BEHAVIOR OF FRP-CONFINED CONCRETE

by

CHING AU

Bachelor of Engineering (Hon), Civil & Structural
The Hong Kong Polytechnic University
(1999)

SUBMITTED TO THE DEPARTMENT OF CIVIL ENGINEERING
IN PARTIAL FULFILLMENT OF THE REQUIREMENTS
FOR THE DEGREE OF

MASTER OF SCIENCE

at the

MASSACHUSETTS INSTITUTE OF TECHNOLOGY

May 2001
June 2001

Signature of Author _____
Department of Civil Engineering
11th May 2001

Certified by _____
Oral Büyüköztürk
Professor of Civil and Environmental Engineering
Thesis Supervisor

Accepted by _____
Oral Büyüköztürk
Chairman, Departmental Committee on Graduate Studies

To my family

for their

Love, Encouragement and Support

BEHAVIOR OF FRP-CONFINED CONCRETE

By

CHING AU

Submitted to the Department of Civil Engineering
On 11th May 2001 in partial fulfillment of the
Requirements for the Degree

MASTER OF SCIENCE

ABSTRACT

The use of fiber-reinforced plastic (FRP) materials as the confinement shells has become an attractive solution to retrofitting, strengthening, and constructing column-like structural systems. The method is considered superior to conventional concrete and steel jacketing methods in terms of confinement strength; post-retrofit ductility, sectional area, weight, and corrosion resistance; application ease; and overall project costs. The confinement effect can be achieved by winding fibers; wrapping and epoxy bonding of fabrics; or installing prefabricated shells. Applications have been extensive in the United States and Japan and there is an increasing trend in Europe and Asia recently.

Despite the extensive use of such new technology, fundamental aspects of the behavior of FRP-confined concrete have not been well understood. Experimental programs at this stage focus on the testing of various composite systems for axial strength increase, which are checked against existing models. Concrete core response, fiber response at various orientations, fiber orientation effects on overall column response, composite stack-up sequence effects, overlap joint effects, air pocket effects, and benefits of using angular fibers have not been fully investigated. Also, reliability and accuracy issues of various instrumentation techniques on composite surfaces have not been sufficiently investigated. The present research work is mostly experimental. It pinpoints various key issues that have not been dealt with previously. Several conclusions are drawn from the present study with respect to the following points: It is found out that gage aspect ratio, resistance, and orientation can have great impact on strain measurements. Concrete core of the column can crush locally and crack globally under high and low confinement strengths respectively. Fracture, buckling, and rigid body reorientation can occur, depending on the orientation of the fibers. Angular fiber wraps generally give more ductile mode of failure. Stack-up sequence of different types of fibers can have positive or adverse effect on the wrapped concrete in terms of failure modes and ultimate strength. Overlap joint can give rise to undesirable bending effect. Air pockets promotes post-peak stress reduction rate.

Thesis Supervisor: Oral Büyüköztürk
Title: Professor of Civil and Environmental Engineering

Acknowledgements

I would like to extend my deepest appreciation to Professor Oral Büyüköztürk, my academic advisor as well as thesis supervisor for his advice, guidance, encouragement, and patience throughout the course of my MS education and thesis work at MIT. He is never too busy to listen to me and discuss about my ideas towards the present thesis work.

I am thankful to Professor Rafael Bras, Department Head of Civil and Environment Engineering at MIT, for granting the funding for material procurement and laboratory resources. This work could not be initiated and completed without this generous financial support.

I am thankful to Dr. John Germaine for his valuable suggestions and help on the instrumentation design and setup, leading to the success of this experimental investigation.

Special thanks to Mr. Robert Fyfe, Mr. Scott Arnold, Ms. Sarah Cruickshank, and Mr. Tyler Maas of Fyfe Co. LLC Ltd. for their provision and installation of their advanced composite systems as well as their suggestions, time and effort in providing and gathering material and technical information, bringing fullness to this work.

I am also grateful for the help and technical assistance of the laboratory research machinist Mr. Steven Rudolph.

Besides, I express my gratitude to my undergraduate research assistance, Alexander Allen, for his arduous efforts, thoughtful ideas, and friendship over the course of the research program.

Last but not the least, I appreciate the valuable and constructive comments, criticisms, and suggestions from fellow students Oguz Günes and Erdem Karaca in my office.

Finally, I would like to thank my love Joanne for taking care of me every single day patiently and unconditionally. Without her love, support, suggestions, and encouragements, I would not have gone through this work so happily.

DISCLAIMER

MISSING PAGE(S)

The Archives copy is missing pages 5 - 13.
This is the most complete version available.

List of Figures

List of Tables

List of Symbols

A	Total cross-sectional area
A_f	Cross-sectional area of fiber
A_m	Cross-sectional area of resin matrix
D	Diameter of concrete cylinder
E	Modulus of elasticity of an isotropic material
E_c	Tangent modulus of concrete
E_f	Modulus of elasticity of fiber
E_{FRP}	Elastic tensile modulus of FRP composite jacket
E_L	Longitudinal elastic modulus of an orthogonal material
E_m	Modulus of elasticity of resin matrix
E_T	Transverse elastic modulus of an orthogonal material
f'_c	Peak strength of unconfined concrete
f'_{cc}	Confined compressive strength
f'_{co}	Unconfined plain concrete strength
F	Applied force
f_c	Confined axial stress at an arbitrary point
f_{FRP}	Tensile strength of the FRP composite jacket
f_{radial}	Radial confining pressure on the concrete core
G	Shear modulus of an isotropic material
n	Kinking shape parameter
R	Radius of concrete core
S	Curve shape parameter of FRP composites
t_{FRP}	Thickness of the FRP composite jacket
α	Angle between the fiber direction and the loading direction
ε	General direct strain
ε_c	confined concrete axial strain

ε_{cc}	Confined concrete axial strain at peak stress
ε_{co}	Unconfined concrete axial strain at peak stress
γ	General shear strain
σ	General direct stress
σ_f	Stress intensity in fiber
σ_m	Stress intensity in resin matrix
τ	General shear stress
ν	Poisson's ratio of an isotropic material
ν_c	Poisson's ratio of plain concrete
Ω	Electrical resistance

Conversion Factors

Parameter	American to S.I. Conversion
Force	1 kip = 4.448 kN
Length	1 inch = 25.4 mm
Pressure	1 ksi = 6.894 MPa

American Units

1 kip = 10^3 lb (pounds)

1 inch = 1/12' (foot)

1 ksi = 1000 psi (pound per square inch)

S.I. Units

1 kN = 1000 N (Newton)

1 mm = 0.001 m (meter)

1 MPa = 10^6 Pa (Pascal) = 1 N/mm^2

CHAPTER 1

INTRODUCTION

1.1 Background

Axial strength and ductility increase of concrete columns is needed whenever repair and strengthening are involved. Repair may be required when columns are damaged under excessive external loads or due to erosion in exposed environments. Strengthening may be required when there is a change of structural use or removal of some adjacent load bearing structural members. In such cases, the required additional load bearing capacity of the existing columns can be provided by external confinements. Lateral confinement has been known to add both strength and ductility in the axial direction for concrete columns and this idea was originally developed back in the 1920s' (Richart et al. 1927, 1928).

Lateral confinements for concrete columns can be in various forms. They appear chronologically as (1) spiral and circular reinforcements; (2) concrete jacketing; (3) steel jacketing; and (4) fiber reinforced plastic (FRP) composite jacketing. Steel has been a conventional and widely used construction material. However, corrosion is one of the largest drawbacks of such material. Weight can be another problem because the construction costs can surge when the installation is labor intensive. Concrete jacketing, though has a lower cost, simply adds weight and cross sectional area to the original structure and may be undesirable. On the contrary, FRP composites, initially developed for aerospace and automobile applications, are found to be a very promising material for civil engineering applications because of their high strength/weight ratio, high corrosion resistance, ease of installation, and relatively low cost of maintenance.

In view of these many advantages, research has been in progress in the past two decades. Experimental investigation and analytical model development are being performed in parallel. Small-scale testing has been the focus of most experimentation programs, although a limited number of large-scale testing has taken place. Analytical models have been proposed base on the basic form suggested in earlier research on spiral reinforcement confinements (Richart et al. 1927, 1928). Coefficients have been proposed empirically. Some stress-strain models are also proposed by refining preceding stress-strain models for steel jacketed concrete and plain concrete behaviors.

Despite all these efforts that have been put into this field of research, several major areas can be identified as insufficiently studied. First, instrumentation issues on composite surfaces have not been addressed yet. Such issues include (1) the installation procedure on composite surfaces that consist of deep ridges due to the fiber roving, (2) the performance of strain gages with different resistance, size, and gage aspect ratio, and (3) the accuracy of strain gages on FRP with different fiber-gage alignments. Second, the behavior of FRP-confined concrete is not well understood. Such behaviors can be categorized into three main areas, namely, loading effects, local effects, and manufacturing effects.

Preceding researches mostly focused on the axial strength and ductility enhancements, which belong to the loading effects category, of the FRP-confined plain concrete cylinders. The concern is that the axial strength increase has often been largely overestimated while the axial strain increase has been largely underestimated. Within the loading effect category, little attention has been paid to the load-deformation behavior, stress-strain curve shapes, failure modes, and stress reduction rates.

For local effects, fiber responses were also not addressed fully. Most researches utilized the fibers in the hoop direction, aiming at producing the maximum confinement effect. However, the possibility of using fibers in different orientations to improve the failure modes and to promote safety should also be considered. Catastrophic failures have been reported unanimously. The roles of fibers in different orientation have not been

investigated and pointed out. The effect of unbalanced overlap design layout was not addressed. Local end condition, which may be correlated to the real world wrapping practice at column ends, needs to be addressed. Designs of strengthening systems in the field mainly rely on the previously developed models that were originally based on steel jacketing and spiral or circular reinforcements. Analytical models and design equations need to be developed and formulated to capture the major observed behaviors demonstrated in FRP jacketed concrete columns.

For manufacturing effects, the effects of composite laminate stack-up sequence need to be adequately studied and reported. Also, initial imperfections such as air pockets and fabric wrinkling, which can be crucial to the overall structural responses, need to be studied.

1.2 Objectives of Present Research

Considering the many areas that need to be further studied, the primary objective of the present research is to study the behaviors of FRP-confined concrete under uniaxial compressive loading as well as to find out the appropriate instrumentation techniques on composite surfaces. The instrumentation and the behavioral studies are categorized into four areas. All studies within each area are briefly summarized below.

Strain Gage Instrumentation Issues

(1) Surface preparation for proper installation and measurement
(2) Performance of various gage types
(3) Fiber-gage misalignment

Loading Effects

(1) Ultimate stress and strains
(2) Time to failure
(3) Failure modes
(4) Load-deformation behaviors

(5) Stress-strain curve shape categorization

Local Effects

(1) Overlap strengthening phenomenon

(2) Bond delamination

(3) Interlaminate shearing between different types of fabrics

(4) Roles of hoop, angular and vertical fibers

(5) Fiber buckling, fracture, and reorientation

(6) Local conditions of confined and unconfined ends

Manufacturing Effects

(1) Initial imperfections such as air pockets

(2) Overlap length and location

(3) Epoxy bond thickness and quality

(4) Fabric stacking sequence

The secondary objective of the present study is to refine the existing analytical models so as to provide an immediate thrust for preliminary design use for the herein composite systems. The study aims at providing an accurate prediction of the peak stress and strain as well as an adequately modeled stress-strain behavior.

1.3 Research Scope and Approach

In order to accomplish the instrumentation objectives stated above, three different types of strain gages are used and compared against the vertical displacement measurements made from extensometers and radial displacement measurements made from two specially designed LVDT devices. Two have a resistance of 350 ohms while the other has a resistance of 120 ohms. All gages have identical gage lengths but the 350-ohm gages have different aspect ratios. They are all made with identical materials in accordance to the suggestions found in the literature (Manual: Tuttle 1989). These gages are tested on three different types of composite surfaces with different fiber weave patterns and

orientations. The gages are also oriented at different angles with respect to the fiber orientations.

To study the behaviors of the FRP-confined concrete cylinders, six wrap configurations are designed. Normal strength plain concrete of about 3500 psi is used. The six configurations are made with different combinations of three types of FRP fabric cloths. All fiber cloths are made with identical E-glass fibers. The first type is made of unidirectional fiber roving; the second type bi-directional weaved fibers in the vertical and horizontal directions; and the third type 45-degree angular weaved fibers. The first three configurations are the most generic and consist only of one ply of the respective FRP fabric. The other three configurations each consist of two plies. All three consist of one ply of angular weaved fibers. Two of the three configurations are made with identical fibers but with different stacking sequence. All six configurations are designed in a way that the fundamental load, local, and manufacturing effects and behaviors can be captured and that each configuration can be compared to at least one other configuration. Details can be referred to Chapter 4 – Experimental Investigations.

To refine the existing peak strength and strain models, the basic form of the confinement equation is utilized and the coefficients are determined by least square fits with the current data. For the stress-strain models, several preceding major models are plotted against the current experimental curves. The closest model is then chosen for the refinement purpose. The refinement of stress-strain models not only includes the change of coefficient by the curve fitting method, but also includes the change of the basic expressions of several major parameters by utilizing the concepts developed from the observed responses of the specimens.

1.4 Thesis Organization

The entire research work is presented in the following logical sequence. First, Chapter 2 gives an overview of the fiber reinforced plastic (FRP) composite materials that are most widely used in column jacketing as measures of retrofit, strengthening, or new

construction. Basic material properties are reviewed. Mechanical behaviors such as stress-strain responses, creep behavior, fatigue and impact resistances are briefly discussed. Environmental effects such as weathering, corrosion, and flammability are also presented.

Then, Chapter 3 reviews some of the preceding researches that represent main contributions. Experimental programs in the US, Canada, and Japan that are concerned about small-scale cylinder testing are presented. Most of them are drawn from the last ten years. Theoretical work developments are also discussed. Analytical models that predict the peak stress and strain, and stress-strain behaviors are presented. Limitations of the reviewed researches are summarized. New directions to further investigations are given.

Chapter 4 presents the experimental program. Material selections and properties, specimen particulars and production procedures, wrap configurations and their design rationales, instrumentation techniques, loading methods, quantitative test results, failure modes, result interpretations and discussions are included in this chapter.

Chapter 5 focuses on the analytical modeling aspect. It first presents the confinement mechanics of circular columns and then evaluates the performances of the existing major models that are presented in Chapter 3. Then, confinement models are proposed to predict the peak stress, peak strain and the stress-strain response of the FRP-confined concrete. The performances of the proposed models are compared against independent results of two other major experimental programs and the results are discussed. Finally, several important design considerations are brought to the surface for serious considerations. Some of these considerations include the proposed progressive failure design concept, the use of a combination of angular fibers and unidirectional hoop fibers, the importance of overlap design within a structural system, and the drawbacks of using large number of hoop wraps.

Finally in Chapter 6, major findings from this research program are summarized. Recommendations for future research work concerning FRP-confined concrete behavior

are given. In the appendix, peak stress, peak strain, and axial stress-strain plots are given for each specimen.

CHAPTER 2

FIBER REINFORCED PLASTIC COMPOSITES FOR CONCRETE REPAIR, STRENGTHENING & NEW CONSTRUCTION

2.1 Introduction

Fiber reinforced plastic (FRP) composites have emerged to be one of the most promising construction materials for reinforcement of concrete members in the past two decades. FRP applications have shifted from the original aerospace and automobile industries to the civil and structural engineering communities because of the superior properties of FRP over other conventional construction materials. The potential applications of FRP reinforcement range widely from new construction to repair as well as strengthening. An extensive number of concrete structural elements can be of benefit. They not only include common elements such as beams, columns, walls, and joints, but also include shell roofs, chimneys, bridge piers, and floor slabs.

This chapter reviews the materials, mechanical behaviors, and environmental resistances of the FRP composites that are most commonly employed in concrete column retrofit, strengthening, and new construction. It also examines the state-of-the-art field applications and industrial developments of such materials. First, the various types of fiber reinforcements and resin matrices are introduced. Second, the mechanical behaviors such as strength, orientation, creep, fatigue, and impact resistance are reviewed. Both isotropic and orthotropic laminates are discussed. Third, environmental effects including weathering, corrosion, and flammability are examined. Finally, current field applications and industrial developments are presented. An example case that exemplifies the existing retrofit practice of reinforced concrete (RC) columns is revealed.

2.2 An Overview of FRP Composite Materials

FRP composites are defined as the materials that consist of high strength/stiffness fiber reinforcements embedded in a resin matrix material. Engineering properties of composites, in most cases, are dominated by fiber reinforcements. More fibers usually give rise to higher strengths. However, low matrix/fiber ratio may lead to strength reduction or premature failure. Fiber lengths and orientations can also affect the properties considerably.

Resin matrix is an adhesive that supports the fibers from buckling under compression, binds the fibers together through cohesion and adhesion, protects the fibers from attack and micro-cracking during service, and provides shearing strengths between fabric layers. The shearing strengths result in resistances to delamination, lap joint debonding and impact damage.

Choice of the particular types of fibers and resins depends on the specific applications. Strength requirement, service life, environmental conditions, and cost are the issues that need to be considered. For example, the choice of composite materials for the retrofit of a group of offshore pier columns would be very different from the strengthening of a group of interior building columns. Load bearing strength, level of exposure, service life, fire and water resistances, ease of installation, and project cost are the major issues that require thorough considerations.

Use of FRP composites in column retrofit and strengthening are mostly in the form of continuous fiber strands and weaved fabric cloths. Fiber strands are used in the process of filament winding using an automated system, a technique that produces column confinement with slight fiber pretensioning. Weaved fabric cloths are wrapped on column surfaces directly using various techniques such as wet lay-up and vacuum bagging. The confinement becomes effective after the fabric cloths are fully cured and hardened. The wet lay-up field installation procedure will be discussed in detail in Chapter Four. For new construction of columns, prefabricated and procured FRP composite shells are used as the concrete pouring forms as well as the permanent confinement shells. The

composite shells can come in different thickness, fiber content, and dimension, depend on the actual design and construction requirements.

2.3 Basic Materials of FRP Composites

As described in Section 2.2, FRP composites are made of two basic materials – fiber reinforcements and resin matrix. Glass, carbon and aramid fibers are the most commonly used in the construction industry owing to their light-weight, superior tensile strength, and corrosion resistance. Figure 2.1 compares the strength and stiffness of a typical carbon fiber composite, glass fiber composite and construction steel.

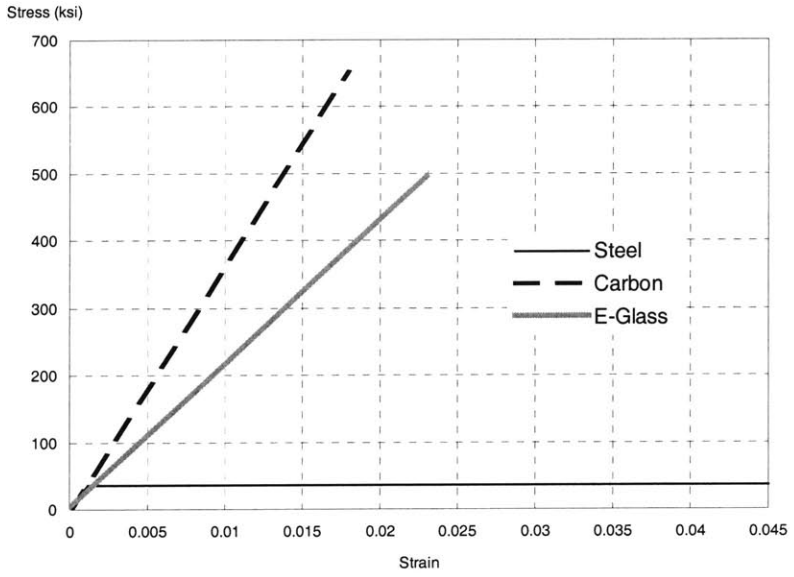

Figure 2.1 Comparison of strength and stiffness of A36 steel, carbon and glass fibers

Epoxies and polyesters are the most popular resins because of their good adhesion capabilities, high toughness, excellent stability and curing properties. In this section, the three types of fiber reinforcements will first be presented, followed by their corresponding forms of existence. Then, the two resin matrices will be examined.

2.3.1 Fiber Reinforcements

A. Glass Fibers

Glass fibers are mainly categorized into E-glass and S-glass. The "E" in E-glass is abbreviated from "Electrical"; the "S" in S-glass is abbreviated from "Structural". In general, E-glass possesses excellent electrical insulation characteristics while S-glass has higher strength and greater corrosion resistance. Both types of glass fibers are calcium aluminoborosilicate formulations. They are inorganic and do not support combustion. E-glass fibers are considered the industry standard and cost less than the S-glass fibers. However, S-glass fibers have higher strengths due to their higher alumina content. Typical filament strength and stiffness values are presented in Table 2.1.

Table 2.1 Mechanical Properties of E-Glass and S-Glass Filaments

Properties	E-Glass	S-Glass
Strength (ksi)	500	670
Stiffness (psi)	10.5×10^6	12.4×10^6

In spite of their chemical resistance, fire resistance, and high tensile strength, glass fibers have a significant draw back. The fiber surface is prone to moisture attack under certain conditions of exposure and above certain stress levels. This attack normally lead to stress-rupture failure if no remedial measure is provided.

B. Carbon Fibers

Carbon fibers are produced by the thermal decomposition of organic precursor fibers such as rayon or polyacrylonitrile (PAN), followed by a stabilization and carbonization procedure. Other alternative precursors are coal, petroleum, and synthetic pitches. The fabrication involves a spinning process. Tensile strength of PAN-based fibers has always been higher than the pitch-based fibers. Therefore, most carbon fibers today are PAN-based. The most important mechanical properties are elastic modulus, tensile strength, electrical conductivity and thermal conductivity. The typical tensile strengths of carbon

fibers are 600-750 ksi, at the higher end of the S-glass fiber strengths. Some even have strengths as high as 1000 ksi, which are less consumed in the industry because of their production cost. Carbon fibers are in general more brittle than glass fibers. But they show exceptional fatigue resistance. Stiffness is higher than all metals.

C. Aramid Fibers

Aramid fibers are aromatic polyamide formulations that are organic in nature. They can be categorized into two main types – para-aramid and meta-aramid fibers. Para-aramid fibers have higher strength and are normally used in high performance applications. One well-known commercial name for para-aramid fibers is the Kevlar fibers. Due to their highly aromatic and ordered structure, aramids have very high thermal resistance. They do not melt prior to decompositions and do not burn when the flame source is removed, although they can be ignited. Compared to inorganic fibers like carbon or glass, aramid are superior in fire resistance because the fibers themselves do not readily conduct heat into the matrix. The typical decomposition temperature is around 450°C. The typical tensile strength and stiffness are 400 ksi and 15 x 10^6 psi. The tensile strength is about that of mid-range carbon fibers. One of the major drawbacks is their weak bending and compressive strengths. They easily buckle or kink under compression forces and the fibers damage. Other major drawbacks include the relatively low adhesion to most resin matrix materials, and high moisture absorption by the fibers.

2.3.2 Forms of Fiber Reinforcements

Reinforcing fibers appear in various forms, depending on the end-use application. The fibers can be in the form of either discontinuous fibers (staples) or continuous fibers (filaments). Staples are usually placed randomly within a matrix to attain isotropic properties so that the load resistance in any direction is almost identical. Continuous fiber filaments can be further fabricated into strands and roving. The fiber bundles can then be weaved into fabric cloths with various patterns. In general, fiber strands have higher tensile strength then the fabric counterparts with respect to weight. This is resulted from the unavoidable kinking within the fabric weave. Each form is elaborated below.

A. Staples

Staples are used to form reinforcing mats or surface mats. In some cases, they are used to reinforce concrete materials by direct addition of chopped fibers with concrete during concrete mixing. The products demonstrate isotropic properties because of the random orientation of the short fibers, which have a length of less than 0.02". The fibers enhance load carrying capacities because they take stresses in their direction and prevent cracks in the matrix or concrete from developing and propagating.

B. Continuous Strands

Continuous strands that are used in column winding are made of many single fiber filaments twisted together or made of several untwisted strands that are adhered together chemically. These continuous strands can be pre-impregnated or impregnated on site simultaneously during the winding process. The strands also act as the basic units of woven fabrics. Continuous strand have higher strength than woven fabrics because they are straight and smooth, without any local stress concentration that may exists when stretched in tension (see below).

C. Fabric Cloths and Tapes

Fabric cloths are weaved in patterns that are similar to textile cloths fabrication. The cloths are weaved using continuous fiber strands with specified fiber contents, depending on application and design requirements. Fabric cloths exhibit lower tensile strength because of the kinking at cross points of the weave. When the fabric is stretched under tensile pull, points of stress concentration forms when the fiber roving tends to straighten up. Points of stress concentration then eventually damage the epoxy bonding and form white dots, demonstrating locally highly stressed resin and relative movements of the fiber roving in orthogonal directions. Fabric tapes show similar behavior and they are trimmed to size from fabric cloths. Woven roving are similar to fabric cloths, but are usually made of thicker fiber roving than the twisted fiber strands. Load capacities of woven roving are in general higher than that of fabric cloths.

Comparison of Cost and Thickness

Table 2.2 shows the cost ratios and size ranges of respective forms of fiber reinforcement. It can be noted that the cost of fiber strands for filament winding is the lowest. Cost of cloth fabrics and woven roving are higher because of the extra fabrication procedure and one more level of quality control during the fabric weaving process.

Table 2.2 Comparison of Cost and Thickness of Various Forms of Fiber Reinforcements (Book: Rosato 1997)

Properties	Continuous Strands	Fabric Cloths	Woven Roving
Cost Factor (per lb)	1 – 2.5	3.5 – 6.5	2 – 3.5
Thickness (inch)	0.0026" – 0.055" (diameter)	0.0010" – 0.045"	0.027" – 0.048"

2.3.3 Resin Matrix

A. Epoxy Resins

Epoxy resins are advantageous in several ways. First, they provide excellent adhesion to a wide variety of fibers because of their inherent polar nature. Second, it has a low level of shrinkage upon curing. Third, there is no release of volatile by-product that causes bubbles or void formation in the curing process. Forth, epoxy has a very high toughness due to their cross-linked structure. Finally, it gives excellent mechanical properties. In view of the many advantages and benefits of epoxy resins, they have been very popular in forming the FRP composites that are used in civil structures. However, epoxy resins have demonstrated a tendency to absorb moisture both in the uncured and cured stage. Also, the elongation to failure is relatively low. The elongation disadvantage has been improved by modified epoxy resin formulations. It was reported that no degradation of the composite materials has been observed even after over 20 years of service exposure (Handbook: Peters 1998). Curing at room temperature and heat accelerated curing are available.

B. Polyester Resins

To date, thermosetting polyester resins are the most widely used of all matrix materials. The thermosetting process consisted of a chemical reaction that cross-links the material so that it cannot be returned to liquid form. At ambient temperatures, the liquid polymers are very stable and can be stored for many months. On the other hand, they can be cured within minutes by adding a peroxide catalyst. Fiberglass reinforced polyester composites in general have excellent mechanical properties and acceptable environmental durability. Comparing with the epoxy resins, polyester resins have a lower cost. However, this resin does not provide adequate adhesion to carbon and aramid fibers. Cure shrinkage is also relatively large. The drawbacks have been deterring its use in the construction industry where carbon and aramid fibers are involved. Curing at room temperature or under heat is available.

2.4 Mechanical Behaviors of FRP Laminates

Mechanical behaviors that will be discussed include behaviors of stress and strain, different orientation, creep, as well as resistances to fatigue and impact. FRP laminates are of major concern. Both isotropic laminates and those with directional properties are examined.

2.4.1 Stress and Strain Behaviors

Stress and strain behaviors can be considered from two perspectives – micro-mechanics and macro-mechanics. Micro-mechanics considers FRP composite materials in the microscopic scale, which considers fiber and matrix as separate entities. Macro-mechanics considers FRP composite materials as in the macroscopic scale, which considers fiber and matrix respond together as one homogeneous material while permits directional properties. Equations in the following subsections that present both micro- and macro-mechanics are extracted from the books of Rosato 1997, Holmes and Just 1983, and Ashbee 1989.

2.4.1.1 Micro-mechanics Representations

A. Isotropic Laminates

When chopped fibers are mixed with resin in random orientation, the laminate has directionless properties and can be treated as an isotropic material. The microscopic behaviors are highly complex and normally consist of interfacial debonding and crack development in the matrix material. Crack propagation direction cannot be generally predicted due to the randomness of the embedded short fibers. Therefore, for isotropic laminates, the macro-mechanics approach is often used.

B. Orthotropic Laminates

For orthotropic laminates, with long continuous fibers embedded in the matrix material, clearly defined bonding interface can be identified. Fibers and matrix are considered as separate entities, although they are adhered together and have considerable interactions under load. The stresses and elastic moduli of the respective materials are considered separately and the effects are superimposed to get the resulting or equivalent stress and elastic modulus of the composite material.

Let us consider a simple case where only unidirectional fibers exist in the laminate and the fibers are aligned with the load vector. For a given tensile pull, the following equation applies.

$$F = \sigma A = \sigma_f A_f + \sigma_m A_m$$

Such that
- F = applied force
- σ = mean stress intensity on entire cross-section
- A = total cross-sectional area
- σ_f = stress intensity in fiber
- A_f = cross-sectional area of fiber
- σ_m = stress intensity in resin matrix
- A_m = cross-sectional area of resin matrix

Assuming a perfect bonding initially between the fiber and the matrix, compatibility condition has to satisfy at the fiber-matrix interface. The two entities have to move together. Therefore, the following equation can be derived.

$$\frac{\sigma_m}{\sigma_f} = \frac{E_m}{E_f}$$

such that E_m = modulus of elasticity of resin matrix

E_f = modulus of elasticity of fiber

Also, the elastic modulus of the composite in the longitudinal direction is given by

$$E\,A = E_f\,A_f + E_m\,A_m$$

where the parameters are defined as before. Since volumetric ratios of the fibers and matrix are directly proportional to their cross-sectional areas, the parameters in the first and third equations that represent the cross sectional areas can be entirely substituted by the respective volumetric ratio parameters V_f and V_m. The total cross-sectional area A can be substituted by unity, which is the addition of the two volumetric ratios that represent fibers and matrix respectively.

2.4.1.2 Macro-mechanics Representations

A. Isotropic Laminate

For isotropic laminates, the familiar engineering equations below apply. Isotropic laminate has an identical elastic modulus in any direction. The stress-strain behavior follows the Hooke's law and the Poisson's ratio ν is related to the shear modulus G and elastic modulus E in the following way.

$$G = \frac{E}{2(1+\nu)}$$

Also, direct stress σ, direct strain ε, shearing stress τ and shearing strain γ are related as follow.

$$\varepsilon = \frac{\sigma}{E}$$

$$\gamma = \frac{\tau}{G}$$

B. Orthotropic Laminate

For orthotropic materials like fabric cloths and weaved roving, the elastic moduli in the longitudinal and transverse directions can be different. Poisson's ratios in the two directions can also differ accordingly and must be determined experimentally. For designs, strains at various arbitrary angles with the applied load are often desirable.

The following presents the relations of the properties of a single-layer laminate in an arbitrary loading direction 1, making an angle α with the longitudinal fiber direction. No shear stress is applied. Superposition methods can be used to determine the resulting stress if more than one load is acted on the laminate, making different angles with the longitudinal fiber direction.

I. Strain Induced in the Direction of the Applied Stress

The applied stress σ_1 causes a strain ε_1 such that

$$\varepsilon_1 = \frac{\sigma_1}{E_1}$$

in which E_1 can be determined from the following

$$E_1 = \left[\frac{1}{E_L}\cos^4\alpha + \frac{1}{E_T}\sin^4\alpha + \frac{1}{4}\left(\frac{1}{G_{LT}} - \frac{2\nu_{LT}}{E_L} \right)\sin^2 2\alpha \right]^{-1}$$

II. Transverse Strain Induced by the Applied Stress

A transverse strain ε_2 that is caused by σ_1 is

$$\varepsilon_2 = - \nu_{12} \varepsilon_1$$

where

$$\nu_{12} = \frac{E_1}{E_L}\left\{\nu_{LT} - \frac{1}{4}\left(1 + 2\nu_{LT} + \frac{E_L}{E_T} - \frac{E_L}{G_{LT}}\right)\sin^2 2\alpha\right\}$$

III. Shear Strain Induced by the Applied Stress

Shear distortion and hence shear strain γ_{12} will appear in the laminate when the applied stress in the 1-direction acts at an angle other than 0 and 90 degrees with the fiber directions. The shear strain can be found from the following.

$$\gamma_{12} = -\frac{m_1 \sigma_1}{E_L}$$

in which m_1 can be determined from

$$m_1 = \sin 2\alpha \left\{\nu_{LT} + \frac{E_L}{E_T} - \frac{1}{2}\frac{E_L}{G_{LT}} - \cos 2\alpha \left(1 + 2\nu_{LT} + \frac{E_L}{E_T} - \frac{E_L}{G_{LT}}\right)\right\}$$

IV. Other General Relationships of the Orthotropic Properties

The Poisson's ratios in both the longitudinal and transverse directions are related as follow.

$$\frac{\nu_{LT}}{\nu_{TL}} = \frac{E_L}{E_T}$$

And G_{LT} can be determined theoretically from the experimentally obtained data ν_{LT}, ν_{TL}, E_L and E_T from the following relations.

$$G_{LT} = \frac{E_L E_T}{E_L(1+\nu_{TL}) + E_T(1+\nu_{LT})}$$

It can be noted that the above two formulas can be decomposed back to the isotropic formulas if E_L equals E_T and that ν_{LT} equals ν_{TL}.

2.4.1 Orientation Behavior

Mechanical behaviors of FRP composites are dominated by the arrangement and interaction of the fiber reinforcement and the surrounding matrix. As pointed out earlier, if chopped fibers are mixed with the resin matrix, the laminate would appear isotropic due to the randomness of the fibers. However, directional properties occur if the continuous roving is placed in orthogonal directions. The maximum strength should occur in the primary fiber direction. When the load and fiber orientation do not align with each other, significant reduction of structural efficiency is resulted. Figure 2.2 shows a typical strength variation with the angle of loading. The variation is computed from the classical laminate theory using typical properties of E-glass unidirectional laminates.

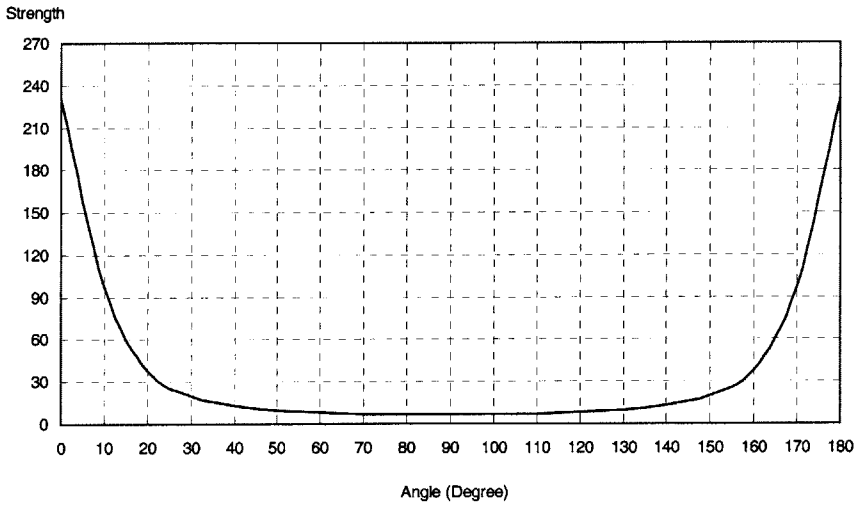

Figure 2.2
Typical strength variation with loading angle in a laminate with unidirectional fibers

Besides the strength difference, failure modes also differ. Unidirectional fibers exhibit fracture upon tensile loading in the fiber direction. The same laminate exhibits resin failure if loaded in the transverse direction because there is no load resisting fibers. Resin-fiber interfacial debonding may occur. If the laminate is rotated to an angle with the applied load, shear plane failure should occur. Fiber may not fracture and the matrix is subjected to substantial shearing stress, a force component decoupled from the tensile pull as demonstrated from the shearing strain equation.

2.4.2 Creep Behavior

Creep behavior is dominated by resin. Creep in the thermoplastic resin matrix is far more substantial than that in the thermosetting resin matrix. Creep experienced is dependent on temperature and the magnitude of the applied stress. The molecular bonds in the resin are strained under a continued application of stress. Responses of these bonds are slow and the state of equilibrium is not reached after a long time. Therefore, the material continues to deform for long periods after application of load. Upon removal of load, unrecoverable deformation occurs. On the other hand, temperature affects the molecular activity. When the temperature is increased, additional creep can be observed. Thermosetting plastic resins such as epoxy are more resistant to the molecular movement by the inherent cross-linking during the curing process. Therefore, creep is less pronounced in thermosetting resins.

2.4.3 Fatigue Resistance

Fatigue resistance of carbon and boron fibers is excellent. The stiff carbon and boron fibers are able to bridge the cracks that occur across the matrix and hence reduce the stress intensity of the crack tip. Fatigue occurs more substantially, however, in glass fiber reinforced plastic composite. Glass fibers are comparatively less stiff and the stress transfer mechanism from the matrix to the fibers is less effectively, making the matrix more prone to large stresses and strains and promoting the crack development under a fewer number of load cycles than carbon and boron fibers. Fatigue tests on fiberglass laminates indicated a deterioration of stiffness, especially at low cycle testing (Handbook:

Peters 1998). It was suggested that the deterioration was due to the creep behavior of the resin matrix.

2.4.4 Impact Resistance

Damage from impact load may reduce the strength of composite laminates, depending on the speed of impact, and the intensity of the impact load. It was indicated from test results (Handbook: Peters 1998) that delamination of the impacted area could be substantial, accompanied by peeling in the direction of the surface laminate fibers. In general, the impact resistance depends on fiber content, weave pattern and weave density. For multi-layer laminate stack up, the resistance also depends on the interlaminate-shearing strength of the resin matrix.

2.5 Environmental Effects

2.5.1 Weathering

In general, weathering capabilities of FRP composites depend highly on the resin matrix characteristics. Degradation can be noted upon extended exposure in outdoor environments. Since the mechanical behaviors such as strength and stiffness are provided almost by the fibers, degradation of the matrix material will not have direct impacts on those behaviors. However, one should remember that the role of matrix is to protect the fibers from micro-crack, moisture attack, as well as to transfer and distribute external loads evenly onto the stress taking fiber reinforcements. Therefore, protection to the matrix is also essential.

Weathering can be in various forms. The most common include ultraviolet (UV) radiation, thermal extremes. UV radiation causes degradation due to molecular weight change and cross-linking decomposition in the resin system. Thermal extremes may occur cyclically in the form of freeze and thaw cycles as well as subjected to high temperatures over a season and low temperature over another. Cyclic thermal fatigue can

occur in such occasions. To tackle these problems, protective coatings have been developed and were found to be effective (Handbook: Peters 1998).

Moisture is known to attack the fibers directly and reduce the original strength through micro-cracking. To tackle the three major weathering problems, protective coatings were developed and were found to be effective in preventing severe degradation of the FRP composite systems under service conditions (Handbook: Peters 1998).

2.5.2 Corrosion

Moisture attack with the presence of oxygen is known to cause severe corrosion in steel. Rusting and cracking of concrete covers are known problems that can hardly be eliminated in the construction industry. Corrosion in FRP composites are found to be minimal, although fibers are prone to moisture attack and can crack prematurely under load. The role of resin matrix is therefore essential in protecting the fibers from moisture attack. Resins developed especially for underwater construction of FRP composites are also developed so that resins cure upon contact with water (Manual: Fyfe 1999).

2.5.3 Flammability

Elevated temperatures due to fire for a prolonged period of time can seriously affect the properties of FRP composites. Matrix softening would occur and is, interestingly, depending on the stacking and humidity. It was found out that quasi-isotropic stacking could effectively reduce the strength reduction at elevated temperature while unidirectional stacking could experience substantial strength reduction. The elevated temperature does not affect only the resin matrix, but also to the fibers, especially the PAN-based fibers. Oxidation was reported from experimental tests for such fibers.

2.6 Retrofit and Strengthening of Reinforced Concrete (RC) Structures

2.6.1 Current Applications and Developments

FRP composite systems find applications in reinforced concrete columns, beams, walls, slabs, chimneys, posts, tanks, and brick or block walls and façades, as well as structural wood elements. The majority of applications are found in RC structures. FRP systems can be in the form of FRP bar reinforcements, bonded plate systems, two-dimensional grid systems, confinement fabrics, and prestressing tendons. These systems mainly replace the traditional roles of heavy steel reinforcements, jackets, or tendons.

The use of FRP bar and bonded plate systems has gained success and maturity in replacing traditional steel reinforcements and strengthening plates. The use of confinement fabrics especially for column-like structures for strengthening and seismic retrofit has been extensive over the past 5 years and there are signs of increasing use of such technique. By mid 1998, there are well over 120 projects that employed such method (Manual: Fyfe 1999). However, analytical models that can be used to predict stress-strain responses accurately are still lacking. Designs are mostly based on previously developed confinement models that have been successfully applied for steel confinements such as steel jackets or spiral and circular reinforcements.

In view of the weathering and degradation problems of the composite systems, materials such as fire resistant coating, corrosion inhibitors, chemical resistant coating, and UV resistant coating have been developed to apply externally on the composites for protective purposes (Manual: Fyfe 1999).

2.6.2 An Example of the Effect of FRP Retrofit of RC Columns

Although analytical confinement models are not fully developed for FRP composites, it has been shown effective that wrapped RC columns could last longer than unwrapped column in the case of exposed bridge columns that consisted of severely corroded steel reinforcement.

According to a study (Manual: Fyfe 1999), three bridge columns located in FDR Drive near Manhattan Bridge at Corlears Park were extensively cracked because of rebar corrosion. The column size was 2' x 4' x 10'. All three columns were repaired with identical procedures with cementatious mortar. Two of the columns were then wrapped with three plies of glass fiber composite fabrics while the third column remained unwrapped. It was found that the unwrapped column cracked again after four years of retrofit while the wrapped columns showed no sign of deterioration.

CHAPTER 3

PRECEDING RESEARCH & STATE–OF–THE–ART

3.1 Introduction

Fiber-reinforced plastic (FRP) confined concrete under static axial, flexural, and cyclic or seismic lateral loads have been under investigation to develop retrofit technologies and new construction methods. Researches have been going on in the last two decades in the United States, Canada, Japan, Singapore, and some other countries. Significant contributions were mainly founded in the past ten years in the US and Japan. This chapter aims to provide a comprehensive review of the major contributions in the framework of FRP confined concrete behaviors under monotonic concentric compression loading. Cylinder tests with normal compressive strength concrete (3500 – 6000 psi) will be focused. No attempt is made to review and discuss topics outside this scope. Also, the review focuses mainly on the development in the North America, because most Japanese research literatures were written in Japanese, which is out of the literacy of the author.

The review that follows is organized into two parts. Major experimental programs will first be presented. Theoretical development will then follow. The two sections are made to remain separate because some researches only contained experimental investigations while some others only focused on theoretical developments. Therefore, research groups do not necessarily appear in both sections. Presentation in respective sections follows the chronological order. Each experimental program will include the aim of tests, materials used, specimen information, FRP confinement mechanism, loading method, failure modes, and the conclusion of what was discovered. A brief comment on what needs to be improved will follow. In the theoretical development section, equations that predict ultimate stress and strain will be presented. In cases where constitutive relations were

developed, the analytical models will also be presented without reproducing the derivation procedures. Finally, a master summary of these advancements and deficiencies will be provided. The logical development and needs of an experimental investigation at MIT will then follow.

3.2 Experimental Programs

The FRP confinement concept in increasing axial strength and ductility of a concrete column is originated from the characteristics of concrete subjected to triaxial stress states. In fact, this confinement concept has been utilized in the form of spiral and circular reinforcement and steel and concrete jacketing in strengthening and retrofitting reinforced concrete columns and bridge piers since decades ago. The use of FRP as the confinement jacket reflects the advancement of materials over time while the fundamental concept remains. This fundamental confinement concept was pioneered in 1927 in University of Illinois under the directions of Richart et al. They formulated a linear analytical model for the prediction of ultimate load (Richart 1928), forming the foundation of all subsequent model developments. With this in mind, there is a need to first review this important initial investigation on triaxial stressed concrete so as to provide more insights on the subsequent findings particularly on FRP confinement such as failure modes and analytical model developments.

3.2.1 Richart, Brandtzaeg and Brown (1928, University of Illinois)

Objectives

The objective of the experimental program was to obtain information on how the ability of concrete to resist stress in one direction was influenced by the presence of stresses in the other directions. It aimed at investigating the validity of a general conception of the process of failure and thus developing a failure mechanism conception for optimal proportioning for strength and durability.

Experimental Particulars

Altogether three series of specimens were produced. The first series contained cylinders subjected to simple axial load and two-dimensional compression respectively. The second series consisted of cylinder subjected to three-dimensional loading with the axial load larger than the lateral compression. The third series had the cylinders subjected to three-dimensional compression with the axial load smaller than the lateral compression. Cylinders sizes of 4" x 8" and 4" x 22" were used. Normal strength plain concrete with lean, medium, and rich mixtures were used. Axial compression was carried out in a testing machine. Lateral compression was produced by oil pressure through a hand pump. The two load types were applied simultaneously. Obviously, active lateral confinement was provided. Vertical load was applied to the specimens with displacement control at a rate of 0.05 in. per minute. Sets of dials were used for displacement measurements.

Findings and Conclusions

It was discovered that the added strength produced by a given lateral pressure was near constant, regardless of the concrete mixtures being studied. Lateral deformation near maximum load was found to have radical increase. Material internal continuity was rapidly being destroyed after that critical state. A wide range of deformation occurred with little change in the accompanying load beyond the maximum load. Most cylinders were still intact when removed from the loading chamber while a few were seen to have developed inclined surface cracks.

It was concluded that the results agreed fairly well with the results of a preceding series, in which spirally reinforced concrete was used. The increase in the ultimate strength produced by the passive lateral pressure developed by the spiral reinforcement was equal to 4.1 times the lateral pressure. The law of resistance was considered essentially the same for concrete restrained by lateral oil pressure, as for concrete spirally reinforced, although lateral confinement was active in the first case while passive in the latter case.

Comments

Although the tests were simple, they have established the fundamental conceptions on the behavior of freshly made concrete under multi-axial compression in terms of failure modes, and ultimate loads with respect to the lateral pressure applied. It is, in fact, quite important to have identified the comparable behaviors and quantitative relationship of concrete under active and passive confinement pressures.

3.2.2 Fardis and Khalili (1981, 1982, Massachusetts Institute of Technology)

Objectives

Fardis and Khalili conducted an early experiment of its kind, using the FRP encasing technique. They aimed at finding out the feasibility and efficiency of this new construction method. This concept was pursued in view of the excellent tensile strength and advantageous properties of FRP, and the drawbacks commonly found in steel jacketing. Such drawbacks include the high weight-to-strength ratio, labor-intensive installation procedure, and steel corrosion problem for exposed structural members. They proposed to simplify the composite system construction procedure by using FRP as a permanent formwork as well as the strength enhancing material.

Experimental Particulars

Concrete cylinders were encased in continuous glass fibers weaved in orthogonal directions (vertical and horizontal). Wrapping instead of encasing was actually performed due to the constraint of available products. Cylinder sizes were 3" x 6" and 4" x 8". Normal strength concrete (4500 – 5500 psi) with water/cement ratio 0.55 was used. Four types of FRP were used. They included balanced weave, unbalanced weave, and unidirectional fibers. Balanced weave implies that the fiber content in one direction is identical to those in the other direction. Circumferential fibers were intended to provide lateral confinement while longitudinal fibers took up tension caused by any unanticipated bending effect. All cylinders were tested under a monotonic, concentric, axial load. Load control mechanism was used at a rate of 20 – 50 psi/sec.

Findings and Conclusions

Cylinders failed under the combined axial load and confining pressure such that the FRP jacket had reached the failure strain in the circumferential direction. Fiber fractured and concrete crushed simultaneously at failure. Axial ductility was enhanced before failure. However, failure modes were all brittle due to sudden fiber breakage upon reaching the elastic limit. It was emphasized that axial stiffness of the FRP casing should not be neglected because local fiber buckling was detected. Premature failures occurred when axially placed fibers buckled locally under compression, inducing early interlaminate shear. It was, therefore, suggested that, for the sake of axial strength enhancement and in terms of economical use of materials, fibers should be placed mostly in the circumferential direction. The presence of fibers in the axial direction should contribute minimal axial strength. Practical issues such as weathering characteristics and fire resistance of the FRP were briefly discussed. Corresponding measures to improve these environmental properties were also reviewed.

The experimental data were compared to Richart's analytical model, which predicts the ultimate strength of confined concrete. It was concluded that, regardless of the type of fiberglass used in the confinement shell, the equation showed general satisfactory predictions of ultimate strength. Scattering of data was noted, though, and it was thought to be due to the FRP strength variation, which was typically exceeding 15% from the mean value.

Comment

The work is considered quite comprehensive. It not only discussed the stress and strain relationships by comparing the experimental finding with an existing confinement model, but also dealt with practical issues including installation procedure, weathering issue, and flammability. This innovative use of FRP material should indeed save significant amount of labor time, construction and maintenance cost. It can also reduce cross-sectional dimensions and safe more floor space.

However, the cylinder size used for investigation is considered too small in order to capture fully the fiber behaviors under load. The radius of curvature is too small when compared to real size columns. Confinement characteristics of the FRP shell may thus have some deviations. On the other hand, the study seemed to have overlooked the overlap effect. Overlap length and method of construction was not reported. One should note that the overlap strength is developed when a certain length of material is lapped so that the total shearing resistance of the matrix material in between equals or exceeds the original tensile strength of the fabrics in the circumferential direction. If the overlap length is too small, strength cannot develop fully. Overlap debonding will thus occur. In the case of small-diameter cylinders, a large percentage of the circumference is overlapped and the true axial strength cannot be revealed because the actual "double-wrapped" condition in the overlapped region exists. Unbalanced forces may also exist when the thickness of the FRP shell is not even around the circumference. Therefore, the comparison of the experimental data with the analytical model developed for uniform active confinement pressure does not truly reveal the accuracy and preciseness of the use of that model in design or prediction of FRP confined concrete strength.

3.2.3 Eckel and Karbhari (1993, University of Delaware)

Objective

This research, from a fabrication perspective, aimed at investigating the feasibility and structural efficiency of the resin infusion technique in the retrofit of columnar structures. It pointed out that the wet lay-up method is difficult to achieve proper and uniform confinement pressure during the installation process. Initial imperfections such as air pockets and fabric wrinkling may lead to possible premature failure. The fiber winding technique was also discouraged because specialized robotic equipments needed be used. The advocated resin infusion technique is capable of simultaneously applying a confining pressure and wetting the wrapped fiber/fabric so that a uniform and smooth composite confinement is achieved. Failure modes and ultimate strength increase were focused.

Experimental Particulars

Normal strength (5500 psi) concrete cylinders of size 6" x 12" were used. Both glass and carbon fiber roving were used. Altogether five fiber architectures were produced. The first two types consisted of woven glass roving with 2 and 4 layers respectively. The third type was a sandwich design with unidirectional axially placed carbon fibers put between two plies of fabrics with horizontally placed carbon fibers. The forth type oriented the middle layer of the third type so that the fibers run horizontally instead of vertically while all the others remained the same. The final type sandwiched a layer of carbon fibers in between single layers of woven glass roving.

During the resin infusion process, resin was injected under a vacuum film using a resin distribution medium to achieve full and rapid infusion of the fabric. The entire assembly was evacuated before the resin was introduced and a vacuum was maintained until the resin was cured. After infusion, the wrapped cylinders were allowed to achieve full cure at room temperature.

All cylinders were loaded monotonically in axial compression until failure. Deformation was measured in the axial direction using dial gage indicators. No lateral deformation information was obtained. Loading mechanism and loading rate were not reported.

Findings and Conclusions

It was reported that doubling the amount of glass fiber composites, the load carrying capacity was effectively doubled above the unconfined concrete strength. The use of glass fabrics in confining concrete reduced the scattering of data common in concrete while the use of carbon fabrics, an apparent wide scatter was found. It was argued that the inherent brittleness of carbon fibers explained the scattering phenomenon. Glass fiber elongation was recorded more substantial than that in carbon fibers. Complete unzipping of the composite jacket was found in Type 3 along the vertical direction. For Type 4, the vertical unzipping was less pronounced. Partial fiber fracture in both the horizontal and vertical directions were recorded in the glass-only jackets. Concrete fracture was found.

For Type 5, the case when combining carbon and glass fabrics, a mix mode that consisted of fabric unzipping, partial fiber breakage, and concrete fracture was found. It was concluded that the use of resin infusion method was effective. Jackets with fibers placed in the hoop direction gave rise to a higher degree of confinement. Also, the combine use of glass and carbon fibers were advantageous in terms of replicating the initial concrete load-deformation behavior because axial stiffness did not increase much. Also, substantial increases in axial load and deformation capacities were noted.

Comments

This research has provided an attractive alternative to solve the problems and difficulties commonly found in the fiber winding and wet lay-up techniques. It is capable of creating a more consolidated wrap during a uniform compaction process. It also introduces initial confinement so that columns after retrofit are immediately effectively confined. Finally, it advocated the use of hybrid composite construction, which made use of both glass and carbon fibers simultaneously.

However, it is not clearly discussed how this technique can be applied in the field. Wrapping small-scale cylinders and full-scale columns definitely require different levels of skills and procedures because of the size effect. The proposed technique may not be easily applied without the fully controlled laboratory-like conditions. Also, it did not mention whether an overlap existed in the wrap when using that technique, and whether that overlap region may produce any undesirable unbalance effect to the column when subjected to axial load. Although the combined use of glass and carbon fabrics was suggested, sound guidelines about how two different materials should be stacked together to obtain optimal design was missing. It also made no attempt to measure and quantify the respective cylinder lateral deformations, which is essential to develop understanding of the overall global behaviors of the different wrap configurations.

3.2.4 Nanni and Bradford (1995, The Pennsylvania State University)

Objective

The purpose of this investigation was to develop experimental data and check for the validity of existing analytical models for the behavior of FRP confined concrete. Prediction models were compared with one another in terms of ultimate strength and stress-strain curve shapes. Three different types of passive FRP confinement techniques were investigated. They included braided aramid FRP tape, filament wound E-glass FRP, and pre-formed glass-aramid FRP shells. The objective of using different types of FRP confinement was to perform a qualitative comparison, especially focusing on various failure modes.

Experimental Particulars

Specimen size 6" x 12" was used. Normal strength and normal weight concrete was used. For the cylinders that were wrapped with aramid FRP tapes, three pitches of 0, 25, and 50 mm were used for the three tape sizes. Tapes were pretensioned and run at an angle with respect to the longitudinal axis of the tape. The pretensioning stress of 4.0 MPa was applied. For the glass filament wound specimens, concrete cylinders were first sand blasted. The fibers were then wound helically onto the surface with an angle of 2 degree from the horizontal plane. Windings were layered to increase the designed thickness. No pretensioning was applied to the fibers during the winding process to prevent any fiber breakage. No detail fabrication description was given for the pre-formed FRP shells.

Axial displacements were measured using LVDTs across the machine crosshead. Load-deformation curves up to failure were obtained. Load cell was used to produce the corresponding loading data. Specimens were loaded monotonically and concentrically in compression. Load mechanism and loading rate were not reported.

Findings and Conclusions

Different failure modes were encountered. For FRP tape confinement, fiber ruptured in tension and concrete disintegrated due to volumetric reduction and lateral tension. In

some cases, shear cone failure occurred before any fiber rupture, bringing the cylinders to failure with no additional load-carrying capacity. In some other cases, tape rupture signified the ultimate life of the specimens. The rest of the specimens confined with FRP tape experienced total concrete disintegration. All specimens in this category experienced an initial phase very similar to the unconfined concrete. The post-cracked phase was practically linear for all specimens. Constant increase in strength was noted to the eventual rupture of the fibers. Concrete between tape-confined (pitches) areas spalled off upon loading.

For filament-wound concrete, all specimens experienced concrete disintegration, followed by a tensile rupture of the confinement at mid-height. Visible bulging was noted at the failure zone before fiber fracture. Discoloration was noted. The stress-strain performance of this group was quite similar to that of the FRP tape group. The stress-strain curve could be represented by a simple bilinear curve with a kink point at the stress level roughly equal to the strength of unconfined concrete.

For pre-formed shell confined concrete, joint failures at the overlap regions dominated the failure mode. The failure occurred at mid-height. Bond separation occurred at the overlap of the two half shells and longitudinal cracks formed on the shell surface. Concrete was partially fractured after examination of the failed specimens. Strength increase in this group appeared to be the weakest. The stress-strain curve shape was similar to the other two groups.

It was concluded that passive FRP confinement systems did not prove to be advantageous under load conditions below the compressive strength of the unconfined material because almost no difference could be noted in the initial stage upon loading. Enhanced strength and ductility were recorded after the kink point. Three major failure modes were noted. They were shear cone failure, concrete disintegration/fiber fracture, and shell joint rupture. As seen in the case of joint rupture, it was proposed that confinement efficiency was directly dependent upon the fabrication technique and quality. Existing analytical models provided a poor prediction on the stress-strain behavior, though the ultimate

strength could be predicted with fair accuracy. Ultimate strain, on the other hand, was grossly underestimated.

Comments

It was verified that existing analytical models were not capable of predicting stress-strain behaviors of FRP confined concrete, regardless of the types of FRP confinement mechanisms. This investigation has, thus, provided important information on how current analytical models needed be refined for design use. The three different failure modes clearly reflect that different confinement mechanism could yield distinct failure modes. Hence, although the stress-strain profiles are similar, the most desired failure mode should be chosen for retrofit and strengthening purposes in favor of safety. Joint failure has indicated the importance of the joint connection and overlap length issue in FRP confinement shells. This can lead to any premature failure, which is often unpredictable and catastrophic. The joint effect should, therefore, be thoroughly investigated. Finally, shear cone failure instead of concrete disintegration occurred in the tape confined concrete with a linear increasing slope in the axial stress-strain curve. This, in fact, violates the fundamental mechanics conception that when concrete is sufficiently confined, only particle disintegration could occur because no cracks could form in any direction. This violation calls for a fundamental revision and investigation of the FRP confinement mechanism concept and a redefinition of the "sufficient confinement" in terms of the slope of stress-strain curves. The violation may signify that even though an inclined slope appears in the stress-strain curve such that strength and ductility both increase, insufficient confinement can actually exist. It may also signify the unique elastic characteristics of the FRP material.

3.2.5 Howie and Karbhari (1995, University of California, San Diego)

Objective

The primary emphasis of this study was to investigate the effect of fiber orientation and composite wrap layering schemes using a tow-sheet-type carbon fabric composite

system. Its main concern was the load-carrying capacity and ductility from a strengthening viewpoint. The work aimed at finding out an optimal wrap configuration such that the confinement would provide enhanced axial strength as well as the capability to constraint failure of the structure, even after the internal concrete failure. Seismic retrofit and rehabilitation were not within the scope of the study.

Experimental Particulars

Plain concrete cylinders of size 6" x 12" were used. Normal strength concrete (6000 psi) was used. Wet lay-up technique was used to install the carbon fiber-weaved fabrics onto the concrete surface. Altogether nine configurations were designed. The first four configurations consisted of unidirectional fiber wraps of one to four plies respectively. These wraps contained fibers in the hoop direction only. The fifth configuration consisted of an inner vertical fiber wrap and an outer horizontal fiber wrap. The sixth configuration added one more horizontal fiber wrap as the inner most layer on the fifth configuration. The seventh and eighth configurations consisted of angular fiber wraps of one and two plies respectively. The final configuration added an inner vertical fiber wrap and an outer horizontal fiber wrap to the seventh configuration. No pretensioning was applied to the fabrics during installation. Overlap on a given layer was approximately 25% of the circumference. Additional plies started 90 degree from the end of the overlap region. All layers were wrapped in the same direction to ensure that the underlying material stayed tightly wrapped. No other consolidation mechanism was used.

Load control mechanism was used. Dials were used to measure both axial and radial deformation. Dial indicator data was collected at 25kN increments without stopping the increase in load. Strain gages were also used to measure local axial, lateral, and angular strains. They were placed on the FRP surface regardless of the fiber directions.

Findings and Conclusions

It was found out that confinement strength was the greatest when all fibers were oriented in the hoop direction. However, it cautioned the reader that one should not immediately

draw a conclusion that only hoop reinforcement was essential. It was pointed out that the overall goal of a composite jacket was to not only increase the load-carrying capacity, but also increase the ductility of the structural element so as to prevent catastrophic failure. Optimization of the overall FRP architecture was considered essential.

Comparing Configuration 2 and 5, the strength increase of Configuration 5, having an inner layer of vertical fibers and an outer layer of hoop fibers, was not as high. However, it did change the failure mode to less catastrophic. The specimens did not fail through pure fiber fracture along the circumferential direction.

When fibers were aligned in the 45-degree direction, which was along the shear plane, the worst results in terms of strength were obtained. They argued that the individual roving tended to slip along those planes, as the specimens were loaded, using energy in movement in those directions. However, those jackets did not show extensive damage at the global level after failure. Rather, the damage occurred in the form of mis-orientation of fabrics from the original positions.

It was concluded that the jacketed systems with jackets containing hoop plies were stiffer than those that contained no hoop plies. The values for structural stiffness were determined from the initial linear portion of the stress-strain profiles obtained on testing each of the specimens. Altogether, three failure modes were encountered. First, the resin in the overlap areas failed in shear. Concrete core, to a large extent, became rubble, and could no longer support load. Second, the concrete crumbled and deformed. Fragments of the constrained concrete pushed into the wrap and locally increased the stress level. The fibers broke and transferred the load to adjacent areas until final failure. Third, a combination of the first two modes was resulted. Both overlap shear and fiber fracture were noted. Stress-strain curves were bilinear, with the change in slope occurring at about the point where the unconfined concrete exhibited failure. Finally, the study pointed out that the use of a model developed for steel confinement would be of great use in determining optimum fiber architectures for use in FRP jackets.

Comments

In the author's opinion, this study is one of the best in capturing the different failure modes and emphasizing the essence of optimal composite system designs, instead of just emphasizing the amount of strength increase over the unconfined concrete counterpart. Although the work was preliminary (without trying to evaluate the effect of rearranging the stack-up sequence of plies with the same materials or changing incrementally the fiber angles), and the measurement method of data was doubtful (using strain gages in directions not aligning to the fiber directions), the ductility issue of the overall composite system was closely paid attention to. It should be pointed out that future researches should include explicitly this issue, without sacrificing the confinement strength and analytical model development. Moreover, it should be noted that the use of the steel model in determining the optimal fiber architecture might prove fatal because of the differences in fundamental material properties of steel and FRP. However, an analytical model that is capable of capturing the stress-strain behavior as well as predicting the ultimate load should be established as soon as possible for design purposes. Finally, the overlap area of 25% was quite substantial. However, the study seemed to have overlooked any effect due to this overlap when odd number of plies were used, giving rise to a substantial unbalance of stress distributed around the circumference.

3.2.6 Picher, Rochette and Labossiere (1996, Universite de Sherbrooke, Canada)

Objective

This study focused on the effect of fiber orientation and the stiffness of carbon fiber confined cylinders. It also studied the effect of rounding corners with various radii of square and rectangular columns. Finally, it tried to verify some mathematical models used to predict the behavior of concrete under multi-axial loads.

Experimental Particulars

Normal strength concrete (40 MPa) wrapped with carbon fibers with cylinder size 6" x 12" was used. Carbon fiber sheets were placed with unidirectional fibers and were

wrapped in a continuously manner. Wet lay-up method was used. Fiber orientation ranged from 0° to 18° in 6° increments. All specimens were loaded in uniaxial compression until failure with a constant strain rate of 10 με/sec. (0.072 in./min.) to allow a quasi-static loading. Axial and lateral strains of cylinders were measured with LVDT devices. Both axial and lateral strain curves were generated.

Findings and Conclusions

Only finding concerning circular cylinders will be discussed here. It was found out that although the curves indicated an increase of ductile behavior, failure of confined concrete cylinders occurred without much apparent warning. Failure was usually caused by a sudden breakage of the composite wrap due to the fragile behavior of carbon fiber wraps. When the confinement failed, the concrete core was unable to withstand the load. Breakage of the confinement thus triggered a fatal failure mechanism. Confined concrete was found to have disintegrated in about one third of the total volume. Delamination between adjacent layers could also be observed. Epoxy adhesion remained effective up to rupture.

Orientation of the confining laminate was a dominant parameter in the failure process. Composite failure was caused by a biaxial loading condition in which radial tensile strains were always lower than axial compressive strains. Ultimate radial strains were lower for confinement configurations with fibers oriented with a larger angle.

It was concluded that although axial stiffness decreases with an increase of angle orientation, ductility (slope of the second portion of the stress-strain curve) remained essentially constant. No improvement in failure mode by varying the orientation of the confinement was observed over the range of fiber orientation, but ultimate strength decreases with the increase in fiber angle with the horizontal plane.

Comments

This investigation has provided more insights on the effect of fiber orientation to the failure modes and ultimate strength. It is found that for angle orientation up to 18 degree from the horizontal would not change the failure mode and they concluded that various fiber orientation does not contribute to any change in failure mode. However, from the study of Howie and Karbhari discussed earlier, failure mode changed remarkably from very brittle to very ductile when the fibers were placed in the 45-degree plane. Therefore, this study may be inconclusive towards the effect of fiber orientation, which should be considered in the design of optimal wrap configuration. Also, since brittle failure was reported for all specimens, a mechanism that could possibly alter the nature of failure mode should be identified.

3.2.7 Mirmiran and Shahawy (1996, 1997, 1998, University of Central Florida)

Objective

The objective of this program was to investigate the performance of the concrete-filled hollow FRP composite column as well as to compare different analytical models with the experimental results. It mainly aimed at providing an alternative to the composite construction of columns and bridge piers. It also addressed the different in behaviors of concrete when confined with elasto-plastic materials such as steel and linearly elastic materials such as FRP.

Experimental Particulars

Normal strength concrete (30 MPa) cylinders of size 6" x 12" were tested under uniaxial compression. FRP tubes consisted of a filament-wound angle ply of polyester resin with unidirectional E-glass fibers at $\pm 15^{\circ}$ winding angle. The FRP shells were preformed and procured with ply numbers of 6, 10 and 14 respectively. In some specimens, stiffening ribs could also be found in the inner surface of the shell so as to increase the bonding between the FRP shell and the confined concrete.

A groove was cut on both ends on the jacket to prevent direct axial interaction of the jacket and the encased concrete. Lateral strains were measured by two 2.36" strain gages placed circumferentially regardless of the inclined fibers. Axial strains were measured by three LVDTs placed at 120° apart around the specimen. Specimens were loaded under displacement control with a constant rate of 0.22 in./min.

Findings and Conclusions

Failure of the hybrid specimens was marked by fiber fracture at the mid-height failure zone. Localized failure near top and bottom ends was reported not due to the friction between the steel platens and concrete end surfaces. Cracking noise was detected during loading. Snapping of the inner composite layer could be heard. White patches also appeared at about 60 – 70 % of ultimate load. Shear failure was the primary mode of failure. Specimens typically remained intact after failure. Bilinear stress-strain behaviors were noted. Dilation rate concept was introduced. A comparison of test data with existing confinement models indicated a gross overestimation of ultimate strength. The discrepancy was believed to be due to the inability of the models in estimating the dilatancy of FRP confined concrete. They therefore concluded that the use of available confinement models that were calibrated for steel might prove detrimental in the design of fiber-rapped or FRP-encased concrete columns.

Comments

This study has proven the overestimation of existing models and the need of a new model that can predict accurately the strength of FRP confined concrete. However, the author doubted the use of strain gages, not aligning with the fiber direction, although the strain gages were quite large, aiming to maximize the capturing ability of global measurement. Also, this study did not explain the originality and advantage of using the high and seemingly non-correlated number of plies for the FRP shells. There is, in fact, no way to relate the thickness effect with the ultimate strength when one would like to make use of the results and develop another analytical model. Finally, the loading rate of 0.22 in/min. was relatively fast comparing to the ASTM standard of 0.05 in./min. and those used by

most other researchers. Therefore, the strength produced from their experiments was likely to be higher than they should be in the real situation, where static loading dominates. And hence, the database established may prove to be at the edge of disadvantage when they are used for any theoretical development.

3.2.8 Miyauchi, Inoue, Kuroda, and Kobayashi (1999, Kagawa Polytechnic College, Tottori University, and Nippon Steel Composite Co. Ltd, Japan)

Objective

The primary goal of this study was to investigate the response of FRP confined high strength and normal strength concrete. Only the findings of those related to normal strength concrete will be reported. It was also aimed to establish the stress-strain relationship for the FRP confined concrete.

Experimental Particulars

Carbon fiber sheets with fibers running in the hoop direction were used. Wet lay-up method was utilized. Cylinder sizes were 6" x 12" and 4" x 8". Lap length was 2.4" for outer layer and 1.57" for inner layers. The laps were carefully located at 180° apart around the circumference in the case of 2 layers, and 120° apart in the case of 3 layers. Uniaxial compression with a displacement control mechanism was used. The displacement rate was not reported. Axial strains were measured by two strain gages on each specimen.

Findings and Conclusions

All cylinders failed by fiber tensile fracture at mid-height, independent of dimensions of specimens, unconfined concrete strength, and number of fiber sheets. Both compressive strength and ductility of confined concrete were enhanced. Rigidity did not change much up to an axial stress of 60% of the ultimate strength of unconfined concrete.

Two major types of stress-strain curves were captured. The first type was referred to the increasing type, which showed a bilinear increasing behavior. The second type was referred to the decreasing type, which showed an increasing then decreasing behavior. The ultimate state for the increasing type was defined to be coincident with the maximum stress sate while that of the decreasing type was defined as the state that the axial stress fell back to the stress level equal to the compressive strength of the unconfined concrete. Not much description was made towards failure modes. However, analytical models were developed for both types of curves.

Comments

This study is considered an important contribution because it has identified a stress-strain curve type that is not bilinear in nature, which is most commonly reported by all other researchers. It also gives more insights on the confinement mechanism of FRP that the bilinear behavior is not necessary. The response of FRP confinement clearly shows more complexity than one might have expected. To the author's opinion, analytical model development should not be performed unless the behavior of the hybrid structure is fully captured. The overlap length and location was also paid close attention to so that a balance load condition was achieved. However, the use of strain gages in the vertical direction with the fibers running in the horizontal direction may have produced some faulty results due to the transverse sensitivity error of strain gages. This is definitely a topic for further research. Finally, the study failed to obtain information regarding the lateral strain response of the wrapped cylinders.

3.3 Theoretical Work Development – Analytical Models of Confinement

Over the past twenty years, a few models were developed for FRP confined concrete. No one model can be applied directly for design with confidence. Moreover, all models for the prediction of ultimate strength of the hybrid column are developed based on the first confinement model that is developed by Richart et al. in 1927. The only changes were the difference in constant coefficient and the power coefficient corresponding to the

confining pressure. They are all developed from regression analysis of the researchers' experimental data. A few stress-strain relationships were also developed so as to model the load-deformation behavior of the confined concrete. These models mainly relied on previously developed models for concrete or soil behaviors under triaxial stresses or confinement stresses. Subsequent modifications were made to fit in the use of FRP confinement.

Most strength prediction models can roughly predict the strength, although they are mostly overestimating the true strength. But the corresponding ultimate strain predictions were mostly poor. Substantial underestimations exist. Also, the stress-strain curves developed from a particular set of experiment do not generally agree with those in other researches.

Finally, it should be pointed out that all these models are only valid, if accurate, for the use of FRP encased concrete construction method, but not for retrofitting or strengthening of concrete. The reason is that from the preceding experiments, FRP were used to wrap on sound concrete instead of cracked concrete, which can have a very different behavior upon initial loading. The FRP materials were also wrapped on initially unstressed concrete specimens. When the specimens were prepared and loaded, both concrete and FRP were stressed together from scratch. In reality, for the case of strengthening or retrofitting, concrete columns are already under stress. The FRP is used to wrap around stressed columns afterwards. The strength increase by FRP confinement may or may not be the as much as predicted because the Poisson's ratio of damaged concrete is much larger than that of concrete stressed in the elastic region, hence activating the FRP confinement much earlier than one might expect due to substantial radial dilation. Plastic zone of concrete is entered not long after additional loading after wrap. Ultimate strain will definitely be different in this case. Nevertheless, some of the major models are discussed below for review purposes.

3.3.1 Fardis and Khalili (1982, Massachusetts Institute of Technology)

Fardis and Khalili were the first who developed an approximation in 1982 at MIT particularly for FRP confined concrete. They made reference to the original equations developed by Richart et al. and Newman and Newman back in 1928 and 1969 respectively for spirally reinforced concrete. Those equations are presented as follow.

Richart et al. (1928)

$$f_{cc}^{'} = f_{co}^{'} + 4.1 f_{radial}$$

$$\varepsilon_{cc} = \varepsilon_{co} \left(1 + 20.5 \frac{f_{radial}}{f_{co}^{'}} \right)$$

where $f_{cc}^{'}$ is the peak confined compressive strength, $f_{co}^{'}$ is the unconfined concrete strength, f_{radial} is the radial confining pressure on the concrete core, ε_{cc} is the peak confined axial strain, and ε_{co} is the unconfined peak concrete axial strain.

Newman and Newman (1969)

$$f_{cc}^{'} = f_{co}^{'} + 3.7 f_{radial}^{0.86}$$

From basic structural mechanics, Fardis and Khalili modified these equations for the specific use of fiberglass-reinforced plastic confined concrete through the use of the following equation of cylindrical shell structures subjected to uniform internal pressure. When thickness of the shell is infinitesimally small when compared with the overall dimension, an approximation can be made.

From mechanics of shells

$$f_{radial} = \frac{f_{FRP} \cdot t_{FRP}}{R - t_{FRP}} \approx \frac{f_{FRP} \cdot t_{FRP}}{R}$$

where f_{FRP} is the tensile strength of the FRP jacket with thickness t_{FRP} and a concrete core of radius R.

Therefore, from Richart et al:

$$f'_{cc} = f'_{co} + 4.1 f'_{co} \left(\frac{f_{FRP} \cdot t_{FRP}}{R \cdot f'_{co}} \right)$$

From Newman and Newman:

$$f'_{cc} = f'_{co} + 3.7 f'_{co} \left(\frac{f_{FRP} \cdot t_{FRP}}{R \cdot f'_{co}} \right)^{0.86}$$

And the corresponding ultimate strain

$$\varepsilon_{cc} = 0.002 + 0.0005 \left(\frac{E_{FRP} \cdot t_{FRP}}{R \cdot f'_{co}} \right)$$

where E_{FRP} is the elastic tensile modulus of the FRP jacket.

Nanni and Bradford (1995) described the above model as "sufficiently accurate for prediction of strength, but grossly underestimated ultimate strain of concrete confined with FRP materials" when comparing with his own experimental data sets as described earlier.

3.3.2 Mander, Priestley and Park (1988, State University of New York at Buffalo, University of California, San Diego, University of Canterbury)

For a confined concrete under triaxial compression with equal lateral effective confining stresses from steel spirals or circular hoops around the circumference, the unified stress-strain model was developed. For an approximate purpose, the equation can be modified by the above mechanics equation so that it can be applied to FRP confinement. In fact, in the industry, this modified equation is currently used for design with various composite

systems. Major companies such as Fyfe Co. LLC has been adopting this equation for years.

$$f'_{cc} = f'_{co}\left(-1.254 + 2.254\sqrt{1 + \frac{7.94\, f'_{radial}}{f'_{co}}} - 2\frac{f'_{radial}}{f'_{co}}\right)$$

Based on an equation suggested by Popovics (1973), they used the following to determine the axial strain in the confined concrete.

$$\varepsilon_{cc} = \varepsilon_{co}\left(1 + 5\left(\frac{f'_{cc}}{f'_{co}} - 1\right)\right)$$

The stress-strain relationship is suggested as follow.

$$f_c = \frac{f'_{cc}\,xr}{r - 1 + x^r}$$

where

$$x = \frac{\varepsilon_c}{\varepsilon_{cc}}$$

$$r = \frac{E_c}{E_c - E_{sec}}$$

$$E_{sec} = \frac{f'_{cc}}{\varepsilon_{cc}}$$

$$E_c = 60.21\sqrt{1000 \cdot f'_{co}} \quad \text{(ksi)}$$

and f_c is the confined concrete axial stress, and ε_c is the confined concrete axial strain.

3.3.3 Cusson and Paultre (1995, University of Sherbrooke, Canada)

Based on a regression analysis of their existing data sets, Cusson and Paultre determined their expression of ultimate strength for confined concrete. When modified with the mechanics equation of shell derived above, the following equation is obtained. One

should note that the original Cusson and Paultre model was derived for high strength concrete instead of normal strength concrete.

$$f_{cc}^{'} = f_{co}^{'} + 2.1 f_{co}^{'} \left(\frac{f_{FRP} \cdot t_{FRP}}{R \cdot f_{co}^{'}} \right)^{0.7}$$

$$\varepsilon_{cc} = \varepsilon_{co} + 0.21 \left(\frac{f_{FRP} \cdot t_{FRP}}{R \cdot f_{co}^{'}} \right)^{1.7}$$

Since high strength concrete does not exhibit the same level of ductility that normal strength concrete possesses, any attempt to compare the models with experimental data should not be applied to normal strength concrete without further investigation.

3.3.4 Karbhari and Gao (1997, University of California, San Diego)

In an attempt to encourage the use of simple design formula, two sets of equations were proposed. The first set was based on the development of a simplistic composite solution set forth by their earlier co-workers. The second set was a modification of the original form suggested by Richart et al. in 1928.

First Model

The first equation assumes a simple bilinear behavior of the FRP confined concrete under uniaxial compression. The end point A of the first slope is described by the following, assuming an overall elastic response of the system until that point and compatibility of FRP and concrete at the bond interface.

$$f_A = f_{co}^{'} + 4.1 f_{co}^{'} v_c \left(\frac{E_{FRP} \cdot t_{FRP}}{R \cdot E_c} \right)$$

where v_c is the concrete Poisson's ratio, and E_c is the tangent modulus of concrete.

The second slope is then described by a stress increment due solely to the confining action of the FRP material. The stress increment, f''_{radial}, is defined as the difference between the ultimate confining pressure and the level of stress at which confining stress starts when concrete damage has achieved.

Therefore,

$$f''_{radial} = \frac{f_{FRP} \cdot t_{FRP}}{R} - f'_{co} v_c \frac{t_{FRP}}{R} \frac{E_{FRP}}{E_c}$$

And since

$$f'_{cc} = f_A + f''_{radial}$$

The stress at failure can be determined as

$$f'_{cc} = f'_{co} + \frac{f_{FRP} \cdot t_{FRP}}{R} + 3.1 f'_{co} v_c \frac{t_{FRP}}{R} \frac{E_{FRP}}{E_c}$$

Second Model

The second model that was modified from the empirical formula is shown as follow. It has the form very similar to the preceding models although the coefficients are different.

$$f'_{cc} = f'_{co} + 2.1 f'_{co} \left(\frac{f_{FRP} \cdot t_{FRP}}{R \cdot f'_{co}} \right)^{0.87}$$

The ultimate strain, however, was argued to be directly dependent on the strength of the composite, rather than indirectly related to the effective confining pressure. When considering the response as a function of increasing confining pressure, one would find that the nonlinear portion of the confined concrete curve is actually unaffected by the modulus of the wrap, but is controlled by the confining pressure developed in the FRP jacket. Therefore, the following parameters were used as the formulation but not using the FRP jacket modulus.

$$\varepsilon_{cc} = \varepsilon_{co} + 0.01\left(\frac{f_{FRP} \cdot t_{FRP}}{R \cdot f_{co}^{'}}\right)$$

3.3.5 Samaan, Mirmiran and Shahawy (1998, University of Central Florida)

The model was derived based on the empirical form similar to that of Newman and Newman (1969) and was generated from their own sets of experimental data. It assumed a bilinear behavior. When compared to other data sets, it appeared to be quite accurate in terms of ultimate compressive strength estimation. Most test results fell within a ±10% margin of error. The model is presented below.

$$f_{cc}^{'} = f_{co}^{'} + 3.38\left(\frac{f_{FRP} \cdot t_{FRP}}{R}\right)^{0.7}$$

The ultimate strain was determined solely from the geometry of the bilinear stress-strain curve. Defining the kink point as A and slope of the second linear slope as E_2, the following is resulted.

$$\varepsilon_{cc} = \frac{f_{cc}^{'} - f_A}{E_2}$$

where $f_A = 0.872 f_{co}^{'} + 0.371 f_{radial} + 0.908$

$E_2 = 52.411(f_{co}^{'})^{0.2} + 2.6912 (E_{FRP}\ t_{FRP} / R)$

From these relationships, a stress-strain model was obtained. The model was based on the four-parameter relationship suggested by Richard and Abbott in 1975 that was augmented from an original soil behavior stress-strain equation. The model is shown in the following.

$$f_c = \frac{(E_1 - E_2)\varepsilon_c}{\left[1 + \left(\frac{(E_1 - E_2)\varepsilon_c}{f_A}\right)^n\right]^{1/n}} + E_2\,\varepsilon_c$$

where $E_1 = 47.586\,(f'_{co})^{1/2}$ and the other parameters were defined above.

3.3.6 Miyauchi, Inoue, Kuroda, and Kobayashi (1999, Kagawa Polytechnic College, Tottori University, and Nippon Steel Composite Co. Ltd)

Most recently, the Japanese researchers cooperated with the industry and developed a stress-strain relationship for concrete confined by carbon fiber sheets. As said earlier in 3.2.8, they classified the curves into the increasing type and the decreasing type. Stress-strain relations for both types were proposed. The ultimate compression capacity is modeled as the same empirical form but with a different coefficient. A linear relationship is assumed.

$$f'_{cc} = f'_{co} + 2.98\,f'_{co}\left(\frac{f_{FRP} \cdot t_{FRP}}{R \cdot f'_{co}}\right)$$

The ultimate strain is modeled as a nonlinear function as follow.

$$\varepsilon_{cc} = \varepsilon_{co} + \varepsilon_{co}(15.87 - 0.093\,f'_{co})\left(\frac{f_{FRP} \cdot t_{FRP}}{R \cdot f'_{co}}\right)^{(0.246 + 0.0064\,f'_{co})}$$

Increasing Type

For the increasing type, the stress-strain relationship consists of a parabola and a straight line that is tangent to the parabola. The point where these two lines meet is defined as point A.

For $0 \le \varepsilon_c \le \varepsilon_A$

$$f_c = f'_{co}\left(2\left(\frac{\varepsilon_c}{\varepsilon_{co}}\right) - \left(\frac{\varepsilon_c}{\varepsilon_{co}}\right)^2 \right)$$

For $\varepsilon_A \le \varepsilon_c \le \varepsilon_{cc}$

$$f_c = f_{cc} - \lambda (\varepsilon_{cc} - \varepsilon_c)$$

where

$$\lambda = \frac{\left\{ -2f'_{co}(\varepsilon_{cc} - \varepsilon_{co}) + \sqrt{4f_{co}\left(f'_{co}\varepsilon_{cc}^2 - 2f'_{co}\varepsilon_{co}\varepsilon_{cc} + f_{cc}\varepsilon_{co}^2\right)} \right\}}{\varepsilon_{co}^2}$$

$$\varepsilon_A = \varepsilon_{co} - \frac{\lambda\, \varepsilon_{co}^2}{2\, f'_{co}}$$

$$f_A = f'_{co}\left(2\left(\frac{\varepsilon_A}{\varepsilon_{co}}\right) - \left(\frac{\varepsilon_A}{\varepsilon_{co}}\right)^2 \right)$$

Decreasing Type

For the decreasing type, a parabola and a straight line representing the falling branch was proposed.

For $0 \le \varepsilon_c \le \varepsilon_A$

$$f_c = f'_{cc}\left(2\left(\frac{\varepsilon_c}{\varepsilon_{co}}\right) - \left(\frac{\varepsilon_c}{\varepsilon_{co}}\right)^2 \right)$$

For $\varepsilon_A \le \varepsilon_c \le \varepsilon_{cc}$

$$f_c = f'_{cc} + \frac{(\varepsilon_c - \varepsilon_{co})(f_{cc} - f'_{co})}{\varepsilon_{cc} - \varepsilon_{co}}$$

3.4 Summary of Limitations of the Preceding Research

Despite the fact that FRP confined columns outperform unconfined concrete columns in terms of strength and ductility and that this topic has been under investigation for almost two decades, there are some inherent limitations of the past research. There is, in fact, much room for improvements and advancement in this field of research before the concept can really be applied in field with confidence. The limitations are categorized into three areas – manufacturing, experimental and theoretical.

3.4.1 Manufacturing

1. Very little data exist comparing the performance of different manufacturing methods such as fiber winding, wet lay-up, resin infusion, and preformed shells.
2. Advantageous effects of combined use of different types of fibers such as carbon and glass in maximizing overall performance, including strength and failure modes, were suggested but not extensively discussed.
3. Use of 45-degree angular fibers was suggested to change the failure mode from brittle to ductile, but no further investigation could be found in maximizing the use of such fabrics.
4. Investigation of the effects of fiber directions was not inclusive enough. Fibers were only oriented up to 18-degree and a conclusion that fiber orientation did not affect the failure mode was drawn.
5. In some cases, large number of plies was used without reporting the rationale. Larger the number of plies may mean a more catastrophic failure mode due to the large energy stored in the system before a sudden release.
6. Effects of initial imperfections such as air pockets and fabric wrinkling were entirely not studied.

3.4.2 Experimental

1. Cylinder sizes of 3" x 6" and 4" x 8" were considered too small for FRP confinement investigations. Local effects, overlapping joint effects cannot be fully captured.

2. Overlap effects such as unbalance stresses or any possible strengthening were not discussed. Overlap lengths and locations were mostly not reported.
3. Failure modes were sometimes not reported, though most failed in brittle mode upon fiber fracture in the jacket.
4. Lateral deformations were not measured in a significant portion in those studies.
5. Strain gage types and sizes were not reported.
6. Effects of strain gage orientation were not investigated. Possible errors of measurement existed when strain gages were not aligned with fiber directions due to transverse sensitivity error of strain gages (Tuttle, 1989). Shearing instead of direct tension is applied to the strain gage if the strain gage and the fiber orientation do not align with each other.
7. Loading rate effect was not studied. In general, the faster the loading rate, the higher the strength of the specimens under compression. Therefore, for any meaningful comparison and model development, the loading rate should be unified.
8. Due to the untraditionally large strains encountered, actual strains instead of engineering strains should be used when converting the experimental data of radial dilation. Significant difference may result.
9. Only short-term loading was studied. Sustained load and axially cyclic load behaviors were not addressed.

3.4.3 Theoretical

1. The concept of constructing new FRP encased concrete, FRP strengthening of stressed but sound concrete, and FRP retrofitting of cracked concrete, was not clearly distinguished. While some models were developed for newly constructed FRP encased concrete, some others developed in the same way but suggested their experimental approaches were developed for strengthening or retrofitting of concrete via the use of FRP confinement.
2. Strength prediction models overestimate the load capacity of FRP confined concrete while strain prediction models severely underestimate the corresponding ultimate strains.

3. Shapes of most stress-strain curves developed do not match with experimental results.
4. The difference between constant active confining pressure and varying passive confining pressure was not addressed. One should note that the development of Richart's model was founded on constant active confining pressure while the development of models for FRP confinement should be founded on varying passive confining pressure. Therefore, the linear relationship may not be applied.
5. Definition of sufficient confinement is not clear, especially when concrete does not become rubble within the FRP confinement but a bilinear increasing curve was obtained.
6. Only one study has indicated the two possible types of stress-strain curves for different level of confinement and developed subsequent stress-strain models. Others seemed to have overlooked the increasing-decreasing type of curve, but only focused on the bilinear increasing type of curve.
7. A parameter that can define a term for meaning comparison of strength increase is lacking. Strength increases reported in all studies have lost the true meaning when not correlated with the degree of confinement.

3.5 Needs for Further Investigation & New Directions

From the discussion in 3.4, the field of FRP confined concrete behavior is apparently immature for real world applications. Discrepancies in model predictions of failure stress and strains speak for themselves. Fundamental behaviors of FRP confined concrete are also not extensively understood. Instrumentation methods were not unified. In view of so many deficiencies and potential areas, a systematic research study is urgently in need.

In the author's opinion, instrumentation method is one of the foremost issues that should first be dealt with. Once the data acquired from the experiments are faulty, it is futile to work diligently on the modeling aspect. The effects of misalignment of strain gage and fibers should be quantified and assessed. The accuracy and appropriateness of strain

gages with different sizes, aspect ratios, gage materials, and resistances should be investigated.

Local effects such as overlap joint effects, bond length and location, interlaminate shear when using different types of fabrics with different fiber directions, and fiber behaviors such as buckling and fracture should be studied. Manufacturing effects such as utilizing different types of confinement techniques, different types of fiber materials, initial imperfections like air pockets and wrinkling should be examined. Finally, failure modes, load-deformation behaviors and ultimate stress and strains of various kinds of wrap configurations should be compared, assessed, and quantify. The most favorable failure mode should then be studied in depth to try and come up with a better FRP stack-up. A simple finite element modeling can be done to see if it is possible to model the orthotrophic properties of the FRP materials. Analytical models can then be proposed for the case of FRP encasement.

After all these initial studies, the focus should move to the more realistic loading and confinement conditions for retrofitting and strengthening. When studying the strengthening behaviors, the concrete should first be loaded to a practical level and then the FRP confinement is applied. For instance, for the strengthening case, concrete can first be loaded up to about 60% of the ultimate load while keeping the specimens sound and undamaged. Stress-strain curves will then be compared with those developed for new construction of FRP encasement while all other parameters remain constant. Analytical models can then be developed particularly for these applications. It should be reminded that the model developed for FRP encasement construction method should not be blindly applied to these two other applications.

After all these studies of fundamental behaviors of static cases, dynamic cases such as axially loaded cyclic behavior, which is common in bridge piers or structural elements in machine rooms, should be investigated.

Despite the many areas that can be done to further improve the state-of-the-art, the present investigation focuses on the study of instrumentation and fundamental behaviors of FRP-confined concrete under static concentric compression load. Owing to the limitations of time and resources, it is impossible to do many variations on each study parameter to determine the best use of instrumentation devices and composite materials. However, the appropriate installation procedure and usage of strain gages on composite surfaces should be identified. Such findings are expected to benefit the research community for future research in similar areas. Fundamental load effects, local effects, and manufacturing effects stated above should be observed, discussed, and interpreted. The observed behaviors will be applied to analytical model conceptual refinements as well as practical design issues. The results are expected to impact the industry with fundamental concepts, in terms of structural behaviors and safety issues, in a way that changes in conventional FRP retrofit practices may be required. Studies involving realistic loading and confinement conditions as well as the other types of loading such as static bending, axial cyclic and lateral cyclic loadings are not within the scope of the current research work.

CHAPTER 4

EXPERIMENTAL INVESTIGATIONS

4.1 Objective

The objective is to investigate four main areas regarding FRP confined normal strength concrete cylinders subjected to monotonic concentric axial load. These four areas are categorized as (1) strain gage instrumentation issues, (2) loading effects, (3) local effects, and (4) manufacturing effects. All studies conducted in each of the four areas are summarized below.

Strain Gage Instrumentation Issues

(1) Surface preparation for proper installation and measurement

(2) Performance of various gage types

(3) Fiber-gage misalignment

Loading Effects

(1) Ultimate stress and strains

(2) Time to failure

(3) Failure modes

(4) Load-deformation behaviors

(5) Stress-strain curve shape categorization

Local Effects

(1) Overlap strengthening phenomenon

(2) Bond delamination

(3) Interlaminate shearing between different types of fabrics

(4) Roles of hoop, angular and vertical fibers

(5) Fiber buckling, fracture, and reorientation

(6) Local conditions of confined and unconfined ends

Manufacturing Effects

(1) Initial imperfections such as air pockets

(2) Overlap length and location

(3) Epoxy bond thickness and quality

(4) Fabric stacking sequence

The rest of this chapter is organized into ten major parts. Following the scope and an overview of the experimental program, construction materials, specimen details, preparation methods and procedures, instrumentation techniques, and loading information will be discussed fully. Test results will then be presented following by a master summary and an in-depth interpretation and discussion section. Finally, a model that has taken the fiber orientation parameter into formulation will be proposed to predict the ultimate strength and strain of FRP confined normal strength concrete under monotonic concentric axial loading.

4.2 Scope

There are a total of six FRP confinement configurations. They are made up with three different types of fiber sheets using different stack combinations. All fiber sheets are made with identical E-glass fibers. The first type of fiber sheet is made of unidirectional fiber roving; the second type bi-directional weaved fibers in the vertical and horizontal directions; and the third type 45-degree angular weaved fibers. Each confinement configuration is designed with one or more specific aim(s). These aims are coherent with the objectives presented earlier in Section 4.1. Different configurations are often used to make direct comparisons with one another. All the confinement configurations will now be described with their corresponding design aims and rationales elaborated. A tabulated summary will be presented at the end of this section in Table 4.1.

Configurations One thru Three

Configurations One through Three consist of cylinders wrapped with only one ply of unidirectional fibers, bi-directional fibers, and angular fibers respectively. These three test cases are the most basic. Seven main areas are targeted.

First, fundamental information such as ultimate strengths and strains and load-deformation behaviors are to be determined. Those values can act as benchmarks for the later test cases with different ply combinations.

Second, the overlap effect can be studied due to the unbalanced stress distribution condition around the circumference.

Third, local fiber behaviors such as buckling and fracture can be identified, if any, in these basic modes. The role of fibers in different orientations can also be identified in Configurations Two and Three because fibers are placed in three different directions in these two cases.

Forth, local end conditions are to be observed. As an initial thought, to prevent fabrics from being directly loaded axially, all cylinders are wrapped from the bottom to slightly below the top end surface. As a result, a slight portion near the top end is unconfined while a full confinement is attained at the bottom. Comparison of the two end conditions can give more insights to the material behavior near the loading platens. It may have direct implications to the wrapping technique in a full size column that whether a gap of unconfined concrete should be left near the slabs or an anchor extending from the column confinement to the slabs is required for continuity.

Fifth, comparisons between the Second and Third configurations can be made with respect to failure modes and ultimate capacities since the tensile strength of these two confinement systems are very similar, although the fiber orientations are different.

Last but not least, the three tasks under "Strain gages instrumentation issues" listed in Section 4.1 are to be carried out for determining the proper strain gage usage. The results

can be directly applied to all subsequent tests. All test cases and details about this study area should be referred to Section 4.6.3.

Finally, some thumb-size air pockets are purposely entrapped into the fabrics of selected specimens before the FRP confinements are fully cured and hardened. Phenomenal changes, failure mechanisms and load carrying capacity are compared with other cylinders without such air pockets.

Configuration Four

Configuration Four consists of one ply of bi-directional fibers being wrapped around by one ply of angular fibers. It should first be reminded that the two materials have similar tensile strengths. Fiber content of the angular wrap is much higher than that of the bi-directional wrap so as to bring the tensile strength level up to about the same. Since the strength is similar, it is useful to compare several properties of this configuration with those in Configurations Two and Three. Four main goals are sought in this configuration design.

First, the linearity of ultimate strength increase over unconfined specimens can be verified by the addition of respective increases of Configuration Two and Three. This is one of the test objectives because the initial curvature of the cylinder surface and the different fabric types may give unexpected interactions so that the linearity law in the Classic Laminate Theory may not hold.

Second, failure modes can be compared among Configurations Two, Three, and Four. Now that the two wraps are combined, it would be useful to see which fiber sheet is more dominating in the resulting failure mode. The domination can then be correlated with the ultimate strengths of the two single ply cases, if any discrepancy in strength is found. This study may lead to the wrap configuration optimization in terms of failure mode and efficient use of materials.

Third, interlaminate shearing behaviors, due to the differential movements of the plies, such as epoxy bond deterioration and delamination between two different fiber-types can be observed.

Finally, local fiber buckling and fracture behaviors can be compared to the two single-ply cases. This can be observed and interpreted in parallel with the corresponding failure modes.

Configurations Five and Six

Configuration Five consists of an inner ply of unidirectional fibers and an outer ply of angular fibers. Configuration Six uses the same materials as Configuration Five but has a reversed stacking order. These two test cases are designed mainly to investigate the failure modes, effects of stacking sequence, and interactions between the two FRP fabrics. The secondary objective is to make comparisons with other cases in terms of the effects of having different inner layers but an identical outer confinement layer. Each of the goals is elaborated one by one.

First, the aim of designing Configuration Five is to improve the failure behavior while retaining the confinement strength. The logic is based on the good confinement strength of unidirectional fiber wraps and ductility enhancement of angular fiber wraps. As an initial thought, it is reasonable to assume that the superposition effect can be applied such that when the two fabrics are added up, both the confinement strengths and failure modes of the two individual plies can be superimposed. The fiber interaction mechanics is however complex because the fibers are running in different orientations in their respective plies. Interlaminate shearing and fiber fracture may be initiated through a different mechanism from the individual-ply cases.

Therefore, the second aim is to investigate the stack-up sequence effects on failure loads and failure modes, giving the motivation to design Configuration Six. By the use of same materials but a different stacking sequence, new insights may be obtained upon a different failure mode and strength. These important information include the validity of

the linearity law for strength estimation of multi-ply situations, failure modes and their corresponding mechanisms, load-deformation behaviors, fiber fracture initiations, origin and effects on neighboring plies, and laminate shearing and peeling effects. If, however, there is not much discrepancy in terms of load carrying capacity and failure modes between these two Configurations, it can be concluded that in designing such FRP confinement systems, the stack up sequence effect can be neglected and strength can simply be added in a linear fashion.

Third, Configuration Five can be compared with Configurations Three and Four in terms of the effect of the inner ply on the overall behaviors of a cylinder with an angular fiber outer-wrap. Strength, strains, local fiber responses, and failure modes can be compared with respect to the benchmarks values and phenomenon in Configuration Three.

Forth and finally, Configuration Six can be compared with Configuration One in a similar way in terms of the responses by adding an inner layer of angular fibers before the wrapping of unidirectional fiber confinement.

Table 4.1 Summary of Test Aims of the Six Wrap Cases

Configurations	Aims of Tests
I, II, III	1. Determine the ultimate strengths and strains, and load-deformation behaviors as benchmarks for subsequent configuration comparisons 2. Study the effects of overlap joint due to the unbalanced stress distribution around the circumference 3. Study the behavior of fibers such as buckling and fracture and the role of fibers in different orientation 4. Differentiate and interpret the cylinder local end responses of confined and unconfined concrete portions 5. Compare failure modes and ultimate capacities under the effects of similar fabric tensile strength but different fiber orientation 6. Determine the proper strain gage usage and apply results to

	subsequent tests 7. Study the effects of initial imperfections, particularly the effects of entrained thumb-size air pockets during the manufacturing process
IV	1. Verify the linearity law of strength increase when using more than one ply of different types of fabric in the confinement shell 2. Determine whether mode domination occurs when using different types of fiber wraps by comparing failure modes with single-ply cases 3. Study bond deterioration and delamination due to the differential movements and interlaminate shearing of different ply materials 4. Compare local fiber effects including buckling and fracture with single-ply cases
V, VI	1. Find out whether failure mode improvement is possible while retaining good confinement strength 2. Investigate the effects of different stack-up sequence using identical amount and type of FRP materials but with a reversed wrapping sequence 3. Compare the difference in strengths and failure modes when using different inner FRP layers but identical angular fiber outer-wrap 4. Compare the difference in strengths and failure modes when using different inner FRP layers but identical unidirectional fiber outer-wrap

Concrete properties are given in 4.4.1. FRP fiber and matrix properties are given in Section 4.4.4. FRP wrap configuration designations for the six systems are designed in a logical and convenient way and are illustrated in Section 4.5.2. Strain gage types and properties are described in Section 4.6.3.

4.3 Experimental Program Overview

This experimental program is focused on studying normal strength concrete cylinders of size 6" x 15", confined in fiber-reinforced plastic sheets and loaded monotonically under axial compression. Altogether six wrap configurations are designed. Three identical cylinders are prepared for each configuration. Each cylinder is wrapped with glass-fiber fabrics using the wet lay-up technique (Fyfe 1999). Unconfined concrete strengths are determined separately from three 6" x 12" and three 6" x 15" specimens respectively. The 15" tall plain concrete cylinders are used to compare with other wrapped cylinders. Three types of strain gages are used in the studies of strain gage usage and performance, as indicated in Section 4.1 and 4.2. LVDT and extensometers are used as independent measurement devices to obtain displacement data in the lateral and axial directions and to compare results with those obtained through strain gage measurements. Except for the study of surface preparation, all the strain gages are installed onto the FRP surfaces using identical techniques (BLH 2000). The LVDT is mounted on a specially made spring support system so that it is capable of capturing the global cylinder dilation at any section up till the ultimate failure point. Axial compression load is made through a displacement control mechanism at a rate of 0.05 in./min. until complete specimen failure. Sign conventions and units used throughout the program are indicated below.

Sign conventions

Since both axial and lateral displacements are measured from the experiments, there is a need to distinguish the two for clarity. Axial shortening is designated as positive. Lateral expansion is designated as negative. These conventions apply to the rest of the chapter including all the stress-strain plots.

Units

The American unit system is used to match with the instrumentation units for convenience. Some readers may find the following conversions useful: (Pressure) 1000 psi (pound/sq. in.) = 6.894 MPa, (Force) 1 kip = 4.448 kN, (Length) 1 inch = 25.4 mm.

Details of the above overview including material selection, specimen information, instrumentation, and loading will be discussed immediately in the following, from

Section 4.4 through 4.7. Experimental results and the corresponding discussions will be starting from Section 4.8 and onwards.

4.4 Material Selection

4.4.1 Concrete

Normal strength concrete was used throughout the program. The concrete was produced from bags of solid form ready-mix, with a mix proportion of 1-2-3 for cement-sand-aggregates. Only water needed be added. The water-cement ratio was set to 0.65 after several trial tests to attain a 28-day compressive strength from 6" x 12" cylinder tests of approximately 4000 psi. No additive was added. Workability was good and no segregation was noted upon compaction. This ready-mix product was chosen over the conventional design mix because concrete itself is not the focus of the study. The only requirements are that the concrete used can perform consistently and that it has a low enough strength to meet with the loading machine capacity.

4.4.2 Capping Material

Top end surface of a vertically cast concrete cylinder is usually not smooth due to hydration during concrete setting. To provide a flat, smooth surface for contact with the steel platens of the loading machine, and to ensure that the top and bottom surfaces of the cylinders are parallel while orthogonal to the loading axis, both ends of the cylinders were capped with high strength gypsum-plaster as stipulated in ASTM C617 - 98. The gypsum used has an ultimate compressive strength of about 10,000 psi, which is much higher than the anticipated maximum compressive strength of all wrapped cylinders. The capping method was, therefore, chosen over the surface grinding method, which would require more tedious work. However, one should use the surface grinding method if the compressive strengths of the specimens exceed the compressive strength of the capping material. Cracks would form within the cap and poor load transfer would be resulted at high load levels in such cases. The thickness of all caps was made as thin as possible to satisfy the maximum average thickness requirement of 1/8" as stipulated in the code. If

the thickness control is done skillfully, the highest irregularity point should show on the capped surface.

4.4.3 Cylinder Molds

Since the non-standard size 6" x 15" cylinders (ASTM C39/C39M – 99) were used, no ready-made molds could be found. A type of disposable cardboard tube was, therefore, chosen due to its abundance and characteristic in making poor concrete surfaces. The interior of the tube was not wax-coated so that the paper adhered slightly to the concrete surface, giving rise to a poor concrete finishing during demolding without sacrificing the strength. The poor finishing was especially desirable in this study because it helped simulate the surfaces of concrete columns that are normally in need of retrofit. Hence, it imposed a challenge to the epoxy bond of the composite systems. Since the cardboard tubes were open in both ends, a reusable wooden base, which comprised of 3 layers of 0.75" solid birch wood, was made for each mold for casting, water stopping and providing a flat concrete surface at the bottom end. The wooden bases fit very well into the tubes and were found to be very effective in preventing leakages without any external aids.

4.4.4 Fiber-reinforced Plastics (FRP) Composites

All fiber-reinforced plastic composites used were manufactured by Fyfe Co. LLC. Three different systems were used. They were the Tyfo® SEH-51A Composite, the Tyfo® WEB Composite, and the Tyfo® BC Composite. All composites were made of E-glass fibers and impregnated in Tyfo® S Epoxy, the matrix material. The SEH-51A consists of unidirectional fiber roving densely placed in the 0° direction with additional sparsely spaced glass fibers in the 90° direction for linking. The WEB is made of $0^{\circ}/90^{\circ}$ bi-directional weaved fibers with equal fiber content running in both directions. The BC is also made of bi-directional weaved fibers but oriented in the $\pm 45^{\circ}$ directions. The 0° direction aligned with the horizontal plane while the 90° direction aligned with the vertical loading axis. Respective composite properties tested in accordance to ASTM D-

3039 were provided by Fyfe Co. LLC and are summarized in Table 4.2. An example of the uncured fabrics is shown in Figure 4.1.

The Tyfo® S Epoxy used was a two-part epoxy for bonding, as shown in Figure 4.2. It could be thickened to use as a primer material. The mix ratio was 100(A) to 42(B) by volume or 100(A) to 34.5(B) by weight. Curing time was a minimum of 72 hours at room temperature. Table 4.3 shows the epoxy material properties provided by Fyfe Co. LLC.

Table 4.2 Tyfo® Composite System Properties

PROPERTIES	SEH-51A	WEB	BC
Ultimate tensile strength in primary fiber direction, psi	83,400	44,800	40,500
Elongation at break	2.2%	1.6%	1.5%
Tensile Modulus, psi	3.79×10^6	2.80×10^6	2.70×10^6
Ultimate tensile strength 90 degrees to primary fiber, psi	3,000	44,800	40,500
Laminate thickness (normalized)	0.05 in.	0.01 in.	0.034 in.

Table 4.3 Tyfo® S Epoxy Properties

PROPERTIES	TEST METHOD	TEST VALUE
Tensile Strength*, psi	ASTM D-638, Type 1	10,500
Tensile Modulus, psi	ASTM D-638, Type 1	461,000
Elongation Percentage	ASTM D-638, Type 1	5.0
Flexural Strength, psi	ASTM D-790	17,900
Flexural Modulus, psi	ASTM D-790	452,000

*Crosshead speed: 0.5 in./min. Testing temperature: 70°F Grips Instron 2716-0055 – 30 kips

Figure 4.1

Tyfo® SEH-51A uncured fabric ready to be trimmed to size for installation

Figure 4.2

Tyfo® S Epoxy ready to be mixed (Left = A; Right = B)

4.5 Specimens

4.5.1 Cylinder Size

Fiber responses, overlap effects, interlaminate shearing and interactions, and failure modes are some of the major issues that require a considerable specimen size for visual interpretations and physical measurements. On the other hand, too small a specimen may make FRP wrapping difficult and unrealistic. Although it is not possible to make columns in their full scales due to time and resource constraints, it is still feasible to make cylinders with a certain diameter and aspect ratio so that the essences of those respective phenomena remain while meeting the requirement of the loading machine capacity. In view of capturing the responses and behaviors under pure uniaxial compression, the size of 6" x 15" was proposed and chosen. This size was believed to be good enough to yield meaningful results and observations. The rationale originates from two perspectives.

First, the radius of curvature of the cylinder surface has to be taken into account for fiber responses, overlap length effects, interlaminate actions, and instrumentation issues such as strain gage installation. Too small a radius would make such observations obscure because the roving-spacing/diameter ratio is too large such that the global and local scales are essentially too close to be differentiable. A diameter of 6" is the largest size that can be handled under normal laboratory resource capabilities. Therefore, 6" is chosen as the diameter of the cylinders instead of some other very common choices such as 4" and 3". Preliminary tests show that 6" cylinders are large enough to demonstrate the local responses that are under investigation.

Second, the frictional force development between the steel platen of the loading machine and the concrete end surfaces in compression tests contaminates the pure uniaxial compressive stress with a three-dimensional stress state that diminishes away from the end surfaces. This three-dimensional stress state stems from a difference in elastic modulus and Poisson's ratio of the two materials. As a result of the uniaxial compression and the lateral friction force acting together on the concrete, shear cone formation becomes the most common failure mode in cylinder compression tests. However, one

should note that when concrete is subjected to pure uniaxial compression, vertical splits should occur.

It was found out that the complex 3D stress state extends from the end surface to a distance of about 0.86D (Van Mier 1984), where D is the diameter of the cylinder under compression. For a cylinder with an aspect ratio of 2 or less, there is hardly any region that experiences the pure one-dimensional uniaxial stress state. Considering a concrete cylinder of size 6" x 12", for instance, 0.86D implies a length of approximately 5.2". When both ends are taken into account, a total of 10.4" is under the influence of the three-dimensional stress state. Only slightly less than 1.6" or 13% is experiencing the pure uniaxial compression.

When holding the diameter constant, the taller the cylinder, the more significant region will be subjected to pure uniaxial compressive stress. An aspect ratio of 2.5 has been considered sufficient for stress analysis. When applying this ratio to the herein case, a central zone of 5" is literally free from the end restraint effects if the cylinder diameter is 6". This 5" length appear to be quite adequate for the observation of fiber responses, interlaminate shearing and interactions, as well as instrumentations. Therefore the length of 15" is chosen as the cylinder height.

In fact, there are some other methods in tackling the end friction problem. Some of these methods include the use of brush bearing platens (Kupper 1969) and different material inserts (Newman 1964). Making longer specimens, however, is the easiest to do on site without employing special resources and equipments. Therefore, this method is chosen over the others.

4.5.2 FRP Wrap Configuration Designations

The rationales of the six wrap configurations were already discussed in detail in Section 4.2. In this section, the designation representing each FRP wrap configuration is presented. They are used throughout the program and are referred extensively in all stress-strain plots for citing and comparison conveniences. The designation system will

now be introduced. All configurations are derived from the following general form, which is read from left to right and corresponds to the layers inside out.

$$C(T) - UC(N) - W(N) - WA(N) - SP(M)$$

where C = Cylinder
UC = Tyfo® SEH-51A (with unidirectional fibers running horizontally)
W = Tyfo® WEB (with fibers running horizontally and vertically)
WA = Tyfo® BC (with fibers running $\pm 45^{\circ}$ to the horizontal)
SP = Specimen number representation
T = Total number of plies wrapped around the cylinder specimen
N = Number of plies of the respective Tyfo® composite system
M = Specimen number ($1 \leq M \leq 3$)

It should be noted that UC, W, and WA are not necessarily presented in the above order. The order arrangements depend on the stack-up sequence counting from the innermost layer. Also, when N = 0, that is when the type of fiber does not exist, the preceded notation (either UC, or W, or WA) will simply be discarded.

Let's consider an example. For instance, when one ply of unidirectional fiber composite is wrapped around by one ply of angular bi-directional fibers and that the cylinder is Specimen number 2 in that configuration, the designation is written as C2 – UC1 – WA1 – SP2. C2 implies that there are altogether 2 plies of FRP wrapping around the concrete cylinder. UC1 immediately following C2 means that the innermost layer that is in contact with the concrete is one layer of unidirectional fibers. WA1 following UC1 means that one ply of angular fibers is wrapping on one ply of unidirectional fibers. SP2 intuitively means Specimen Number 2. Table 4.4 lists the six FRP configurations investigated in this experimentation program. The listed configurations and sequence can be directly correlated with the descriptions elaborated in Section 4.2. It should be noted that the SP(M) designation is dropped when the group of FRP configuration instead of a particular specimen is referred to.

Table 4.4 FRP Wrap Configuration Summary

CONFIGURATIONS	DESIGNATIONS
I	C1 – UC1
II	C1 – W1
III	C1 – WA1
IV	C2 – W1 – WA1
V	C2 – UC1 – WA1
VI	C2 – WA1 – UC1

For respective FRP material properties, please refer to Table 4.2 in Section 4.4.4 for the manufacturer provided test data.

4.5.3 Concrete Casting Procedure

Altogether 30 concrete cylinders were cast in two batches. The casting procedure was done in accordance to ASTM C192/C192M – 98. Each batch consisted of 15 cylinders including three 6" x 12" cylinders and twelve 6" x 15" cylinders. The procedure was slightly simplified from the code requirement because ready-mix concrete instead of design-mix was used. An electric operated mixer was used. Details are described below.

Before pouring in the ready-mix, the interior of the mixer was wetted. Water was drained out with the mixer rotating for two minutes. Then, half of the weighted mixing water was poured in and the corresponding ready-mix followed. The rest of the water was finally poured in with the mixer rotating continuously. After all materials were in the mixer, they were allowed to mix for three minutes. The mixer was then stopped for two minutes to allow for initial chemical reactions to take place. A plastic lid was used to cover the mixer opening to prevent moisture escape. The mixer was then turned on for further mixing of another three minutes before the concrete was poured out onto a plastic, non-absorptive tray.

Concrete was then vertically cast into the cardboard molds, which had mold oil hand brushed onto the inner surface beforehand. The concrete was first shoveled in the tray with a trowel so that a consistent paste was achieved. Then, the concrete was inserted in three layers and tamping was done using a tamping rod 25 times for each layers. After the third layer was tamped, extra concrete filled the top and excessive materials were rolled off using the tamping rod leveled with the top edge of the mold. The top surface was smoothened and leveled with a trowel and a non-absorptive plastic sheet was covering the top to prevent moisture escape.

The concrete was allowed to set in a stationary condition for 24 hours before demolding and moving to the water bath for 7-day curing. After submerging the cylinders in the lime saturated water bath for 7 days, the cylinders were moved to a curing room to complete the 28-day curing cycle. When they were fully cured, all cylinders were removed from the curing room and air-dried for a week before capping and installing the respective composite systems. 28-day strength was tested after full curing had taken place. The tests were carried out within 8 hours after the 28-day period.

4.5.4 FRP System Installation Procedure

The FRP system installation was done in accordance to the Fyfe Co. LLC Quality Control Manual under the supervision of the manufacturer. The quality and workmanship of the installation were considered exemplary in the field practice. The entire installation procedure consisted of three major phases. They were (1) surface preparation, (2) fabric preparation, and (3) fabric installation. Fabric sampling was also done to acquire the corresponding FRP material properties to check with the manufacturer provided values. Before going into the details of the installation procedure, the overlap length consideration is discussed.

Overlap Consideration

The overlap length of all specimens in this program did not follow the suggested value stipulated in the Fyfe Co. LLC Quality Control Manual. The suggested value was 6" and was considered an absolute value regardless of the column size in the field. This length

was believed to be capable of developing sufficient epoxy bond strength at the overlap region, which is discontinuous. Viewing from a mechanics perspective, the overlap length is dependent on the shear strength of the epoxy that forms the bonding, the type of lap joint, the structural geometry such as initial curvature, and the loading direction. Therefore, the length is considered an absolute value instead of a circumferential percentage for a given set of initial conditions and epoxy properties.

Nevertheless, it was not reasonable to take the 6" or 32% overlap length on a 6"-diameter cylinder confined in one ply of FRP because the desired and assumed uniform stress distribution around the circumference would be significantly upset. In view of the cylinder size and by learning from some previous researches, a 3" overlap was adopted. The 3" length implied a 16% overlapping over the circumference. Should there be any stress unbalance in the one-wrap cases, this percentage of overlap would, in an engineering sense, give a measurable magnitude in terms of differential displacement.

For Configurations IV, V, and VI, which contained two FRP wraps, the overlaps were designed to be 180 degrees apart so that they were located exactly opposite to each other in order to attain a more balanced structural layout.

Phase I – Surface Preparation

The surface preparation is largely dependent on the type of structural element being strengthened, according to the Fyfe Co. LLC Quality Control Manual. For concrete columns, no special treatment is required except a broom cleaning (Figure 4.3). In general, the surface should be free from fins, sharp edges, and protrusions. Existing voids in concrete can be filled with the Tyfo® epoxy filler, which is made by thickening the Tyfo® S Epoxy at a rate of 500 rpm for 5 minutes (Figure 4.4). The contact surfaces should be free from moisture at the time of application. Following the cleaning of application surface, a prime coat of the Tyfo® S Epoxy should be applied (Figure 4.5) and allowed to cure for a minimum of one hour (Figure 4.6). The following pictures show the procedures.

Figure 4.3
Broom cleaned cylinders ready for prime coat application

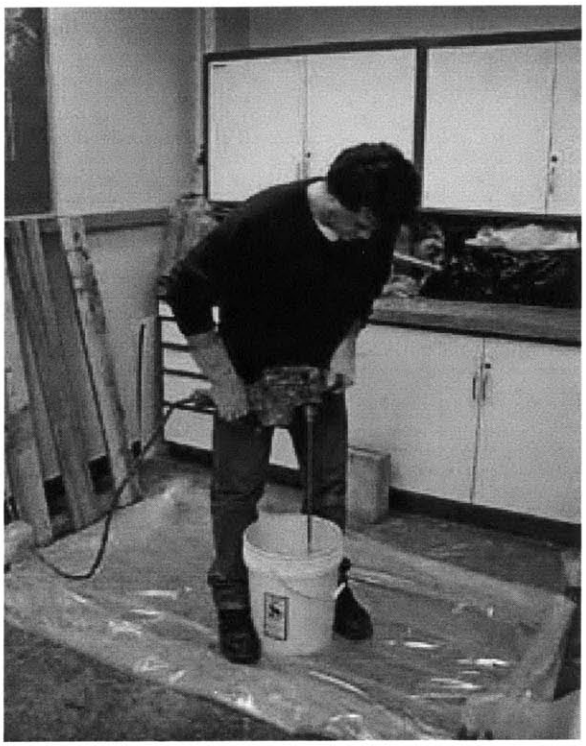

Figure 4.4
Tyfo® S Epoxy mixing and thickening for prime coat application with a mechanical mixer operating at 500 rpm for 5 minutes

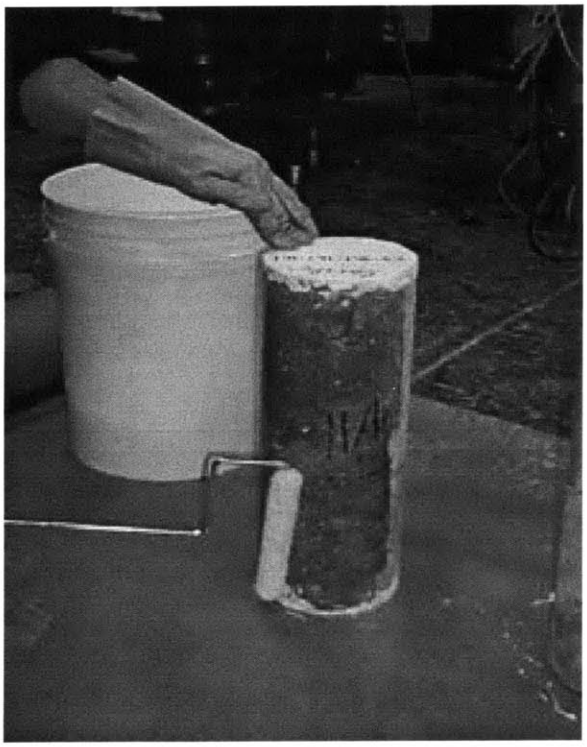

Figure 4.5
Prime coat application by a roller

Figure 4.6
Primed cylinders under curing for at least one hour (surfaces were darkened by the prime coat)

Phase II – Fabric Preparation

Fabrics should first be trimmed into shape. Operators should wear gloves and protective clothing for not getting glass fibers onto the clothes and skins. Saturation of the fabric then follows. A calibrated saturator should be used to achieve a specified volumetric ratio on site in large-scale construction in order to attain a consistent saturation for all composite systems to be installed. However, the saturator was not available at the time of installation. In view of the small-scale construction herein, the epoxy was instead rolled onto the fabric using a hand roller (Figure 4.7). To prevent any contamination of the composite systems, clean non-absorptive plastic sheets were used for backing the fabric saturation operation. As a rule of thumb, the composite system follows a volumetric ratio of 10:8 (fiber : epoxy) by weight. In order to facilitate the FRP installation process, the fabrics, after impregnation, were made to a roll such that during the installation, unrolling of fabric in place could be achieved.

Figure 4.7

Impregnation/saturation of the fabric with a hand roller

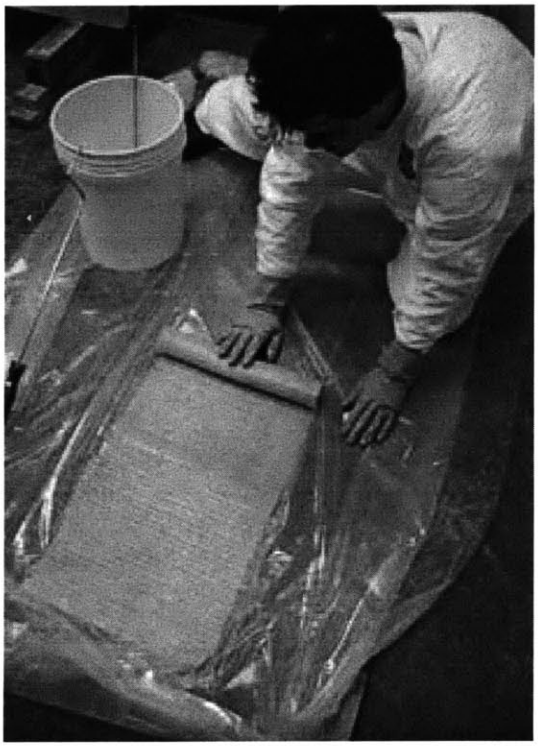

Figure 4.8

Saturated fabric rolled to shape and ready for installation

Phase III – Fabric Installation

Saturated fabrics were applied to the concrete surface by hand using the wet lay-up method. When unrolling the fabric into place (Figure 4.9), a slight constant pull was applied across the width of the fabric so that the fiber sheet was flatly adhered to the concrete according to the surface curvature. Hand pressure was applied to squeeze out air pockets and to press against the preceding layer to ensure sound adhesion between the two (Figure 4.10). Proper orientation of fibers was checked by naked eyes. A final coat of epoxy was applied to the wrapped specimens for complete saturation. The composite system was then allowed to cure for 72 hours at room temperature. Finally, fabric sampling was done on site with identical materials on a smooth, flat, leveled surface covering with polyethylene sheeting. A 12" x 12" sample was made. Air bubbles were squeezed out. The sample was not allowed to move for at least 48 hours. Both the wrapped specimens and the sample were protected from moisture contact for more than 24 hours.

Figure 4.9

Unrolling saturated fabric onto the cylinder surface

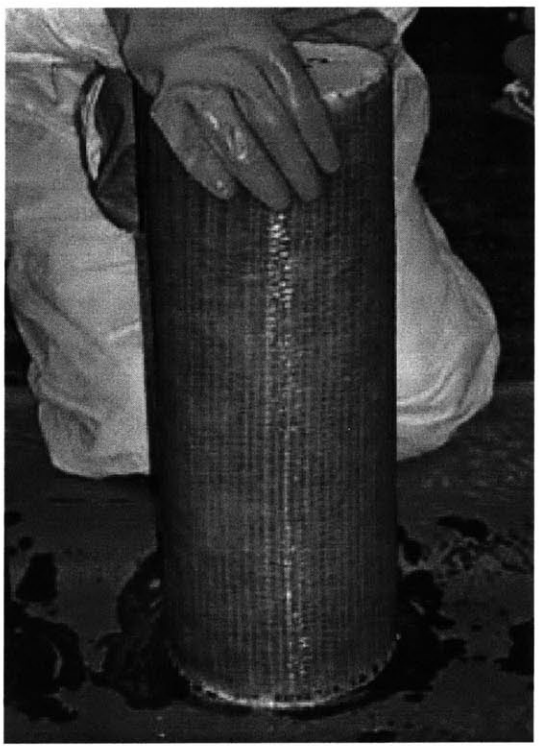

Figure 4.10

Squeezing entrapped air and ensuring a smooth finishing

4.5.5 Strain Gage Installation Procedure

Phase I - Surface Preparation

Fiber roving had given rise to dense ridges such that the composite surfaces were not flat enough for good strain gage fixation. This problem was more pronounced for all the UC outer-wraps because the fiber content was relatively much higher. Roving diameter was thus much greater than the other two systems.

Except a few preliminary tests that had strain gages installed regardless of the surface ridges, epoxy was used to fill the troughs of the ridges before normal strain gage installation procedure was carried out. Isopropyl alcohol was used to clean up the targeted surface areas before epoxy filling to ensure proper bonding. Dust and grease precipitated during composite curing and subsequent handling were removed through this process. A Teflon film with a sharp edge was used to apply and smoothen the epoxy filler onto the targets. The epoxy was then allowed to set and cure for 48 hours.

After a flat, smooth surface was prepared at the site, isopropyl alcohol was used again for degreasing purpose. The site was targeted to be chemically clean so that the adhesive could properly wet the surface and bond to it. To attain this level of cleanliness, a new, uncontaminated cotton swab was used for every site. The ambient environment was also cleaned beforehand to prevent airborne contamination from dust on working benches.

The appropriate roughness was then obtained by sanding the site with circular abrading motion, producing multi-directional marks with a 400-grit silicon carbide paper. The residues were then cleaned with alcohol in a gentle action. Two crossed lines were marked on the surface at the point where the strain gage was to be positioned. Ballpoint pen was found to be more appropriate than a 4H pencil as the marking tool on the epoxy material. The surface was then cleaned again by alcohol, followed by a neutralizer immediately before strain gage installation.

Phase II – Gage Mounting

For the herein application, the strain gages could be handled and positioned with the assistance of normal scotch tapes (BLH 2000). The foil gages did not require cleaning of the backing material while not contaminated by fingers. Therefore, the gages were always handled with the aid of a pair of clean, flat-nosed tweezers by holding the backing material. The foil elements were never touched by fingers or by any other means except clean scotch tapes.

Since the peeling strength between the backing and the foil was sufficient, tapes were applied across the entire foil area. Also, because a cyano-acrylate adhesive or "Superglue" was used, the tape chosen was much wider than the gage width in order to protect the fingers from adhesive spread during operation.

To pick up a strain gage, a tape was cut out and placed upside down on a prepared clean surface. The gage was then removed by the tweezers from the original packing and was placed also upside down onto the tape. The picked up gage was positioned accurately onto the site with pre-marked lines. Thumb pressure was applied over the gage on the tape so that entrapped air between the tape and the foil was squeezed out in order to prevent adhesives running in between.

One end of the tape assembly was then removed from the mounting surface at a slight angle for adhesive application. The free end was then tucked under and pressed to the surface, forming an arc shape, exposing the backing material for the application of adhesives.

Minute amount of adhesives was then applied on the backing of the gage and the tape was roller back to place slowly and simultaneously squeezing out excessive adhesives to the sides. Thumb pressure was applied for 30 seconds over the gage area on the tape and the tape was removed at a slight angle to prevent sucking up the attached gage. A magnifying glass was used to check for proper bonding of the gage or potential air bubbles entrapped in between.

Phase III – Curing

Although the curing required for the adhesive was 5 minutes, all cylinders were not tested at least 24 hours after strain gage installations. Scotch tapes were used to cover the strain gages from dust and moisture contamination in the mean time.

Phase IV – Soldering

Soldering was done close to the compression test machine. Water-soluble flux was brushed onto the encapsulated lead wires and the connection cables to enhance soldering quality. The ordinary 63/37 (tin/lead) solder was recommended (BLH 2000) and used.

Phase V – Verification

Finally, after the entire strain gage installation process, circuit voltages were checked to ensure that the soldering was done properly and no connection was loose, short circuited, or not conductive. For a balanced circuit, the voltage across the strain gage should read close to zero.

4.6 Instrumentation

4.6.1 Data Acquisition System

The entire data acquisition system consisted of a computer, an HP3497A Data Acquisition/Control Unit, and a cable connection box. This system collected both displacement and load data from strain gages, LVDT (Linear Variable Displacement Transducer), extensometers, and load cell in real time with a data logging time step of one second. Two circuits were built for strain gage data acquisition respectively for the two different resistances of 120 ohm and 350 ohm. The data collected were in the form of resistance fluctuation. Conversion was done for each set of data to transform the raw results into interpretable results through the use of calibration factors. Each piece of equipment was recalibrated before put into use since old calibration factors might not be applicable. The data logging time step of one second was the fastest possible, although a higher rate would be more desirable. The data logging software was unable to display

real time curves at the time of data logging. But it was capable of recording a maximum of 20 channels simultaneously with no time running limit. Figure 4.11 shows the entire data acquisition system that was used in the experimental study.

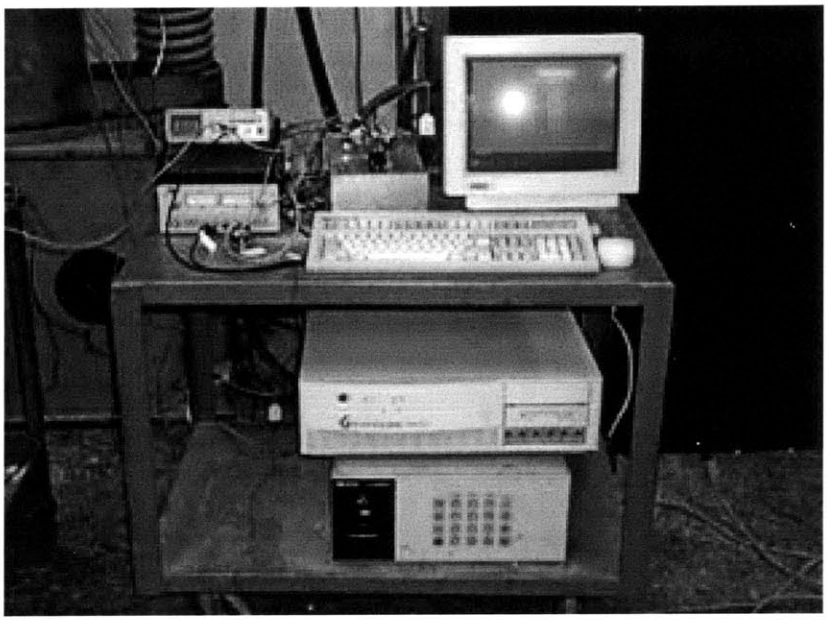

Figure 4.11 Data acquisition system

4.6.2 LVDTs and Extensometers

Trans-Tek LVDTs were used to measure radial displacements while HP LVDTs were used to measure crosshead displacements. Two Trans-Tek LVDTs were mounted respectively on two identical specially designed spring systems (Figure 4.12) that were capable of measuring the radial expansion of a 6"-diameter cylinder at a horizontal plane through the spring system clamping action. These two LVDT systems were responsible of measuring the radial dilations of the mid-height section and another section that was 2" below mid-height.

The two HP LVDTs were mounted respectively on two adjustable stands with vertical clamps, which were placed 90 degrees apart, to measure the crosshead displacements. They were placed at 90 degrees instead of 180 degrees for averaging solely because of

the spatial limitations of the setup. Nevertheless, from preliminary tests, the two LVDTs produced congruent results.

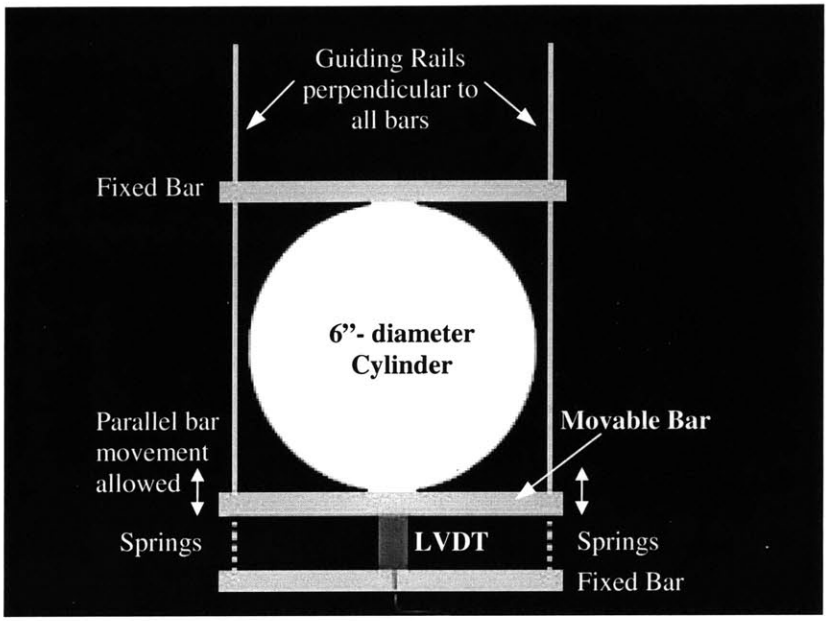

Figure 4.12 LVDT mounting spring system

Local discrepancies in axial displacement were captured by extensometers. This is particularly useful in the study of overlap effect. Any stress unbalance would be reflected from the differential axial strains on the lap and at the location 180-degree from the lap. The extensometers used had a gage length of 3.5" and were mounted onto the FRP surface within the mid-height region of 5" by the use of tight rubber bands, which prevented as much as possible any surface slippage.

4.6.3 Strain Gages

4.6.3.1 Locations and Orientations

All strain gages were installed at mid-height. On all fiber types, strain gages were installed in the hoop direction and the vertical load direction. On WA surfaces, strain gages were also installed in the 45-degree direction to align with the fibers. There were altogether four test cases and in each case, the strain gages were installed with different orientations. In some instances, when space was available, two cases were combined on one cylinder. All gages were installed following the procedure described in Section 4.5.5

with the surface smoothening technique. The comparative study of surface smoothening preparation effect is discussed in the following section. Each individual case will now be discussed.

Case 1 – Comparison between Strain Gage and LVDT (Hoop direction)

Four gages of the same type were placed 90 degrees apart in the hoop direction for data averaging. Since four gages were used, it would be almost up to par to compare with the global strains obtained from the LVDT device (Figure 4.12). Also, individual gage measurement would give some local information that would not be possible by the LVDT. The centerline of the overlap acted as the starting location of installation. For WA surfaces, this case act as Case 4 described below.

Case 2 – Comparison between Strain Gage and Extensometer (Vertical direction)

Two identical gages were installed next to the extensometers in the vertical load direction side by side. One set (gage + extensometer) was placed 180 degrees apart from the other set. This case was to compare the local measurements at the same site with two different devices. In some cases, the devices were placed on and opposite to the overlap. In some other cases, the devices were placed 90 degrees from the centerline of the overlap. For UC and WA surfaces, this case acted as Case 4 described below.

Case 3 – Comparison between Two Types of Strain Gages (Hoop & Vertical)

Two gages of one type were placed 180 degrees apart while the other type was placed side by side. The two types of strain gages were placed in the same orientation. The data collected from each type of gage were then averaged and compared to the LVDT and extensometer measurements accordingly, depending on the gage orientations.

Case 4 – Study of Fiber-Gage Alignment Effects

This case studied the performance of strain gages when not aligned with fiber directions. For UC surfaces, strain gages were placed in the vertical direction. For WA surfaces, strain gages were placed in the hoop, vertical, and fiber directions. Since extensometers and LVDT devices were not adhered onto the FRP surface, they were not directly

affected physically by the fiber orientations. Therefore, their respective measurements acted as the benchmarks for comparison with strain gage data. Angular measurements were then transformed and decoupled in the hoop and vertical directions and compared with the benchmarks.

4.6.3.2 Study of Composite Surface Smoothening Effect

As discussed in the beginning of Section 4.5.5, composites are weaved by fiber roving and thus normally do not exhibit a smooth and flat surface for strain gage installation, except when additional epoxy matrix material is used to fill the ridges. Since the surface preparation issue has not been discussed, if any, in the literature, there is a need to identify the responses and report errors of strain gages when the site of installation is not flat and smooth.

In view of this, a preliminary investigation was done to compare the strain gage performance on epoxy filled and unfilled sites. Two cylinders were installed with an extra strain gage without any epoxy filling on the installation site. Adhesion quality and gage quality were checked by a magnifying glass and circuit voltage was checked by a voltmeter. Results were then compared to strain gages with epoxy filled sites.

4.6.3.3 Gage Types and Properties

Three types of strain gages were used. They were the 120-ohm steel gages, 350-ohm composite single gages and tee gages. Respective gage properties are presented in Table 4.5. The steel gages used herein were those popular gages normally used for strain measurements on steel. The composite gages, on the other hand, were made in accordance to the recommendation given by some researches that focused on experimentation methods in composite materials (Book: Tuttle 1989).

Steel gages were chosen as one of the study objectives because (1) they are probably some of the most abundant gages in laboratories and (2) some researchers have been using them for strain measurements on FRP composites (Tan 2000). Normally, these gages differ from composite gages or concrete gages by possessing different gage

properties such as resistances, gage materials, and strain limits. The exact gage type should, in fact, depend on the particular application material, structural geometry and test environment (Book: Tuttle 1989). As a preliminary study, resistance was chosen as the parameter under investigation. Other parameters that can be varied include gage size, aspect ratio, backing material, and gage metal.

Table 4.5 Summary of Strain Gage Properties

PROPERTIES	STEEL GAGE	COMPOSITE SINGLE GAGE	COMPOSITE TEE GAGE
Series Designation	FAE – 25 – 12 – S6EL	FAE – 25 – 35 – S0EL	FAET–25B–35–S0EL
Gage Material	Cu-Ni (Constantan)		
Backing Material	Polyimide		
Lead Wire	Lead wires encapsulated		
Gage Factor	2.03 ± 0.5%	2.01 ± 0.2%	2.03 ± 0.5%
Resistance, Ω	120.0 ± 0.25%	350.0 ± 0.2%	350.0 ± 0.2%
Grid Length, in.	0.25		
Aspect ratio	2.0	2.0	1.0

The grid length employed was the minimum value suggested (Tuttle 1989). Although larger grid length could have been used, they were made to match with the common grid length of steel gages. The flexible Polyimide carrier material was chosen because it has a minimum bending radius of 0.06 in. and a maximum strain limit of 4%. This material was suitable because the FRP surface on which the strain gage was fixed was curvilinear and relatively large strains were expected from the hybrid system due to increased ductility. The gage alloy was made of copper-nickel (or commonly called Constantan) foil. The lead wires that were pre-encapsulated with the gages made soldering and wire connections much easier, especially on the temperature sensitive composite materials.

4.6.3.4 Gage Adhesives

A modified cyano-acrylate that requires only 30 seconds thumb pressure for initial set and less than 5 minutes curing time, was chosen as the adhesive for all gages. The strain

limit of this adhesive is approximately 10%, which well exceeded the requirements for the program use.

4.6.3.5 Barrier Coating and Gage Terminals

No barrier coating was used because no moisture that would contaminate the strain gages was expected in the test environment. Strain gage terminals that serve as junction points for connecting strain gages to instrumentation leads were not used because of their clumsiness on the diligently instrumented FRP surface. Teflon tapes were used instead to tackle the problem of straining of lead wires due to connection cable gravity.

4.7 Loading

A Baldwin 200-kips loading frame (Figure 4.13) was used to test all specimens under monotonic compression. It operates hydraulically and is computer-controlled (Figure 4.14). The crosshead is fixed while the platform moves upward according to the input loading rate or displacement rate. The steel platen affixed to the crosshead can be adjusted so that it can either be fixed to form a parallel surface to the platform or be released to become swivel. Since the all cylinders were capped and checked for orthogonality with the vertical axis, the platen was released to allow for the detection of any unbalanced stress. In fact, this simulated the beam-column situation such that the loading and displacement would follow the easiest and weakest path. Load redistribution would take place incrementally if any unbalance stress existed. This pointed directly to the study and observations of the overlap joint effect.

Load displacement control at a rate of 0.05 in./min. was used. The displacement control was used over the load control mechanism in order to obtain relatively less catastrophic failures near peak load when the plastic region was entered. During the plastic deformation, axial displacement would take place at a much faster rate under the same load increment. Therefore, if the otherwise were chosen, the axial displacement would have taken place too quickly so that the material responses and fracture mechanisms could not be observed as clearly.

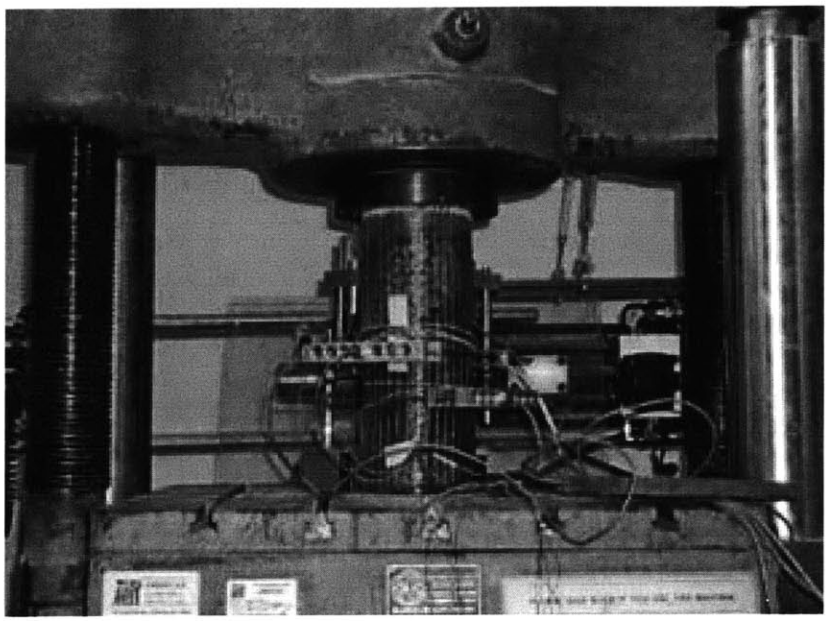

Figure 4.13

Baldwin 200 kips loading frame with a specimen and the full setup

Figure 4.14

Computer-controlled system

4.8 Test Results

Test results are categorized into four major areas as of the objectives listed in Section 4.1. They are (1) instrumentation issues, (2) loading effects, (3) local effects, and (4) manufacturing effects. The results will first be briefly summarized to shed a light on the findings of the entire experimental program. For simplicity, configuration numbers will be quoted instead of the corresponding designations. Configuration numbers can be referred back to Table 4.4 in Section 4.5.2. Details of the findings of each area can be found in subsequent subsections. Results interpretations should be directed to Section 4.9.

An Overview

From the preliminary tests, it was confirmed that epoxy surface filling technique on the composite surface is required for proper strain gage installation and data acquisition. 350-ohm single gage, which has an aspect ratio of 2.0, produced congruent results with the LVDT measurements. The 120-ohm steel gage grossly underestimated the strains while the 350-ohm tee gage measurements were not consistent. When strain gages did not align with the principal fiber and stress directions, poor results were obtained. Remarkable underestimations and overestimation were also noted when strain gages were orientated in such a way that significantly stressed fibers were running through that gage area, depending on the strain gage type.

The ultimate load capacities of Configuration I was higher than II while II was higher than III, although fabrics in II and III had similar tensile strengths in the hoop direction. Configuration IV and VI showed approximate linearity relationship in the capacity increase for two combined fiber types. Configuration III and V showed scattered results. Configurations V and VI, which were made of identical materials but had different FRP stack-ups, showed very different ultimate load capacities.

Lateral strains at peak were generally less than the corresponding axial strains. Lateral expansion was most pronounced at mid-height. Configuration II had very little lateral expansion at failure while III had tremendous expansion at mid-height without significant fiber fracture even after peak load.

Failure modes of all six configurations were distinct, though IV was a mix of II and III while V was a mix of I and III. Catastrophic failure was recorded for I, II and V. Very ductile failure was noted for III. The rest exhibited failures between the two extremes. Most failure occurred in the mid-height region due to fiber fracture. Concrete cores were either cracked or crushed, depending on the cases. Crushing was confined in the middle third and did not take place throughout the entire cylinder height. When crushing took place at mid-height, concrete in both top and bottom thirds usually remained sound. Time to failure of III was the longest while II was the shortest. In IV, when wrapping II with WA fabric, time to failure was prolonged several folds.

Stress-strain curves appeared in two major shapes. The first shape was bilinear increasing. The second shape was a combination of increasing and decreasing slopes. Initial slopes of all curves were close to that of unconfined concrete. The point of changing slope in the bilinear increasing curve type had an upward shifting tendency with higher peak load. Whenever the confinement consisted of a WA wrap, the descending tail of all curves, regardless of the type, had a slope approximately parallel to that of one ply of WA (Configuration III) alone.

Overlap of FRP in all one-ply cases had given rise to a bending effect, evidenced from differential axial shortening. When two overlaps appeared in opposite sides of a circumference, only minute differential axial shortening was noted. All FRP cracks terminated right before the overlap region. Overlap length of less than 3" was found to be insufficient for full bond strength development; overlap debonding was noted for such cases.

Intact bonding was found in Configurations IV and V; no delamination was noted. Fabric peeling phenomenon was noted for Configuration VI. Fiber buckling was noted for confinement shells with axial fibers. Fiber reorientation was noted on all angular fiber outer-wraps at the mid-height failure zone without significant fiber fracture. Fiber fracture and progressive snipping was noted for hoop fiber outer-wraps. The snipping action signified the breakage of linking fibers. Elephant foot (bottom end bulging)

phenomenon was noted for cylinder ends with axial fiber outer-wraps. Top end unconfined concrete was not crushed in all cases.

Initial imperfections such as thumb-sized air pockets and slight wrinkling did not promote strength deterioration. However, they acted as nuclei for delamination flow. The flow represents the development of air channels between air pockets of all sizes. Time to failure shortened significantly for cases with entrapped air pockets. Delamination flow accelerated especially after peak load. For configuration V, thinner epoxy bonding between the two different fabric layers, higher the ultimate strength was recorded. For all other cases, epoxy thickness variation did not contribute to major variations in ultimate strengths.

4.8.1 Strain Gage Instrumentation Issues

4.8.1.1 Epoxy Surface Filling

Four 350-ohm single gages were used in this study. Two were installed onto the UC surface of Configuration I. The other two were installed onto the W surface of Configuration II. The two different surfaces were chosen for investigation because they had the highest and lowest levels of surface bumpiness among the three types of FRP fabrics, resulted from the roving ridges that depended on fiber contents. One of the two strain gages on the same surface was installed with epoxy surface smoothening while the other was installed without that smoothening procedure. Visual checks and voltage checks were done using a 2.5X magnifying glass and a voltmeter respectively when the gages were installed and cured. Except for the smoothening procedure, the rest of the installation was done in accordance to Section 4.5.5.

In the case that had the strain gage installed without epoxy filling the UC surface, sanding was done before gage fixation, aiming at obtaining a flat and slightly roughened surface for proper gage adhesion. However, the sanding process was ceased when some visible damages to the fibrils in the roving were detected.

Another site was then chosen. The strain gage was installed after minimal sanding followed by thorough cleaning and degreasing. After adhesion was done under thumb pressure, it was immediately noted that part of the edges were not fully adhered to the composite surface and the gage foil was somewhat distorted due to the thumb pressure and irregular, bumpy roving geometry. When checked with a voltmeter, the closed circuit reading was abnormal; normal reading should read zero volts.

For the other strain gage that was installed onto the same UC surface, epoxy was used to fill the troughs of the roving ridges. Excessive fills were removed such that the applied epoxy was just slightly covering the targeted area without flooding the roving troughs. Full cure was allowed and the gage was installed accordingly. After installation, it was checked with a magnifying glass that sound adhesion was achieved. The gage laid flatly on the surface without any distortion. Circuit voltage was very close to zero.

Identical procedure was followed for the W case. The only difference was that the ridge troughs were less deep such that the adhesive was able to fill the voids partially. However, the gage was distorted slightly and part of the adhesives squeezed out upon the applied thumb pressure. The distortion imaged the roving pattern. Circuit voltage was, nevertheless, appeared normal.

In the case that had the epoxy filled on the W surface before subsequent installation procedure, sound adhesion, no distortion, and normal voltage were resulted.

Conclusion: Epoxy filling technique is an essential first step in the strain gage installation procedure on fabric type FRP, which surfaced with roving ridges, for proper gage fixation without distortion or damage to the gage. Sound adhesion can be assured all over the gage and voltage of the strain gage circuit will not be adversely affected by any foil distortion.

4.8.1.2 Strain Gage Performance

Performances of three types of strain gages were compared. As discussed in Section 4.6.3, the strain gages used were 120-ohm steel gage, 350-ohm composite single gage,

and 350-ohm composite tee gage. The 350-ohm composite gages were made in accordance to the suggestions in the literature (Tuttle 1989).

It was found that the 350-ohm single gages gave congruent results with the LVDT measurements in the case of Configurations I and VI while 120-ohm steel gages grossly underestimated the strains on UC surfaces. Figure 4.15 and 4.16 show the plots of averaged lateral strains measured from 350-ohm single gages and 120-ohm steel gages on C1 – UC1 – SP3 and C2 – WA1 – UC1 – SP1 and are compared with the LVDT measurement. It should be reminded that the only variable in the strain gage measurements was resistance. All other gage properties and installation procedures were the same.

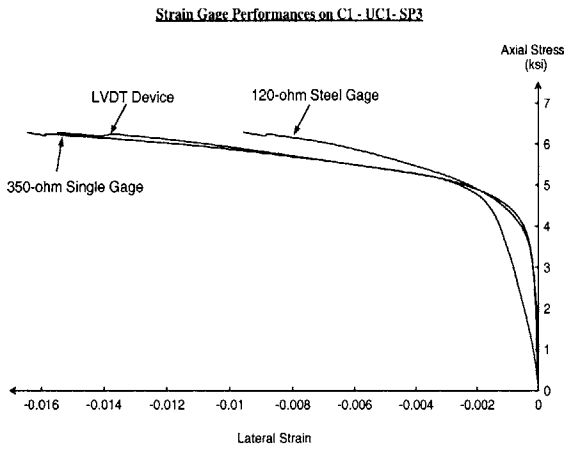

Figure 4.15
Comparison of 350-ohm single gage and 120-ohm steel gage on C1 – UC1 – SP3

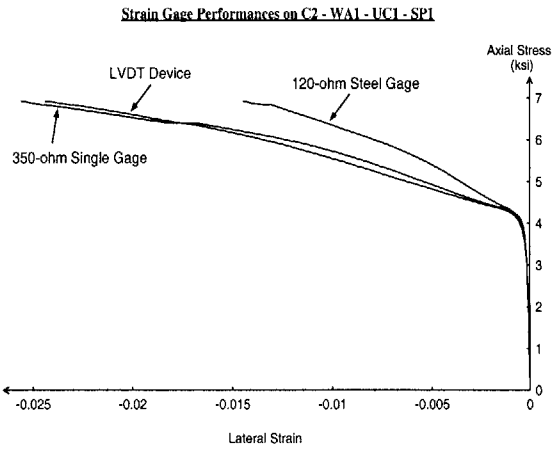

Figure 4.16
Comparison of 350-ohm single gage and 120-ohm steel gage on C2 – WA1 – UC1 – SP1

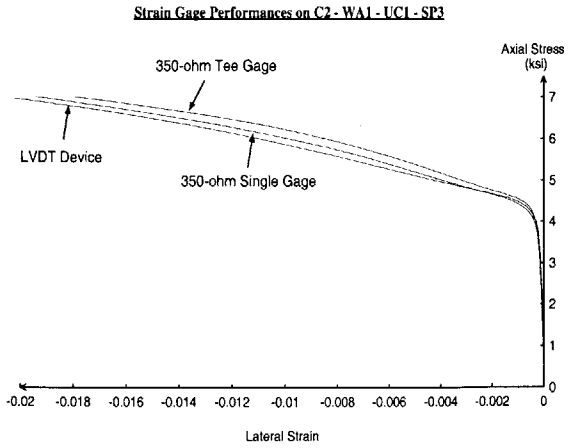

Figure 4.17
Comparison of 350-ohm single gage and 350-ohm tee gage on C2 – WA1 – UC1 – SP3

350-ohm tee gage measurement on UC surfaces was close to that of the 350-ohm single gage, although not as accurate when compared to the benchmark values produced from the LVDT device (Figure 4.17).

When strain gages were installed onto W surfaces, where fibers were weaved in a bi-directional pattern, and aligned with the fiber directions, poor results were obtained from all strain gages, regardless of types. The good performances of the 350-ohm gages that were noted on UC surface no longer appeared on the W surfaces. The 120-ohm steel gage continued to underestimate the strains in the fiber direction. The 350-ohm tee gage now consistently underestimated the strains while the 350-ohm single gage produced severe overestimations. Figure 4.18 and Figure 4.19 show the measurements of two specimens of the C1 – W1 group. The 350-ohm single curve in Figure 4.19 was dropped from the plot because the strain was more than doubled the LVDT measurement.

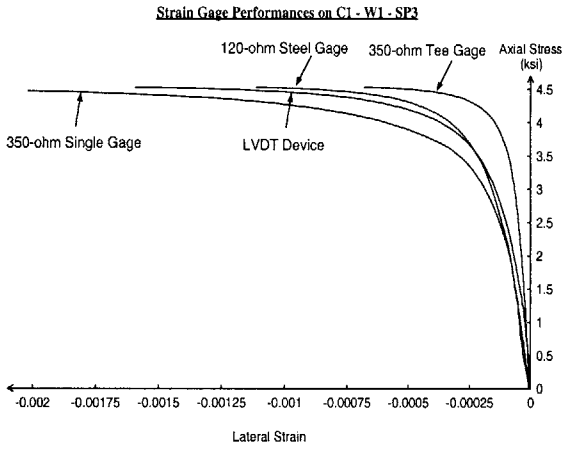

Figure 4.18
Comparison of all strain gages on C1–W1–SP3

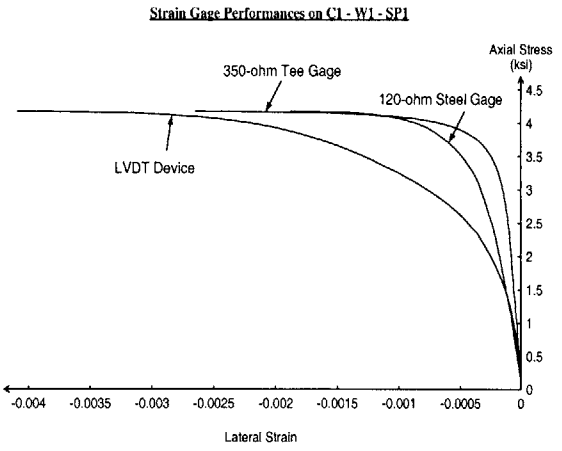

Figure 4.19
Comparison of all strain gages on C1–W1–SP1

Strain gage performances on WA surfaces are discussed in the next section because the fiber-gage misalignment effect is involved.

Conclusion: Upon the measurements on UC surfaces of hoop lateral strains, 350-ohm single gage with an aspect ratio of 2.0 produced good results. 350-ohm tee-gage with an aspect ratio of 1.0 produced acceptable results. 120-ohm steel gage showed significant

underestimation. In the case of W surface measurements, 350-ohm single gage significantly overestimated the lateral strains while the other two strain gages consistently made underestimation in all specimens.

4.8.1.3 Fiber-Gage Misalignment

In this study, the results obtained from the strain gage performance study were used as the benchmarks. Since 350-ohm single gage performed well on UC surfaces, this type of strain gage was used to investigate the effects of fiber-gage misalignment on the specimens with UC outer-wraps. The unaligned primary direction of the UC surfaces was the vertical load direction; the strain gages were, therefore, placed side by side to the extensometers to compare the axial strain measurements.

Figure 4.20 shows that the averaged axial strain measured by the 350-ohm gage was less than that obtained by extensometers. Also, the curve shape was quite different from that of the extensometers and the vertical LVDT device. It is also noted that the extensometer measured axial strain is less than that of the vertical LVDT due to the local axial strain variation. The LVDT curve is also included for curve shape indication only.

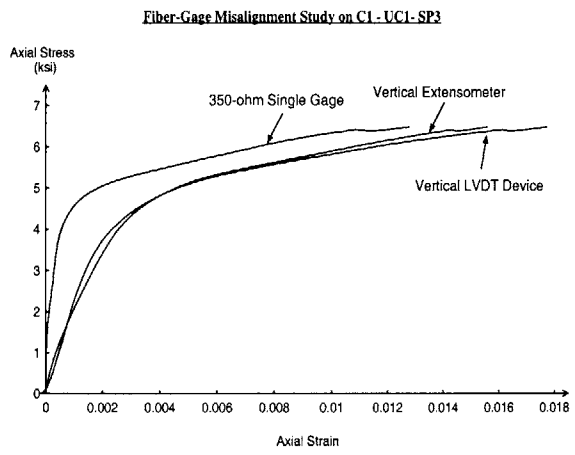

Figure 4.20
Fiber-gage misalignment study on C1-UC1-SP3

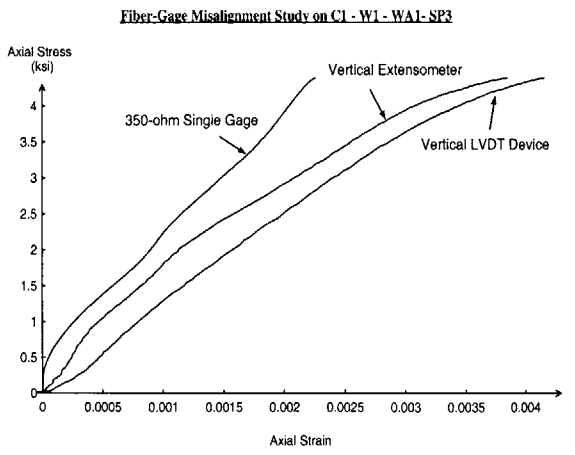

Figure 4.21
Fiber-gage misalignment study on C2–W1–WA1–SP3

In the case of WA surface, strain gages were placed in the hoop and vertical directions such that the fiber-gage misalignment angle was 45 degrees. Figure 4.21 shows again the

significant underestimation as high as 32% of the 350-ohm single gage when the gage was not aligned with the fiber orientation on the WA surface. Also, the slope deviates from the other two curves when it approaches the peak stress.

In the case of W surface, since the vertical fibers run through the horizontally placed gages, fiber-gage misalignment can be considered. The results were already presented in Figure 4.18 and Figure 4.19. Overestimation was noted for the 350-ohm single gage and underestimation for the other two gage types.

Conclusion: Whenever the strain gage is not aligned with the fiber direction, underestimation will be resulted in most cases. Stressed fibers running underneath a gage causes poor results. Both overestimation and underestimation can be resulted, depending on the gage type.

4.8.2 Loading Effects

4.8.2.1 Peak Stress

Table 4.6 summarizes the peak stresses of all six configurations including the unconfined concrete. The six configurations are ranked in ascending order. All stresses were actual stresses instead of engineering stresses. The continually dilating cross-sections were used to compute the actual peak stresses. This step is emphasized because there is a substantial difference between the two stress values due to the unusual dilation encountered in the wrap cylinders, especially for the two-ply configurations.

Although only averages were presented in Table 4.6, it should be pointed out that scattered results were obtained for Configurations III and V while uniform results were obtained for all the other configurations. Scattered results had a percentage standard deviation of about 10%. Uniform results had a percentage standard deviation of less than 3%.

Table 4.6 Summary of Ultimate Load Capacities

RANK	CONFIG.	DESIGNATIONS	PEAK STRESS (Average), psi	CAPACITY INCREASE (average), %
1	VI	C2 – WA1 – UC1	6990	99
2	I	C1 – UC1	6351	81
3	V	C2 – UC1 – WA1	6184	76
4	IV	C2 – W1 – WA1	4615	32
5	II	C1 – W1	4327	23
6	III	C1 – WA1	3916	12
7	Unconfined	–	3507	–

It can be noted that substantial increase in load capacity resided on all configurations that contained a UC ply. Configurations II and III had very little increase in strength but it is readily seen that IV demonstrated a linearity relationship. When summing up the average load increases in II and III, a total load increase approximately equals that of IV. A similar relationship can be found by adding up the average load increases in I and III, getting a total load increase that approximately equal that of VI.

When paid attention to Configurations IV and VI, it can be discovered that different load increases were resulted, although identical number of wraps were used. The load increases in II and III were unequal, although the two materials had similar tensile strength in the hoop direction. The load increase in II almost doubled III.

Conclusion: Two major observations can be noted. First, the linearity of load capacity increase is valid for most 2-ply cases. However, possible adverse interactions between different ply types may upset this linearity behavior. Second, similar fabric tensile strengths do not guarantee identical strength increase. Orientation of fibers plays a significant role in the amount of load increase.

4.8.2.2 Peak and Ultimate Strains

Peak strains and ultimate strains should be differentiated in this study. Peak strains are strains that correspond to peak stresses. Ultimate strains are strains that correspond to the complete failure of the specimens. Since in some cases, the complete failure is difficult to define, ultimate strains are determined as the strains that correspond to the 50% peak stresses in the plastic region. Table 4.7 summarizes the average peak strains and ultimate strains of all the six configurations in the descending order of axial strains at peak. The axial strain is used for ranking purpose because it is a relatively more objective measures. Lateral strain is often affected by the local behavior of the FRP fabrics at failure. According to the defined sign conventions in Section 4.3, lateral expansion is negative while axial shortening is positive.

Table 4.7 Summary of Peak Strains and Ultimate Strains

AXIAL STRAIN RANK	PEAK STRESS RANK	CONFIG.	DESIGNATIONS	STRAIN AT PEAK STRESS		ULTIMATE STRAIN	
				Axial	Lateral	Axial	Lateral
1	1	VI	C2 – WA1 – UC1	0.0260	-0.0221	0.0298	-0.0393
2	3	V	C2 – UC1 – WA1	0.0166	-0.0148	0.0245	-0.0478
3	2	I	C1 – UC1	0.0163	-0.0143	0.0221	-0.0369
4	4	IV	C2 – W1 – WA1	0.0055	-0.0056	0.0150	-0.0274
5	6	III	C1 – WA1	0.0050	-0.0076	0.0159	-0.0272
6	5	II	C1 – W1	0.0043	-0.0038	0.0084	-0.0315
7	7	PLAIN	C0	0.0036	-0.0015	0.0055	-0.0089

In general, lateral strains at peak stresses were smaller than axial strains. The only exceptions were Types III and IV. For Type III, lateral strain at peak stress is greater than the corresponding axial strain by more than 50%. For Type IV, although the averaged axial strain is smaller than the averaged lateral strain at peak, the two values are essentially identical.

Ultimate lateral strains were all larger than the ultimate axial strains. The increase in axial strain from peak stress to half of the peak stress ranges from 14.6% (Type VI) to 218% (Type III). The increase in lateral strain, on the other hand, ranges from 77.8% (Type VI) to 389.3% (Type IV), excluding the exceptionally large dilation of Type II.

From the ranking listed, it can be noted that the axial strain ranking is literally following a similar order of the peak stress ranking. In other words, the higher the stress a specimen can take, the larger the axial strain it experienced. Also, except III and IV, generally speaking, the order of lateral strains at peak follows that of the corresponding axial strain.

Conclusion: In general, lateral strain at peak stress is smaller than the corresponding axial strain. Ultimate lateral strain is, however, larger than the corresponding axial strain due to the change in dilatation rate before and after the peak stress. Higher is the loading capacity, higher the axial strain is experienced.

4.8.2.3 Time to Failure

Time to failure after peak is expressed in the form of rates of stress reduction and axial strain increase. Stress reduction rate and axial strain increase rate are defined as follow.

$$\text{Stress reduction rate} = \frac{\sigma_{50\%\,peak} - \sigma_{peak}}{t_{50\%\,peak} - t_{peak}}$$

$$\text{Axial strain rate} = \frac{\varepsilon_{50\%\,peak} - \varepsilon_{peak}}{t_{50\%\,peak} - t_{peak}}$$

where σ, ε, t are the axial stress, axial strain, and the corresponding time respectively. The subscript $_{50\%\,peak}$ represents the state at the 50% post-peak stress level. The subscript $_{peak}$ represents the state at the peak stress level. These rates are noteworthy due to the safety issues that will be discussed in a later section. Table 4.8 shows the respective rates and the configurations are ranked in the descending order of stress reduction rate.

Table 4.8 Summary of Rates of Stress Reduction and Axial Strain Increase

RANK	PEAK STRESS RANK	CONFIG.	DESIGNATIONS	Stress Reduction Rate, psi/sec	Axial Strain Rate, sec^{-1} ($x10^6$)
1	5	II	C1 – W1	-63.63	120.59
2	3	V	C2 – UC1 – WA1	-38.17	28.79
3	2	I	C1 – UC1	-30.83	56.31
4	1	VI	C2 – WA1 – UC1	-26.48	97.53
5	4	IV	C2 – W1 – WA1	-15.38	63.33
6	6	III	C1 – WA1	-9.69	53.96

It can be noted that Configuration II had the fastest stress reduction rate while III had the slowest. When taking a view on the rankings according to stress reduction rate, it can be noted that the rate does not necessarily correlate with the peak stress ranking. In other words, the configuration that has the highest or lowest load capacity does not necessarily imply the highest stress reduction rate.

It is also interesting to note that IV, the combination of II and III in terms of FRP materials, the stress reduction rate decreased dramatically. On the other hand, however, in V, the combination of I and III has led to a slight increase of the stress reduction rate. Also, the rate was different for V and VI, although they were made of the same materials.

Conclusion: The stress reduction rate does not necessarily correlate with the peak stress. Configuration III, which solely consists of angular fibers, demonstrates the slowest stress reduction rate. On the other hand, by combining two different types of materials, the stress reduction rate can either increase or reduce depending on any possible interlaminate adverse effect that exists.

4.8.2.4 Failure Modes

From the observations, it can be claimed that there are altogether six modes of failure for the six configurations. In other words, each configuration gave rise to a distinct failure,

although some configurations had a failure mode that composed of two basic modes. Basic modes are defined as the failure modes of Configurations I, II, and III. Since they were all single-ply wrapped, the failure modes were mainly determined by the type of wrap. Configurations IV, V, and VI all demonstrated mixed modes. It is interesting to note that V and VI failed very differently, despite the fact that they were made of the same materials. Each of these modes will be presented complemented by a picture that captured the exemplary failures of the three specimens within the same group. In all cases, all specimens within the same group showed identical failure. The mode number follows the same sequence of the configuration number defined in Table 4.4. Mode I, II, and III are basic modes. Mode IV, V, and VI are mixed modes.

Basic Modes

A. Mode I – (C1 – UC1)

Mode I represents the failure of C1 – UC1 specimens. All specimens failed catastrophically in the middle third sections under the coupling of fiber fracture and concrete crushing. Fiber fractures consistently initiated on the opposite site to the overlap region. Concrete crushing was highly localized. Sound concrete was detected in the top and bottom thirds.

The failure started with a cylinder bowing action in a way that more axial shortening took place on the opposite side of the overlap. The top third leaned slightly forward while the bottom third remained vertical. This action was evidenced by the changing orientation of the vertical longitudinal fibers upon loading. Concrete crushing took place locally and volume gradually reduced as more concrete was crushed into rubble form. Concrete was crushed before substantial fiber fracture. Lateral expansion became pronounced after a significant amount of concrete was transformed into powder and pressed against the FRP confinement. Axial shortening rate reduced and lateral expansion took over. The pressure exerted on the inner face of the FRP confinement was transformed into hoop tension in the FRP. Upon reaching the elastic limit of some of the fibers, fractures occurred suddenly without warning.

Two fracture wings were formed and opened up upon further loading. Crushed concrete spalled off as the wings opened and snipping took place gradually. The longitudinal fibers that held the hoop fibers in place were snipped off one by one as the wings opened wider and extended towards the overlap. A large gap was noted as concrete spalled off in the middle. As an increasing volume of concrete spalled off due to the wing open-up, the bowing phenomenon became even more pronounced and visible. The gap was now closing due to the bowing action and lateral expansion was gradually moved to the sides, thus pushing against the FRP and forcing the wing to open up further on the sides. Figure 4.22 illustrates the fiber fracture and fracture wing formation.

Figure 4.22 Failure mode I (C1 – UC1)

These series of concrete spalling and wing open-up ceased when the wings reached the overlap region. The wing size was growing from the fracture point to about one forth of the cylinder height near the overlap region. The overlap remained intact without any visible damage. The fiber fracture was catastrophic. Huge noise was produced due to sudden release of energy at fiber rupture. The snipping of longitudinal fibers was also swift.

FRP-concrete interfaces remained intact as evidenced in the fractured wings. Chunks of concrete were still adhered to the fractured fabric, although the inner concrete was

crushed into powder. Fabrics above and below the failure region remained intact, as of the confined concrete core. No major crack could be found in the top and bottom third except that some white dots could be detected in those regions. The white dots appeared at all locations where the hoop fibers and longitudinal fibers crossed, signifying the movements of the fibers during the loading process.

B. Mode II – (C1 – W1)

Mode II represents the failure of C1 – W1 specimens. The specimens failed swiftly and catastrophically after the peak stresses were reached, as could be implied in Table 4.7. All specimens failed in the common modes of plain concrete cylinders. The cone and split mode and the cone and shear mode were noted as illustrated in Figure 4.23.

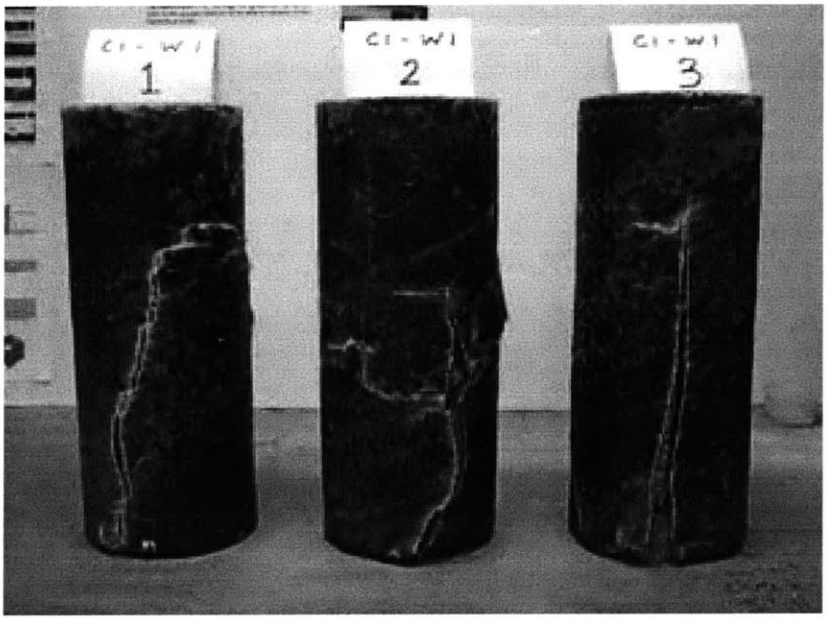

Figure 4.23 Failure mode II (C1 – W1)

All failures were initiated from the bottom end through local bulging (denoted as the elephant foot behavior to be discussed in a later section) and local fiber buckling. The buckling of longitudinal fibers crinkled the fabric and hence imposed large tensile strains on the crossing hoop fibers. Hoop fiber fracture therefore occurred at the bottom and the jacket crack surged upward upon further loading. The pattern of the upward surging crack resembled the concrete cracking pattern inside because of the intact concrete-FRP

interface. It should be noted that in this mode, no concrete crushing had occurred. Concrete cracked instead.

For specimen one, two large shear cones were formed. The concrete shear cone displaced along the shear plane and the top sharp edge of the cone pressed against the FRP confinement, crinkling the fabric in that region. As the cone displaced more, the sharp horizontal edge cut through the crinkled fabric; the longitudinal fibers broke under such concentrated stress. The confinement effect vanished when the longitudinal fibers fractured. The specimen became two separate cones with the undamaged fabrics remained firmly adhered to the separate concrete cones.

For specimen two, shear cracks were formed in the lower half. Initial crack was at a 45-degree angle and then became vertical after about one inch of development. It then surged up to the one-third level and developed two other individual sideway cracks. The initial crack continued to surge upward and terminated at mid-height. The sideway cracks were approximately horizontal. Fabrics crinkled slightly at the one-third level.

For specimen three, a vertical split surged all the way from the bottom to two thirds of the cylinder height. The split was straight and the unzipping was very swift. When the specimen was dissembled, a shear cone was found at the top end while a long vertical crack divided the lower portion of the cylinder.

C. Mode III – (C1 – WA1)

Mode III represents the failure of C1 – WA1 specimens. These specimens failed in a very ductile manner. No severe fiber fracture could be noted at a load level as low as 30% of the peak stress during plastic deformation. Fiber reorientation at mid-height was pronounced. Global shear cracks could be noted in the concrete core after dissembling. As shown in Figure 4.24, all three specimens failed similarly.

Figure 4.24 Failure mode III (C1 – WA1)

As in Mode II, this mode has cracks initiated from the bottom for all three specimens. Crack propagated upward at a 45-degree angle to about one half to one third of the specimen height and then the crack orientation changed to approximately vertical throughout the middle section. After the crack had reached about two thirds of the height, it changed back to the 45-degree angle. The crack, in fact, occurred within the concrete core only. Fabrics at the end of the crack surge wrinkled and local fiber buckling (Section 4.8.3.3) occurred. Fibers in the middle section did not tear apart, but rather, reoriented. The cracks shown in Figure 4.24 were made by cutting the reoriented fibers for detail inspection of the concrete quality.

Overall radial expansion was significant. Bulging of the middle portion was very pronounced because fibers did not fracture and no concrete had spalled out until the cease of loading. The bulging continued until 30% of the peak stress in the plastic region. These specimens were not tested until fiber fracture for fear of the sudden release of the huge energy absorbed.

Mixed Modes

D. Mode IV – (C2 – W1 – WA1)

Mode IV represents the failure of C2 – W1 – WA1 specimens. These specimens failed in a mix mode consisting of Mode II and III, although III dominated. The failures of all three were quite ductile. No concrete spalled off and fibers did not fracture. Instead, fibers reorientation took place just like those in Mode III. Shear cones were resulted in all three cases, in addition to some local horizontal cracks at around mid-height. Figure 4.25 demonstrated this mix mode of failure. Most of the failure resembled specimens one and two of Mode II and those in Mode III.

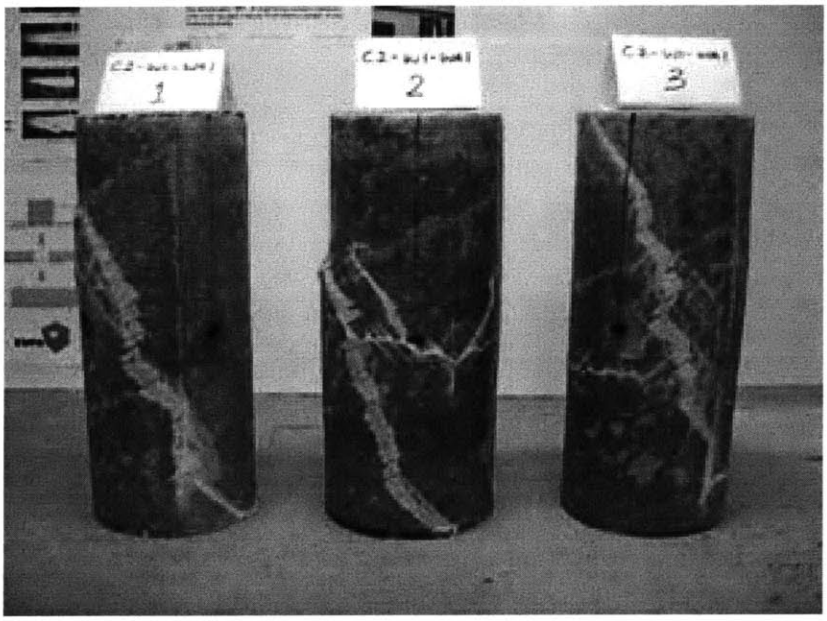

Figure 4.25 Failure mode IV (C2 – W1 – WA1)

Failure started at the bottom as usual due to local fiber buckling. The crack surged up with a 45-degree angle. After a few inches of crack propagation, the angle increased to about 75. It was, however, not as vertical as those in Mode III. Upon reaching about two thirds of the cylinder height, the crack terminated. Concrete shear cone inside displaced along the shear plane and the sharp edge pushed against the FRP fabrics as usual. However, this time the edge was not able to cut through the fabrics. It produced local bulging and fabric crinkling, though.

For specimen three, the FRP was applied all the way from top to bottom, without any gap left in the top. This cylinder demonstrated the crack initiations on both ends. A large shear crack ran from top to bottom all the way, and was not only cracking two thirds of the cylinder. The two cracks started at both ends at about the same time and then met approximately in the middle. The other behaviors of this particular specimen were the same as the other two.

Delamination was not noted between the two different layers. The bowing action that occurred in Mode I also did not occur in this Mode. Finally, all cracks terminated right in front of the overlap as all the other modes did.

E. Mode V – (C2 – UC1 – WA1)

Mode V represents the failure of C2 – UC1 – WA1 specimens. In this mode, the failure was initiated through the fiber fracture mechanism at around mid-height with a tendency of extending to the lower part of the upper third. About one third of the concrete was crushed and spalled off continuously upon opening up of the fractured fabric. Fibers did not buckle or crinkle near the ends, as in the case of Mode I. Figure 4.26 shows the distinct failure mode.

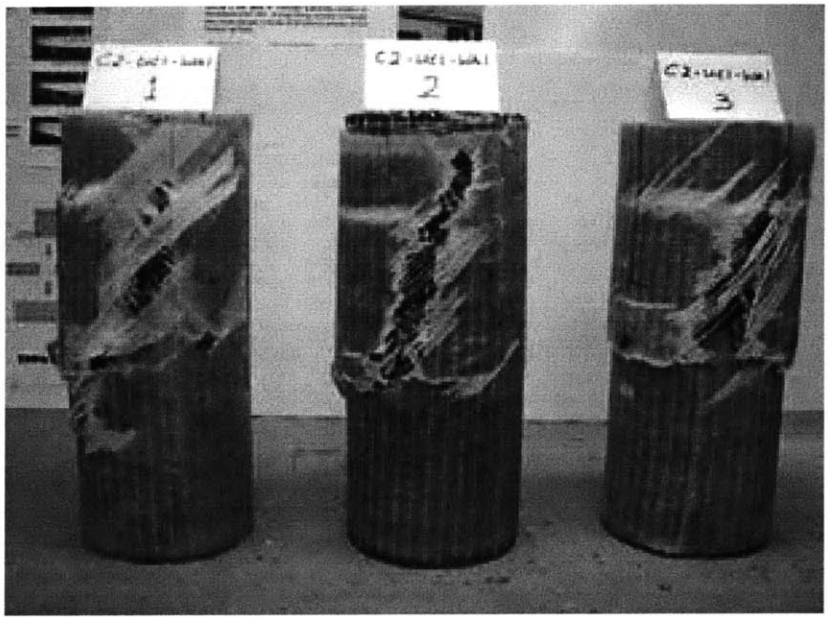

Figure 4.26 Failure mode V (C2 – UC1 – WA1)

Fiber fracture started at the middle third region. Upon further loading, the crack propagated upward at an almost vertical orientation. When the crack had extended to the upper third zone, it terminated in the vertical direction and began to stretch to the sides. A fracture wing was developed as in the case of Mode I. However, the fracture wing in this mode is much larger than the size in Mode I at the onset. The snipping action as described Mode I applied until, again, in front of the overlap. The crack initiation location was more random, though. The location was not predictable and did not just occur on the opposite side of either the UC overlap or the WA overlap. Failure was catastrophic and swift. Huge noise was heard upon jacket rupture. Upon dissembling, no clear shear crack could be found. Bonding between the two layers of different FRP was generally intact. No delamination occurred except some localized delamination occurred at the top of specimen one.

F. Mode VI – (C2 – WA1 – UC1)

Mode VI represents the failure of C2 – WA1 – UC1 specimens. This mode was very similar to Mode I in terms of outward appearance as shown in Figure 4.27. Fracture wings were formed within the middle third, though more uniform in width around the circumference. Catastrophic failure and swift failure were recorded.

Figure 4.27 Failure mode VI (C2 – WA1 – UC1)

The distinct phenomenon, however, was the debonding between the two layers. No concrete spalled off. No fracture was detected in the inner WA layer at all. And obviously, the failure mode was different from Mode V, in which the specimens employed the same materials but a different stack-up sequence of the fabrics.

Upon reaching the peak stress, the hoop fibers ruptured as normal at mid-height due to hoop tension failure. As the fracture wings developed and continuously opened up on each side, delamination between the two fabrics took place with an accelerated pace accompanied by a large peeling noise. After the peeling action, no concrete spalling off and the wings stopped opening up. Instead, a recoiling force brought them back to place right after the massive peeling. Then the load dropped significantly and eventually the test was stopped. When the specimens were inspected closely, it was found that the fibers of the WA layer did not reorient themselves as in the case of Mode III. All fibers remained the same as if nothing had happened.

For specimen three, overlap debonding instead of fiber fracture occurred due to insufficient bond length. The same peeling action took place and no damage was done to the inner WA layer as the other two specimens. The overlap debonding will be discussed in a later section in more detail.

Conclusion: Failure modes can be divided into basic modes and mixed modes. Basic modes represent the failures of single-ply wrapped cylinders. Mixed modes represent the failures of double-ply wrapped cylinders. It is noted that whenever hoop fibers are involved, the failures tend to be more catastrophic and swift. It is also noted that whenever angular fibers are involved, the failures tend to be more gentle and gradual. For the mixed use of hoop and angular fibers, the failure mode lies somewhere between the two extremes. Nevertheless, one should note that different stack-up sequences may yield distinct failure modes. For the composite materials used in the present study, when angular fibers are used as the inner wrap while the hoop fibers are used as the outer wrap, the angular fibers are capable of preventing any concrete spalling from the core, enhancing the safety of the damaged columns, as explained in a later section.

4.8.2.5 Load-Deformation Behaviors

Load-deformation behaviors can be most easily visualized by looking at the plotting. They can be categorized into three behavioral representations – axial, lateral, and volumetric. Stress-strain curves were plotted for each representation. The plots are (1) axial stress vs. axial strain, (2) axial stress vs. lateral strain, and (3) axial stress vs. volumetric strain. For clarity, only one set of curves representing a configuration type was selected for plotting. Peak values should not be directly compared because some scattering existed within a configuration. The values should be referred directly back to Sections 4.8.2.1 and 4.8.2.2. Figure 4.28 and 4.29 show the respective plots of axial strains and lateral strains versus axial stress. Respective peak stress and peak strain data are shown in Appendix D. Individual plots are shown in Appendix E.

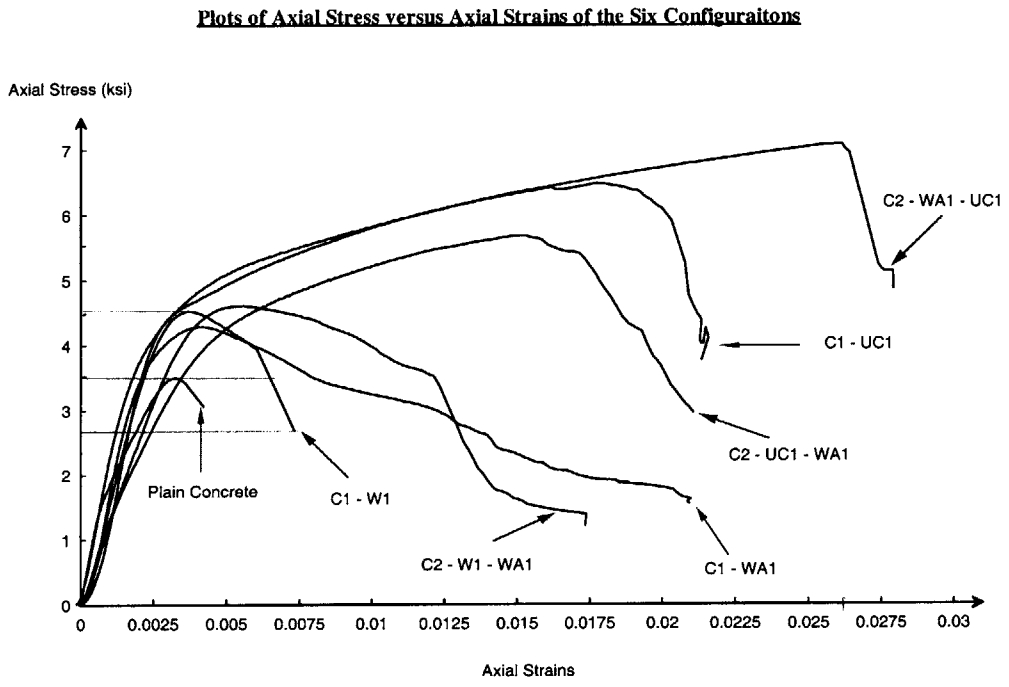

Figure 4.28 Plots of axial stresses versus axial strains

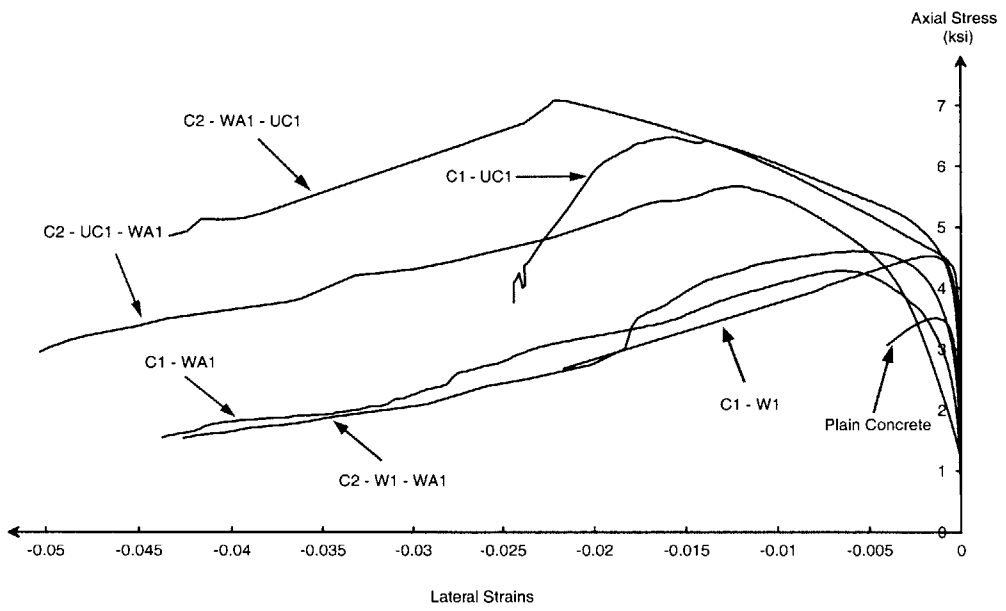

Figure 4.29 Plots of axial stresses versus lateral strains

Axial strain data used for plotting were obtained from the average measurements of the two vertical LVDT devices. Lateral strain data used for plotting were obtained from the lateral LVDT device. Measurements from LVDT devices were chosen over those of strain gages and extensometers in order to capture the global behavior of specimens. Also, strain gage results were reliable in a few particular cases only, as presented in Section 4.8.1.

Volumetric strains were computed from the axial strains and lateral strain by the following equation.

$$\text{Volumetric Strain} \quad \varepsilon_v = \varepsilon_a + 2\,\varepsilon_r = \varepsilon_a + 2\,\varepsilon_l$$

where ε_a is the axial strain, ε_r is the radial strain, and ε_l is the lateral strain. The sign convention follows the defined system in Section 4.3. It can be proved from mechanics that the radial strain equals the lateral strain in the case of a cylinder. Figure 4.30 shows the plot of volumetric strains versus axial stress.

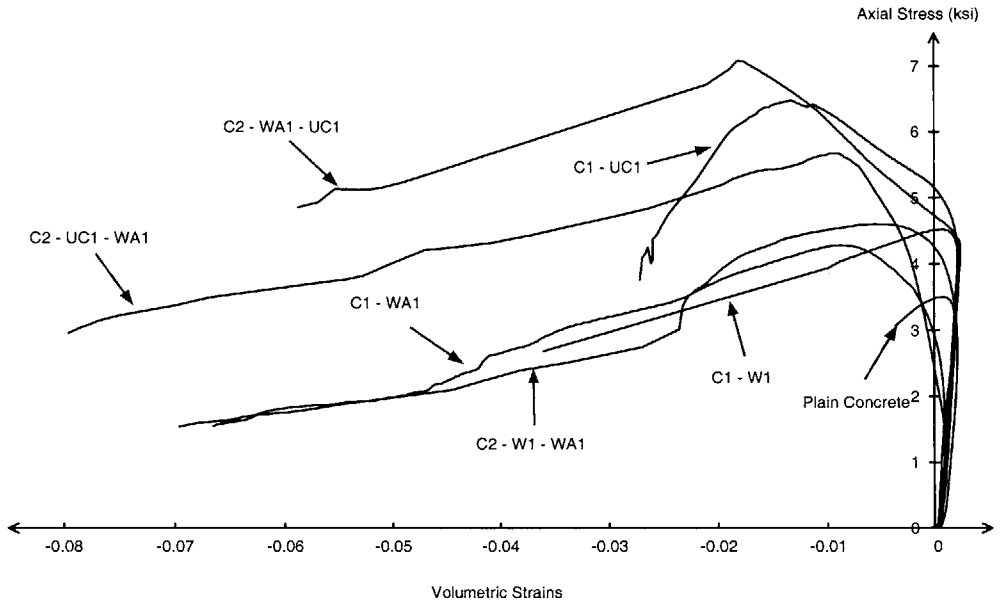

Figure 4.30 Plots of axial stresses versus volumetric strains

From the above plots, three major phenomena can be observed. First, the points, where the change of slope, occur do not coincide with each other. Some occur close to the unconfined concrete peak stress while the others far exceed that level. There shows a trend that the change of slope occurs at a higher level of stress when the peak stress of the specimen is higher. The vice versa applies.

Second, two major curve shapes can be observed. The first type demonstrates an approximate bilinear increasing behavior follows by a decreasing tail as shown in Figure 4.31. The second type consists of an increasing slope and a decreasing slope as shown in Figure 4.32. Among the six types, three are classified as Type I and the other three as Type II. The shapes apply to both axial and lateral strains. That is, for a given axial strain plot that appears as Type I, its corresponding lateral strain plot should also appear as Type I.

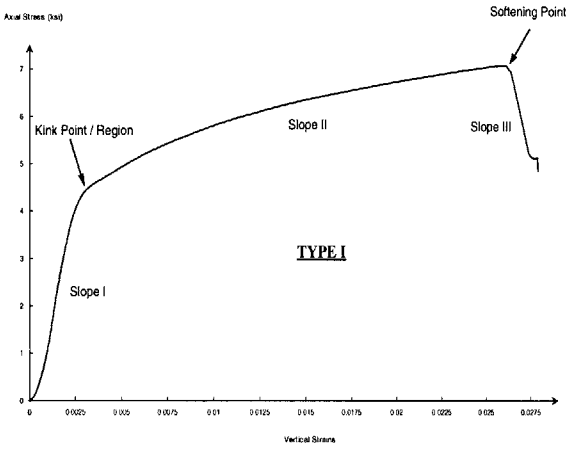

Figure 4.31 Axial strain curve Type I

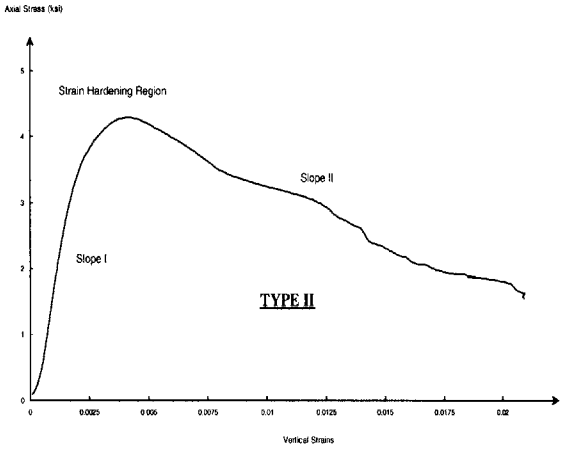

Figure 4.32 Axial strain curve Type II

Third, whenever WA wrap was involved, no matter it was the outer-wrap or inner-wrap, the descending tail had a slope that approximately follow that of WA alone (Configuration III). This phenomenon applies to all curves, regardless of the curve types categorized above.

Conclusion: Load-deformation behaviors can be divided into two main types. The first type is bilinear increasing. The second type is increasing-decreasing. Change-of-slope points occur at different stress level depending on the confinement strength. Slope of all descending tails are similar for those configurations that involve the angular fiber wrap. Brittle failures normally associate with the bilinear increasing behavior with a steep tail that follows the peak stress. Ductile failures normally associate with the increasing-decreasing behavior with a gentle and long tail that follows the peak stress.

4.8.3 Local Effects

4.8.3.1 Overlap Strengthening

For the one-wrap configurations, unbalance stress distribution could be found around the circumference. This phenomenon stands out when the axial strains on and opposite to the

overlap is compared. Figure 4.33 illustrates the differential axial shortening on a specimen of Configuration I measured by extensometers mounted on the fabric surface. The difference in strain was up to about 40%, hence considered significant. This phenomenon did not occur in all the two-wrap configurations, which had overlaps placed on opposite sides.

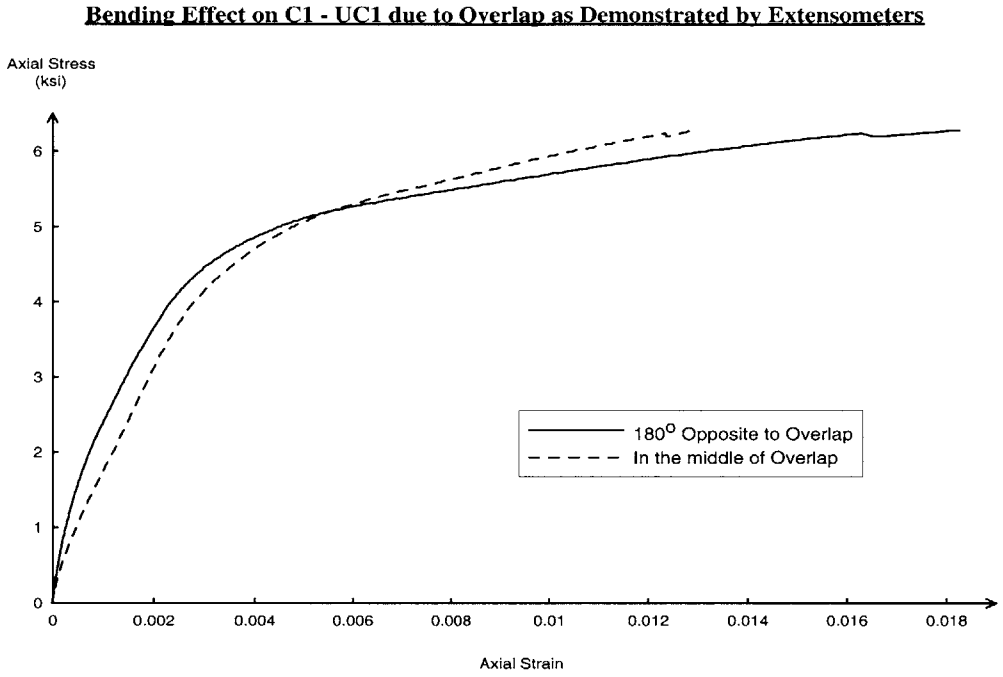

Figure 4.33 Differential axial strains due to an overlap

Conclusion: Differential shortening or bending effect is noticed for cylinders with an odd number of overlap joint. Unbalanced structural layout is resulted from the odd number of overlap joint. This effect is pronounced for the one-ply, one-overlap specimens. For specimens with an even number of overlap joints that are arranged symmetrically, the bending effect could not be detected.

4.8.3.2 Bond Delamination

Bond delamination occurred in some specimens of the two wrap-configurations. Configuration VI exemplified this phenomenon. Figure 4.34 showed the delamination between the outer UC layer

and the inner WA layer. Complete debonding occurred at the interface. No damage was done to the inner layer. This debonding was due to the peeling action as discussed in Section 4.8.2.4.

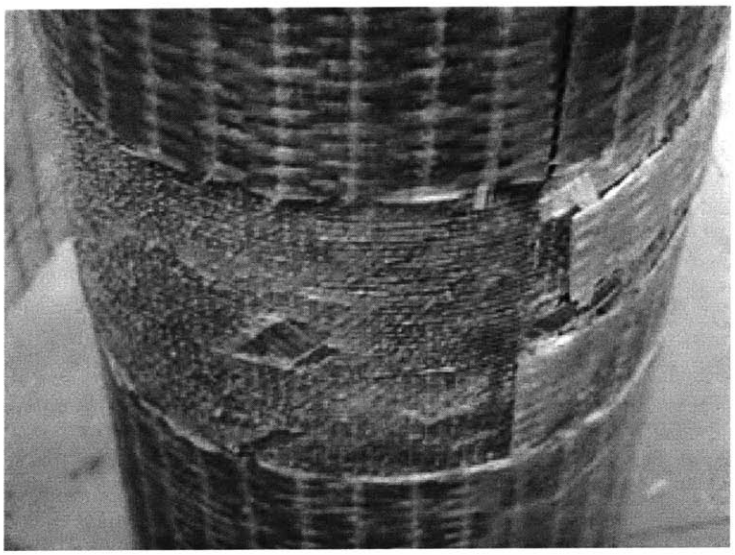

Figure 4.34

Complete delamination of C2 – WA1 – UC1 – SP3

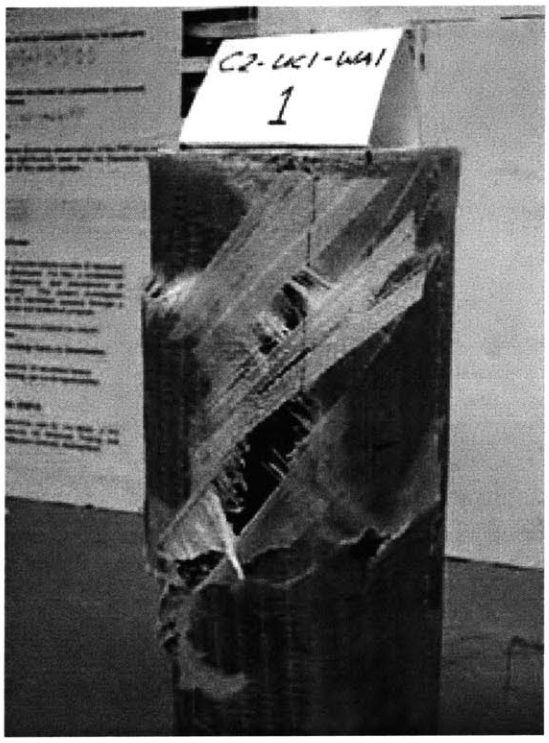

Figure 4.35

Partial delamination of the WA layer of C2 – UC1 – WA1 – SP1 near the top end (improper epoxy bonding result)

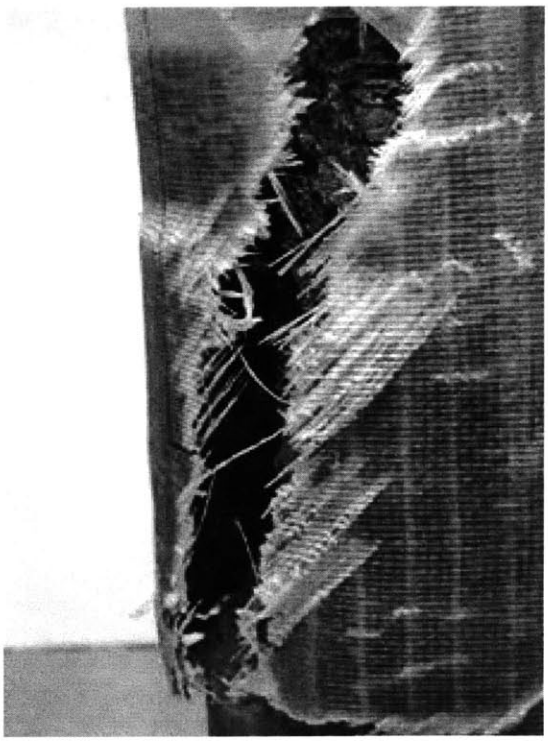

Figure 4.36

Intact bonding of C2 – UC1 – WA1 – SP2 at fracture (proper epoxy bonding result)

Figure 4.35 shows a localized debonding of part of the fabrics in a specimen of Configuration V due to poor epoxy bonding in a particular area near the top end. Figure 4.36 shows another specimen in Configuration VI that demonstrated no delamination at all.

Conclusion: Bond delamination does not occur in most cases. It only occurs in Configuration VI that consists of two different types of wraps. For this configuration, a peeling action is noted after the fracture of the hoop fibers. No damage is done to the inner angular fibers after the total delamination has occurred.

4.8.3.3 Fiber Buckling

Fiber buckling was found in all specimens that contained a vertical force component. Either the W fabric or the WA fabric was susceptible to some fiber buckling. All buckling occurred locally.

In the case of W fabric, where vertical fibers existed, local buckling gave rise to crack initiation at the bottom end, which was fully wrapped. The vertical fibers buckled and posed increasing tension to the crossing hoop fibers until they reached their elastic limits and fractured. The buckling out of the vertical fibers at the bottom edge gave rise to a phenomenon that can be described as an elephant foot like appearance. However, it could not be captured clearly after the cracks had developed and surged up the cylinder because the elephant foot had burst out.

In the case of WA fabric, where angular fibers existed, local buckling also occurred. The buckling mode was quite different from that in the W fabrics, though. Fibers did not buckle individually and broke subsequently the adjacent fibers. Rather the fibers buckled together to form a buckling ring around part of the circumference.

Fiber reorientation (Section 4.8.3.4) was seen in and around the ring but no fiber fracture occurred. In essence, the fabric wrinkled locally as shown in Figure 4.37. Local delamination occurred.

In the case of UC fabric, where unidirectional hoop fibers and some relatively sparse vertical linking fibers existed, local buckling did not occur at all. The bottom ends were not damaged and they were not the origin of crack development and propagation.

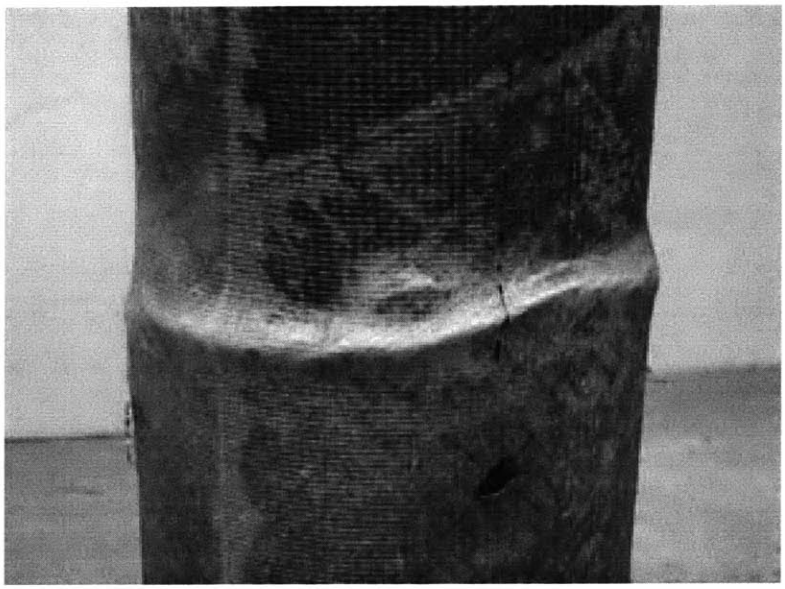

Figure 4.37 Local fiber buckling / fabric wrinkling in C1 – WA1 – SP3

Conclusion: Local fiber buckling is seen near the end surface whenever vertical fibers are involved. The fibers that buckle are not subjected to direct compression. Fiber buckling is found to initiate jacket failure. Local fiber buckling does not occur in angular fiber wrapped cylinders. Global fiber buckling is noted. A buckling ring is formed in the way of fabric wrinkling at about mid-height.

4.8.3.4 Fiber Reorientation

Fiber reorientation took place in angular fabrics of Configurations III. Figure 4.38 illustrates a change in fiber angle in the mid-height region after load. Fibers did not fracture but they elongated. When cutting through the fibers manually after test for inspection, it was found that the concrete inside experienced severe shear failure, as shown in Figure 4.39. The shearing angle was almost perpendicular to the reoriented angle of the fibers at mid-height. For instance, as shown in Figure 4.38, the reoriented

angle was 25-degree. The concrete shearing angle shown in Figure 4.39 was about 65-degree to the horizontal. When computing from geometry, the shear cone height is about 12", which is quite close to that shown in Figure 4.39. Specimens 1 and 2 show very similar fiber reorientation angles and shear cone heights as illustrated in Figure 4.24.

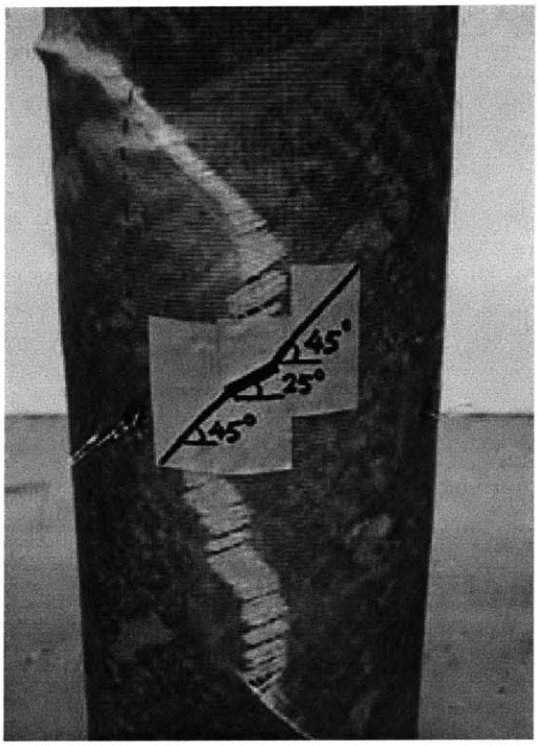

Figure 4.38
Fiber reorientation in C1 – WA1 – SP2

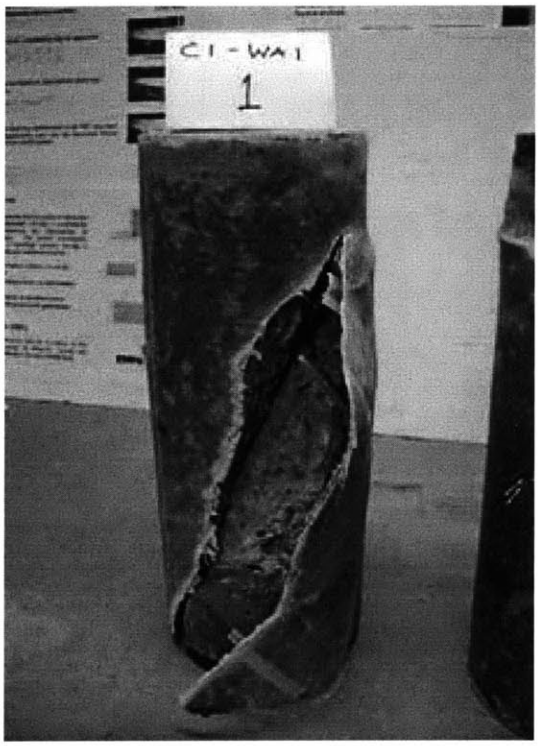

Figure 4.39
Concrete shearing fracture within fabric

Conclusion: Fiber reorientation is a unique phenomenon to the angular fibers. It is a rigid body motion and result in more capacity for fiber elongation up till their elastic limit. The reorientation occurs mostly within the mid-height region.

4.8.3.5 Fiber Snipping Action

Fiber snipping action occurred mainly in Configuration I. The snipping took place when the fabric wing opened up and tried to tear apart the longitudinal linking fibers. When a linking fiber was snipped, the fabric wings were able to open up and allow more crushed concrete to fall off from the core. This action was enhanced by the sound adhesion of the fabric immediately above the fracture wings. Figure 4.40 shows a close up of the

snipping action of the final linking fiber just after failure. The linking fiber was sheared and the fiber angle changed at the snipping plane. Figure 4.41 shows the fabric wings with intact FRP-concrete bonding and the crushed concrete core.

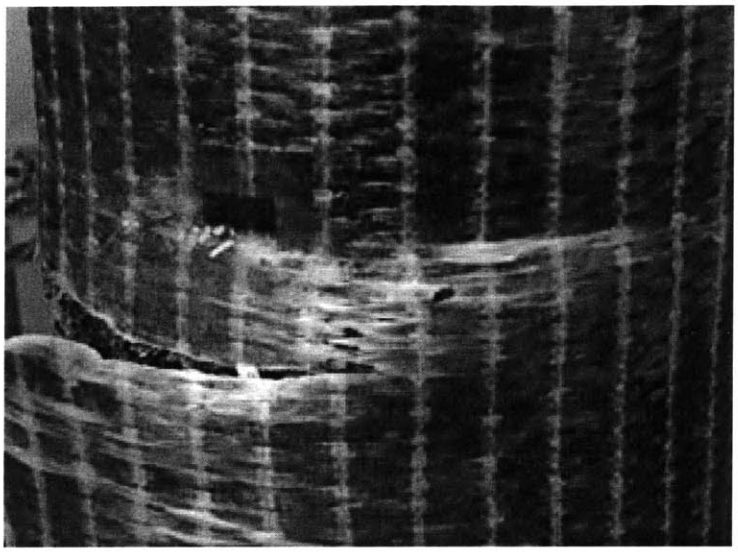

Figure 4.40

Close-up of the snipping action on the longitudinal fibers of C1 – UC1 – SP3

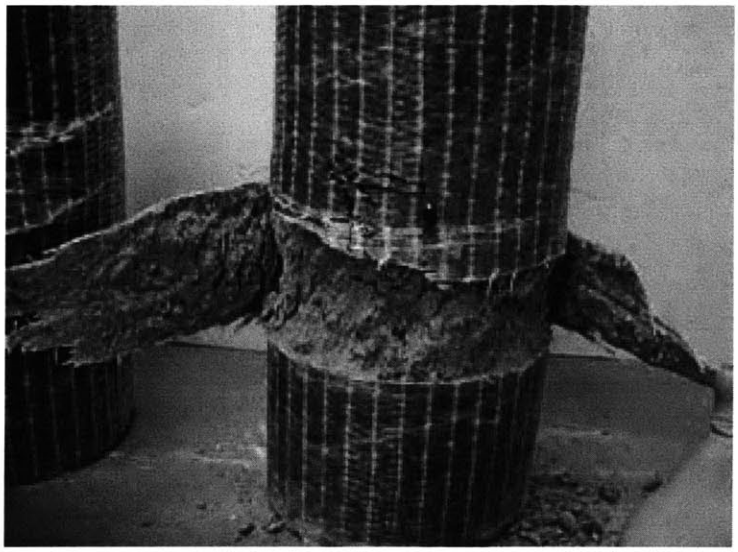

Figure 4.41

Fracture wings straightened up manually after test; crushed concrete core; intact FRP-concrete bond on the wings

Conclusion: Fiber snipping occurs in Configuration I. It represents the shearing of the longitudinal fibers by the fracture wing. The snipping action takes place gradually one by one as the fracture wing opens up due to concrete expansion.

4.8.3.6 Local End Condition of Unconfined Concrete

Concrete at the top end, which was unconfined did not break in all specimens. Figure 4.42 shows the sound condition at the top and a crack that surged up from the bottom to about two thirds of the specimen height in C1 – W1 – SP2. The picture was taken right after the specimen being removed from the loading machine.

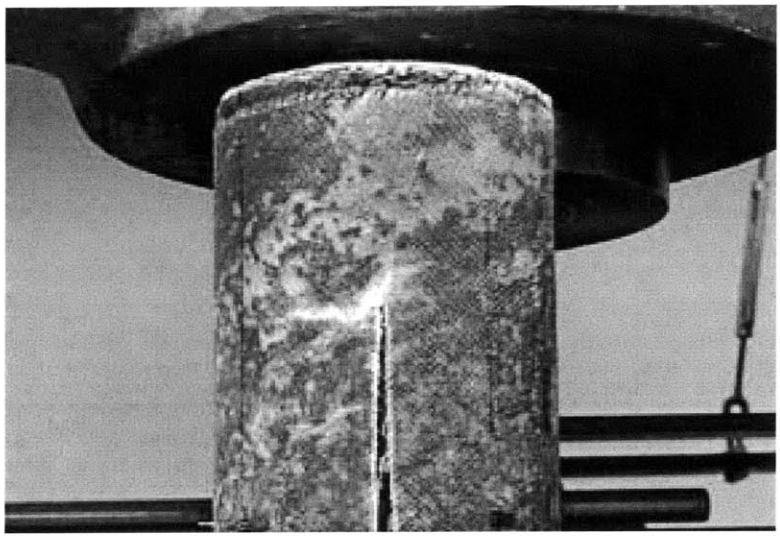

Figure 4.42

Sound concrete condition at the unconfined top

Conclusion: Unwrapped concrete of 0.5" height at the end surface does not fail in crushing.

4.8.4 Manufacturing Effects

4.8.4.1 Air Pockets

A few thumb-sized air pockets were entrapped in two specimens in Configurations II and IV. The air pockets were located randomly, although more of them were in the upper portion of the specimens. In both cases, the air pockets acted as nuclei for delamination. Delamination normally occurred mainly from the cracks and then starting from there, the delamination would flow to the closest nuclei. Air pockets that were not close to the cracks did not establish the airflow channel. Instead, localized whitening patch could be

seen growing around the air pocket, signifying a growing delamination area. Although localized delamination occurred, the ultimate load capacity did not seem to have changed. But, the stress reduction rates of those specimens with entrapped air were in general faster than the others after peak load.

Conclusion: Air pockets are seen to form airflow channels and enhance delamination growth especially after the peak stress. It is noted that thumb-sized air pockets do not affect the peak strength of the cylinders.

4.8.4.2 Overlap Debonding

Overlap debonding was detected in one specimen that had a shorter overlap. The overlap length was 2.5" (or 13% of the circumference) while all the others were 3" (or 16% of the circumference). This specimen belonged to Configuration VI, which showed the peeling action between the two fiber types.

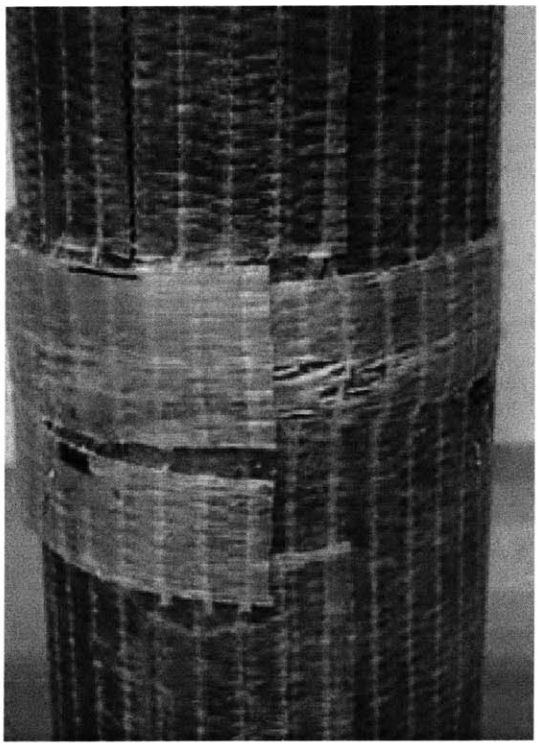

Figure 4.38
Overlap debonding in C1 – WA1 – UC1 – SP3

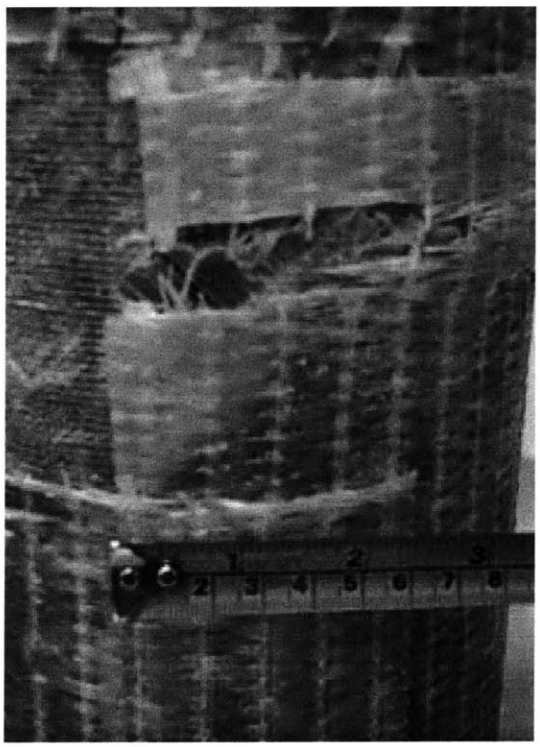

Figure 4.39
Overlap bond length of about 2.5" (or 13% of the circumferential length)

The failing mechanism of this specimen was not fiber fracture on the outer-wrap, but solely due to debonding. Ultimate load of this specimen was slightly less than the other two. Figure 4.43 shows the close-up of the overlap debonding. Figure 4.44 shows the overlap length measurement after bond failure.

Conclusion: Overlap bond failure occurs when the overlap length is too short. In the present study, the sufficient overlap length is found to be 3" and is believed to be epoxy property dependent.

4.8.4.3 Effects of Epoxy Bond Quality on Strength

Epoxy bonding quality was proved to be influential to the ultimate strength of a wrapped specimen to a large extend in some cases. In Configuration V (C2 – UC1 – WA1), it was reported that significant scattering of data took place. The range of the ultimate load capacity was large. When comparing the initial wrapped cylinders and the final tested cylinders from the snapshots in terms of color reflection, it was found out that the strength could be correlated to the laminate bond quality and thickness.

It was discovered that for the cylinder that had a lighter surface color, reflecting a thinner epoxy bonding, the ultimate load was higher. On the other hand, the cylinder that had the darkest surface color, signifying sound adhesion between the two layers, the ultimate load was lowest.

The dark color that showed on the wrapped cylinder represented that the wraps were tightly adhered to the cylinder surface such that the wetted concrete color, which was dark gray, showed up on the surface. The lighter color resembled the discoloring during delamination upon loading. This reflected a gap existed in between the layers because light was reflected in the gap layer instead of reflected from the wetted concrete surface.

In other words, in the two-ply cases that consisted of a mix use of materials, the epoxy bonding may influence the axial strength. This phenomenon will be discussed in detail in a later section.

Conclusion: Epoxy bond quality is found to have impact on the peak strength. Better bonding seems to lead to a faster initiation of defects development in the adjacent layer. For other cases where no adverse interlaminate effect exists, the bond quality is not influential to the peak strength and failure mode.

Master Summary of Results

The results will now be summarized and tabulated to give the essences of the findings. Details are not described and should be directed to previous subsections. Table 4.9 shows the instrumentation issues of strain gages. Gage performance, fiber-gage misalignment effects and epoxy surface filling effect are presented in a qualitative manner. Table 4.10 summarizes all the results of all six wrapped configurations including peak stresses, strains at peak and at ultimate, stress reduction rates, failure modes, load-deformation behavior type, local effects, and manufacturing effects.

Table 4.9 Summary of Strain Gage Instrumentation Issues

Gage Type	Performances on Test Surfaces (Gages aligned with fibers)			Fiber-Gage Misalignment Effect	Epoxy Surface Filling Preparation
	UC	W	WA		
350-ohm Single Gage	Excellent	Significant Overestimation	Poor	Significant Underestimation	Required
350-ohm Tee Gage*	Good	Significant Underestimation	Poor	Significant Underestimation	Required
120-ohm Steel Gage	Significant Underestimation	Underestimation	Poor	Not tested	Required

* Aspect ratio of this gage type was 1.0. The other two were 2.0.

Table 4.10 Summary of FRP-Confined Concrete Responses

Configurations	Peak Stress (av.), psi	Strains**		SRR*** (average) psi/sec.	Failure Modes	Load-Def. Behavior ****	Local Effects	Manufacturing Effects
		@ Peak Stress	@ Ultimate					
I C1 – UC1	6351	A = 0.0163 L = -0.0143	A = 0.0221 L = -0.0369	-30.83	• Catastrophic • Fiber fracture • Concrete crushing • Overall bending stress development	Type I	• Overlap strength-ening • Longitudinal fiber snipping	None
II C1 – W1	4327	A = 0.0043 L = -0.0038	A = 0.0084 L = -0.0315	-63.63	• Catastrophic, swift • Shear, split • Concrete cracking • Fabric unzipping and fracture up till 2/3 of height	Type II	• Fiber buckling at bottom end • Local fabric delamination with concrete	• Air pockets encouraged delamination flow
III C1 – WA1	3916*	A = 0.0050 L = -0.0076	A = 0.0159 L = -0.0272	-9.69	• Very ductile • Fiber elongation without rupture • Concrete crack in shear	Type II	• Fiber reorientation at mid-height • Fabric wrinkling at mid-height	None
IV C2 – W1 – WA1	4615	A = 0.0055 L = -0.0056	A = 0.0150 L = -0.0274	-15.38	• Ductile • Fiber elongation without rupture • Localized fabric cracking at mid-height • Concrete cracking without spalling	Type II	• Fiber reorientation at mid-height • Local fabric delamination	• Air pockets encouraged delamination flow
V C2 – UC1 – WA1	6184*	A = 0.0166 L = -0.0148	A = 0.0245 L = -0.0478	-38.17	• Catastrophic • Fiber fracture • Concrete crushing	Type I	• Bond delamination in one specimen	• Good epoxy bond induced lower ultimate strength
VI C2 – WA1 – UC1	6990	A = 0.0260 L = -0.0221	A = 0.0298 L = -0.0393	-26.48	• UC fiber fracture • No damage to WA • 1/3 concrete crushing • Fabric delamination through swift peeling	Type I	• Bond delamination with peeling action	• Overlap debonding due to shorter overlap length (2.5")

* Significant scattering of results (about 10% standard deviation)

** A = axial strain; L = lateral strain

*** SRR = Stress Reduction Rate

**** Type I = bilinear increasing-decreasing; Type II = increasing-decreasing

4.9 Results Interpretations and Discussions

Following the result presentations in Section 4.8, this section focuses on the corresponding interpretations and the possible applications to real-world problems and further researches in this area. The following is organized into six subsections. The first four subsections follow the order of the investigated areas as presented in Section 4.1. The last two subsections respectively discuss the possible inferences and applications from the current experimental results to real-world retrofit and strengthening practices as well as to further researches in the same area.

4.9.1 Strain Gage Instrumentation Issues

4.9.1.1 Need of Epoxy Surface Filling before Strain Gage Installation

It was found out that strain gages need to have flat surfaces to function normally. Gage foils should not be distorted if the correct initial circuit voltages and subsequent accurate measurements are to be obtained. The gage foil is responsible for strain detection through the resistance change mechanism. Resistance change and the corresponding strains are correlated linearly. Once the gage is distorted non-uniformly in directions that do not align with the principal gage direction, the resistance change linearity response may not hold, giving rise to erroneous results. On the other hand, firm adhesion of the entire gage backing is needed to develop sufficient sensitivity of local strain transfers and to enable accurate averaging of strains under the gage area. Therefore, on composites that consist of deep and dense roving ridges, the epoxy surface filling procedure is an imperative before any strain gage fixation to take place.

4.9.1.2 Influence of Gage Resistance

Gage resistance is found to have significant influence on the results. In this investigation, both 120-ohm and 350-ohm strain gages were studied. Low resistance seems to have adverse effects to the accuracy. When using two gage types with identical gage properties but different resistances, affixing on identical sites and oriented in the same directions, it was found that the lower resistance gage (120-ohm) gave rise to significant underestimation of the measured strains. The strains measured by the 350-ohm gage were

close to that of an independent measuring device (LVDT). One should note that the lower the resistance, the higher is the current running through the gage foil for a given input voltage because of the following relationship.

$$V = I \times R$$

such that V = input voltage, I = current, R = resistance. The higher the current, the more heat is generated. Unlike steel or concrete, FRP composites consist of epoxy, a matrix material that is heat sensitive. Therefore, the exothermal foil gage will have changed the material properties locally and the material that lie underneath the gage acts as a heat sink, if the heat release is substantial.

4.9.1.3 Effects of Gage Aspect Ratios

Comparing the results of the two 350-ohm strain gages, one with an aspect ratio of 1.0 while another with an aspect ratio of 2.0, there is no substantial difference in measurements in the case of unidirectional fiber surfaces. However, it could be noted that the gage with the lower aspect ratio, the results tended to be slightly underestimated. From a structural point of view, differential strains should occur in the fibers and in the matrix material because of their different elastic properties and Poisson's ratios. Also, the deformation of FRP composite is dominated by the fibers because they are the major load-resisting elements. When the gage is narrow and is installed on top of the fiber roving, the measured strains will reflect closely that of the fiber roving itself.

On the contrary, when the gage is wide, for a given gage length, the percentage coverage of both the matrix and fiber roving has increased. Thus, it can capture the local strains produced in the fiber roving as well as the matrix. Now that the roving is strained more than the matrix locally, the average strain captured by the strain gage will be lower. Hence, the measurements show some underestimations. This underestimation was amplified when this type of gage was used on the bi-directional fiber surfaces, which had substantial amount of stressed fibers running underneath the gage foil in a deviating direction (explanations see below).

4.9.1.4 Poor Results of Fiber-Gage Misalignment

Strain gages are designed to measure strains in the principal gage direction. The performance is best when the straining direction align with the principal gage direction. When gages and fibers do not align with each other, the gage foil will be strained to a certain extent in the transverse direction. This transversivity effect can produce significant error in measurements (Book: Tuttle 1989).

In the current study, it was found out that an underestimation of as high as 32% could occur in some specimens if there was fiber-gage misalignment. In fact, when there are stressed fibers running underneath a gage, the gage is strained in more than one direction significantly.

For instance, having a strain gage installed in the hoop direction of a WA surface, the 45-degree fibers are running across the gage in orthogonal directions. When the cylinder is compressed axially and expand laterally, the fibers are stressed and there are literally four significantly stressed directions pulling and pushing the gage foil locally. Local shear stress develops as a result and is evidenced in the fiber reorientation as shown in Figure 4.38.

In some part of the foil, it is in tension; in another part, it is in compression. The worst is that the gage is not pulled or pushed in the foil filament direction such that the filaments do not extend or contract longitudinally; they are subjected to the stresses transversely. Since the gage is not capable of decoupling the strains to align with the filaments and total them to get the net strain, erroneous readings are resulted.

For a simpler case such as that in Configuration III, in which the W fabric was the measuring surface, the effect is more readily visualized. Let us consider the following example.

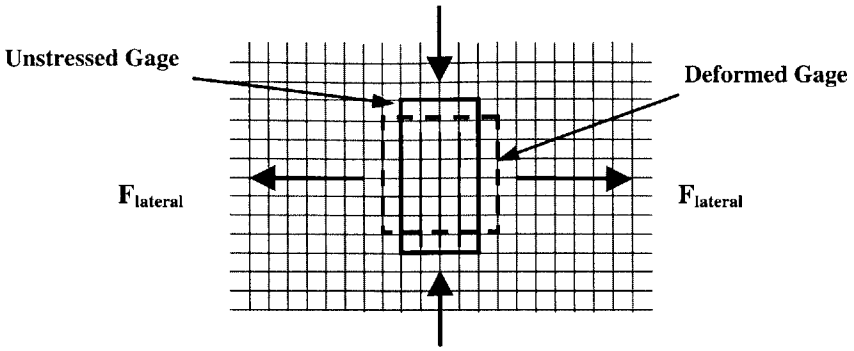

Figure 4.45 Doubly stressed actions on a strain gage

As shown in Figure 4.45, when a gage is installed vertically to measure the axial strain on a loaded cylinder, the gage is actually subjected to both hoop and axial stresses simultaneously. Owing to the simultaneous vertical compression and horizontal pull, the gage will deform in the way as shown in exaggerated shape in the diagram. Now that the gage is shortened and widened by the horizontal pull to a certain extent due to the in-plane Poisson's effect on the gage material, the actual axial shortening detected by the gage in the vertical direction will be smaller. The stress in the orthogonal direction to the stress that aligned with the gage filament had, therefore, an effect of pseudo-strain-reduction. Consequently, the change in resistance in the filament is less and hence a smaller average axial strain under gage is resulted. This logic also applies to the case when the gage is installed in the hoop direction while vertical stressed fibers are running underneath the gage. As a result, underestimations were recorded for all gages mounted on the W surfaces.

4.9.2 Loading Effects

Configurations I, V and VI, that consisted of UC fibers showed the highest peak stresses because of the higher tensile strength of the UC materials themselves. Load-deformation curves showed a bilinear increasing behavior in these three configurations. Those consisted of W and WA fibers showed lower strengths. Load-deformation curves did not show any bilinear increase. Instead, the increasing-decreasing behavior was observed.

Configurations V and VI showed quite different average ultimate strengths, strains, stress reduction rates, and failure modes, although they were made of identical FRP materials in the confinement shell. Configurations II and III also did not show similar failure modes, and stresses and strains, although similar strength of FRP were used in the hoop direction. However, the fiber orientations in these two cases were different.

Strains were observed to have some correlations with the level of peak stresses. In all test cases, the higher the peak stress usually implied the higher the corresponding strains and the ultimate strains due to more energy absorption from aggregate disintegration and air void compression. Lateral strains were normally less than the corresponding axial strains at peak. But the ultimate lateral strains were, in all cases, larger than the corresponding axial strains. Moreover, stress reduction rate was the slowest for the most ductile failure, which was Configuration III; the fastest stress reduction occurred in Configuration II, which had the lowest lateral fiber content and fiber buckling initiation of fabric crack. Finally, stress increases in IV and VI showed linearity while V did not.

4.9.2.1 Inter-relationships Among Confinement Mechanisms, Load-Deformation Behaviors, and Failure Modes

It was found out that the load-deformation curve shape was highly dependent on the confinement level. Failure modes were also a reflection of the confinement mechanisms and the curve types. Therefore, they were discussed together in the following, which is organized into UC, W, and WA confinement cases. Only the basic modes are dealt with in here. Mixed modes will be discussed in later sections

Case UC

When the high strength unidirectional UC fabrics were used, the curves showed a bilinear increasing behavior. This signified significant energy absorption by the confinement after the concrete has crushed and failed to take up any further loading. Slope II of the bilinear curve showed more ductility than Slope I (Figure 4.31). This implied that a wrapped concrete cylinder was much less brittle than an unwrapped concrete cylinder. Concrete crushing instead of cracking occurred in such cases of high level of confinement. Voids

entrapped in the concrete were minimized and aggregates were disintegrated. During the particle disintegration process, energy was consumed. When the disintegration could not take place any further, they were forced to expand upon further axial compression due to volumetric dilation according to the hybrid bulk modulus. The crushed particles pushed against the confinement, which in turn took up the internal pressures and transformed them into hoop tension in the fibers. Since the pressure increased with more lateral dilation, energy was stored in the wrap during the expansion process. Hence, Slope II was seen to be less steep than Slope I. The linear elastic properties of the fibers were reflected in the second linear increasing slope, which signified linear energy absorption. When reaching the elastic limits, the fibers ruptured catastrophically right after the peak stress, signifying a sudden energy release. Complete failure took place when excessive fibers ruptured and concrete spalled off from the core severely such that the cylinder could no longer bear additional axial compression.

Case W

When the lower strength W fabrics were used, the cures showed the increasing-decreasing behavior instead. This curve type resembled that of unconfined concrete. Insufficient confinement allowed the concrete core to crack as if it was unconfined. The cracking dissipated external energy and the core expanded when the blocks of cracked concrete moved against one another, along with their respective expansion under load. This expansion imposed a tension on the fibers of the confinement. Upon further radial expansion, the fibers were stressed to their elastic limits in the hoop directions and fractured momentarily. Since the energy absorption by the fibers was comparatively small, the fibers broke before any additional ductility could develop. Therefore, Slope II of curve Type I could not took place as in the case of UC. The decreasing slope was then immediately entered because the cylinder could not take any further loading.

Case WA

The curve shape of specimens that were wrapped with WA fabrics was very similar to that of specimens that were wrapped with W fabrics. The concrete cracking mechanism

was also similar to that of the W confinement. However, fibers did not fracture. They instead reoriented and elongated to allow for the chunks of cracked concrete to further dislocate and move against each other along the shear plane in order to expand. The fiber reorientation could actually be seen as a rigid body rotation. When decomposing the force component from the hoop direction to the angular fiber direction, the actual loads experienced by the fibers were substantially smaller. Therefore, fibers did not fracture because they were not loaded up to their elastic limits yet, even after the entire cylinder could not take any further loading due to the large gaps found within the concrete core. The reorientation took place spontaneously to redirect the fibers to the principal load direction, which occurred circumferentially, to help absorb as much energy as possible. This rigid body rotation took up energy because the fibers had to overcome the traction of the epoxy matrix and had to deform adjacent fibers in order to allow the rotation to take place. This energy dissipation mechanism was found to produce surprisingly ductile failure mode to a stress level as low as 30% of the peak load without fiber fracture.

4.9.2.2 Change-of-Slope Upward Shift Phenomenon

The point where change of slope occurred from Slope I to Slope II in curve Type I is defined hereafter as the kinking point. Comparing the three Type I composite systems, kinking shifted up the stress scale as the confinement strength and ultimate load capacity increased. The shift signified that the concrete core allowed more external energy absorption and delayed its substantial expansion until a higher stress level when all fibers were stretched and stiffened up.

The increase energy absorption and delayed activation of the composite jacket was due to the aggregate disintegration action and the closing up of air voids in the concrete core. The higher the confinement level, the more the aggregates disintegrated themselves because the confinement shell was able to hold the aggregates inside the shell without significant lateral dilation. The aggregates transformed the axial compression to lateral expansion due to the Poisson's effect. This Poisson's ratio increased when the particles became more incompressible because the air voids could not be closed and the energy could not be dissipated further due to the action of aggregate disintegration. Until a point

where the aggregates possessed a high Poisson's ratio such that they exerted substantial pressure on the confinement shell, the shell would move and the kinking took place, as noted from the change of slope from Slope I to Slope II in curve Type I. This kinking, from the above arguments, should shift upward upon having a higher level of confinement pressure. Theoretically, the kinking upward shift should stop at a certain level of confinement for a given type of concrete because the concrete could not infinitely absorb energy by compressing the air voids and disintegrating aggregates. There should exist a point where the air voids are completely compressed and the aggregates are completely disintegration such that the lateral dilation has to take place no matter how many more number of wraps is added to the confinement.

4.9.2.3 Load Responses due to Different Fiber Stack-up Sequence

It was proved that different fiber stack-up sequence could have tremendous impact on the confined concrete in terms of ultimate strength, strains at peak stress, stress reduction rate, and failure mode. Configurations V and VI aimed to study this effect. In V, WA wrapped around UC while in VI, the order was reversed. The result was that the ultimate load increase of VI was much higher than that of V. The outer-wrap of VI peeled off from the inner layer. This did not occur in V. The two layers of FRP in V stayed intact together without any delamination.

The failure modes can be explained from the mechanics point of view. In the following, it will be assumed that a perfect bond existed initially between the WA and UC fibers when unstressed and that the WA has a lower tensile strength and Young's Modulus than UC. It is also assumed that the two fabrics had the same thickness so as to simplify the arguments.

Case VI

For Configuration VI, considering a piece of combined fabrics with unit width subjected to a simple tensile pull individually, without attaching onto a concrete cylinder, a bending stress will be generated due to the differential stiffness of the two materials. The more ductile WA1 fibers displace more than the UC fibers under a given load. When the

displacement compatibility condition at the interface is to hold due to the perfect initial bond assumption, bending has to occur with the center of curvature on the side of the stiffer material. WA fibers will fail first, when the loading has past the strength of the fibers, because of their lower tensile strength.

If, however, the combined fabrics are not allowed to bend by keeping straight the tensile pull, for a given displacement, the stress developed in UC will be higher because it is a stiffer material, as shown in Figure 4.46.

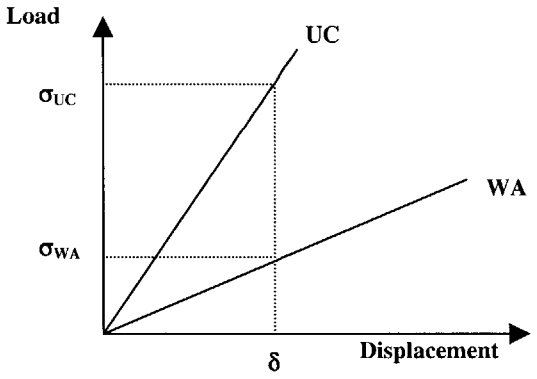

Figure 4.46 Different stresses for a given displacement on UC and WA fibers

Since the WA fibers can elongate and reorient themselves to accommodate the large displacement under the tensile pull, the UC fibers will eventually break first, due to the higher stresses developed. Once the UC fibers fracture, they tend to contract back to the original length due to the elastic property. This contraction imposes a shearing force at the interface and hence on the epoxy bonding. When the contracting force exceeds the shearing strength of the epoxy, delamination occurs. The above argument holds for the test case when we consider a finite length that is tangent to the cylindrical surface of the wrapped cylinder in the hoop direction, which is subjected to surface tension.

In reality, the cylinder surface is not straight. When the UC fibers on the surface start to fracture, the shearing action will move incrementally along the circumference. The shearing eventually becomes a peeling action when the finite tangent length grows to a length with substantial curvature due to the circumferential geometry. The fractured

fibers, after releasing the energy, have a tendency to align tangentially with the curved stressed portion of the same continuous fibers that are not yet detached from the inner layer. This tangential alignment action promotes further accelerated failure, which was seen during test. Once the peeling action has started, it will propagate along the circumference with a constant force of initialization until the energy is completely dissipated. Figure 4.47 shows the fractured UC fibers and the undamaged inner WA fibers. It should be noted that the fibers on the right of the picture shows the natural tangency after the delamination, validating the above arguments.

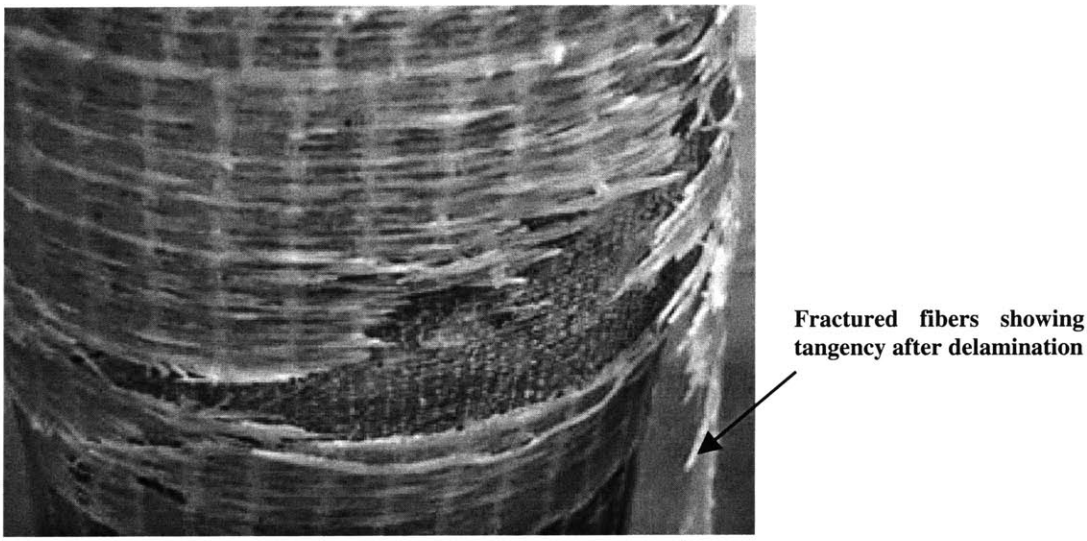

Figure 4.47 **Intact inner WA layer but ruptured outer UC layer of C2 – WA1 – UC1 – SP1**

Case V

The same basic mechanism also applies to Configuration V, which had the fibers stacked up in the reversed order. Now that the UC inner layer ruptures first for a given elongation, the broken fibers cannot follow the tangency and peel off freely outward due to the confinement of the WA layer and the inner pressure exerted by the concrete core. The UC layer now acts as the middle layer of the sandwich system. The fractured fibers transferred the load spontaneously to the adjacent layer suddenly. Hence, the stress surged up locally in that periphery within the WA layer and the fibers have to break upon reaching the elastic limit. The failure therefore appeared that the fibers failed together at the same time. But in fact, it was the inner layer failed first and the load was transferred

to the outer layer, although the process of load transfer to the reaching of the elastic limits of the WA fibers could take a short time. Both layers ruptured and concrete was crushed and spalled off from the core.

Effects of Epoxy Bonding Thickness and Quality

It was also noted that for a poorer initial epoxy bonding between the two layers of fibers, a higher ultimate strength could result. Moreover, within Configuration V, scattering of results was pronounced. When one looks at the load-transfer mechanism closely, the phenomenon can be explained. As said, the UC fibers break first within the wrap of the WA fibers. When those fibers break, the epoxy matrix that surrounds the fibers also fractures. Now that the epoxy that surrounds the UC fibers also surrounds, in part, the WA fibers on the side at the interface. The fracture of the epoxy will lead to the fracture of the WA fibers. Therefore, with a sound bond between the fabrics, the load transfer will be accompanied by a premature fracture of the WA fibers when the UC fibers fracture just started to initiate. This premature fiber fracture in the WA fabric would, in turn, affect adversely the UC fibers that were not fractured due to tensile straining. Hence, when comparing the ultimate loads of Configurations I and V, it could be seen that I even had a higher strength than V. When a poor bond exists in between, for instance an air gap exists, the fracture of the WA fibers had to wait until the elastic limits of their own have reached when the UC fibers are fractured severely so as to lost the confinement effect, instead of triggered by the fracture of the UC fibers alone. Therefore, the load increase of those cylinders with poorer bonds was higher while those with sound bonds was lower due to the premature fiber fracture in WA outer layer.

4.9.2.4 Load Responses due to Different Fiber Orientations

It was discovered that the load responses of the W wrapped cylinders were very different from the WA wrapped cylinders. W wrapped cylinders failed in brittle mode with fiber buckling and fabric unzipping. WA wrapped cylinders failed in ductile mode with fiber elongation, localized fabric buckling and no fiber fracture. Also, the failure loads of W wrapped cylinders were higher while that of WA wrapped cylinders were lower, although

the two fabrics had similar tensile strength. This signified the different roles of fiber orientations as a confinement shell.

Case W

One should note that all the wraps were not wrap from top to bottom all the way to prevent direct axial compression of the fibers. However, interestingly, the vertical fibers still buckled under load. This has confirmed that the vertical fibers resisted vertical loads through the distributed shearing stresses at the interface that was in contact with the concrete while the vertical stresses vanished towards the exposed surface of the fibers. Due to the local differential surface shear stress distribution, the fibers had to buckle out, although not subjected to direct compression. This shear resistance gave rise to the higher ultimate load of the W wrapped concrete specimens. Since the vertical fibers buckled locally mostly at the bottom end, the crossing hoop fibers were strained due to the buckling action. Eventually, the hoop fibers were strained to their elastic limit and fractured. Now that the fibers were weaved in orthogonal directions, the seams between the ridges provided guided rails for the crack that initiated from the bottom to propagate upward. This propagation was accelerated up the height because the hoop stress became increasing larger when traveling up to mid-height. The hoop fibers were therefore snipped one by one until the wrapped specimen could not take further load. The brittleness was therefore due to the crack propagation as well as the swift fiber snipping action.

Case WA

For the WA wrapped specimens, the failure mechanism was very much different. Fibers did not fracture because their elastic limits could not be reached. However, as the cylinder was shortened by compression and dilated by the shear displacement of the cracked concrete, the fibers could reorient themselves more to the hoop direction to allow more lateral expansion. When the reorientation of 20 degrees took place, the horizontal width of the fibers that were originally 45 degrees to horizontal now became 10% longer due to rigid body rotation alone. This action therefore allows a lot more room for the

concrete core expansion before the fibers are actually strained. Moreover, this rigid body motion absorbs much of the energy and so, even if the fibers finally fracture due to straining, the energy release should not be as much as the other fabric types.

4.9.2.5 Implications of the Stress Reduction Rate

Stress reduction was found to relate directly to the fiber content in the hoop direction as well as the type of fibers used in the confinement. When comparing the rate of I to II, it can be noted that II reduced stresses much faster than I did. The reason is that fiber fractures incrementally within the roving. From a statistical point of view, the fiber strength should vary according to the Gaussian distribution. The weakest fiber breaks first, then followed by the stronger fibers. Therefore, for a fabric with higher fiber content, the stress reduction rate should be lower than that of a fabric with lower fiber content. Therefore, it should be intuitive that II failed much faster than I.

On the other hand, the stress reduction rate also depends on the fiber orientation. Configuration III shows the slowest stress reduction because the fibers actually did not break because of the fiber reorientation action. It is noticed that whenever WA is involved in the confinement, the rate of stress reduction will go much slower. For instance, the rate for II was -63.63 psi/sec. When II was wrapped with a layer of WA fabric, the rate immediately reduced to −15.38 psi/sec. A similar phenomenon also happened to UC fabrics, for instance comparing VI and I. However, one should pay attention to the rate increase of V from I. Though a layer of WA was added to the UC fabric, the rate increased nevertheless. This is mostly due to the premature failure of WA fibers as discussed earlier.

4.9.2.6 Linearity of Strength Increase Phenomenon

Linearity of strength increase was observed for Configurations IV and VI. In other words, when there is no adverse effect on the fiber fractures from adjacent layers (i.e. premature fiber fracture), the total increase in strength can be computed by simply adding the increase in strength of the respective individual wraps. The total increases matched with the individual add-ups with a low margin of scattering, which is lower than 3%. This

addition law is, however, not applicable to Configuration V, which demonstrated severe premature fiber fracture, as discussed earlier.

4.9.2.7 Mode Domination of 2-Ply Wrap Configurations

Mode dominations were found in Configurations IV and V. In IV, although a mix mode was noted, the effect of WA was much more than that of W in terms of failure mode and stress reduction rate. Brittleness at failure did not appear and the serious global shear cracks within the concrete core was found. At the surface, fiber reorientation took place and fiber unzipping could not be severely noted. The stress reduction rate appeared to be in between those of WA and W alone, but was obviously closer to that of WA.

In V, concrete spalling and crushing still occurred and the failure time was close to that of I. Fiber fractured in the hoop direction, regardless of the effects of the angular fibers in the WA fabric. Failure occurred at mid-height and was confined. Shear cracks did not appear entirely.

These domination phenomena were attributed to the stacking sequence as well as the closeness of material property and fiber orientation of the different fabric types. When comparing Configuration V and VI, with the same fabrics but having a different stacking sequence, mode domination occurred in the former while a completely new mode of failure was found in VI. Therefore, whether mode domination would occur should consult the failure mechanism before drawing any conclusion.

4.9.2.8 Optimal Configuration in terms of Strength and Failure

Considering both strength enhancements and failure mode appearances, Configuration VI was the optimal configuration among all the six wrap types. This series of specimens not only gave rise to significant strength enhancement (in fact they were the highest), but also protect any concrete from spalling after failure. Concrete spalling can be considered as a dangerous event because once a portion of the concrete volume is removed from the core, significant displacement in the axial direction could take place, giving rise to immediate collapse of the structure above. Moreover, in view of strengthening, the use of

unidirectional fibers in the hoop direction is the most effective because fibers are loaded in tension directly. Finally, the local fiber behaviors are the most predictable – fiber fracture. Fiber buckling has never occurred on the specimens in this series and this is considered a plus to the overall column behavior. Fiber buckling, as discussed, would give rise to fabric crack initiation. And very often, the buckling phenomenon is swift and unpredictable.

4.9.3 Local Effects

4.9.3.1 Overlap Strengthening

Overlap strengthening was observed in the case of Configuration I through the use of extensometer measurements. It was found out that differential axial shortening occurred on and opposite to the overlap positions. It should be pointed out that if the overlap bond strength could be developed to a level as high as the fabric tensile strength in the primary fiber direction, the overlap is literally providing an extra layer of local confinement. Therefore in all cases, it was noted that the overlap joint did not fail through cracking or any kind of fiber damage. This overlap provided unbalanced circumferential stress. Lateral strain on the confinement within this region was less than its opposite side. The same amount of lateral stress was shared equally between the two layers. Concrete core therefore expanded more on the opposite side because it was weaker and hence generated more axial shortening due to volumetric compatibility of the concrete material. The axial shortening was pronounced because one layer of fabric that was overlapped by the same thickness would mean a 100% increase in thickness locally. For the cases of II and III, the overlap strengthening effect was less because concrete cracking occurred instead of concrete crushing. Therefore, the local bulging of crushed concrete did not occurred. Lateral expansion was due solely to the movement of the cracked concrete along the shear planes. For cases IV, V and VI, very little, if any, differential shortening was recorded. This is due to the balanced structural layout of the overlap designs. Thickness of the regions at the overlap and that opposite to the overlap was closer in magnitude and hence an even confining effect was resulted on opposite sides.

4.9.3.2 Bond Delamination

Bond delamination mainly occurred in Configuration VI. It took place when the shearing or peeling strength of the epoxy was lower than the applied shearing stress. The mechanism has already been discussed extensively in "Load Responses due to Different Fiber Stack-up Sequence" in Section 4.9.2 and will not be repeated here. Overlap debonding should refer to the next subsection.

4.9.3.3 Fiber Buckling

Fiber buckling occurred whenever vertical fiber exists. The buckling near the cylinder bottom may act as the origin of crack initiation. The vertical fibers buckled even if they were not loaded directly in the axial direction. Mechanisms of the buckling mode should be referred to the discussion of "Load Responses due to Different Fiber Orientations" in Section 4.9.2.

4.9.3.4 Fiber Reorientation

Fiber reorientation only occurred in WA fabrics and when the concrete core did not crush but crack. It may serve the purpose of energy dissipation and cause a very ductile failure mode. The action may also alleviate the brittleness and stress reduction rate of FRP confined cylinders to a large extent when the WA fabric is used in addition to other fabrics. Mechanisms of the reorientation mode should be referred to the discussion of "Load Responses due to Different Fiber Orientations" in Section 4.9.2.

4.9.3.5 Roles of Fiber in the Hoop, Vertical, and Angular Directions

The role of hoop fibers is to confine the cylinder from expansion due to concrete failure. The confinement is considered effective because the fiber direction is aligned with the principal load direction. The role of vertical fibers is to take up some vertical stresses through the surface shearing distribution mechanism. However, buckling can occur due to the non-uniform shearing stress distribution on the fiber-roving surface. The role of angular fibers is to increase ductility of the entire column through the fiber reorientation mechanism. This mechanism is found to be extremely effective in preventing concrete

spalling from the core. It can be used in enhancing the safety of retrofitted or strengthened columns in the events of structural failure.

4.9.3.6 Local Behavior of Unwrapped Concrete Portion at Top End

Since the fabrics were designed not to subject to direct overall axial compression, the top end of the cylinder was not wrapped while the bottom end was wrapped. Therefore, part of the cylinder at the top was unconfined while the rest was fully confined. Nevertheless, there was no concrete failure at the unconfined portion of concrete in all specimens. This was mainly because of the stiffening of concrete due to the frictional force between the steel platen and the concrete in contact. The friction gives rise to a pseudo-confinement that has prevented the concrete from failure.

4.9.4 Manufacturing Effects

4.9.4.1 Detrimental Effects of Air Pockets

It was discovered that entrapped air pockets did not contribute to significant peak strength deterioration. Instead, their roles tend to be more dominant in the post-peak region. Air pockets was found to act as nuclei of local delamination. The pockets grew large under load, regardless of position on the cylinder surface. When the pockets were close to significant delamination site, flow channels would be developed to hook up each other and form a larger delaminated area. Stress reduction rate was faster in specimens with air pockets than those without.

When stressed axially and circumferentially, the pocket surface was tensioned in the hoop direction while compressed in the axial direction. The stresses on the pocket would grow and eventually reach a state that the edges had to stretch out so as to release the stresses on the pocket surface spontaneously. This edge movement was promoted by the stress concentrations due to the discontinuity of the fabric smoothness.

4.9.4.2 Effect of Overlap Length on Overlap Bond Strength

The lower bound of the bond length was found to be 3" (16% of circumference) for the composite system used in the current study. Overlap debonding occurred for the cylinder that consisted of a 2.5" (13% of circumference) overlap length. It is believed that whether the overlap can develop sufficient bond strength depends highly on the shearing strength of the epoxy as well as the type of lap joint made. Stress concentration, which depends on the lap type, initial curvature and loading direction, also contribute to the initiation of bond failure and the overall strength of the bonding.

4.9.4.3 Effects of Epoxy Bond Quality on Strength

Since the wet lay-up method was used and that the epoxy was hand rolled onto the fabrics, the epoxy thickness control could not be precise. Despite this fact, the epoxy bond quality variation did not have major impact on most specimens. The only exception was those specimens in Configuration V. Details of the effects of bond quality and thickness should be referred to "Load Responses due to Different Fiber Stack-up Sequence" in Section 4.9.2.

4.9.5 Applications of Results to Real-World Problems

In view of the performances and failure modes of the six wrap configurations, there are a few suggestions to the application of the FRP confinement in the field. First, the use of unidirectional fibers in the hoop direction alone should give the highest possible confinement effect. However, one should also note that the failure was catastrophic, reflecting the sudden enormous energy release upon fiber fracture. Second, the use of bi-directional fibers in the directions that aligned with the vertical loading axis and the horizontal expansion axis is not advisable for concentric static loading. Fiber buckling was found to initiate cracks in the jacket and the failure was often swift. The use of vertical fibers may, however, be effective in taking up bending tension in the case of beam-columns, but significant fiber buckling should be expected on the side of compression. Third, the use of bi-directional fibers at substantial angles can help change

the failure mode, although some previous studies indicated that no significant difference could be noted for fibers oriented up to 18 degrees (refer to Section 3.2.6). It was shown that when the fibers are oriented to a degree up to 45 degrees to the hoop direction, the fibers were able to accommodate large lateral displacement without letting the concrete to spall off the core through the fiber reorientation mechanism. Also, fibers were not strained to their elastic limit due to the longer length of fibers in the horizontal component after the fibers had rotated in a rigid body motion. Forth, in view of the combined use of materials, it was confirmed that angular fibers could substantially reduce the catastrophic behaviors at failure. If the fabric is used as the innermost layer, a safety jacket is provided because concrete cannot spall off while required evacuation and destructive evaluation could take place even after structural failure, retaining a certain level of rigidity.

4.9.6 Applications of Results to Further Research

In terms of instrumentation, strain gages with at least 350-ohm resistance should be used. Gages with 120-ohm resistance, which is the most used in structural steel specimens, were proved to significantly underestimate the actual strains. Aspect ratio (length/width) of the gage is recommended to be large in order to capture the information of primary fiber directions. Gage size of 0.25" was found to be sufficient in yielding accurate results if following the strain gage installation procedure in Section 4.5.5, along with the use of 350-ohm resistance. When stressed fiber and gage do not align with each other, poor results were obtained. Thus, in no case should the gage be placed on stressed fibers that are running across the gage area.

The fundamental behaviors of cylinders confined in three different types of FRP composite materials were captured. The use of angular fibers in column retrofit should not be overlooked. Though they do not confine columns in the hoop direction effectively, they are able to significantly change the column response. Therefore, the combination use of hoop fibers and angular fibers should be further studied in an extensive manner. Variables such as fiber contents, ply thickness, stacking sequence, and manufacturing

process should be focused. The development of a fabric that consisted of weaved fibers in both the angular and hoop directions, is recommended as an immediate research topic.

Finally, since the tests were carried out with sound unloaded concrete, they should not be immediately applied to retrofitting damaged columns or even to strengthening undamaged columns. The stress-strain responses should demonstrate a different behavior for wrapping loaded concrete and unloaded concrete. Further research is required in the area of simulating the confining action of already loaded columns.

CHAPTER 5

ANALYTICAL MODELING AND DESIGN CONSIDERATIONS OF FRP-CONFINED CONCRETE COLUMNS

5.1 Introduction

Confinement models have been proposed for concrete column retrofit using FRP composites over the last two decades. Major models were introduced in Section 3.3. The performances of each of these models are reviewed and compared against the six sets of experimental data in this chapter. Three major parameters are compared. They are (1) peak stress, (2) peak strain, and (3) axial stress-strain curve shapes.

This chapter first discusses the confinement mechanics of circular columns as a basis for developing insights into the general form used in the analytical model formulation. Performances of the six major analytical models are then compared against the six sets of experimental results obtained from the herein experimental program as discussed in Chapter 4. Modifications of the stress and strain models then follow. The modification is essentially a calibration for the current test data, which depends heavily on the specimen fabrication workmanship, compression loading rate, and instrumentation techniques. Stress-strain models are also proposed and are refined from two existing models. These models are checked against two other independent experimental programs. Concepts, essences, and directions for further model development are as well discussed. Finally, concerns and possible approaches about the design of FRP-confined concrete columns are addressed.

5.2 Confinement Mechanics of Circular Columns

Confinement can be provided in a passive or active manner. Active confinement pressure is often produced by means of external oil pressures such as those generated in a 3-dimensional loading chamber. Passive confinement pressure is provided by transverse reinforcement such as spiral and circular reinforcements or external jackets such as FRP, steel, and concrete jackets. The confining pressure in passive confinement exists only after the concrete has experienced significant radial expansion, tensioning the jacket with internal pressure. At the FRP-concrete interface, both the force equilibrium and the displacement compatibility conditions have to be satisfied. From mechanics of shells (Book: Hearn 1997), the following equation can be derived, as stated in Section 3.3.1, as a representation of the force equilibrium equation.

$$f_{radial} = \frac{f_{FRP} \cdot t_{FRP}}{R - t_{FRP}} \approx \frac{f_{FRP} \cdot t_{FRP}}{R}$$

where f_{radial} is the radial confining pressure, f_{FRP} is the average hoop stress in the FRP confinement shell, t_{FRP} is the thickness of the shell, and R is the radius of the concrete core.

In general, the confinement pressure f_{radial} can be related to the confined axial strength f'_{cc} and the unconfined concrete strength f'_c. Although a linear relationship was first suggested (Richart 1927), the following nonlinear relationship, which was proposed by Newman in 1969, was more commonly adopted in FRP confinements.

$$f'_{cc} = f'_c \left(1.0 + k_1 \left(\frac{f_{radial}}{f'_c}\right)^n\right)$$

where k_1 and n are constants determined from experiments. Figure 5.1 shows the nonlinear relationship by curve fitting the herein experimental database.

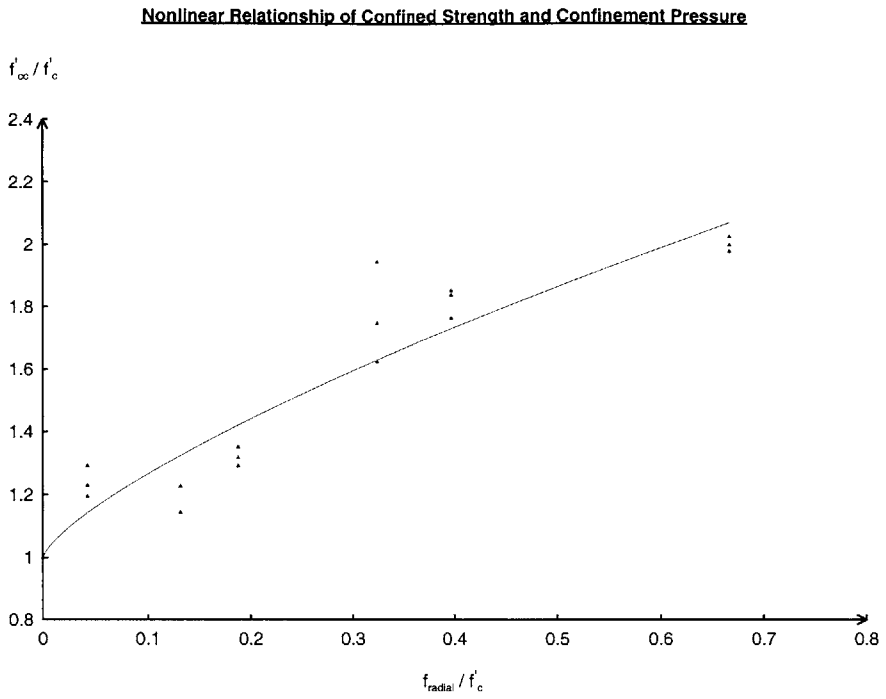

Figure 5.1 Nonlinear relationship of confined strength and confinement pressure

The nonlinear relationship reflects that the confinement is less effective at a higher level of confinement. As the confinement strength increases, the increase in confined axial strength becomes less.

On the other hand, a nonlinear relationship can also be noted relating peak strain and the corresponding confinement pressure. The non-linearity increases as the confinement pressure gets larger, reflecting the concrete core being more compressible as the pressure increase. However, this increasing non-linearity in axial strain is expected to become linear as the confinement pressure increases to a level that the concrete material becomes finally incompressible. This was discussed in Section 4.9.2.2.

Figure 5.2 shows the nonlinear relationship by curve fitting the experimental data. It should be noted that the non-linearity is not pronounced due to the limited range of confinement pressure of the designed specimens in the experimental program.

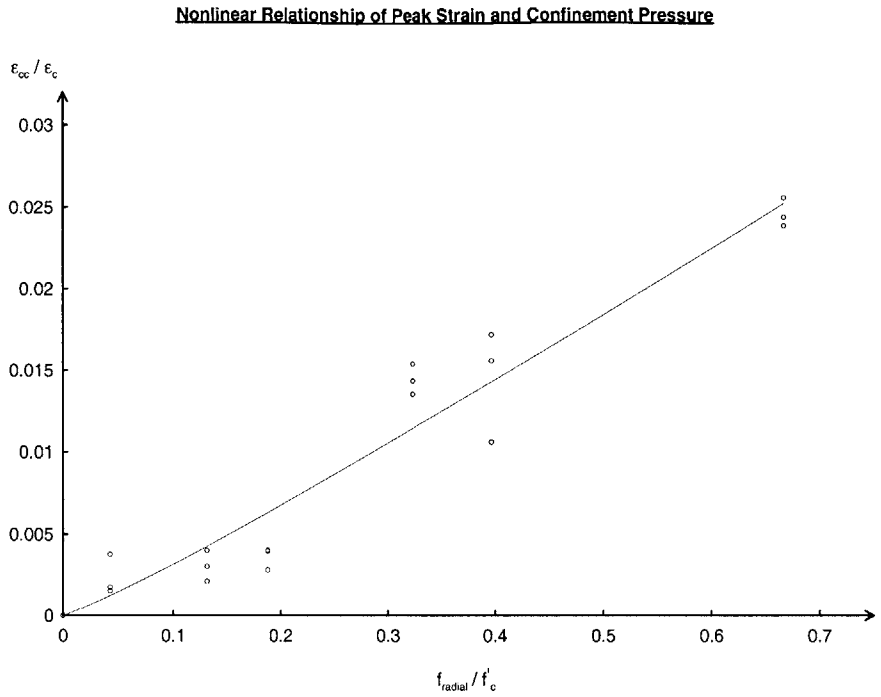

Figure 5.2 Nonlinear relationship of peak strain and confinement pressure

The unified confinement model developed originally for steel jacketing and spiral reinforcements by Mander, Priestley, and Park (1988) has a different general expression from the typical nonlinear model form presented above. That model utilizes the energy approach that assumes that the additional ductility available in the confined concrete is due solely to the energy stored in the confining jacket. The compatibility condition at peak stress is not generally satisfied. The model is insensitive to the variation of the continuous concrete dilation. This model is presented in Section 3.3.2 and will not be repeated in this section.

5.3 Performances of Existing Analytical Models

Performances of the six major analytical models described in Chapter 3 are evaluated by plugging in the material and geometric properties of the various wrap configurations. The performances are divided into two main groups according to the load-deformation behavior categorization discussed in Section 4.8.2.5. The first group represents load-deformation behavior Type I, which demonstrates a bilinear-increasing behavior. The second group represents behavior Type II, which demonstrates an increasing-decreasing

behavior. For simplicity hereafter in quoting the six models, a unique model designation is assigned for each of them. They are summarized below in Table 5.1.

Table 5.1 Summary of Model Designations

Model Designations	Researcher Teams	Year of Proposal
FK	Fardis and Khalili	1982
MPP	Mander, Priestley, and Park	1988
CP	Cusson and Paultre	1995
KG	Karbhari and Gao	1997
SMS	Samaan, Mirmiran, and Shahawy	1998
MIKK	Miyauchi, Inoue, Kuroda, and Kobayashi	1999

It should be noted that all models have proposed their peak stress and peak strain prediction equations based on their own experimental data sets. However, only three models have also proposed their original stress-strain relationships to simulate entirely the load-deformation behavior from zero to failure load. These three models are namely the (1) MPP, (2) SMS, and (3) MIKK models. The rest mainly refer to the stress-strain relationship used in the MPP proposal. Thus, the plots of the three models that have not proposed their original stress-strain behaviors are produced via a combination of the MPP stress-strain relationship and their respective peak stress and strain predictions.

On the other hand, the MIKK model is the only one that provides two distinct simulations of the load-deformation behaviors Type I and Type II. All other models use a single stress-strain relationship in tackling both behaviors. In the case of SMS, no attempt is made in simulating the Type II behavior. The bilinear behavior has been assumed and used throughout. As one can see later, the SMS model fails in predicting the increasing-decreasing type response entirely, although it simulates quite well the bilinear response.

In this section, the performances of the analytical models are first presented and compared with one another and against the experimental data. General curve shapes are discussed with comments on the kinking point, initial slope, peak stress, and peak strain in a qualitative manner. The peak stress and strain predictions of all six models are then summarized and tabulated for each wrap configuration. Percentage of deviation is also given. Experimental averages are used as benchmark values. Finally, general comments on the use of existing models are given. Modifications of the prediction models are given in the section that follows.

5.3.1 Load-Deformation Curve Shape Type I

5.3.1.1 Configurations and Computation Methods

Three wrap configurations are categorized as Type I. They are C1 – UC1, C2 – WA1 – UC1, and C2 – UC1 – WA1. These three configurations all demonstrate a bilinear increasing behavior upon axial compression. For the latter two configurations, the same materials were used but a reversed stack-up sequence was adopted. Nevertheless, the input parameters of these two configurations for the analytical models are identical and the following equations are used in the computations of the stress-strain responses. The equivalent elastic modulus is computed as $E_{Total}\ A_{Total} = E_{WA}\ A_{WA} + E_{UC}\ A_{UC}$; total jacket thickness as $t_{Total} = t_{WA} + t_{UC}$; and total jacket confinement strength per unit width (in kips) as $f_{Total}\ t_{Total} = f_{WA}\ t_{WA} + f_{UC}\ t_{UC}$. The parameters E_{UC}, E_{WA}, f_{UC}, f_{WA} are respectively the tensile moduli and the tensile strengths of the UC and WA fabrics in the hoop direction. Since the equivalent jacket properties are the same for the two different wrap configurations, the model prediction curves are the same. The experimental curves are plotted on the same graph for comparison purposes, as the analytical curves of these two configurations are basically one set.

5.3.1.2 Change-of-slope Considerations

Only the SMS and MIKK models have given specific treatments to the point where the change of slope occurs. The SMS model is more versatile in that it can control the radius

of curvature of the slope changing point by varying the magnitude of a variable in the model. This variable can be literally calibrated for different material systems. The MIKK model, on the other hand, assumes that the kinking point occurs at a level very close to the unconfined concrete strength and ductility comes in when the external load has surpassed such level of stress when concrete is fully crushed inside. It fails to include the kinking point upward shift phenomenon as discussed in Section 4.9.2.2. Comparing with the rest, the MIKK model demonstrates in general the smallest radius of curvature at kinking, follows by that of the SMS model. The other models generally yield a large radius of curvature, forming a smooth transition between the first and second slope of the bilinear curves. However, it should be pointed out that such a large radius does not match with the reality as in the case of composite wrapped concrete.

5.3.1.3 Bilinear Curve Shapes

Figure 5.3 and 5.4 show respectively the analytical model comparisons of the C1 – UC1 and the C2 – WA1 – UC1 & C2 – UC1 – WA1 series. Figure 5.3 shows only the results of the C1 – UC1 series. Figure 5.4 shows the results of both C2 series. It can be noted that, in general, the shapes of the models in the two figures are very similar. The general discussion hereafter applies to both figures unless otherwise specified. The SMS, MIKK, and CP models show clear-cut bilinear behaviors. The rest predict shorter second slopes.

Among all the curves, the SMS model appears to be the most successful in simulating the first and second slopes. Except for the C2 – UC1 – WA1, it is able to accurately simulate the level of stress where the change of slope occurs. However, this model assumes that the second slope is a straight line and hence fails to cater for the increased ductility that has taken place in C2 – WA1 – UC1 near the failure load. Curve deviation starts at about 90% of the experimental peak stress in this configuration.

The MIKK model fails to give a close representation of the second slope because the kinking point starts at a relatively low stress level while the peak stress is substantially overestimated. It also assumes a straight line for both the first and second slopes respectively.

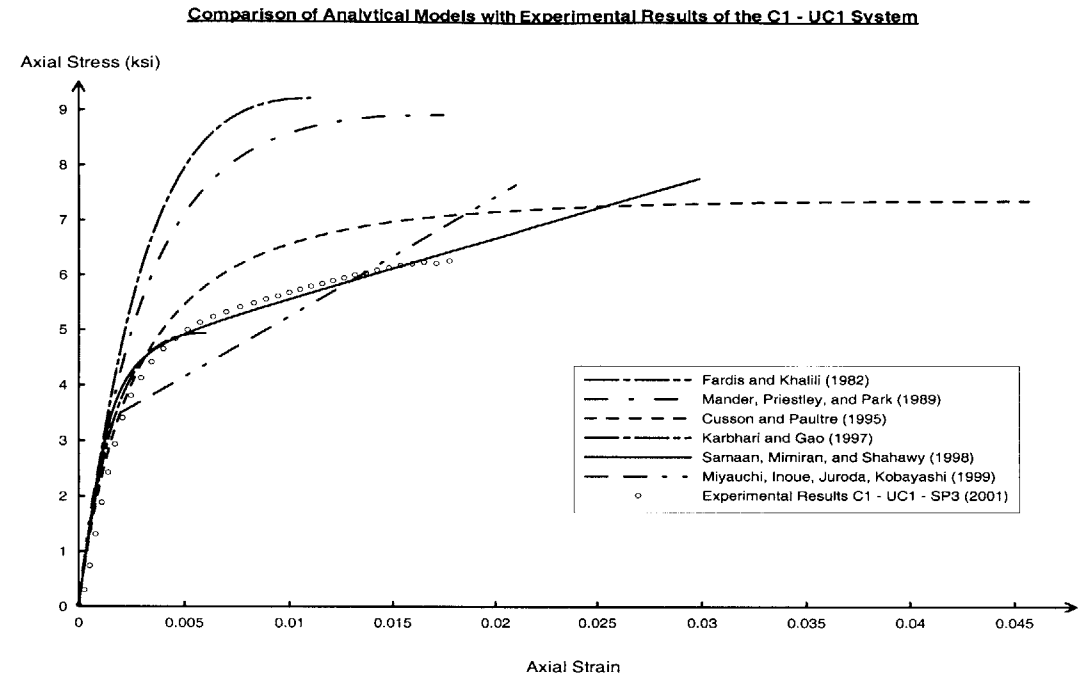

Figure 5.3 **Comparison of analytical models with experimental results of the C1 – UC1 composite system**

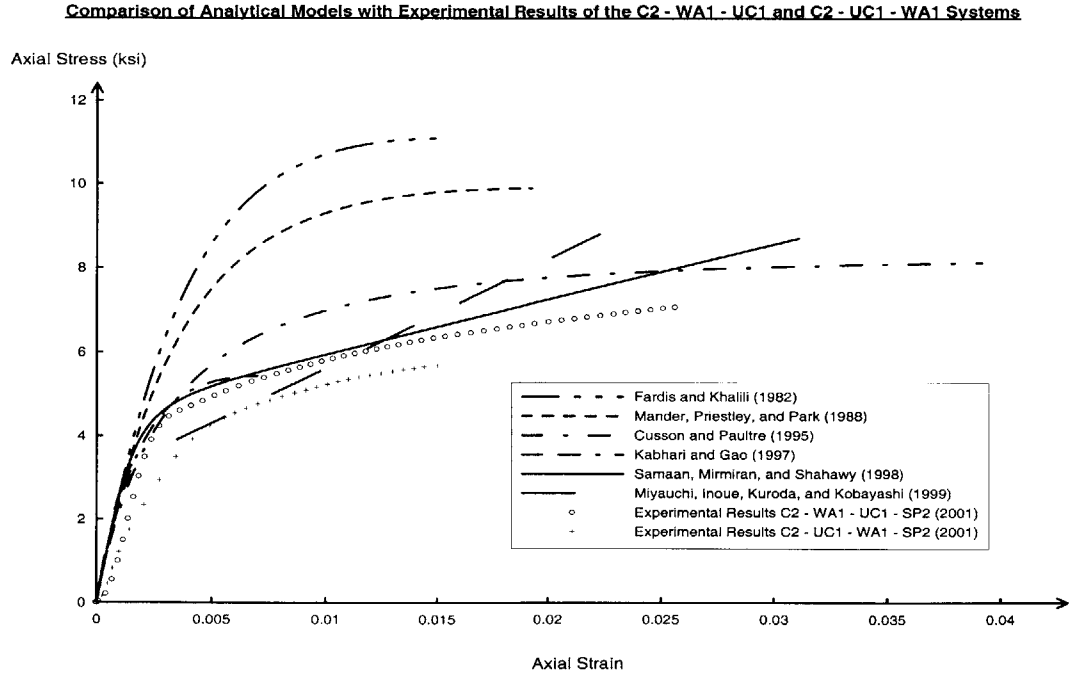

Figure 5.4 **Comparison of analytical models with experimental results of the C2 – WA1 – UC1 and C2 – UC1 – WA1 composite systems**

The CP model shows a flat second slope with a very large axial strain at peak. The change of slope occurs in a gentle manner. The FK and MPP models predict the specimens to be as stiff as the initial stage of unconfined concrete until a high level of stress and then show ductility not long before the peak stress is reached. Their curve shapes are obviously deviated from the experimental results and are considered inappropriate for designs and analyses.

Finally, the KG model is successful in simulating the first and second slope as well as the kinking region. However, this model significantly underestimates the ultimate strength and the corresponding strain, resulting in an unrepresentative overall stress-strain behavior simulation.

Considering the C2 – UC1 – WA1 experimental curve, it can be noted from Figure 5.4 that the initial slope tends to be lower than the other two configurations. The kinking point, therefore, occurs at a larger strain and at a lower stress level than the C2 – WA1 – UC1. This exceptional phenomenon has already been discussed in Sections 4.9.2.1 and 4.9.2.3 in details and will not be repeated here. As a result, none of the models is able to predict this behavior. This has confirmed that stack-up sequence effect and the compatibility of different types of fibers have to be first investigated before applying in the design.

5.3.1.4 Peak Stress and Strain Predictions

Except for the KG model, all models overestimate the ultimate strength to a large extend. Particularly, the peak stress model originally proposed by Richart et al (1927) and later suggested and modified by Fardis and Khalili (1982) shows the highest overestimation. The MPP model that was originally used for steel confinement shows the second highest overestimation. The peak stress proposed by the SMS model and the MIKK model are similar as indicated in Figures 5.3 and 5.4 and that proposed by the CP model is the closest to the experimental values. The KG model consistently underestimates the ultimate load capacity to a large extent. The proposed values are only slightly over the load level where the change of slope occurs.

Predictions of strain at peak stress vary greatly among models. In all cases, the KG model and the FK model are the two that underestimate the most. The CP model consistently overestimates the strain, follows by the SMS model with a lesser extent. The strain estimations by the MIKK model matches closely with the experimental values while that by the MPP model in the C1 – UC1 case is almost perfect but has some underestimations in the C2 – WA1 – UC1 case.

5.3.2 Load-Deformation Curve Shape Type II

5.3.2.1 Configurations and Computation Methods

The other three wrap configurations are categorized as Type II. They include C1 – W1, C1 – WA1, and C2 – W1 – WA1. These configurations all demonstrate an increasing-decreasing load-deformation behavior without any sign of bi-linearity. The peak stress takes place with a slight ductility increase after the initial linear slope and the declining tail is immediately entered. Except for the MIKK model, which has a different set of equations to compute the load-deformation responses, all the other models make use of the same equation to simulate the response accordingly. For the C2 series, the same equivalent relations, which are employed in the curve Type I computations, are used in this curve Type.

5.3.2.2 Initial Slope Considerations

It should be pointed out that the initial slopes of all Type II experimental curves are less steep than those of Type I, although the same concrete was used. The reason was already discussed in Chapter 4 and will not be repeated here. Nevertheless, one should note that only the MIKK model is capable of modeling this change of initial slope while all the other models still assume the same initial slope that is computed based on the unconfined concrete strength. Except for the C1 – WA1 system, the MIKK model is able to capture the initial slope quite accurately. This model actually computes the slope from the peak stress and the corresponding strain. Once the two parameters are well predicted, the initial slope is of excellent agreement with the experimental data. The deviation herein

between the MIKK model and the test curve is solely because of the difference in the peak parameter predictions. It must be pointed out that although the stress-strain model is good at predicting the initial slope, the peak strain predictive relation has not been established yet. But the ultimate strain is proposed. The ultimate strain is proposed as the strain when complete collapse and fiber fracture occurs and this strain is not equal to the peak strain.

5.3.2.3 Increasing-Decreasing Curve Shapes

Since the phenomena are similar for all three configurations, the following discussion applies to all of them unless otherwise specified. Figures 5.5, 5.6, and 5.7 show the comparison of analytical models with experimental results of the C1 – W1, C1 – WA1, and the C2 – W1 – WA1 composite systems respectively. Both the MIKK and KG models appear to be the most promising in modeling the increasing-decreasing curve shapes. The descending branch modeled by the KG model simulates the slope correctly, although at times the starting points, or peaks, can be quite different. It should be pointed out, however, that the descending branch of the MIKK curve is in effect arbitrary because the ultimate strength (not peak strength) has to be specified manually in the model.

Among all the models, the SMS model is the only one that fails to encounter the increasing-decreasing behavior. Despite the fact that the bilinear behavior does not exist under lower confinement strength because of concrete cracking but not crushing, the model still predicts a bilinear increasing behavior. For the MPP model, the descending branch is essentially an almost horizontal slope. The descending tails are not trivial. Similar situation occurs in the CP model when predicting the C2 configuration. The FK model is simply not accurate although it is able to predict the increasing-decreasing behavior consistently and that the slope of the descending tail is closer to the experimental curves when compared to the SMS, MPP, and CP models.

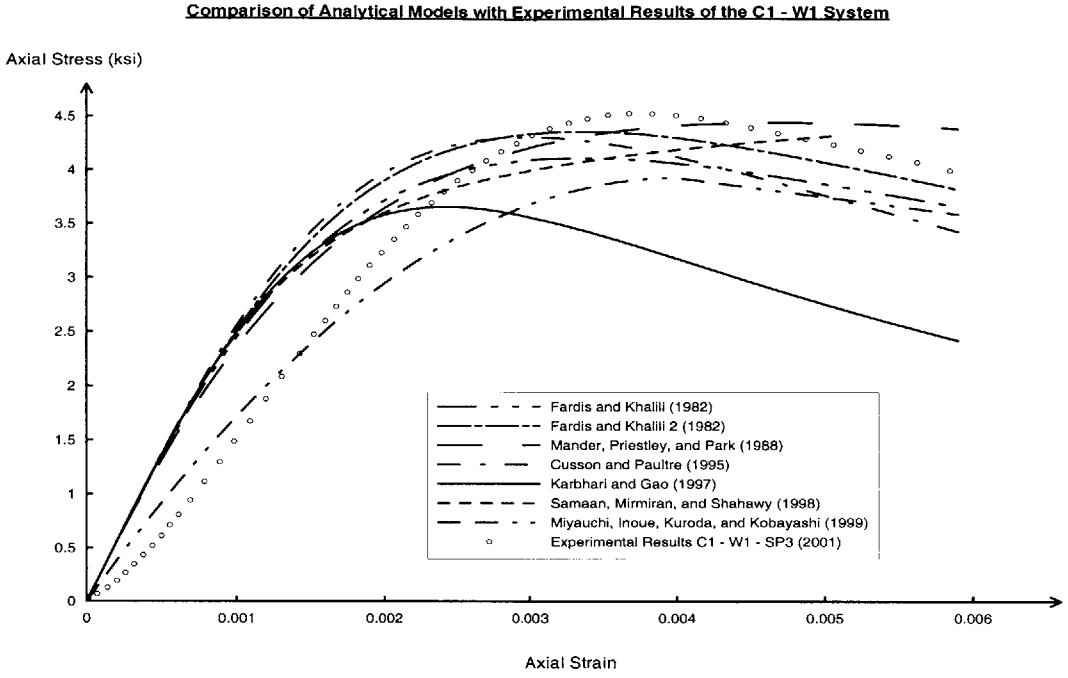

Figure 5.5 **Comparison of analytical models with experimental results of the C1 – W1 composite system**

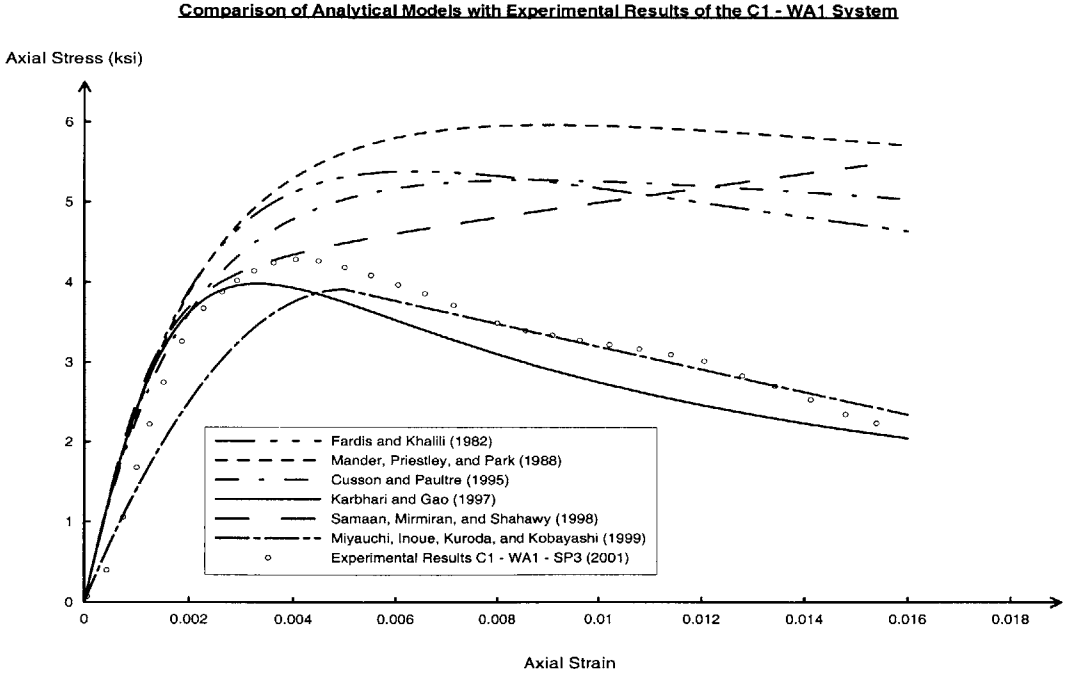

Figure 5.6 **Comparison of analytical models with experimental results of the C1 – WA1 composite system**

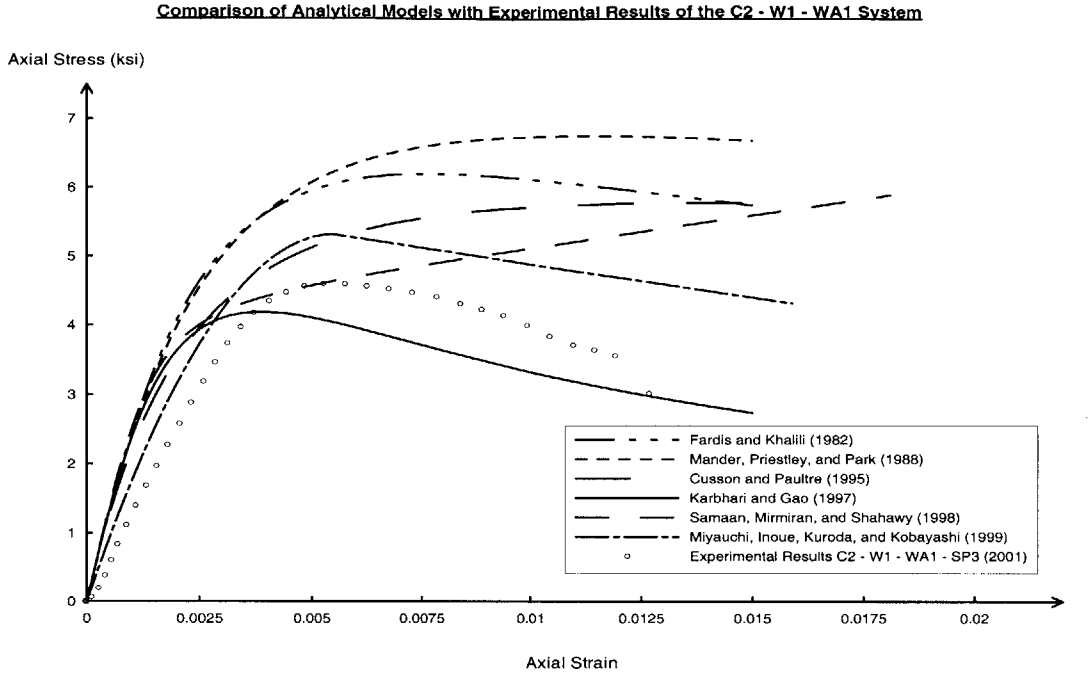

Figure 5.7 Comparison of analytical models with experimental results of the C2 – W1 – WA1 composite system

When comparing the three configurations, it can be seen that the discrepancies in the C1 – W1 model are far less than those in the other two configurations. It can be noted from Figure 5.5 that the peak stress of the experimental curve is actually the highest among and is close to all the other curves. The usual overestimations by most analytical models seem to have disappeared because of the incline actual loading of the specimen. This inclined load is most probably due to the effects of vertical fibers, which also contribute in taking axial load in the form of distributed shearing stress in part of the fiber-roving circumference at the concrete-fabric interface as described in Section 4.9.2.4. This additional load carrying capacity is obviously out of the capturing ability of the analytical models. Thus, the smaller discrepancy phenomenon arises in the case of C1 – W1 specimens.

5.3.2.4 Peak Stress and Strain Predictions

Except for the C1 – W1 configuration, which is exceptional as explained above, the KG model predicts quite well the peak stress and the corresponding strain although there are

consistent underestimations. The MIKK model, which pioneers the concept of using a different model for prediction of the Type II behavior, is unable to provide the estimation of the peak strain. The peak stress is underestimated in each of the C1 series while overestimated in the C2 series. In general, most models overestimate the peak stresses and strains substantially.

5.3.2.5 Ultimate Stress and Strain Predictions

Since all except the MIKK model has given thoughts to the two different curve types, those models have not distinguished or even define the ultimate state and the peak state. For curve Type I, which the bilinear increasing behavior appears, the peak state and the ultimate state are used interchangeably because fiber fracture occurs at the peak stress and generally brings the specimens to an ultimate condition. Therefore, most researchers normally do not consider or care about the descending branches of curve Type I. However, for curve Type II, the ultimate state of the specimen can be very different from the peak state. The stress reduction rates of Type II specimens are usually much lower as indicated in Table 4.10. After the peak state of such specimens, there are basically still "life" and load carrying capacity. Fiber rigid body motion and substantial elongation can occur, helping to prevent the concrete from spalling off. An intact concrete core still exists to resist external load, although not at the same level as sound concrete. Regrettably, most models do not consider these details. Hence, the predictions are confined in the peak stress and strain estimations, not including the parameters at the ultimate state. In view of this, the ultimate states of the curves, in fact, make use of the experimental results. One can, therefore, note that all curves end at about the same strain level. Obviously, there is a need to correlate the stress reduction rate and the composite material and structural properties to produce some ultimate stress and strain estimations.

5.3.3 Summary of Peak Stress and Strain Predictions

In this subsection, all the peak stress and strain predictions from the six analytical models are summarized and tabulated in Table 5.2 and Table 5.3 respectively. The predictions are compared directly with the experimental data averages of the respective wrap

configurations. Result deviations are given in percentages and are rounded off to the nearest whole number. C2 – WA1 – UC1 and C2 – UC1 – WA1 are compared with the same set of analytical predictions due to the reason stated earlier. Peak stresses are expressed in ksi.

From Table 5.2, it can be noted that the predictions by the FK and MPP models are very high. The KG model, the CP model, the MIKK model and the SMS model give a closer estimation to the experimental peak stress. Particularly, the KG model is consistently underestimating the strength while the CP and SMS models give consistent overestimations. The consistent overestimation made by the CP and SMS models may be due to several reasons. First the CP model is originally developed for high strength concrete and not normal to low strength concrete. Second, the composite systems are different. The SMS model made use of the prefabricated composite casing instead of the fabric cloth wrapping. Third, the SMS model is developed based on the testing program with a loading rate of 0.22 in/min., which is more than four times larger than the rate used in the herein experimental program. It is well known that the faster is the loading rate, the higher is the resulting measured strength.

From Table 5.3, it can be noted that most peak strain estimations are done fairly poor. The MPP model is, however, able to predict quite well the configurations with hoop fiber dominations such as C1 – UC1 and C2 – WA1 – UC1 while it fails in predicting correctly the strains for the specimens with angular fibers. On the other hand, the KG model gives similar phenomenon on the specimens with angular fibers dominations such as C1 – WA1 and C2 – W1 – WA1. The predictions are considered acceptable when compared with the other models. But this model fails in predicting the hoop fiber dominated specimens with significant underestimations. The MIKK model, as described earlier, is not capable of giving the peak strains for the increasing-decreasing type specimens. However, it should be pointed out that the estimations of the bilinear increasing type specimens are relatively well.

Table 5.2 Comparison of Peak Stress Predictions

Composite Systems	Exp. Av.	FK		MPP		CP		KG		SMS		MIKK	
		f'_{cc}	Err.	f'_{cc}	Err.	f'_{cc}	Err.	f'_{cc}	Err.	f'_{cc}	Err.	f'_{cc}	Err.
C1 – UC1	6.35	9.20	45	8.91	40	7.35	16	4.94	-22	7.76	22	7.65	20
C1 – W1	4.33	4.11	-5	4.44	3	4.31	0	3.66	-15	4.39	1	3.93	-9
C1 – WA1	3.92	5.38	37	5.96	52	5.27	34	3.98	2	5.46	39	3.91	0
C2-W1-WA1	4.62	6.19	34	6.75	46	5.78	25	4.19	-9	5.89	27	5.31	15
C2-UC1-WA1	6.18	11.08	79	9.89	60	8.20	33	5.42	-12	8.70	41	9.01	46
C2-WA1-UC1	6.99		59		41		17		-22		24		29

Experimental averages shown are the same as those in Table 4.6. Deviation errors are shown in percentages.
Negative signs (-) means underestimation, positive signs (+) means overestimation.

Table 5.3 Comparison of Peak (Axial) Strain Predictions

Composite Systems	Exp. Av.	FK		MPP		CP		KG		SMS		MIKK	
		ε'_{cc}	Err.	ε'_{cc}	Err.	ε'_{cc}	Err.	ε'_{cc}	Err.	ε'_{cc}	Err.	ε'_{cc}	Err.
C1 – UC1	0.0163	0.0110	-33	0.0175	7	0.0457	180	0.0060	-63	0.0299	83	0.0209	28
C1 – W1	0.0043	0.0033	-23	0.0047	9	0.0030	-30	0.0024	-44	0.0051	19	-	-
C1 – WA1	0.0050	0.0064	28	0.0090	80	0.0086	72	0.0033	-34	0.0151	202	-	-
C2-W1-WA1	0.0055	0.0077	40	0.0113	105	0.0142	158	0.0039	-29	0.0181	229	-	-
C2-UC1-WA1	0.0166	0.0154	-7	0.0203	22	0.0730	340	0.0073	-56	0.0311	87	0.0231	39
C2-WA1-UC1	0.0260		-41		-22		181		-72		20		-11

Experimental averages shown are the same as those in Table 4.7. Deviation errors are shown in percentages.
Negative signs (-) means underestimation, positive signs (+) means overestimation.

5.3.4 General Comments on the Analytical Models

Existing analytical models have limitations in correctly predicting the load-deformation responses of the composite systems tested in the herein experimental program. Peak stress and strain are in most cases wrongly predicted. Overestimations are noted for peak stress predictions in most cases while both overestimations and underestimations are noted for peak strain predictions.

Nevertheless, for bilinear increasing responses, the MIKK and the SMS models are able to give truly bilinear behavior predictions with special attention dedicated to the change of slope region. Particularly, the SMS model seems to be the better one because it caters for the change-of-slope upward shift phenomenon and it allows a versatile adjustments or calibration to that region by defining a variable especially for the purpose. The MIKK model, on the other hand, need to reassess the kinking point occurrence stress level. Both the peak stress and strain predictions are not applicable to the current experimental results. It should be noted that the second slope of the MIKK model is directly depending on the peak and thus, once the predictions are incorrect, direct consequences can be resulted on the slope itself. Once the peak predictions are correct and that the kinking point level is corrected, the model can be as powerful as the SMS model. In the mean while, the SMS model is more flexible in that the second slope is not solely determined by the peak stress and strain. Therefore, although the SMS model overestimates the peak parameters, a close fit is also obtained between the predicted second slope and the experimental second slope. The stress-strain relationships simply cannot be applied due to the very different curve shapes and kinking behaviors.

For the increasing-decreasing responses, the MIKK model and the KG model are the best in terms of curve shape modeling, although the peak strain and the ultimate stress relationships cannot be predicted by the MIKK model and need manual input while the ultimate stress and strains cannot be predicted by the KG model. All the other models are neither capable of capturing the correct curve shapes, especially the descending branch, nor the peak and ultimate responses. The SMS model, though powerful in the bilinear response predictions, fails to give even an approximation of the increasing-decreasing

behavior. In the author's opinion, the MIKK model is worth to be further developed and refined for low composite confinement specimens modeling. Once the two missing parameters can be predicted, the model will become very powerful.

5.4 Confinement Model Modifications and Proposals

Now that the existing models are not capable of predicting well the stress-strain response and the peak parameters of the specimens that are tested in the herein program, there is a need to establish new prediction equations so that safe structural design can take place. It should be noted that under all circumstances, overestimation of the strength of a composite system could be very dangerous. If the newly retrofitted or strengthened structure were subjected to a service load that actually exceeds or is close to the ultimate strength of the structure, either material damage or excessive deformation would occur, and often swift and catastrophic. Serious consequences could then follow. Moreover, one should bear in mind that for FRP-wrapped concrete structures, the concrete core is actually severely cracked or crushed depending on the confinement level, when the unconfined concrete strength is exceeded. When the FRP jacket fails, the structure literally remains no strength resistant capabilities. The peak strength estimation is, therefore, very vital and the design load specified cannot be even close to the ultimate state because post-peak ductility is normally not significant for regular hoop wrapped systems.

In the following, the peak stress and the corresponding strain will be estimated by equations that are resulted from least square fits of the available data. It should however be warned that such relations are not recommended for use in the designs of structural systems with all types of commercially available composites. They are solely pertinent to the current specified wrapping and testing conditions and are obviously not universally applicable. Also, the available set of data for each wrap configuration is actually very limited from a statistical point of view. Only three specimens were tested for each of the six wrap configurations. Furthermore, when comparing the predictive equations with other sets of data, similar testing conditions and instrumentation techniques are expected.

It is known that the peak stress and strain are highly dependent on the loading rate. The best-fit curves are essentially true for the selected loading rate. Adjustments are definitely needed if the equation is aimed at applying to other sets of data that are based on a different rate of loading.

Further validations of the model across different composite types, testing and instrumentation methods are required to yield a truly effective set of design equations for most composite systems. A designer should not blindly use a single strength prediction equation to design various complex and untested wrapping configurations, particularly those with different fabric stack-ups. More design issues will be further discussed in section 5.5. The peak stress and strain prediction models will be checked against two independent datasets provided in the papers by Karbhari and Gao (1997) and Nanni and Bradford (1995). The datasets chosen for the validity check are those produced from similar composite systems, instrumentations and loading conditions. The predictions are computed for each configuration and tabulated in Table 5.4. Besides, two stress-strain relationship models are proposed and they are based on the basic form of the MIKK and SMS stress-strain relationships. Some major conceptual alterations of the parameters are made.

5.4.1 Proposed Peak Stress Prediction Model

Now that the concrete core failure mechanism of the bilinear-increasing type of specimens is different from that of the increasing-decreasing type of specimens, two separate models are proposed for the peak stress. The models are produced from the least square fit of the experimental data. The relations are given as follow. They are categorized by the confinement ratio f_{radial} / f'_c, which indicates the range that correspond approximately to the confinement level of the two curve types. This ratio is considered the confinement strength index. It should be pointed out that specimens having a ratio between 0.4 and 0.7 (Case 1) are classified as the high confinement category while those having a ratio lower than 0.2 are classified as the low confinement category. Specimens that have confinement ratios between 0.2 and 0.4 are considered having a critical confinement level, which distinguish concrete cracking from concrete crushing within the

core. Although from an earlier study (Soon 1987) that the critical confinement was defined with a ratio of about 1.33, which is quite far from the range in the current study, that categorization based on an active constant confinement pressure while the current study based on a passive varying confinement pressure. Moreover, the concrete crushing occurred more extensively in that early study while that in the current study was found to be very local. Therefore, a direct correlation between the critical confinement level of the two studies may not be valid.

Case 1: Bilinear Increasing Curves

For $0.4 \leq (f_{FRP}\, t_{FRP} / R\, f'_c) \leq 0.7$

$$f'_{cc} = f'_{co} + 1.17\, f'_{co} \left(\frac{f_{FRP} \cdot t_{FRP}}{R \cdot f'_{co}} \right)^{0.39}$$

Case 2: Increasing-Decreasing Curves

For $0.0 \leq (f_{FRP}\, t_{FRP} / R\, f'_c) \leq 0.2$

$$f'_{cc} = f'_{co} + 0.39\, f'_{co} \left(\frac{f_{FRP} \cdot t_{FRP}}{R \cdot f'_{co}} \right)^{0.25}$$

5.4.2 Proposed Peak Strain Prediction Model

For a similar reason as in the peak stress prediction models, two equations are proposed for the two distinct cases. Both models are also nonlinear. They are again categorized by the confinement strength index.

Case 1: Bilinear Increasing Curves

For $0.4 \leq (f_{FRP}\, t_{FRP} / R\, f'_c) \leq 0.7$

$$\varepsilon_{cc} = \varepsilon_{co} + 0.033 \left(\frac{f_{FRP} \cdot t_{FRP}}{R \cdot f'_{co}} \right)^{0.77}$$

Case 2: Increasing-Decreasing Curves

For $0.0 \leq (f_{FRP}\, t_{FRP} / R\, f'_c) \leq 0.2$

$$\varepsilon_{cc} = \varepsilon_{co} + 0.0055\left(\frac{f_{FRP} \cdot t_{FRP}}{R \cdot f'_{co}}\right)^{0.27}$$

5.4.3 Performances of the Proposed Peak Stress and Strain Models

The performance of the above proposed models are checked against two sets of data that can be found in the literature Karbhari and Gao (1997) and Nanni and Bradford (1995). Table 5.4 tabulates the respective experimental and predicted results. Both unidirectional and angular wrap configurations are checked against.

Table 5.4 Performance of Proposed Peak Stress and Strain Models

Data Sets	Experimental Peak Stress	Experimental Peak Strain	Predicted Peak Stress	Percentage Error	Predicted Peak Strain	Percentage Error
Karbhari and Gao (1997)						
[0°]	6.51	0.011	6.76	4	0.0075	-32
$[0°]_2$	8.65	0.013	9.28	7	0.0155	19
$[0°]_3$	11.26	0.022	10.01	-11	0.0200	-9
$[0°]_4$	12.97	0.024	10.94	-16	0.0271	13
[0°/ 90°]	7.00	0.008	6.92	-1	0.0079	-1
[0°/ 90°/ 0°]	9.68	0.017	9.53	-2	0.0169	0
[+45°/-45°]	6.14	0.006	6.28	2	0.0062	4
$[+45°/-45°]_2$	6.00	0.005	6.48	8	0.0067	35
[90°/+45°/-45°/ 0°]	7.47	0.009	6.98	-7	0.0080	-11
Nanni and Bradford (1995)						
F01	8.06	0.0148	11.34	41	0.0156	5
F02	9.23	0.0120	11.34	23	0.0156	30
F03	9.69	0.0161	11.34	17	0.0156	-3
F04	10.92	0.0169	11.34	4	0.0156	-8
Current Experiment (2001)						
C1 – UC1	6.35	0.0163	6.36	0	0.0182	12
C1 – W1	4.33	0.0043	4.12	-5	0.0043	1
C1 – WA1	3.92	0.0050	4.32	10	0.0052	4
C2 – W1 – WA1	4.62	0.0055	4.40	-5	0.0055	0
C2 – UC1 – WA1	6.18	0.0166	6.14	-1	0.0159	-4
C2 – WA1 – UC1	6.99	0.0260	7.00	0	0.0262	1

From Table 5.4, it can be seen that except for the peak stress datasets of Nanni and Bradford (1995), all predictions are very close to the experimental values. Moreover, the peak strain predictions are also well within the proximity of the experimental values. Most results fall within the ±10% margin. The relatively large deviations of the predictions in the Nanni and Bradford (NB) datasets are probably due to the premature failure of their specimens. It was reported in the paper that joint failure occurred, which was inconsistent with the other failure mechanisms in the program. In fact, from the experience gained in the herein program as previously presented in Section 4.8.4.2, premature failure and lower ultimate strength was reported for the specimen with joint debonding failure due to insufficient bond length. This premature failure can occur at an unpredictable stress level, depending on the conditions of the overlap joint. Therefore, the four specimens reported in the NB datasets actually show a scatter with all ultimate strengths lower than the predicted value.

In general, the equations can be applied with confidence to composite systems that are consisted of a confinement strength index within the specified proposed ranges and are manufactured by the wet lay-up method. For systems outside the specified ranges, further validations are needed because the concrete responses and the overall volumetric responses are different at high levels of confinement, for instance those found in the SMS model (with a confinement strength index close to 2.0).

5.4.4 Proposed Stress-Strain Models

The SMS model is chosen for modification in the bilinear stress-strain behavior because its basic form is the most versatile and accurate by far. The model was originally proposed by Richard and Abbott in 1975.

The MIKK model is chosen for modification in the increasing-decreasing behavior because of its potential in developing into a flexible, simple, but accurate model for low confinement strength composite systems. The model was originally proposed by Hognestad in 1951 for reinforced concrete behaviors under axial compression.

Although the original form of the SMS model is used, the subsequent parameters are literally all modified. Particularly, the initial slope is further reduced as observance of the concrete behaviors in the herein program. Also, the point where change of slope occurs is set to a nonlinear relationship instead of the originally proposed linear relationship. This is due to the fact that the upward shift of the kinking point would vanish with increasing confinement because of the corresponding incompressible concrete core under high confinement strength. This was already discussed in detail in Section 4.9.2.2 and will not be repeated here. The previously proposed peak stress and strain relationships in Sections 5.4.1 and 5.4.2 are used and the plastic slope (E_2) is now dependent on the proposed peak parameters as well as the change-of-slope point. The originally proposed relationship is no longer used.

A. Proposed Bilinear Increasing Model

Governing Equation

$$f_c = \frac{(E_1 - E_2)\varepsilon_c}{\left[1 + \left(\frac{(E_1 - E_2)\varepsilon_c}{f_A}\right)^n\right]^{1/n}} + E_2\,\varepsilon_c$$

Peak Stress Relations

$$f'_{cc} = f'_{co} + 1.17 f'_{co}\left(\frac{f_{FRP} \cdot t_{FRP}}{R \cdot f'_{co}}\right)^{0.39}$$

Peak Strain Relations

$$\varepsilon_{cc} = \varepsilon_{co} + 0.033\left(\frac{f_{FRP} \cdot t_{FRP}}{R \cdot f'_{co}}\right)^{0.77}$$

Elastic Slope

$$E_1 = 37.0\,(f'_{co})^{1/2}$$

Plastic Slope

$$E_2 = \frac{f'_{cc} - f_A}{\varepsilon_{cc}}$$

Kinking Point

$$f_A = f'_{co} + 1.137 f'_{co} \left(\frac{f_{FRP} \cdot t_{FRP}}{R \cdot f'_{co}} \right)^{0.1227}$$

Kinking Shape Parameter

n = 3.0 = constant for fiberglass composite wet lay-up systems

B. Proposed Increasing-Decreasing Model

Governing Equations

For $0 \leq f_c \leq f'_{cc}$

$$f_c = f'_{cc} \left(2\left(\frac{\varepsilon_c}{\varepsilon_{cc}}\right) - \left(\frac{\varepsilon_c}{\varepsilon_{cc}}\right)^2 \right)$$

For $f'_{cc} \leq f_c$

$$f_c = f'_{cc} + S * (\varepsilon_{cc} - \varepsilon_c)$$

Curve Shape Parameter

S = calibrated from experiments depending on the composite system
= approximately equals 180 ksi for angular fibers
= approximately equals 530 ksi for bi-directional fibers
= $\sum \alpha_i S_i t_i / \sum t_i$ for combined use of fibers

where α is a weighting factor to cater for mode domination. This is to be determined experimental observations and calibrations.

Peak Stress Relationship

$$f'_{cc} = f'_{co} + 0.39 f'_{co} \left(\frac{f_{FRP} \cdot t_{FRP}}{R \cdot f'_{co}} \right)^{0.25}$$

Peak Strain Relationship

$$\varepsilon_{cc} = \varepsilon_{co} + 0.0055\left(\frac{f_{FRP} \cdot t_{FRP}}{R \cdot f'_{co}}\right)^{0.27}$$

5.4.5 Performances of the Proposed Stress-Strain Models

A. Bilinear Increasing Model

Figures 5.8 and 5.9 show the performances of the proposed model on C1 – UC1 and C2 – WA1 – UC1. The original SMS model curves and the experimental data are also plotted on the same graph for comparison purposes.

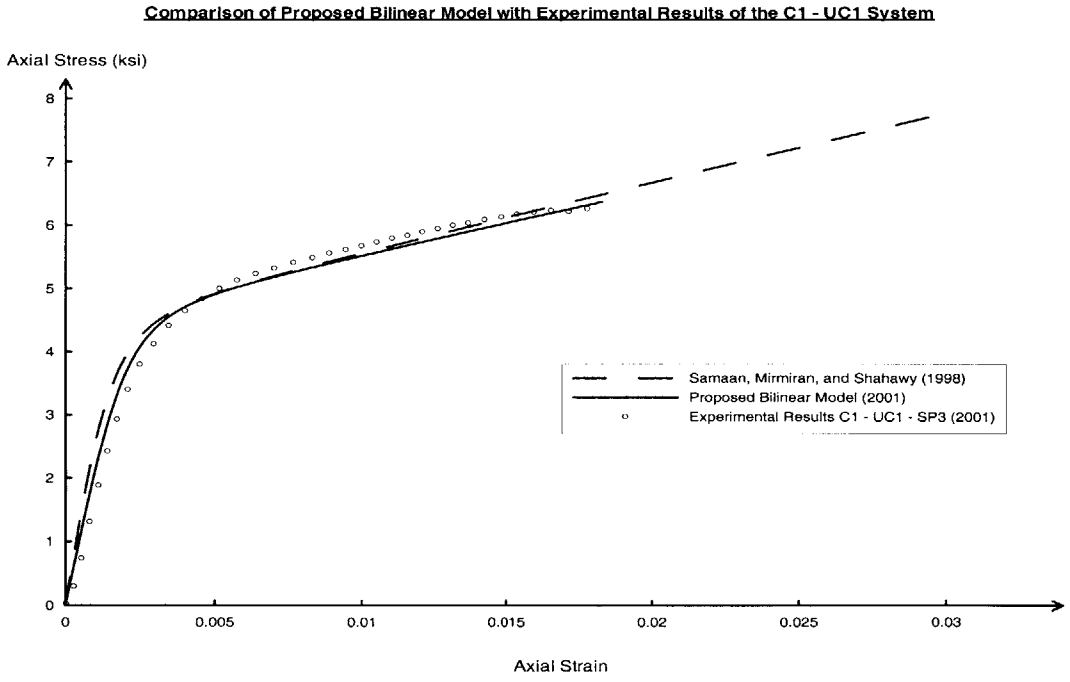

Figure 5.8 Comparison of the Proposed Bilinear Model with experimental results of the C1 – UC1 composite system

It can be noted from Figure 5.8 that the peak stress and the corresponding strain are now in good fit with the experimental data. The second slope of the proposed model is also slightly lower than the original SMS model.

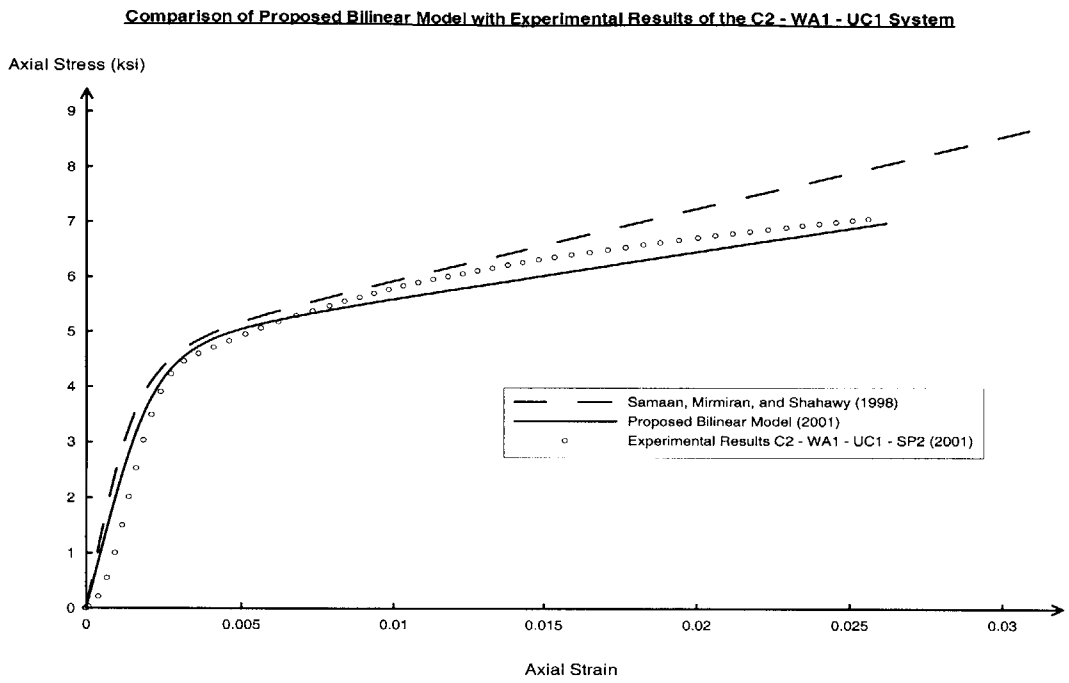

Figure 5.9 **Comparison of the Proposed Bilinear Model with experimental results of the C2 – WA1 – UC1 composite system**

From Figure 5.9, it is obvious both the initial and second slopes are modified from the original SMS model. Both proposed slopes are less steep than those proposed by the SMS model. Besides, the second plastic slope is now approximately the average of the experimental data while that of the SMS model underestimates the ductility of the combined wrap composite system.

B. Increasing-Decreasing Model

Figures 5.10, 5.11, and 5.12 show respectively the predicted responses of the C1 – W1, C1 – WA1 and the C2 – W1 – WA1 composite systems. It can be seen that the C1 – W1 prediction is slightly underestimating the peak stress while the peak strain is well predicted well. The underestimation is due solely to the vertical fiber effect that was discussed previously. The proposed peak stress model is completely unable to capture such behavior because none of the input parameters reflect the additional strength resistance of the vertical fibers. However, such underestimation is on the safe side in terms of structural design.

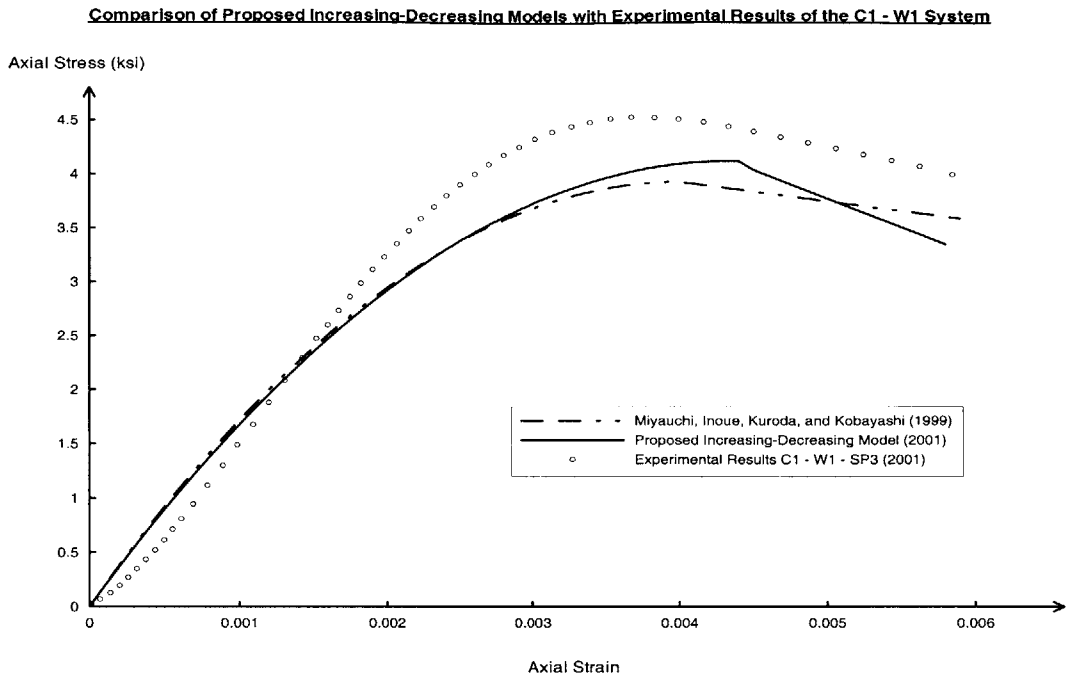

Figure 5.10 **Comparison of the Proposed Increasing-Decreasing Model with experimental results of the C1 – W1 composite system**

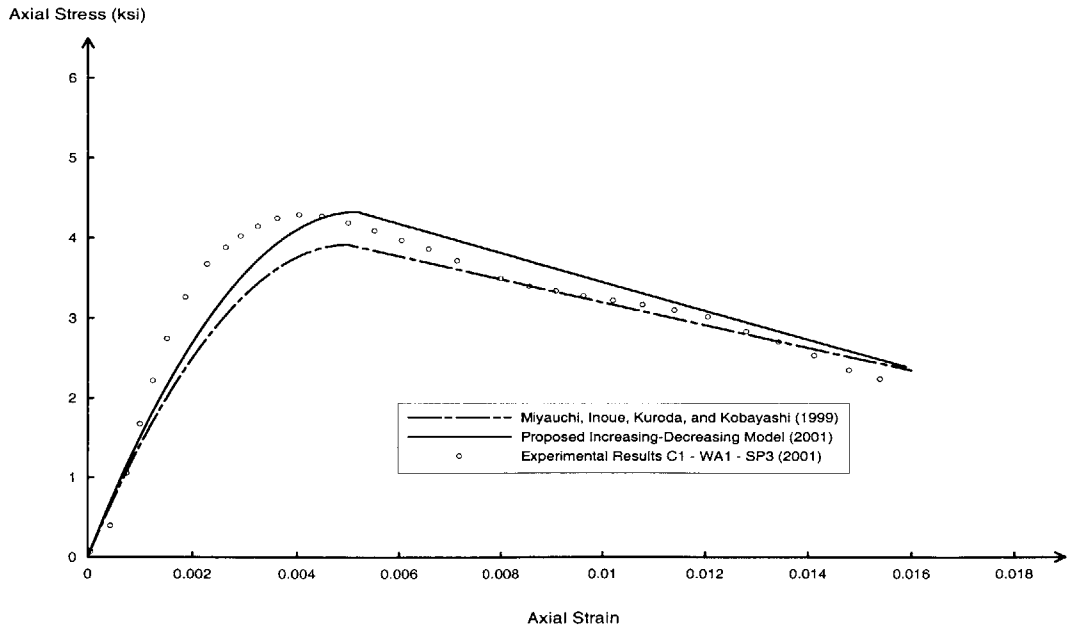

Figure 5.11 **Comparison of the Proposed Increasing-Decreasing Model with experimental results of the C1 – WA1 composite system**

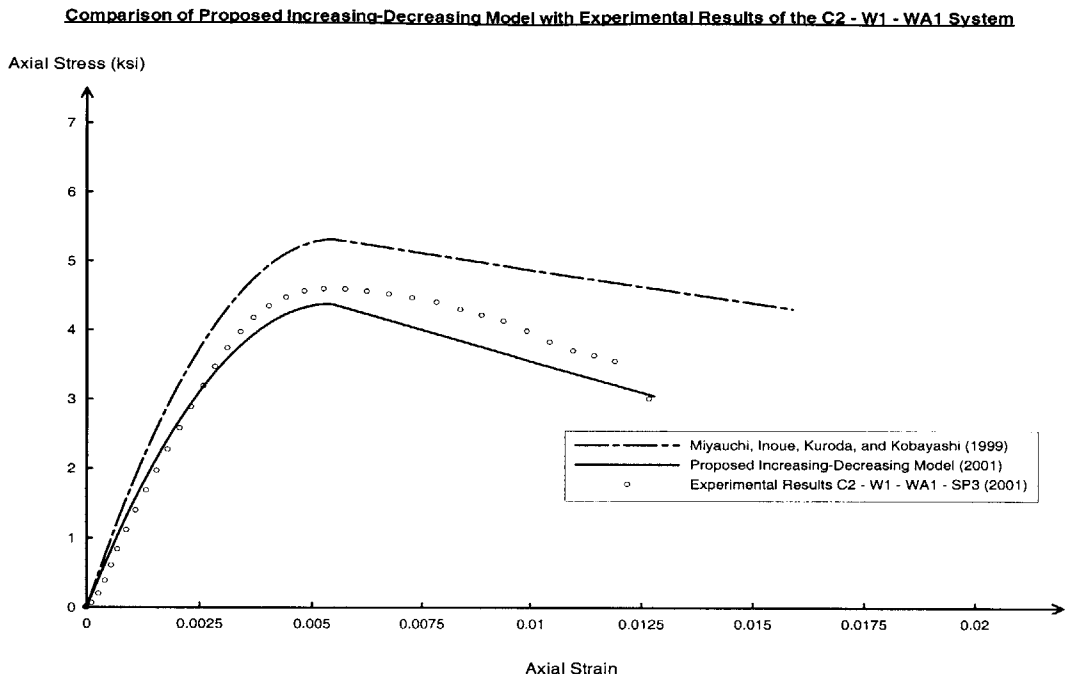

Figure 5.12 Comparison of the Proposed Increasing-Decreasing Model with experimental results of the C2 – W1 – WA1 composite system

Generally speaking, the proposed models fit quite well with the experimental curves. Nevertheless, slight deviations exist in the C1 – WA1 and C2 – W1 – WA1 composite systems due to the more scattering load responses, reflecting the statistically more varied concrete cracking and fiber rigid body motion and elongation of angular fibers.

5.5 Design Considerations of FRP-Confined Concrete

5.5.1 Objectives of Utilizing FRP Confinement: Strengthening, Retrofitting, or New Construction

A. Differences in Concrete of the Three Cases

A structural designer should be clear about the objective of the design assignment. Whether it involves the innovative design of a new structural member with composite forms or it involves the design of a strengthening or retrofitting system implies very different interpretations and use of the proposed models. First, one should distinguish the various concrete conditions of the three different cases. From a macroscopic point of view, freshly poured concrete, in the case of new construction, is unstressed (except from

its self gravity load) and undamaged. Sound concrete in a structural system, in the case of strengthening, is undamaged but stressed due to the service loads. Cracked concrete, in the case of retrofitting, is damaged and stressed with high stress concentrations. Non-uniform stress distribution can be expected.

B. Problems of Applying Proposed Models to Real World Designs

In the design of new structural members, satisfying the inherent restrictions of the proposed models such as confinement strength indices, wrapping methods, and composite systems, the equations can be considered applicable in a rough manner. Some important parameters such as size effects and embedded reinforcement effects are not yet considered. Nonetheless, the models should give a sound estimation of peak strength and deformation to designs of new structural members.

Whenever strengthening and retrofitting are involved, the designer should be cautious about the use of the models. One can see from those models that the unconfined concrete strength and strain at peak are involved and this has several vital implications. First, the unconfined strength does not really mean the existing unconfined concrete strength of the member that is usually evaluated by concrete coring or some other non-destructive testing methods. Instead, the term should be interpreted as the remaining concrete capacity if the new design load is the possible strength increase. One should bear in mind that the inherent service load has already taken up most part of the concrete capacity. Moreover, it is true that after about 30% of the unconfined concrete strength, the stress-strain relationship of concrete becomes nonlinear. This non-linearity is accompanied by a continually changing Poisson ratio and at a high level of stress (e.g. 70% of the concrete strength), the Poisson ratio of 0.2 can no longer be assumed. As a consequence, the stress-strain behavior should not be congruent with the proposed model because the concrete would enter the crushing or cracking stage soon after it is given additional loads. The concrete dilatation characteristics also change because of the larger Poisson ratio at the time when the composite system is installed. The energy absorption would be quickly dominated by the composites and the concrete core is basically failed if additional loading that exceeds the original concrete strength is imposed. It should be pointed out

that the stress-strain behavior of wrapping structural members that are initially stressed or damaged is still not clear. In fact, this is a topic of research that is left untouched at this stage.

C. Possible Implementation of the Proposed Models to Structural Strengthening

In reality, the proposed models may still find its worth in the strengthening practice. Now that the models are proposed for the wet lay-up of composite systems that are unstressed initially, one may find a similar situation when the structural members immediately adjacent to the columns that need strengthening are jacked up and supported by temporal struts so as to simulate the pseudo unstressed load level during fiber wrapping. When the struts are removed upon completion of the composite installation, the concrete and the composite wraps are stressed together from the beginning, giving a closer simulation of the laboratory testing conditions.

5.5.2 Choice of Fibers and Matrices

Choice of materials depends highly on the particular structural requirements of the project involved as well as the available budget sum. In general, for lower project cost, glass fibers are chosen due to its lower material cost. When higher structural performances such as fatigue and corrosion resistances are expected, carbon fibers would be a good choice. However, to the author's opinion, fiberglass is the recommended fiber type for column strengthening and retrofit because of its higher ductility. Matrix material such as epoxy resin would be a good choice because of its superior adhesion property and toughness. Good adhesion is essential for the reduction of the possible debonding between the fiber and the matrix. High toughness is also imperative in preventing matrix failure as well as enhancing the ductility of the wrapped structure.

5.5.3 Benefits of Using Angular Wraps in Conjunction with Hoop Wraps

A. Fundamental Behaviors of Angular and Hoop Wraps

From the experimental test results, one can see clearly that the 45-degree angular fibers are able to change substantially the failure mode. The combine action of rigid body

motion and fiber stretch of the angular fibers upon lateral expansion delays the fibers from reaching their elastic limits, hence prolonging their lives. Also, concrete, though crushed or cracked in the core, does not fall out of the jacket because the jacket essentially does not fail in fiber fracture, keeping the materials inside intact. On the other hand, it can be noted that the unidirectional fiber wraps are the most effective in giving strength increase. But one major drawback of such fiber type is that the failure mode is extremely catastrophic.

B. Angular Fiber Jacket as the Bottom Line of Failure

In view of such behaviors, one should consider the combined use of the angular fibers as well as the unidirectional fibers such that both the strength requirement and the ductile failure mode can be obtained. However, as shown in the study of stack-up sequence effects, the use of different types of fibers can be very tricky. If used properly, both strength and failure modes are improved. Otherwise, premature failure may occur. In the case of C2 – WA1 – UC1, the inner angular fiber jacket does not fail at all while fiber fracture of the outer unidirectional fiber jacket is noted. Also interlaminate peeling action is recorded and the concrete core remain intact, with no concrete spalling after structural failure. These traits are very beneficial in terms of post-failure considerations. If the outer jacket fails with the damaged concrete still in place, deformation of the failed structure is highly confined and controlled.

Consider a simple structural frame with four columns on the sides, supporting a flat slab that is being loaded evenly. If after structural failure, the concrete is spalled off from the core because of complete jacket failure, the columns will deform substantially in bending because of the uneven material distribution within the core of the columns. The slab, due to the excessive differential axial shortening and bending, will probably collapse. However, if the concrete core is held in place by a final jacket, deformation will certainly take place in a lesser extent. It is therefore suggested to use an angular fiber jacket as the innermost layer for safety purpose. It is also suggested to research on such a topic for more efficient use of materials and to prevent any possible premature failure that takes place with the C2 – UC1 – WA1 configurations.

5.5.4 Progressive Failure Design Concept

The worst failure scenario of composite jacketed columns is that all the fibers in the middle fail suddenly all at once without warning. Such failure normally occurs when only the unidirectional hoop fibers are used and that the several layers of composite materials act like one.

Learning from the results of the C2 – WA1 – UC1 specimens and viewing from an energy dissipation mechanism point of view, it is thought that when a wrap configuration that is capable of allowing interlaminate shearing and peeling of the outer-wraps one by one progressively, the energy will be dissipated in a more gradual manner in the post-peak region, leading to a progressive ductile failure mode. To attain such a progressive failure mode, a wrap configuration can be designed as one having a stepping stiffness. In other words, it would be more desirable to have the composite system with the stiffest FRP layer on the outside and gradually diminishing stiffness moving towards the core. As explained in Section 4.9.2.3, for a given displacement, the stiffer material ply will break first, assuming all plies posses identical tensile strength in the hoop direction. When the plies are arranged such that the outer layer always breaks first, the retracting force due to the elastic properties of the composite materials will lead to a shearing action at the laminate interface, peeling off the fractured layer one by one until the innermost layer is reached. An additional energy dissipation process, besides fiber fracture, is experienced. Theoretically, the tougher the matrix, the more energy can be dissipated. A beneficial by-product of such wrapping configuration is that it provides sufficient warning that the structure is failing.

5.5.5 Drawbacks of Using Large Number of Hoop Wraps

From an energy perspective, the unidirectional hoop fiber wraps absorb the most energy before break. The higher is the number of hoop wraps, the larger is the amount of energy stored in the composite system. For the same reason, at failure, identical amount of energy is released because the composite materials are essentially elastic. No plastic deformation during the loading stage helps dissipate the externally input energy. From a structural design point of view, this is highly undesirable because the sudden burst of

such a large amount of energy means that catastrophic structural failure is to take place. Therefore, it is not recommended to apply many plies of composite wraps to concrete columns as a strengthening or retrofit measures.

On the other hand, the confinement efficiency also reduces with the increase in number of wraps. This is actually shown in Figure 5.1 that when the confinement pressure increases, the ultimate strength increase rate reduces. Therefore, considering efficient use of materials, larger number of wraps means higher cost. A study about the confinement efficiency should be conducted to determine the maximum overall thickness, number of plies or fiber content to be used for design purposes.

5.5.6 Importance of Overlap Design for Structural Systems

Learning from the results of the experimental program, overlap may result in a bending effect on the wrapped column. The reason about the bending effect has been explained and will not be repeated here. However, the author would like to emphasize that such an overlap effect would eventually vanish with the increase in number of plies. This is so because the percentage thickness of influence of the overlap decreases with the increase in total thickness. For instance, for a one-ply wrap configuration, the overlap means a 100% increase in thickness in that region. For a two-ply wrap configuration, however, the overlap reduces to a 50% thickness increase. Even though, it should be pointed out that the positions of the overlap in a group of columns in a structural system should be designed with care. For a one-overlap wrap configuration, a structurally balanced layout should be strictly followed to prevent any undesirable structural response to occur.

5.5.7 Concerns about the Top and Bottom Ends

It was observed that whenever a column is wrapped with fabrics that contain vertical or angular fibers such that the fibers are subjected to or close to the proximity of direct compression, local fiber buckling or fabric wrinkling would occur. Such buckling or wrinkling initiates crack in the jacket. On the other hand, such behaviors do not appear in the case of unidirectional hoop fiber wraps. In practice, it is recommended that all fabrics should be wrapped in such a way that a margin is left between the top or bottom edge of

the fabric and the confining slabs. Although unidirectional hoop wraps do not initiate cracks because of such reason, for fear of confusion, all wraps are best to be wrapped in this fashion to prevent premature failures to occur. Moreover, it is noted that the unconfined concrete at the proximity of the loading does not fail because of the frictional effect between the concrete and the steel platen. In reality, such a frictional effect does not exist and thus, one may worry about the concrete crushing problem at the column ends. However, one should first look into the reinforcement detailing at the beam-column joint before drawing immediate conclusion to the strength at those regions. Usually, the joints are heavily reinforced with steel for fear of beam-column joint failure and to provide column-column continuity from one floor to another. In most cases, the inherent confining effect should be much higher than that at mid-height. Also, leaving a 1" margin at the ends, for instance, should practically not be of significant influence to a typical 9' column.

CHAPTER 6

SUMMARY, CONCLUSIONS, AND RECOMMENDATIONS

This thesis provides an overview of the behavior of FRP-confined plain concrete cylinders under uniaxial monotonic compression. It also presents the performance of various instrumentation techniques as well as new experimental data on the mechanical behavior of FRP-confined concrete with various wrap configurations and fiber directions. Finally, analytical models are suggested to simulate respective behaviors. Section 6.1 summarizes the objectives of this research and the primary approach of the investigation. Section 6.2 presents the main conclusions from this study. Section 6.3 provides recommendations for utilizing the present test results to field applications, followed by the suggestions for future research to further improve the knowledge on FRP-confined concrete behavior.

6.1 Research Summary

A literature review of existing information on FRP-confined concrete columns has indicated that mechanical behavior under uniaxial monotonic compression is not well understood and that the instrumentation techniques on composite material surfaces need to be studied. The study of mechanical behavior has been mostly qualitative. Axial strength increase has been the focus of most experimental program for previous studies. Composite wraps mainly consisted of unidirectional fibers in the hoop direction and the study of fiber orientation effect was scanty. Stack-up sequence effect was not fully studied. Use of combined materials in obtaining a better failure mode was not generally addressed. Initial imperfections and overlap joint effects were not studied. Lateral deformations were seldom measured. Analytical work mainly relied on previously

developed models and axial stress-strain behaviors were assumed to be bilinearly increasing. On the other hand, many researchers utilized strain gages for axial and lateral strain measurement by affixing the gages on the composite surfaces. The gage-fiber misalignment effect was not considered. These considerations have therefore provided the incentives for the current experimental study. The current work also included some analytical work was also done in view of the substantial deviations of predicted peak stress, peak strain and the stress-strain behaviors by existing models from the experimental data.

The objectives of this research are categorized in five main areas:

I. Strain Gage Instrumentation Issues

(a) To provide new information on the effect of surface preparation on composite materials for strain gage installation

(b) To compare the performances of various types of strain gages on composite surfaces with other independent devices such as LVDT and extensometers

(c) To study the effect of fiber-gage alignment

II. Loading Effects

(a) To correlate the peak stress and strain with different wrap configurations

(b) To correlate the stress reduction rate with different wrap configurations

(c) To study the failure modes and the possible improvements through the combined use of composite materials

(d) To study and categorize the load-deformation behaviors

(e) To correlate the stress-strain curve shapes with the level of confinement

III. Local Effects

(a) To study the overlap joint effect

(b) To observe and bond delamination at the composite-composite interface and the composite-concrete interface

(c) To observe any possible interlaminate shearing between two different kinds of composite materials

(d) To determine the roles of fibers being oriented at different angles

(e) To examine closely the fiber behaviors such as buckling, fracture, and reorientation under load

(f) To study the end conditions of the cylinder with and without wrap

IV. Manufacturing Effects

(a) To study the effects of initial imperfections such as embedded thumb size air pockets

(b) To study the effects of overlap length and locations

(c) To examine the fabric stacking sequence

(d) To observe qualitative the effect of epoxy bond quality on failure loads and failure modes

V. Analytical Modeling

(e) To derive a model empirically that is capable of predicting peak stress and the corresponding strain for all wrap configurations in the present study

(f) To establish a stress-strain model that can simulate the stress-strain behavior of all the wrap configurations by modifying previously developed models

In the investigation, three different types of strain gages, two identical extensometers and two specially designed lateral LVDT devices were used on six distinct wrap configurations. Three major types of fiber wraps were used. The first one consisted of unidirectional fibers placed in the hoop direction. The second one consisted of bi-directionally weaved fibers placed in the vertical and hoop direction. The third one consisted of bi-directionally weaved fibers placed in the 45 degree directions. The first strain gage type was a 120-ohm steel gage. The other two types of gages were of 350-ohm resistance. All gages had identical gage length. The first and second gages had a gage aspect ratio of two while the third gage had a gage aspect ratio of one.

The six wrap configurations were designed in such a way that any one configuration could be compared directly to at least another one. These six configurations were able to

yield sufficient information and were capable of covering the study areas stated in the objectives above.

Analytical models were proposed empirically. They are categorized by the confinement strength of the jackets. Peak stress and strain predictions were performed and compared to the current data sets. Two other independent experimental studies were also compared against with the predictive models for verification purposes. Stress-strain models were proposed by modifying two existing models. The expressions of some parameters were changed as a reflection of the change of some fundamental concepts.

6.2 Major Conclusions from Present Study

Based on the results obtained, the following conclusions regarding (1) the instrumentation technique on composite materials, (2) the behaviors of FRP-confined concrete and (3) the analytical modeling approach and its use, are drawn:

(1) In view of the deep ridges of the fiber roving on the composite wrap surfaces, epoxy filling is necessary before any strain gage installation is to take place.

(2) Strain gage resistance can substantially affect the strain measurement results. 350-ohm strain gages were found to be consistently more accurate and reliable than the 120-ohm strain gages.

(3) Higher gage aspect ratio is generally needed for more accurate measurement on materials with orthotropic properties such that the longer side of the gage is parallel with the primary (stronger) axis of the material surface.

(4) Whenever strain gages are not aligned with the fibers or when highly stressed fibers run across the gage area, faulty measurements may be obtained. In other words, strain gages are not recommended on composites with bi-directional weaved and stressed fabrics to measure strains.

(5) Strain gages with size 0.25" were found to perform sufficiently accurate in the measurement of direct tensile strains on unidirectional fiber wraps.

(6) Stress-strain curves can be categorized into two main types, depending on the confinement strength. For higher confinement strength, a bilinear increasing behavior should be expected. For lower confinement strength, an increasing-decreasing behavior should be expected.

(7) High confinement strength in the current study implies the specimens with jacket strength ratio f_{radial}/f'_c larger than 0.4.

(8) An upward shift of the kinking point is noted with increasing confinement strength.

(9) The use of identical composite materials with different or reversed stack-up sequence can give rise to a totally different stress-strain response and ultimate load and displacement.

(10) Adverse effect may be resulted from the different stiffness of the combined use of composite fabrics because of the different exposed stress level under the identical displacement under tension.

(11) Unidirectional fibers in the hoop direction mainly fail in fiber fracture when radial expansion of the core is experienced under axial compression.

(12) Vertical fibers often experience fiber buckling even if the fibers are not directly loaded. Uneven shear stresses distribute on the fiber-roving surface. The side that is in contact with either the concrete surface or another inner layer of fabrics is stressed while the outer side of the same fiber roving is not stressed. This differential stress distribution results in the buckle-out mode of failure.

(13) Angular fibers do not generally fail in fracture. When loaded in the hoop direction in tension, the angular fibers experience rigid body motion such that the matrix material that is originally in place fails. Due to the longer hoop component of the reoriented fibers, they are not stressed to their elastic limit and thus no fiber fracture takes place.

(14) Linearity of strength increase is observed for two-ply cases. This, however, is true only if there is no adverse effect between the two different kinds of fiber wraps.

(15) Mode domination may take place depending on the fundamental behaviors of the fabrics. It is also dependent on the fabric strength and fiber orientation. In the case of C2 – W1 – WA1, the angular fiber mode of failure dominates over the bi-directional fiber mode of failure. Stress reduction rate is significantly reduced when compared to the C1 – W1 case alone.

(16) The higher the stress reduction rate, the more catastrophic the failure is. For instance, C1 – W1 has the fastest stress reduction rate, it failed all in a sudden without any warning.

(17) By using an angular fiber wrap as the inner wrap and a unidirectional fiber wrap as the outer wrap, an optimal behavior is obtained. This wrap configuration demonstrates the highest strength increase while the failure mode and stress-reduction are moderate. The inner angular fiber wrap serves as a safety jacket and prevents the concrete from spalling out of the core. The outer unidirectional fiber wrap serves as the strength-enhancing layer.

(18) Overlap joint is found to give rise to a bending effect for the one-wrap cases. Differential axial shortening was recorded. For two-wrap cases, which had the overlap joints placed opposite to each other, the bending effect disappeared.

(19) Overlap debonding can occur when the overlap length is too short. The debonding action may cause a premature failure and a lower-than-normal ultimate load may be resulted.

(20) In all cylinder tests, unwrapped ends do not fail in concrete crushing due to the additional confinement effect from the frictional force between the steel platen and the concrete end.

(21) Wrap ends, if consisted of fibers in the directions under than the hoop direction and that the wrapping edges reach the end surface, consistently

initiate failure of the fabric materials through the local fiber buckling mechanism.

(22) Thumb size air pockets do not usually affect the ultimate strength of a column. But they act as nuclei sites for delamination flow and help accelerate the post-peak failure rate.

(23) Regarding to the design of FRP-confined concrete, the objectives have to be clear. The designer should distinguish among new construction, strengthening and retrofit. The three cases require three different interpretation and utilization of the confinement models.

(24) Progressive failure design concept should be employed in order to yield the safest and most ductile failure once the load level has exceeded the ultimate strength of the wrapped column. This progressive failure can be attained by deploying the stepped-stiffness strategy such that the stiffness composite wrap is used as the outermost layer while a decreasing stiffness is used as the plies move inward to the concrete core.

(25) The use of large number of wraps are discouraged because of the enormous buildup of energy and the sudden release at failure.

(26) The use of a combination of angular fibers and unidirectional hoop fibers are encouraged in order to attain both a ductile failure mode and the high strength requirement.

(27) Most existing analytical models overestimate the peak stress of the FRP-confined cylinders. Peak strain estimation is also poor. To attain a more reasonable estimation, different models have to be developed for specimens with different confinement strength. This is so because of the concrete failure mechanism at different ranges of confinement strength behave very differently. Cracking dominates when the confinement level is low while crushing dominates when the confinement level is high.

(28) When developing a stress-strain model, the kinking shift phenomenon must be encountered. It is proved that in most cases, the kinking points do not occur at the peak stress level of unconfined concrete.

6.3 Recommendations for Future Work

Based on the experience gained from this study, the following recommendations are made for further research and field applications:

(1) Performances of different sizes of strain gages should be investigated with a gage resistance of 350 ohms on the unidirectional hoop fiber wraps.

(2) Loading rate effect needs to be studied so that the rate effect can be calibrated for use of analytical models derived from a specific rate of loading.

(3) Size effect of the cylinders need to be investigated. For instance, varying heights and section sizes were not studied in the current experimental program. However, these pieces of information are of vital importance for the application of the laboratory test results to real world column applications.

(4) Very little data has been established to compare the mechanical behaviors of various composite systems with the same strengths. Such systems may include the wet-lay-up composite wraps, fiber winding systems, and preformed composite shells.

(5) Investigation on the fiber orientation is also needed so as to evaluate the possible beneficial effects of angular fibers.

(6) Effects of different kinds of initial imperfections including larger sizes of air pockets, fabric wrinkling, and initially broken fibers are needed to correlating with the stress-strain behaviors as well as the ultimate strength of the columns.

(7) Overlap effects should be studied with increasing number of plies to see whether such an adverse bending effect would vanish as predicted with an increasing number of plies because of the decreasing percentage of overlap thickness to overall jacket thickness ratio.

(8) Ductile failure modes should be found by optimizing the wrap configurations and combined use of materials.

(9) Long-term loading such as sustained load, and dynamic loading such as axial and lateral cyclic loads should be investigated.

(10) Eccentric load effect should be investigated to find out the mechanical behavior of the FRP-confined concrete under both bending and axial compression.

(11) Investigation of the effects of wrapping on cracked and initially stressed concrete is needed so as to simulate the real world concrete conditions in the cases of strengthening and retrofitting.

(12) In field applications, large factor of safety is still recommended due to the insufficiently studied analytical models, which mostly overestimate the peak strength.

(13) Also, untested wrap configurations are not recommended due to the possible adverse interactions between two different composite materials that would lead to undesirable premature failure.

(14) An angular fiber wrap is recommended as the bottom line safety jacket as the innermost layer so that concrete does not fall off the core after structural failure.

(15) Overlap joint layout needs to be balance within a structural system so as to prevent the differential bending stresses developed on adjacent or supporting structural members.

References

Books, Manuals, and Thesis

1. ACI Manual of Concrete Practice Part 5 – 2000, Committee 440R-96, State-of-the-art report on fiber reinforced plastic (FRP) reinforcement for concrete structures. Technical report, American Concrete Institute (1996)

2. American Society for Testing and Materials, ASTM Manual C192/C192M: Standard Practice for Making and Curing Concrete Test Specimens in the Laboratory (1998)

3. American Society for Testing and Materials, ASTM Manual C39/C39M: Standard Test method for Compressive Strength of Cylindrical Concrete Specimens (1999)

4. American Society for Testing and Materials, ASTM Manual C617: Capping Cylindrical Concrete Specimens (1998)

5. American Society for Testing and Materials, ASTM Manual D3039/D3039M: Standard Test Method for Tensile Properties of Polymer Matrix Composite Materials (2000)

6. Ashbee K, Fundamental Principles of Fiber Reinforced Composites, TA481.5.A83 (1989)

7. Berthelot J M, Composite Materials: Mechanical Behavior and Structural Analysis, TA418.9.C6.B467 (1999)

8. BLH Catalogue: Strain Gages for Stress Analysis, Catalogue Number 100-6 (2000)

9. Calvi G M, Priestley M J N, Seible F, Seismic Design and Retrofit of Bridges, TG300.P64 (1996)

10. Editor: Gdoutos E E, Pilakoutas K, Rodopoulos C A, Failure Analysis of Industrial Composite Materials (2000)

11. Editor: Kawahara W, Reese R T, Handbook on Structural Testing, TA646.R36 (1993)

12. Editor: Kelly A, Concise Encyclopedia of Composite Materials, TA418.9.C6C635 (1989)

13. Editor: Nanni A, Fiber-Reinforced-Plastic (FRP) Reinforcement for Concrete Structures: Properties and Applications, TA683.F45 (1993)

14. Editor: Peters S T, Handbook of Composites 2nd Edition, ISBN 0 412 54020 7 (1998)

15. Editor: Tuttle M E, Pendleton R L, Manual on Experimental Methods for Mechanical Testing of Composites, TA418.9.C6.M36 (1989)

16. Editor: Window A L, Strain Gauge Technology 2nd Edition, TA413.S72 (1992)

17. Fyfe Co. LLC, Design Manual for the Tyfo® Fibrwrap® System Rev.2 (1999)

18. Haftka R T, Hajela P, Gurdal Z, Design and Optimization of Laminated Composite Materials, TA418.9.L3.G87 (1999)

19. Hearn E J, Mechanics of Materials, TA405.H3 (1997)

20. Holmes M, Just D J, GRP in Structural Engineering, TA455.P55.H65 (1983)

21. Howie I, A Study on the Use of Composite Wraps for Rehabilitation of Deteriorated Concrete Columns, Master Thesis, University of Delaware (1995)

22. ICBO Evaluation Service, Inc, AC125: Acceptance Criteria for Concrete and Reinforced and Un-reinforced Masonry Strengthening Using Fiber-Reinforced Composite Systems (1997)

23. Newman A, Structural Renovation of Buildings: Methods, Details, and Design Examples, TH3401.N49 (2001)

24. Rosato D V, Designing with Reinforced Composites: Technology – Performance – Economics, TA455.P55.R58 (1997)

25. Shahawy M, Mirmiran A, Analytical and Experimental Investigation of Reinforced Concrete Columns Encased in Fiberglass Tubular Jacket and Use of Fiber Jacket for Pile Splicing, (1997)

26. Soon K A, Behavior of Pressure Confined Concrete in Monotonic and Cyclic Loadings, PhD Thesis, Department of Civil Engineering, MIT (1987)

Journal Papers and Proceedings

1. Abbott B J, Richard R M, 'Versatile Elastic-Plastic Stress-Strain Formula', *J. Engg Mech, Proceedings of the ASCE,* V.**101**, No.EM4, Aug., 511-515 (1975)

2. Bogetti T A, Gillespie J W, Hoppel C P R, 'Design and Analysis of Composite Wraps for Concrete Columns', *J. Reinforced Plastics and Composites*, V.**16**, No.7, 588-602 (1997)

3. Bogetti T A, Gillespie J W, Hoppel C P R, Howie I, Karbhari V M, 'Analysis of a Concrete Cylinder with a Composite Hoop Wrap', *Infrastructure Repair Methods*, 191-198

4. Bradford N.M., Nanni A., 'FRP Jacketed Concrete Under Uniaxial Compression', *Const. & Building Mat.,* V.**9**, No.2, 115-124 (1995)

5. Brandtzaeg A, Brown R L, Richart F E, 'A Study of the Failure of Concrete Under Combined Compressive Stresses', *University of Illinois Bulletin*, No. 185, Vol. XXVI, No.12, Nov., pp 3 – 103. (1928)

6. Cusson D, Paultre P, 'Stress-strain Model for Confined High-strength Concrete', *J. Struct. Engg.*, V.**121**, No.3, Oct., 468-477, (1993)

7. Eckel D A, Karbhari V M, Tunis G C, 'Strengthening of Concrete Column Stubs through Resin Infused Composite Wraps', *J. Therm. Comp. Mat.*, V.**6**, 92-106 (1993)

8. Ehsani M R, Li M W, Saadatmanesh H, 'Strength and Ductility of Concrete Columns Externally Reinforced with Fiber Composite Straps', *ACI Struct. J.*, V.**91**, No.4, July.-Aug., 434-447 (1994)

9. Fardis M N, Khalili H H, 'Concrete Encased in Fiberglass-Reinforced Plastic', *ACI Journal*, Nov. - Dec., 440-446 (1981)

10. Fardis M N, Khalili H H, 'FRP-encased Concrete as a Structural Material', *Magazine of Concrete Research*, V.**14**, Dec., 191-202 (1982)

11. Fujimaki T, Iso M, Honda Y, Kaneto M, Nakamura H, Shirai N, Toyoshima M, Watanabe K, 'Confinement Effect of FRP Sheet on Strength and Ductility of Concrete Cylinders Under Uniaxial Compression', *Proceedings of the Third International Symposium*, V.**1**, 233-240 (1997)

12. Hakamada F, 'Experimental Study on Retrofit of RC Column Using CFRP Sheet', *Proceedings of the Third International Symposium*, V.**1**, 419-426 (1997)

13. Hoshikuma J I, Hosotani M, Kawashima K, 'A Study on Confinement Effect of Concrete Cylinders by Carbon Fiber Sheets', *Proceedings of the Third International Symposium*, V.**1**, 209-216 (1997)

14. Howie I, Karbhari V M, 'Effect of Tow Sheet Composite Wrap Architecture on Strengthening of Concrete Due to Confinement: I – Experimental Studies', *J. Reinforced Plastics and Composites*, V.**14**, Sept., 1008-1030 (1995)

15. Inoue S, Kuroda T, Kobayashi A, Miyauchi K, 'Strengthening Effects of Concrete Column with Carbon Fiber Sheet', *Transactions of the JCI,* V.**21**, 143-150 (1999)

16. Inoue S, Miyauchi K, Nishibayashi S, 'Estimation of Strengthening Effects with Carbon Fiber Sheet for Concrete Column', *Proceedings of the Third International Symposium*, V.**1**, 217-232 (1997)

17. Karabinis A I, Kiousis P D, 'Effects of Confinement on Concrete Columns: Plasticity Approach', *J. Struct. Engg.*, V.**120**, No.9, Sept., 2747-2767 (1994)

18. Karbhari V M, Gao Y, 'Composite Jacketed Concrete Under Uniaxial Compression - Verification of Simple Design Equations', *J. Mat. in Civil Engng.*, 185-193 (1997)

19. Katsumata H, Kobatake Y, 'Retrofit of Existing Reinforced Concrete Columns Using Carbon Fibers', *Proceedings of the Third International Symposium*, V.**1**, 555-562 (1997)

20. Kupper H, Hilsdorf H K, 'Behavior of Concrete Under Biaxial Stresses' *ACI Journal*, V.**66**, Aug. 656-666 (1969)

21. Labossiere P, Picher F, Rochette P, 'Confinement of Concrete Cylinders with CFRP', *Fiber Composites in Infrastructure: Proceedings of the First International Conference on Composites in Infrastructure, Tuscon*, Jan., 829-841 (1996)

22. Mander J B, Park R, Priestley M J N, 'Observed Stress-Strain Behavior of Confined Concrete', *J. Struct. Engg.* V.**114**, No. 8, Aug., 1827-1849 (1988)

23. Mander J B, Park R, Priestley M J N, 'Theoretical Stress-strain Model for Confined Model', *J. Struct. Engg.* V.**114**, No. 8, Aug., 1804-1826 (1988)

24. Mirmiran A, Shahawy M, 'A New Concrete-Filled Hollow FRP Composite Column', *Composites: Part B,* **27B**, 263-268 (1996)

25. Mirmiran A, Shahawy M, 'Dilation Characteristics of Confined Concrete', *Mech. Of Cohesive-Frictional Mat.,* V.**2**, 237-249 (1997)

26. Mirmiran A, Shahawy M, 'Behavior of Concrete Columns Confined by Fiber Composites', *J. Struct. Engng*, V.**123**, No.5, 583-590 (1997)

27. Mirmiran A, Shahawy M, Samaan M, 'Model of Concrete Confined by Fiber Composites', *J. Struct. Engg.,* V.**124**, No.9, Sept., 1025-1031 (1998)

28. Mirmiran A, Shahawy M, Samaan M, Echary H E, Mastrapa J C, Pico O, 'Effect of Column Parameters on FRP-Confined Concrete', *J. Comp. for Const.,* V.**2**, No.4, Nov., 175-185 (1998)

29. Mirmiran A, Shahawy M, Samaan M, Kargahi M, 'Composite FRP-Concrete Column with Bi-directional External Reinforcement', *Fiber Composites in Infrastructure: Proceedings of the First International Conference in Composites in Infrastructure ICCI '96* (1996)

30. Mirmiran A, Shahawy M, Samaan M, 'Strength and Ductility of Hybrid FRP-Concrete Beam Columns', *J. Struct. Engng*, V.**125**, No.10, 1085-1093 (1999)

31. Newman K, Lachance L, 'The Testing of Brittle Materials Under Uniform Uniaxial Compressive Stress', *ASTM* V.**64**, 1044-1067 (1964)

32. Van Mier, JanG.M., 'Complete Stress-strain Behavior and Damaging Status of Concrete Under Multiaxial Conditions', *RILEM/CEB Symposium on Concrete Under Multiaxial Conditions*, INSA, Toulouse, May, Session 3 (1984)

33. Tan K H, Department of Civil Engineering, National University of Singapore, *Personal email letter*, Obtained upon request to the current thesis author (2000).

34. Yanagisawa M, Yanase T, 'An Experimental Study on Existing Reinforced Concrete Columns Jacketed with Carbon Fiber Sheets', *Proceedings of the Third International Symposium*, V.**1**, 427-434 (1997)

Other General References

1. Araki N, Fukuyama H, Kataoka T, Nakano K, Matsuzaki Y, 'Ductility of Retrofitted RC Columns with Continuous Fiber Sheets', *Proceedings of the Third International Symposium*, V.**1**, 547-554 (1997)

2. Arockiasamy M, Amer Ahmed, Chidambaram S, Shahawy M, 'Long Term Behavior of Concrete Columns with CFRP', *Engineering Mechanics*, 1050-1053 (1996)

3. Asai H, Iwata M, Shimbo H, Yamada K, Yonekura A, 'Aseismatic Retrofit of Concrete Piers with CFRP Ring and Expansive Concrete', *Proceedings of the Third International Symposium*, V.**1**, 363-370 (1997)

4. Bahng E Y, Feng M Q, 'Damage Assessment of Jacketed RC Columns Using Vibration Tests', *J. Struct. Engng*, V.**125**, No.3, 265-271 (1999)

5. Bisarnsin T, Green A, Hashem Z, Yuan R L, 'Fiber Reinforced Plastic Composite Columns', Advanced Composite Materials, 205-211

6. Brown C B, Cameron B, Roeder C W, 'Composite Action in Concrete Filled Tubes', *J. Struct. Engng*, V.**125**, No.5, 477-484 (1999)

7. Chaallal O, Shahawy M, 'Performance of Fiber-Reinforced Polymer-Wrapped Reinforced Concrete Column under Combined Axial-Flexural Loading', *ACI Struct. J.*, V.**97**, No.4, July-Aug. 659-668 (2000)

8. Chai Y H, 'An Analysis of the Seismic Characteristics of Steel-Jacketed Circular Bridge Columns', *Earthquake Engng. Struct. Dyn.* **25**, 149-161 (1996)

9. Chai Y H, Priestley M J N, Seible F, 'Analytical Model for Steel-Jacketed RC Circular Bridge Columns', *J. Struct. Engng.*, ASCE, V.**120**, No.8, 2358-2376 (1994)

10. Chai Y H, Priestley M J N, Seible F, 'Seismic Retrofit of Circular Bridge Columns for Enhanced Flexural Performance', *ACI Struct. J.*, V.**88**, No.5, Sept.-Oct., 572-584 (1991)

11. Dotiwala F S, D'Souza J T, Pincheira J A, 'Seismic Analysis of Older Reinforced Concrete Columns', *Earthquake Spectra*, V.**15**, No.2, 245-272 (1999)

12. Echary H E, Mirmiran A, Shahawy M, 'Acoustic Emission Monitoring of Hybrid FRP-Concrete Columns', *J. Struct. Engng*, V.**125**, No.8, 899-905 (1999)

13. Eckel D A, Karbhari V M, 'Effect of Cold Regions Climate on Composite Jacketed Concrete Columns', *J. Cold Reg. Engng.*, V.**8**, No.3, 73-85 (1994)

14. Ehsani M R, Jin L, Saadatmanesh H, 'Repair of Earthquake-Damaged RC Columns with FRP Wraps', *ACI Struct. J.*, V.**94**, No.2, Mar.-Apr., 206-215 (1997)

15. Ehsani M R, Jin L, Saadatmanesh H, 'Seismic Retrofitting of Rectangular Bridge Columns with Composite Straps', *Earthquake Spectra.* V. **13**, No. 2, 281-304 (1997)

16. Feng M Q, Haroun M A, Sultan M, 'Cyclic Qualification Testing of Jacketed Bridge Columns in Flexure and Shear', *University of California, Irvine, Comprehensive Testing Program Report*, 1770-1776

17. Filippou F C, Spacone E, Taucer F F, 'Fiber Beam-Column Model for Non-Linear analysis of R/C Frames: Part 1. Formulation', *Earthquake Engng. Struct. Dyn.* **25**, 711-725 (1996)

18. Filippou F C, Spacone E, Taucer F F, 'Fiber Beam-Column Model for Non-Linear analysis of R/C Frames: Part 2. Applications', *Earthquake Engng. Struct. Dyn.* **25**, 727-742 (1996)

19. Gamble W L, Hawkins N M, Kaspar I I, 'Seismic Retrofitting of Bridge Pier Columns', *41st International Symposium*, 1004-1014 (1996)

20. Gergely J, Pantelides C P, Reaveley L D, Volnyy V A, 'Retrofit of RC Bridge Pier with CFRP Advanced Composites', *J. Struct. Engng*, V.**125**, No.10, 1094-1099 (1999)

21. Hsu H L, Lin J L, 'Experimental Evaluation on Seismic Performance of Sandwich Box Columns', *Earthquake Engng. Struct. Dyn.* **28**, 823-840 (1999)

22. Innamorato D, Hegemier G A, Priestley M J N, Seible F, 'Seismic Retrofit of RC Columns with Continuous Carbon Fiber Jackets', *J. Comp. for Constr.*, V.**1**, No.2, 52-62 (1997)

23. Iso M, Matsuzaki Y, Sonobe Y, Nakamura H, Watanabe K, Watanabe M, 'Experimental Study on Seismic Behavior of Reinforced Concrete Columns with Wing Walls Retrofitted by Carbon Fiber Sheets', *Proceedings of the Third International Symposium*, V.**1**, 579-586 (1997)

24. Kage T, Lee H S, Noguchi T, Tomosawa F, 'Effect of CFRP Sheets on Shear Strengthening of a Reinforced Concrete Column Damaged by Rebar Corrosion', *Proceedings of the Third International Symposium*, V.**1**, 451-458 (1997)

25. Kakuta Y, Kazuteru S, Sato Y, Sirbu G, Ueda T, 'Seismic Resistance of Reinforced Concrete Pier with Carbon Fiber Sheet Retrofitting', *Proceedings of the Third International Symposium*, V.**1**, 571-578 (1997)

26. Kishi N, Mikami H, Matsuoka K G, Sato M, 'Strengthening Effects of Winding Materials on RC Columns due to Axial Impact Loads', *Proceedings of the Third International Symposium*, V.**1**, 249-256 (1997)

27. Ma R, Xiao Y, 'Seismic Retrofit of RC Circular Columns Using Prefabricated Composite Jacketing', *ACI Struct. J.*, V.**123**, No.10, Oct., 1357-1364 (1997)

28. Macrae G A, Myojo T, Nosho K, Stanton J, 'Carbon Fiber Retrofit of Rectangular RC Gravity Columns in Seismic Regions', *Proceedings of the Third International Symposium*, V.**1**, 371-378 (1997)

29. Martin G R, Wu H, Xiao Y, 'Prefabricated Composite Jacketing of RC Columns for Enhanced Shear Strength', *J. Struct. Engng*, V.**125**, No.3, 255-264 (1999)

30. Mills R H, Pantazopoulou S J, 'Microstructural Aspects of the Mechanical Response of Plain Concrete', *ACI Mat. J.,* V.**92**. No.6 Nov. –Dec., 605-616 (1995)

31. Nagasaka T, Okamoto T, Tanigaki M, 'Shear Strengthening Effectiveness of Aramid Fiber Tapes on Existing R/C Columns', *Proceedings of the Third International Symposium*, V.**1**, 539-546 (1997)

32. Pantazopoulou S J, 'Role of Expansion on Mechanical Behavior of Concrete', *J. Struct Engg.,* V.**121**, No.12, Dec., 1795-1805 (1995)

33. Pantelides C P, Volnyy V A, 'Bond Length of CFRP Composites Attached to Precast Concrete Walls', *J. Comp. for Constr.*, V.3, No.4, 168-176 (1999)

34. Priestley N M J, Seible F, Verma R, Xiao Yan, 'Steel Jacket Retrofitting of Reinforced Concrete Bridge Columns for Enhanced Shear Strength - Part 1: Theoretical Considerations and Test Design', *ACI Struct. J.*, V.**91**, No.4, July-Aug., 394-405 (1994)

35. Priestley N M J, Seible F, Verma R, Xiao Yan, 'Steel Jacket Retrofitting of Reinforced Concrete Bridge Columns for Enhanced Shear Strength - Part 2: Test Results and Comparison with Theory', *ACI Struct. J.*, V.**91**, No.5, Sept.-Oct., 537-551 (1994)

36. Priestley N M J, Seible F, Xiao Yan, 'Seismic Assessment and Retrofit of Bridge Column Footings', *ACI Struct. J.*, V.**93**, No.1, Jan.-Feb., 79-94 (1996)

Appendix A

Summary of
Channel Numbers and Input Voltages of
Instrumentation Devices

Summary of Channel Numbers and Input Voltages of Instrumentation Devices

Channel #	Device Type	Input Voltage	Notes
1	Extensometer 1	4.0	For vertical strain
2	Extensometer 2	4.0	For vertical strain
3	120-ohm strain gage	5.5	Single element steel gage
4	120-ohm strain gage	5.5	Single element steel gage
5	200 Kip Load Cell	5.5	Baldwin 200 kips loading frame
6	Lateral LVDT 1	5.5	Mid-height, lateral strain (over 6" diameter)
7	Lateral LVDT 2	5.5	2" from mid-height, lateral strain (over 6" total length)
8	Crosshead LVDT 1	5.5	Vertical strain (over 15" total height)
9	Crosshead LVDT 2	5.5	Vertical strain (over 15" total height)
20	350-ohm strain gage	4.0	Either single or tee gage
21	350-ohm strain gage	4.0	Either single or tee gage
22	350-ohm strain gage	4.0	Either single or tee gage
23	350-ohm strain gage	4.0	Either single or tee gage
30	Input voltage	4.0	For 350 ohm strain gage

Appendix B

Formulas of Conversion from Raw Data (Voltages) to
Displacements and Direct Strains

Displacement Conversion Formula for LVDT Devices

$$\text{Displacement} = \frac{\Delta(\text{voltage}_{\text{out}})}{\text{voltage}_{\text{in}}} \times (\text{Calibration Factor})$$

Direct Strain Conversion Formula for Strain Gages

$$\varepsilon = \frac{4 \times (\Delta V_{\text{out}})}{(\text{Gage Factor}) \times (V_{\text{in}}) \times (\text{Active Arms})}$$

Appendix C

Summary of Calibration Factors and Device Measuring Ranges

Summary of Calibration Factors and Device Measuring Ranges

Device	Voltage Range	Calibration Factor	Measuring Range
Lateral LVDT 1	±2V	0.28348 in/v/v	±0.1 in
Lateral LVDT 2	±2V	0.28667 in/v/v	±0.1 in
Crosshead LVDT 1	±2V	0.93140 in/v/v	±0.35 in
Crosshead LVDT 2	±2V	0.85231 in/v/v	±0.3 in
Extensometer 1	±0.015V	32.0252 in/v/v	±0.1 in
Extensometer 2	±0.015V	34.1192 in/v/v	±0.1 in
200 kip Load Cell	Not applicable	8510 kips/v/v	0 – 200 kips

Appendix D

Peak Stress and Strain of Respective Specimens

Summary of Peak Stress and Peak Strain of All Individual Specimens

Test Specimens	Peak Stress (ksi)	Peak Strain (in./in.)
C1 – UC1 – SP1	6.17	0.01263
C1 – UC1 – SP2	6.43	0.01763
C1 – UC1 – SP3	6.28	0.01809
C1 – W1 – SP1	4.18	0.003545
C1 – W1 – SP2	4.30	0.005691
C1 – W1 – SP3	4.52	0.003678
C1 – WA1 – SP1	4.00	0.006070
C1 – WA1 – SP2	3.48	0.004963
C1 – WA1 – SP3	4.29	0.004117
C2 – W1 – WA1 – SP1	4.52	0.004818
C2 – W1 – WA1 – SP2	4.73	0.005965
C2 – W1 – WA1 – SP3	4.61	0.006023
C2 – UC1 – WA1 – SP1	6.80	0.01605
C2 – UC1 – WA1 – SP2	5.68	0.01524
C2 – UC1 – WA1 – SP3	6.12	0.01708
C2 – WA1 – UC1 – SP1	6.92	0.02768
C2 – WA1 – UC1 – SP2	7.08	0.02602
C2 – WA1 – UC1 – SP3	6.99	0.02582

Appendix E

Stress-Strain Plots of Respective Specimens

Plot of Axial Stress – Axial Strain of C1 – UC1 – SP1

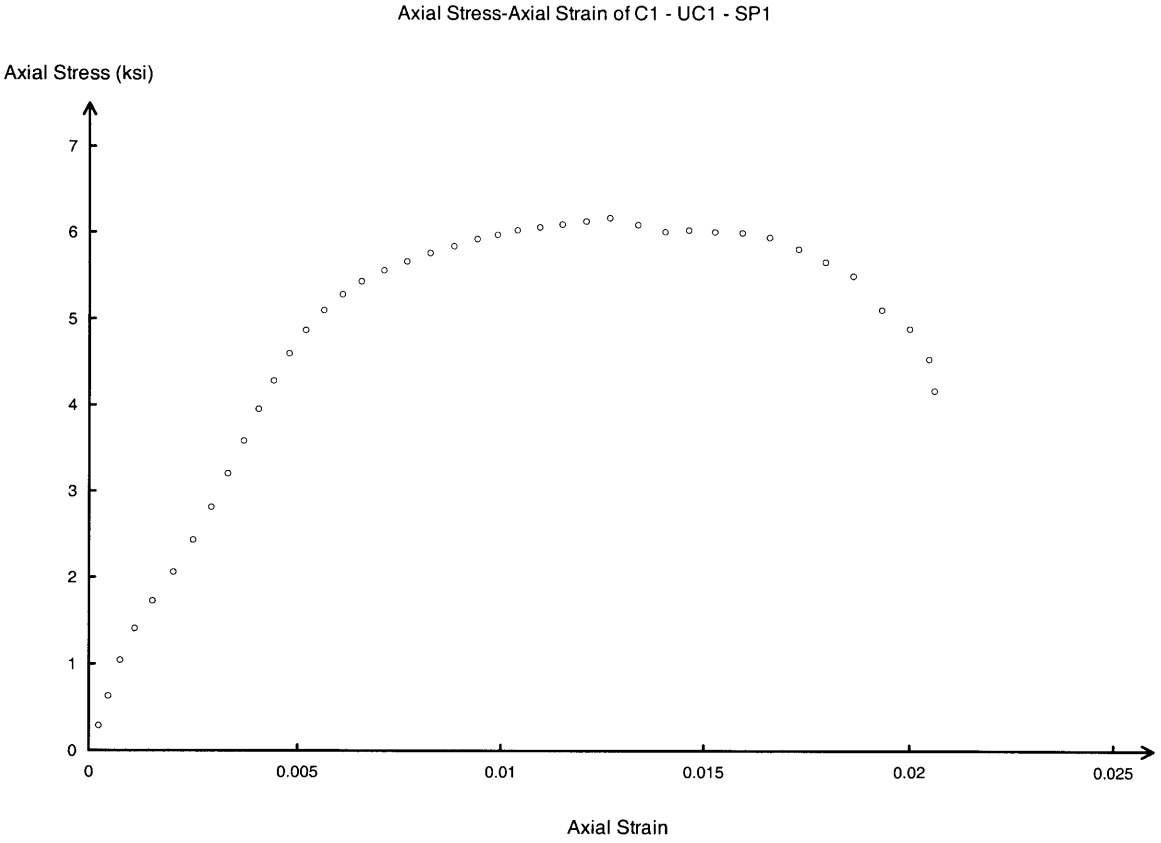

Plot of Axial Stress – Axial Strain of C1 – UC1 – SP2

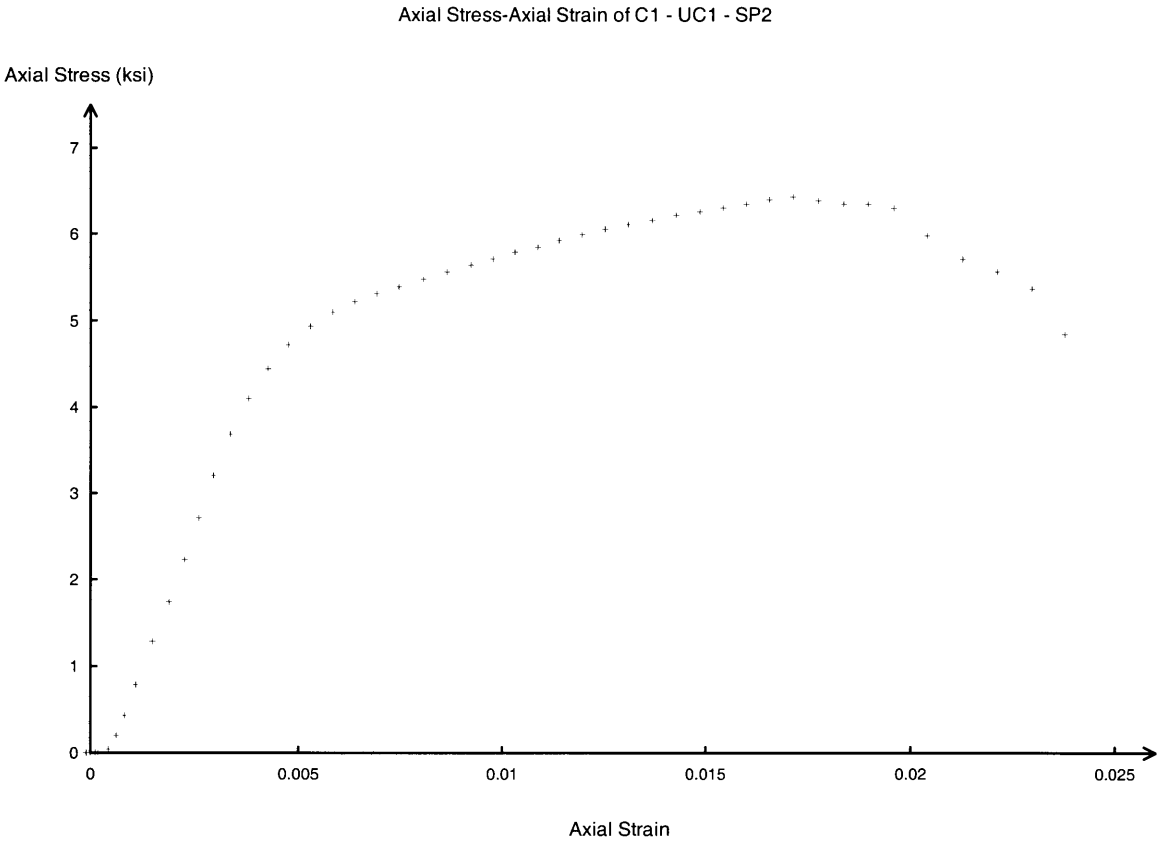

Plot of Axial Stress – Axial Strain of C1 – UC1 – SP3

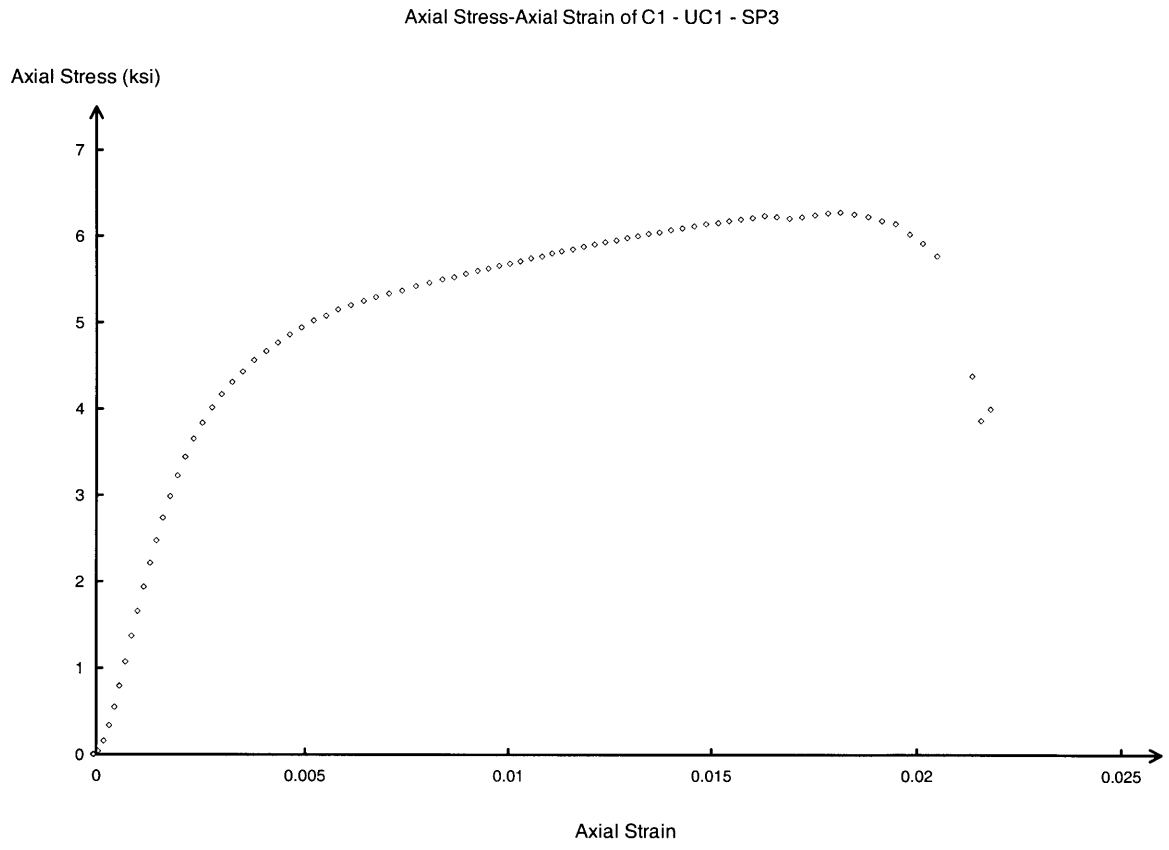

Plot of Axial Stress – Axial Strain of C1 – W1 – SP1

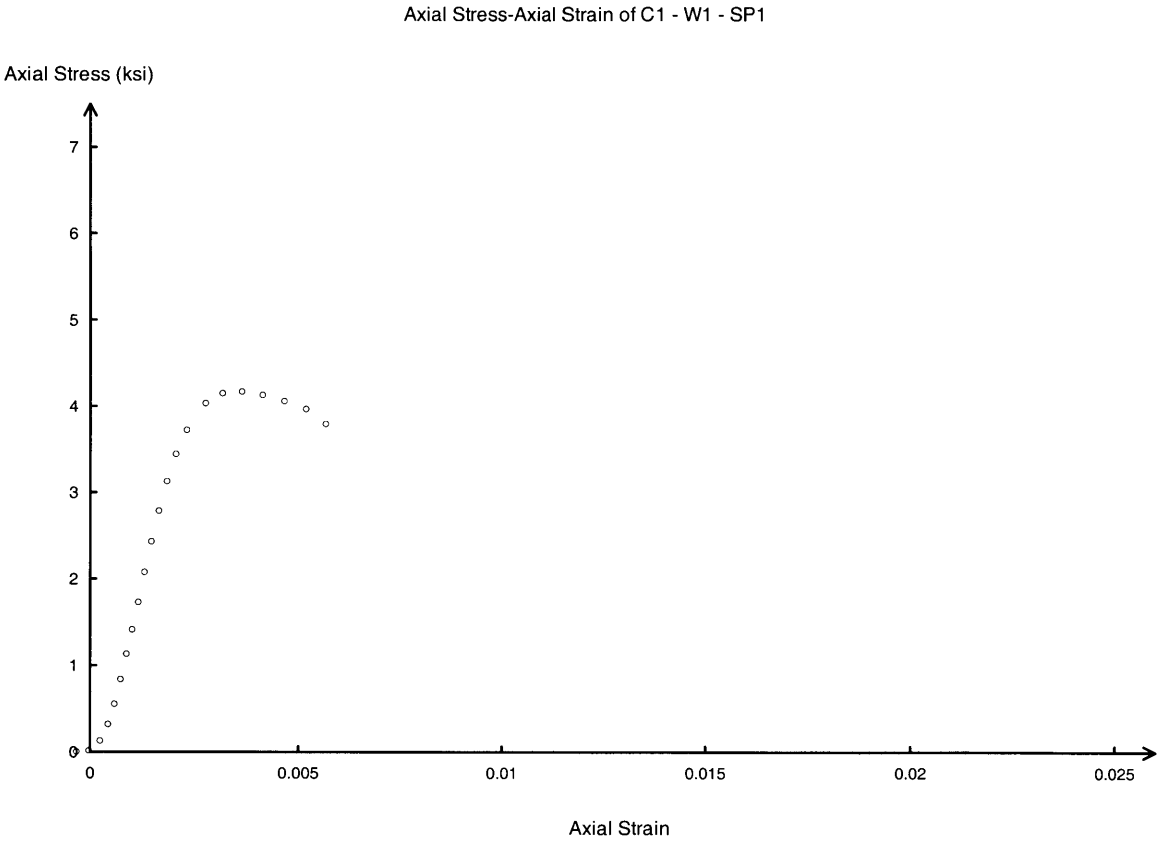

Plot of Axial Stress – Axial Strain of C1 – W1 – SP2

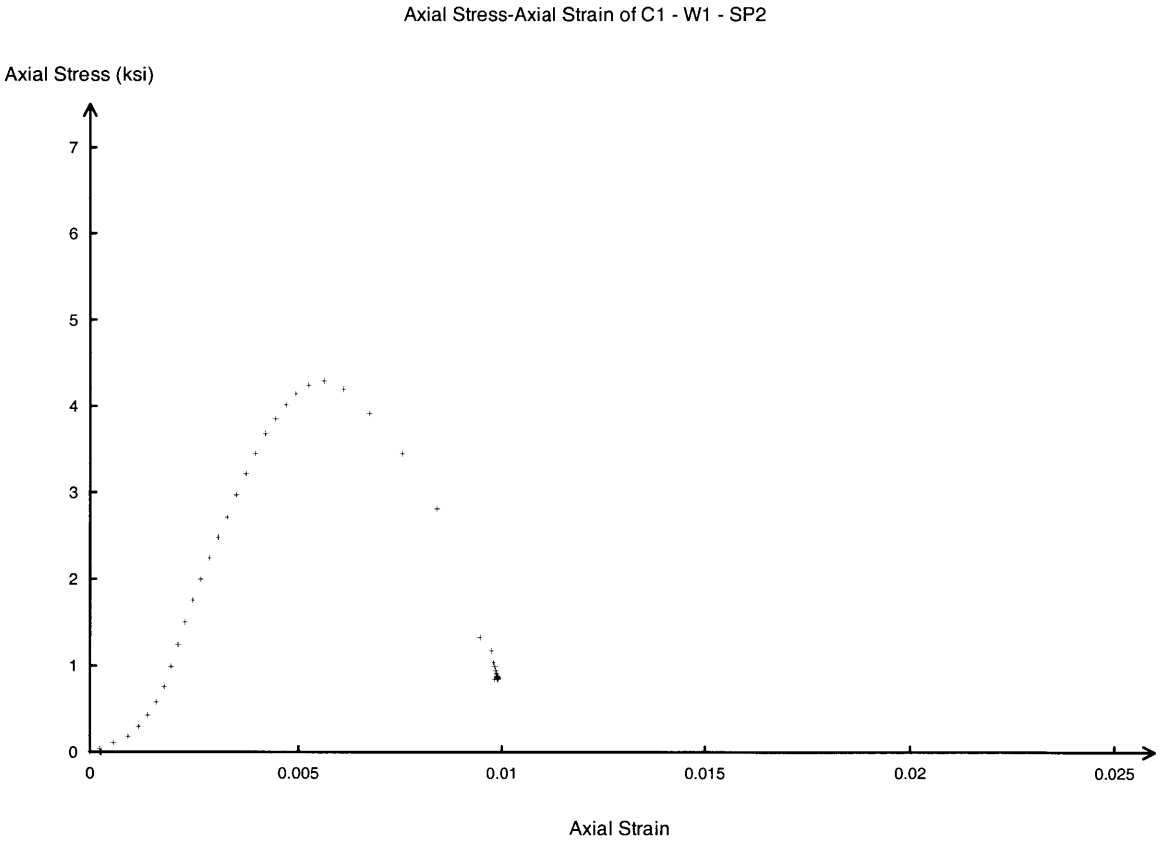

Plot of Axial Stress – Axial Strain of C1 – W1 – SP3

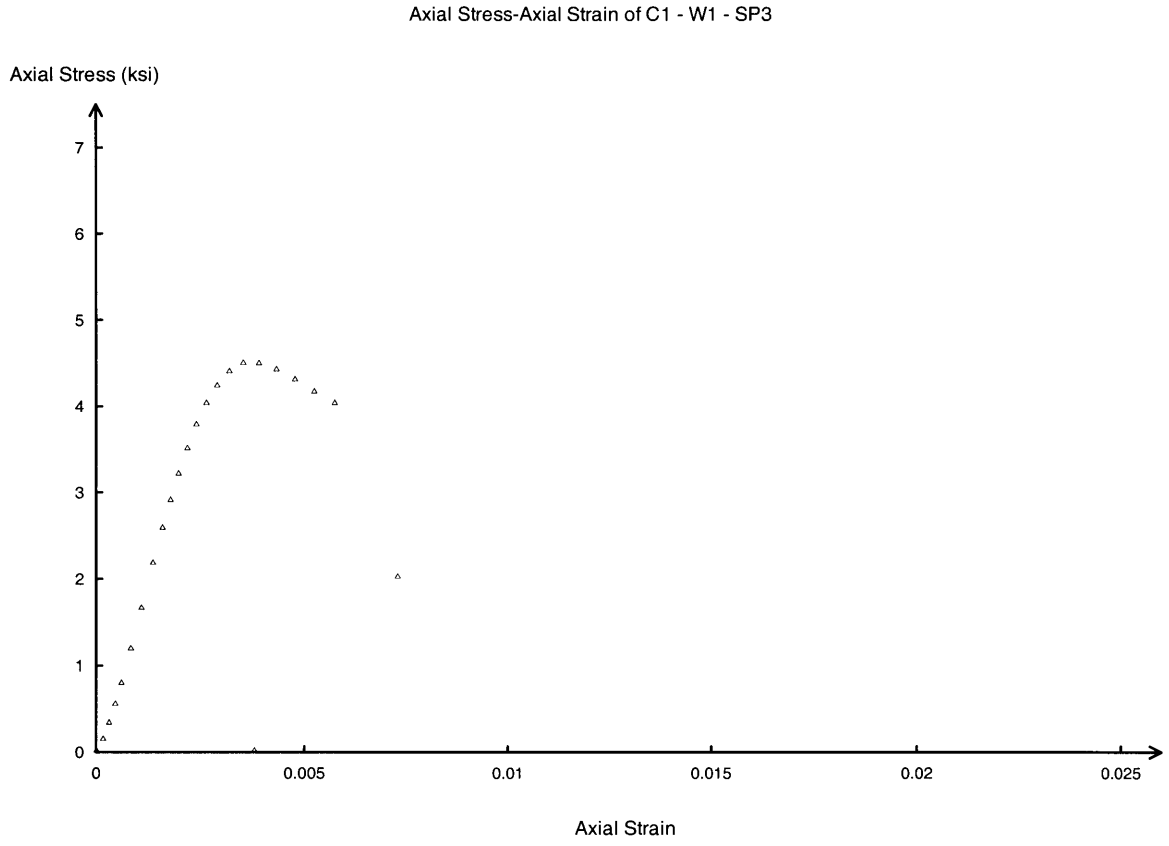

Plot of Axial Stress – Axial Strain of C1 – WA1 – SP1

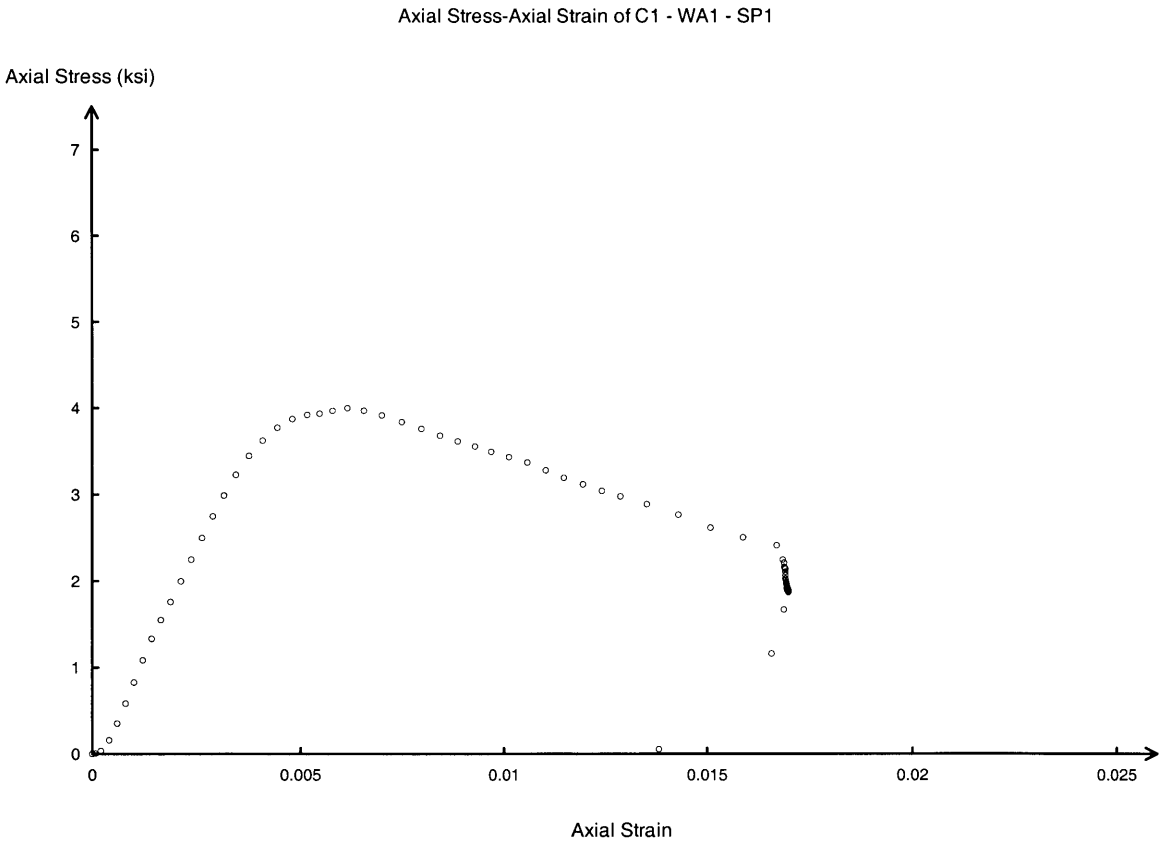

Plot of Axial Stress – Axial Strain of C1 – WA1 – SP2

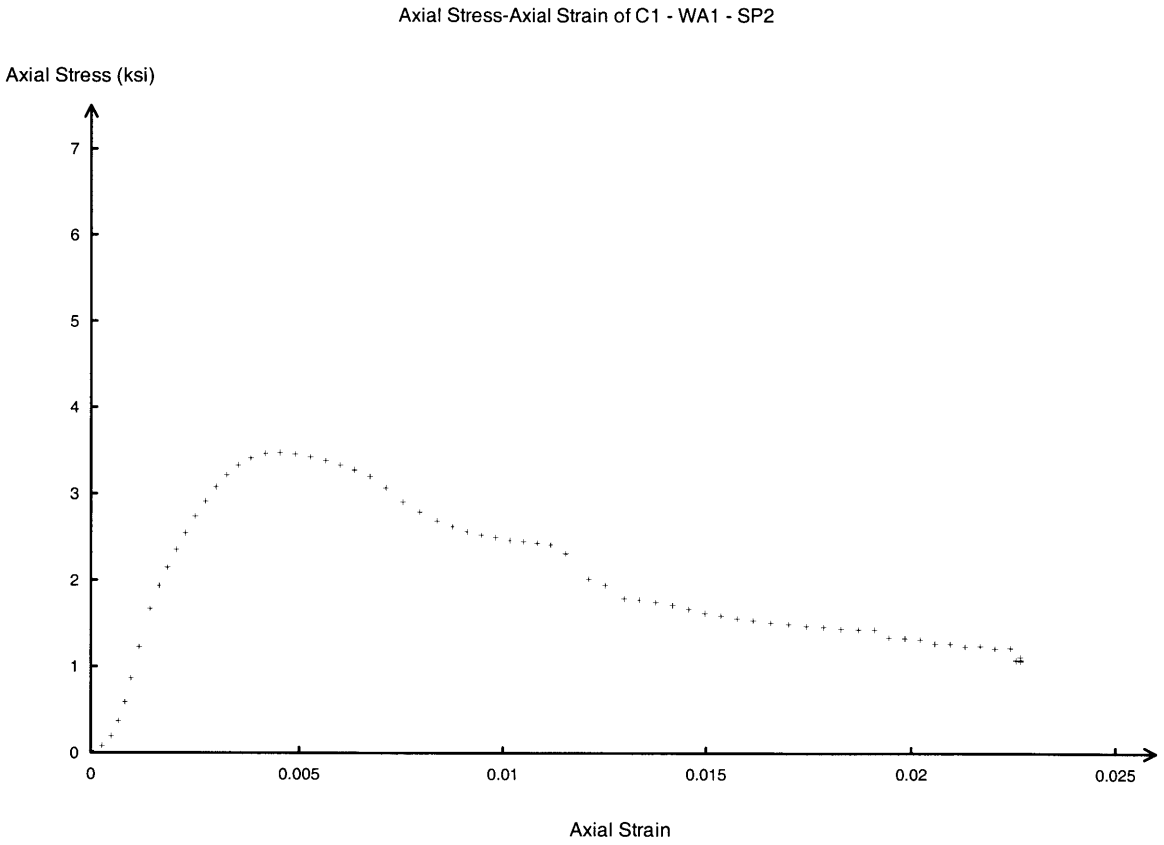

Plot of Axial Stress – Axial Strain of C1 – WA1 – SP3

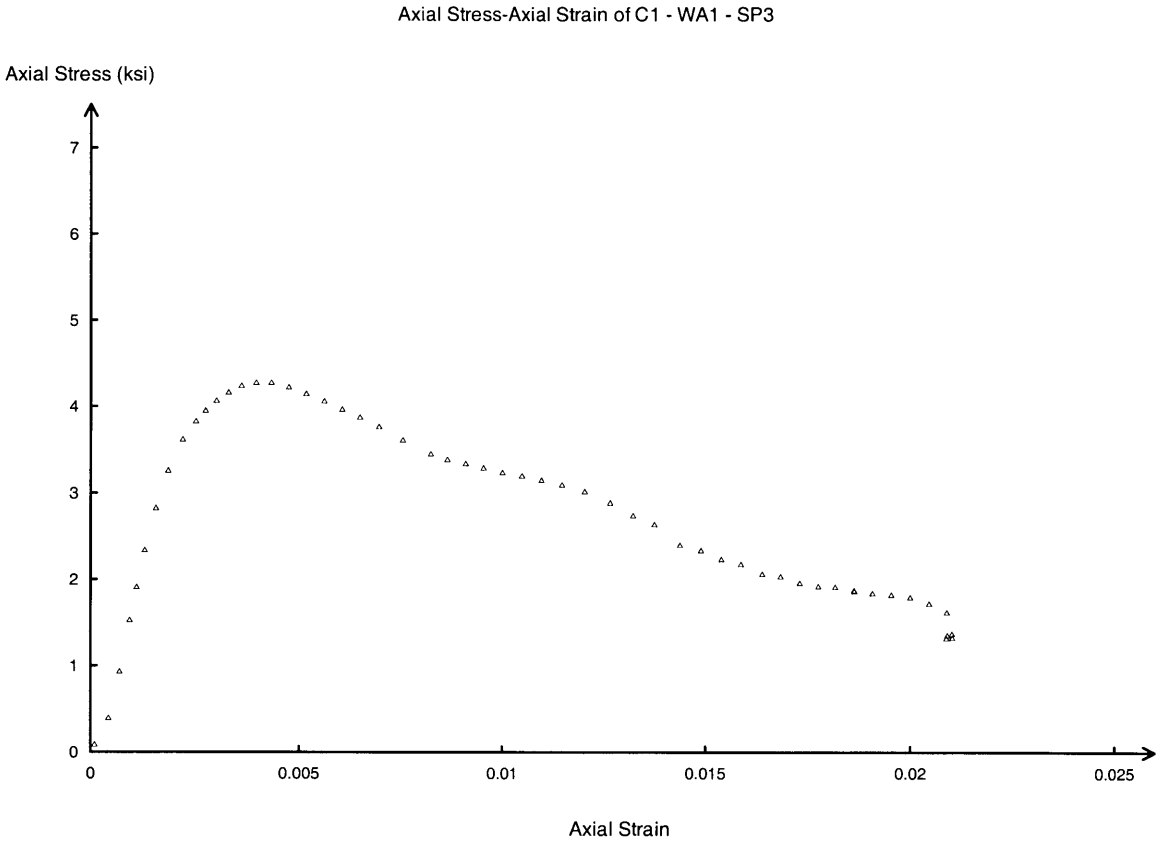

Plot of Axial Stress – Axial Strain of C2 – W1 – WA1 – SP1

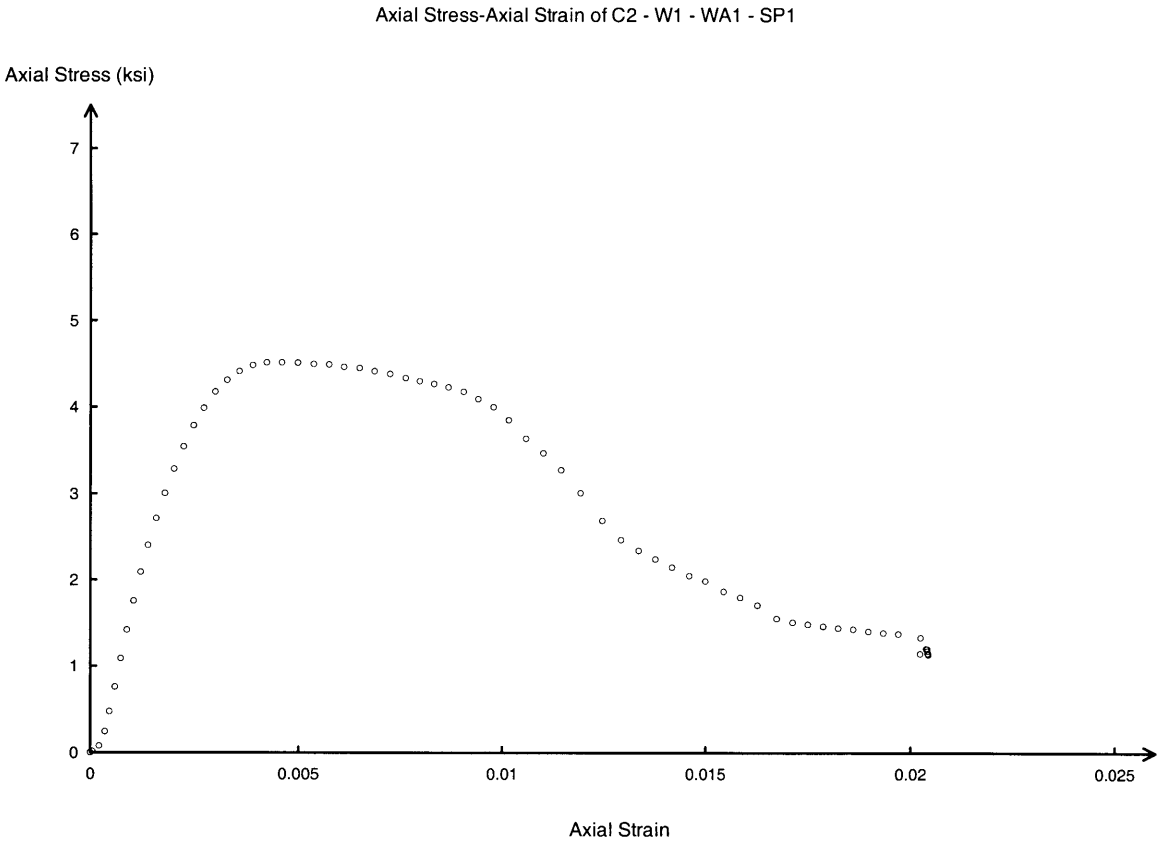

Plot of Axial Stress – Axial Strain of C2 – W1 – WA1 – SP2

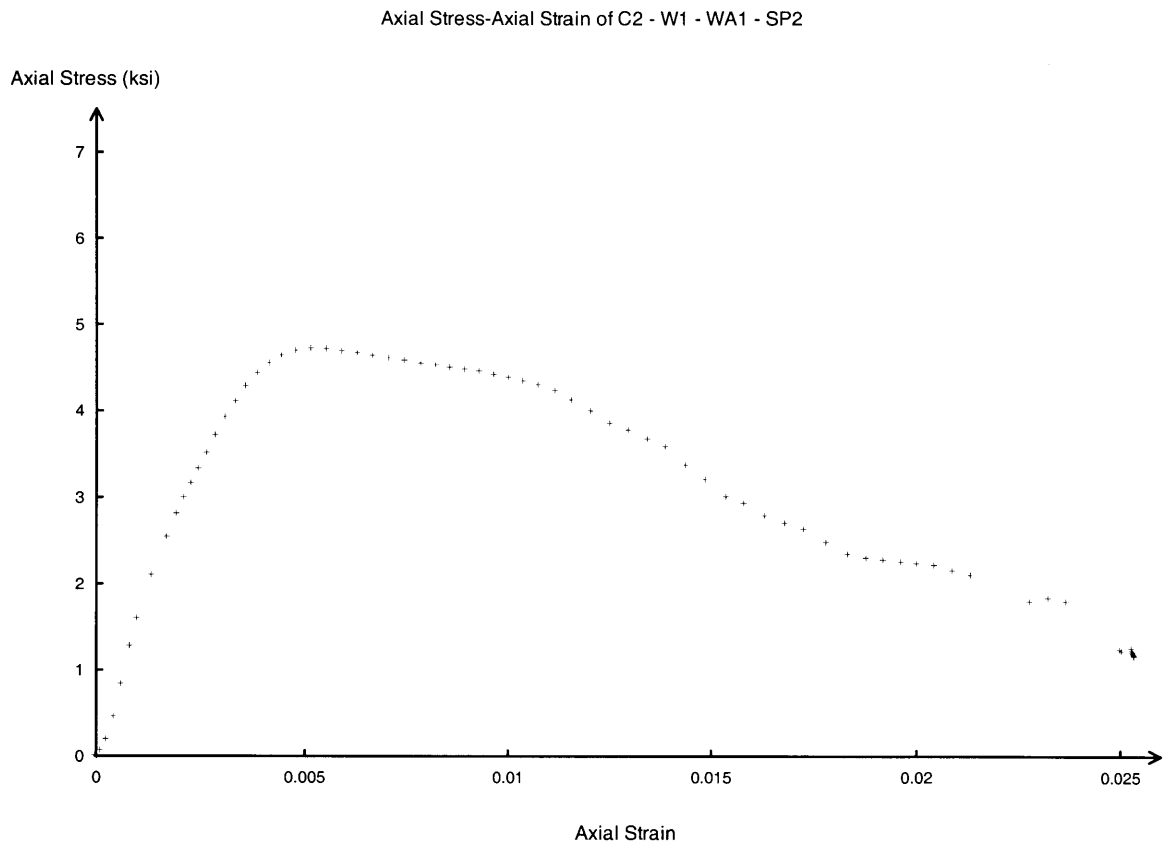

Plot of Axial Stress – Axial Strain of C2 – W1 – WA1 – SP3

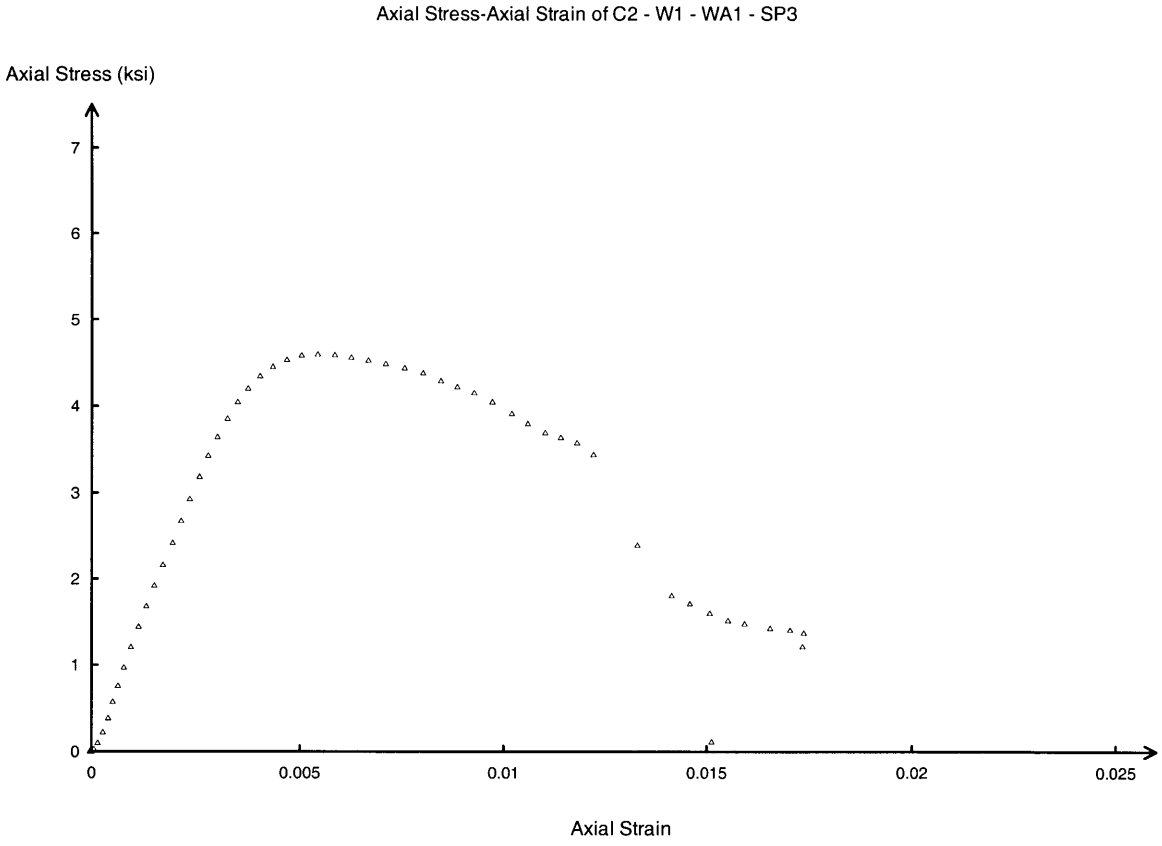

Plot of Axial Stress – Axial Strain of C2 – UC1 – WA1 – SP1

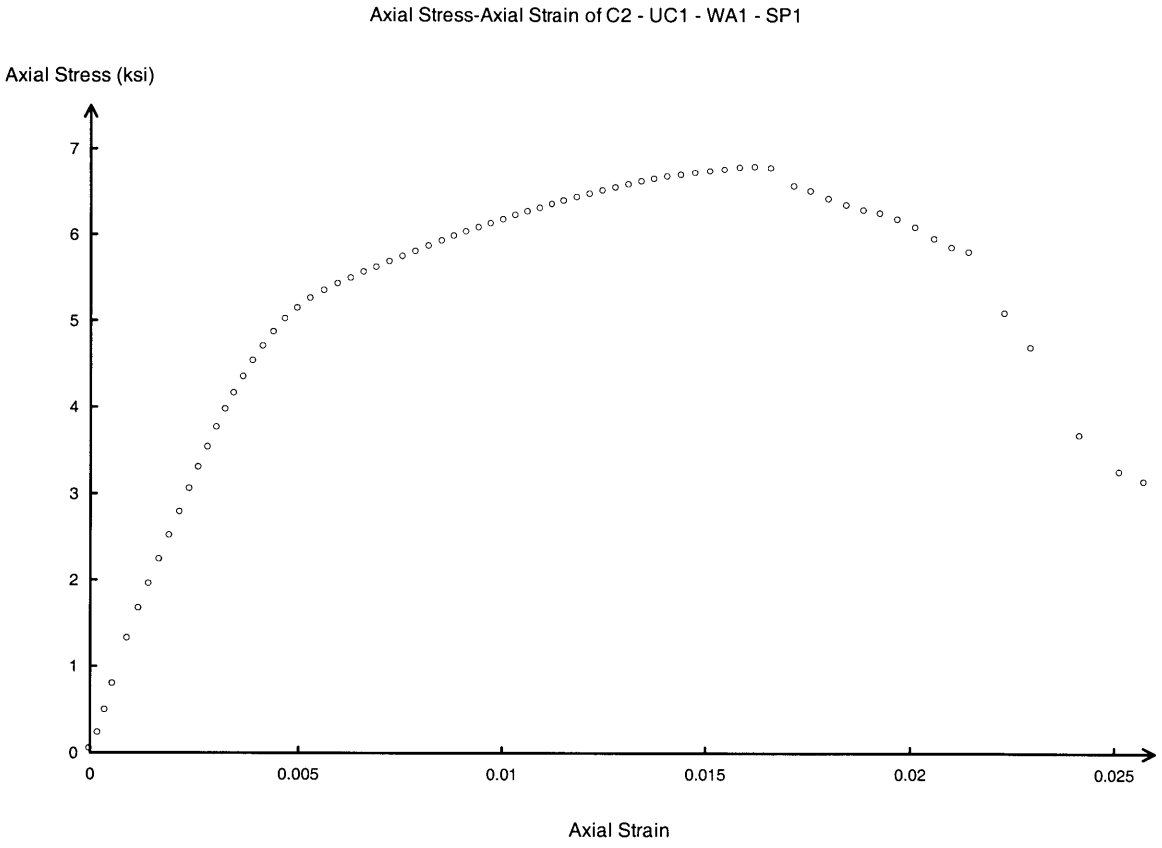

Plot of Axial Stress – Axial Strain of C2 – UC1– WA1 – SP2

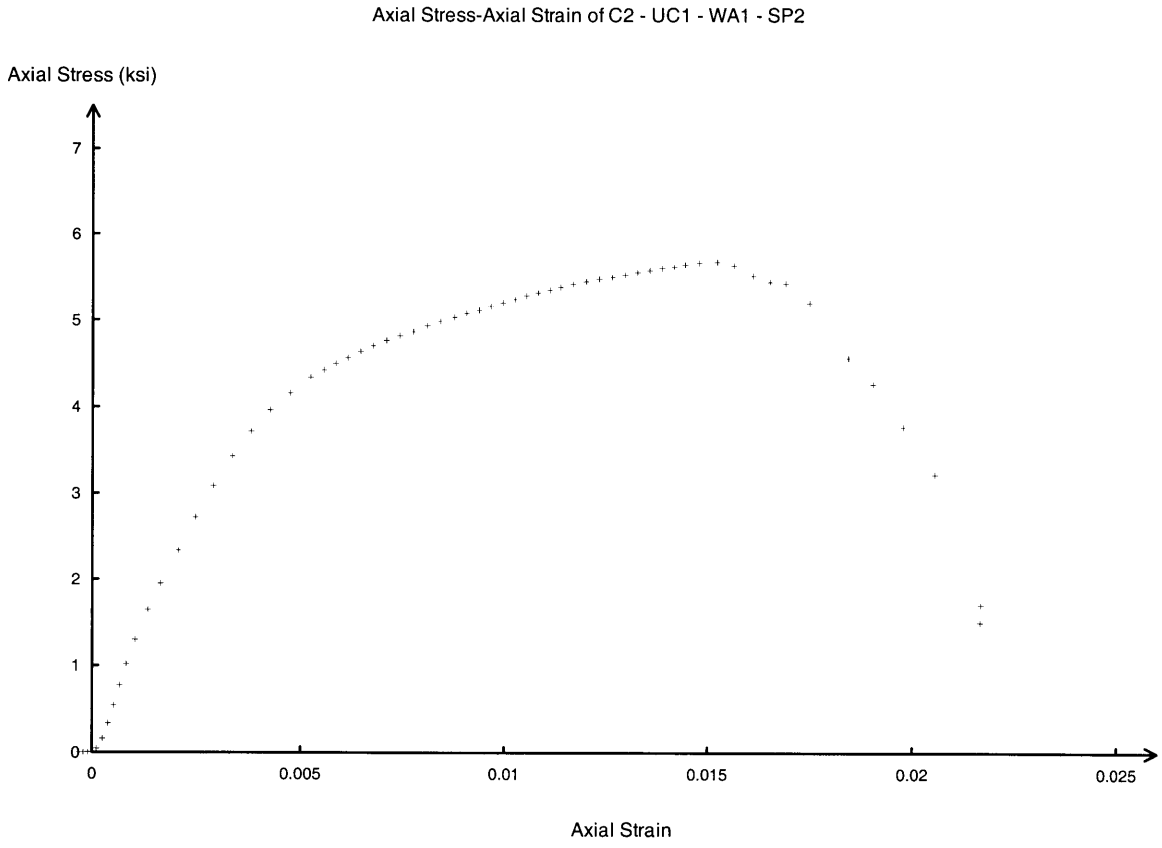

Plot of Axial Stress – Axial Strain of C2 – UC1– WA1 – SP3

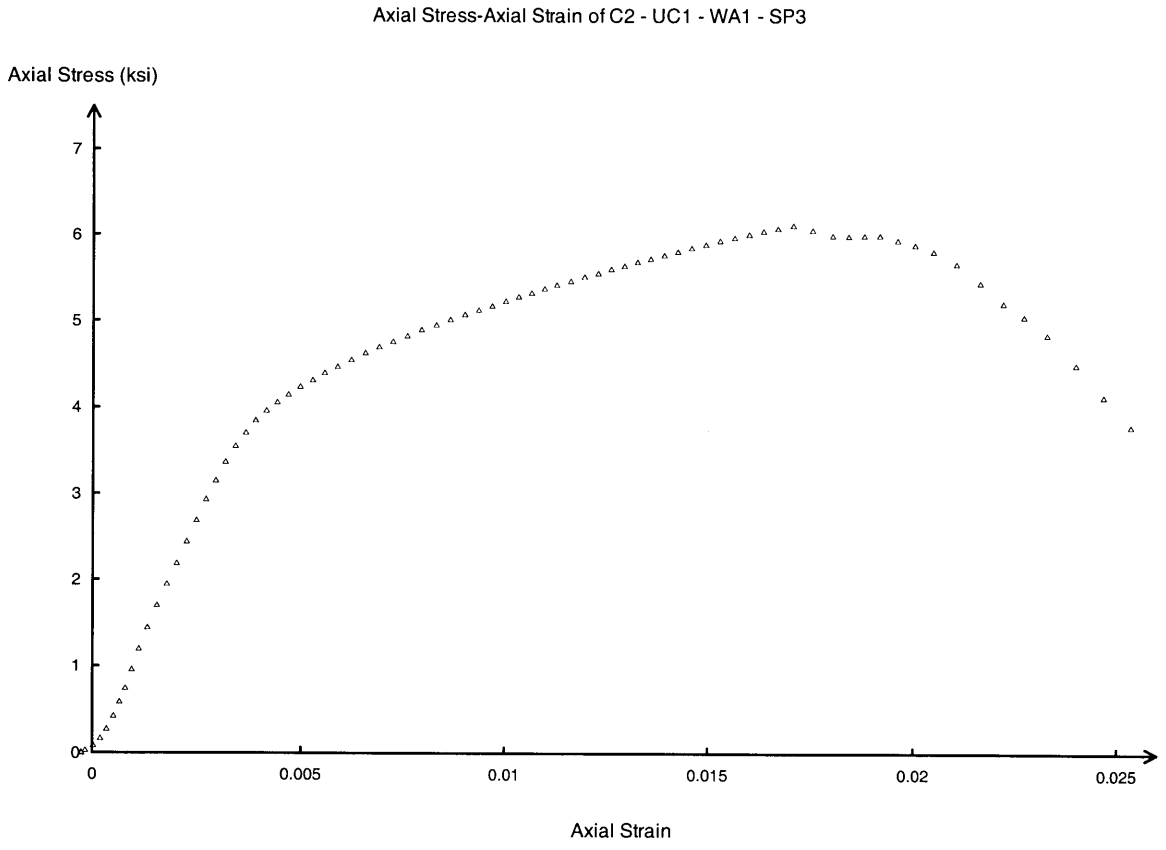

Plot of Axial Stress – Axial Strain of C2 – WA1 – UC1 – SP1

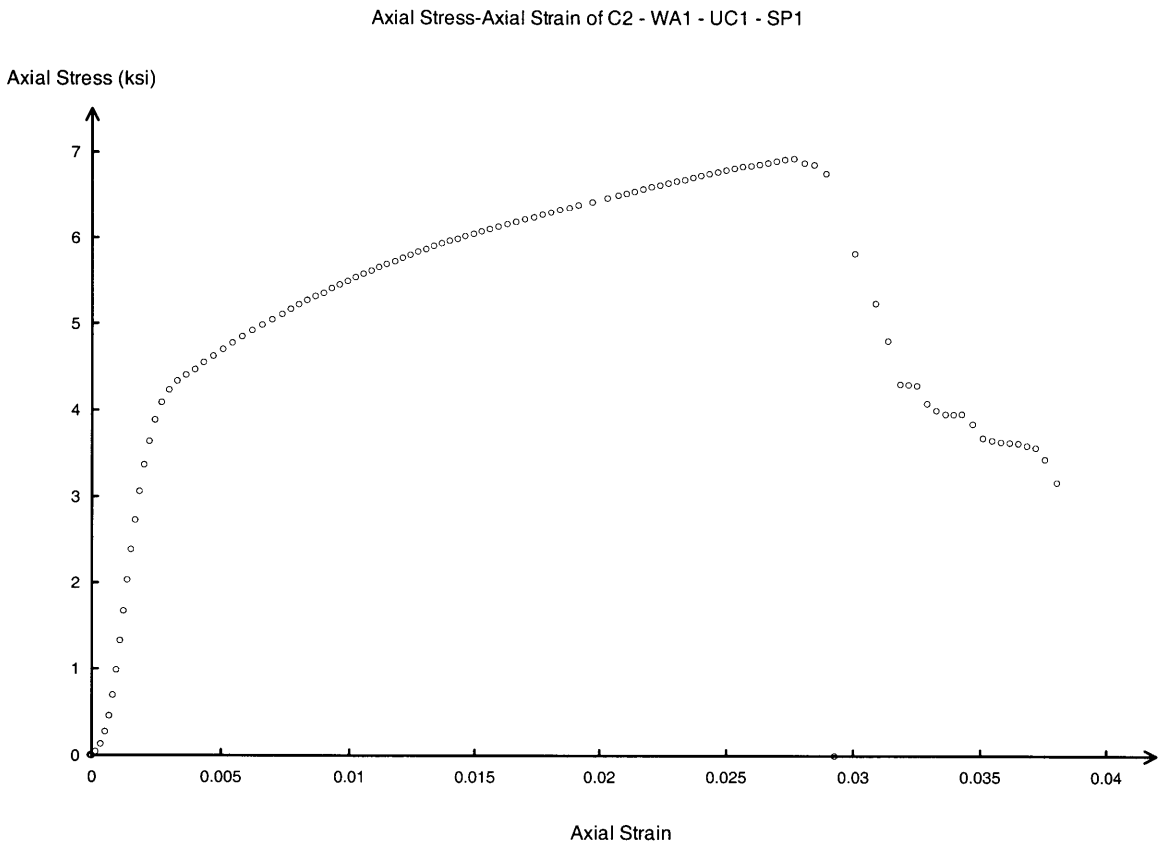

Plot of Axial Stress – Axial Strain of C2 – WA1 – UC1 – SP2

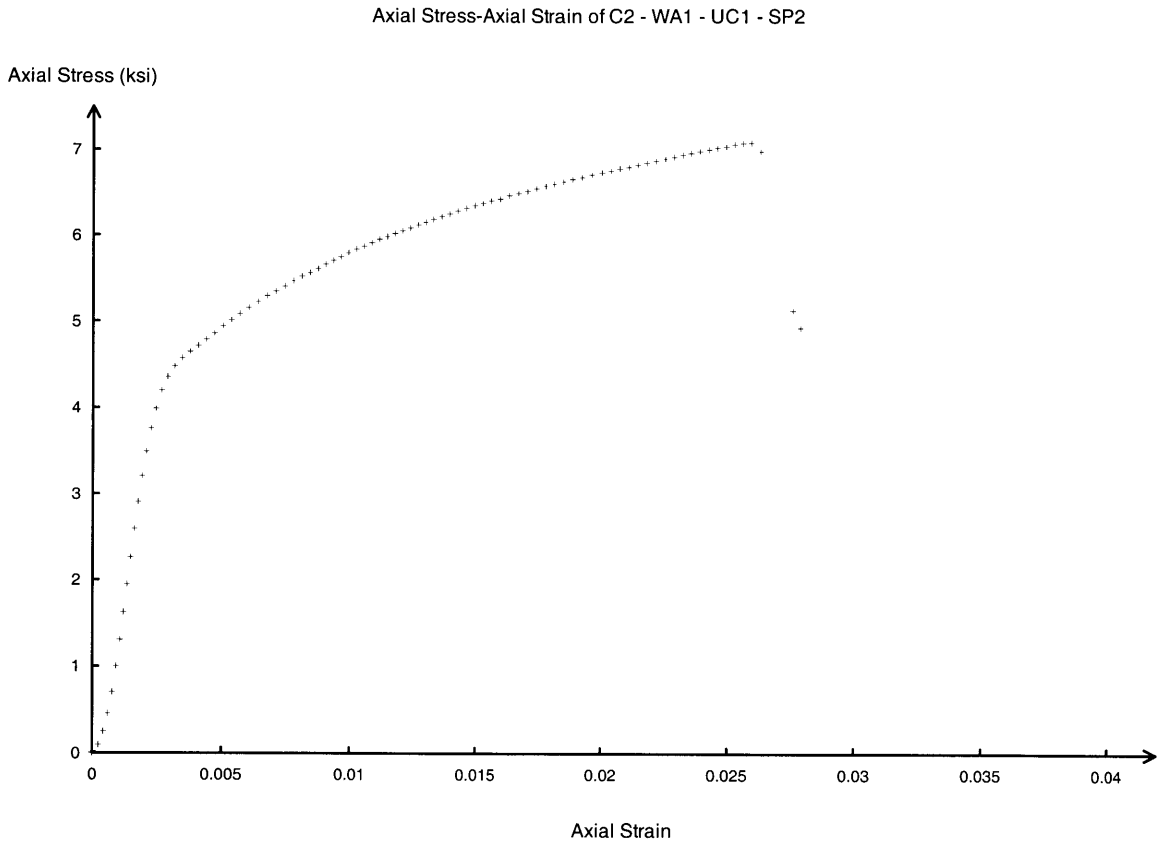

Plot of Axial Stress – Axial Strain of C2 – WA1 – UC1 – SP3